SYSTEM AUGMENTATION AND OPTIMAL FEEDBACK AUXILIARY SIGNALS FOR INTERROGATING NONLINEAR SYSTEMS

by

Kiran X. D'Souza

A dissertation submitted in partial fulfillment
of the requirements for the degree of
Doctor of Philosophy
(Mechanical Engineering)
in The University of Michigan
2009

Doctoral Committee:

Associate Professor Bogdan I. Epureanu, Chair
Professor Noel C. Perkins
Professor Armin W. Troesch
Adjunct Associate Research Scientist Matthew P. Castanier

To my parents

ACKNOWLEDGEMENTS

I would like to express my gratitude to my advisor and chair of my doctoral committee Professor Bogdan Epureanu. His generous support and guidance have made this work possible. I would like to thank Dr. Castanier, Professor Perkins and Professor Troesch for their valuable comments and suggestions, and serving on my doctoral committee. Also, I would like to acknowledge the National Science Foundation Graduate Research Fellowship and East Asia and Pacific Summer Institutes programs for their support.

I would also like to thank the current and former members of the Vibrations and Acoustics Laboratory who have helped me through their insights, comments and friendship, in particular I would like to thank: Steve Yin, Zhijiang He, Adam Hendricks, Jarrod Rivituso, Joosup Lim, Andrew Sloboda, Chulwoo Jung, Sung Kwon Hong, Darren Holland, Andrew Madden and Akira Saito. Additionally, I would like to thank all my friends who have helped me along the way.

I would also like to express my appreciation for my entire family, in particular all my uncles, aunts and cousins who have always been there for me. Finally, I would like to thank my parents, Arun, Jen, Kai, Deepak, Grace, Ryan, Stefanie, Meghan, Elijah, Ian and Vinay for their love and support.

TABLE OF CONTENTS

LIST OF FIGURES

Figure

LIST OF TABLES

Table

CHAPTER I

Introduction

1.1 Dissertation Objective

Nonlinear dynamics are of crucial importance in many engineering fields. The research in this dissertation is focused on the applications of nonlinear dynamics in the areas of structural health monitoring, system identification and sensing. In the structural health monitoring field, the goal is to replace the current common methods of visual inspection and time-based maintenance approaches with online monitoring and condition-based maintenance. This important transformation is based largely on current damage detection techniques, which are focused on identifying changes in linear features such as mode shapes and natural frequencies. However, nonlinearities are pervasive in many systems affected by damage, and thus linear techniques fail, because, for example, the presence or level of damage cannot be distinguished by linear methods from the nonlinear healthy dynamics. In the sensing field, current vibration based methods do not take advantage of nonlinear dynamics but minimize it, even though nonlinear-based methods can provide greater sensitivity and performance. The objective of this work is to develop general methodologies that can be applied to realistic, nonlinear systems, and exploit the greater sensitivity and performance that can be achieved using nonlinear dynamics.

1.2 Dissertation Background

Many structures have nonlinearities that play an important role in their dynamics. For example, geometric nonlinearities and (Colomb) friction are often present. These nonlinearities are typically neglected in applications such as structural health monitoring, and linear approximations are used. These approximations are motivated mainly by the fact that damage detection methods are much more developed for linear systems than nonlinear ones. However, the effects of neglected nonlinearities limit the accuracy and performance of the linear techniques (when applied to nonlinear models). The techniques presented in this dissertation address this problem, and allow for capitalizing on well developed linear techniques to perform accurate model based damage detection and sensing in nonlinear systems.

1.2.1 Linear and Nonlinear Analysis and Damage Detection

Typically, damage detection methodologies use information about the healthy and damaged systems. This information can exist in various forms, including a discrete or continuous model of the healthy system, or modal properties of the healthy (linearized) system. Most methodologies then extract system properties such as natural frequencies and mode shapes (for the linearized system) to detect damages. These linear features are obtained by using linear modal analysis, which is well established. The linear modal analysis field can be broken into single input single output, single input multiple output and multiple input multiple output (MIMO) approaches. Each of these approaches have in turn been developed for both the time and frequency domains. Yang et al. [2] surveyed the time-based MIMO methods and discussed their characteristics. In particular, there are the free and impulse response methods such as the poly-reference complex exponential [3], eigensystem realization algorithm [4] and Ibrahim time domain [5] methods. Also, there

are forced response methods such as auto-regressive moving average vector [6] and direct system parameter identification (DSPI) [7], which use the forcing from natural excitations to determine modal properties. The use of the natural excitations makes most of these methods well-suited for online damage detection.

In contrast, the *nonlinear* experimental analysis field is still under development. Worden and Tomlinson [8] separate the research in this field into three main areas. The first area uses the basic theory and philosophy of linear modal analysis by characterizing the nonlinear system in a way such that the amplitude invariance is lost. The study of the frequency response functions (FRF) distortion was one of the early studies in this area by Ewins [9]. The second area consists of extending the linear approach of modal analysis to encompass quantities that are amplitude invariants of nonlinear systems. For example, Gifford [10] developed a technique in this area which is based on Volterra series [11] and obtained the linear parameters from a nonlinear optimization step and the nonlinear parameters from a linear least squares analysis of higher order FRFs (HFRF). The third area of the study of nonlinearity in modal analysis requires the discarding of the linear theory and the creation of new theories to address the nonlinearity directly, such as nonlinear normal modes [12–16] and center manifold theory [17, 18].

In a model based approach, once model parameters are identified, they can be used for structural health monitoring. Ibrahim [19] and Heylen [20] provide a review of the four general categories of linear nondestructive evaluation. The first category is sensitivity methods, where recently Leung [21] proposed a more accurate solution technique for inverse sensitivity equations for asymmetric systems. The second is eigenstructure assignment techniques, which place eigenvalues and/or eigenvectors of the closed loop system. A good review of different eigenstructure assignment techniques can be found in the work by Andry et al. [22]. Lim [23] developed a constrained eigenstructure assignment for

damage detection that formed a direct relation between the feedback control and structural parameter changes, while Jiang et al. [24] developed optimal controllers for sensitivity enhancement by eigenstructure assignment. The next category are optimal matrix update methods [25, 26], which can be used for both system identification and damage detection. These methods update the system model by minimizing a cost function (e.g. the minimum Frobenius norm for the update) for a given set of constraints (e.g. maintaining the sparsity pattern of the original finite element model). The last category are minimum rank perturbation methods [1, 27–30], which solve for damage as the minimum rank solution to the perturbation equations.

1.2.2 Sensor Placement for Damage Detection

Most current sensor placement methodologies are focused on maximizing the controllability and observability of the healthy structure. For example, Cherng [31] identified the optimal placement of sensors and actuators for controllability and observability. That method examines the whole structure and selects sensor locations to maximize the signal to noise ratio in the system. Other approaches examine ways to minimize the information entropy norm, which is a measure of the uncertainty in the model parameter estimates. For example, Yuen et al. [32] proposed a sensor placement method designed for system identification and based on reducing entropy. That method requires choosing a number of damageable areas (each with an associated parameter) and placing an equal number of sensors to minimize the uncertainty in parameter estimates. Another technique, called the effective independence distribution vector (EIDV) method, selects sensor locations that make the measurements as linearly independent as possible while capturing as much information as possible in the desired mode shapes in the measured data [33].

Recently, there have been proposed several techniques which are focused on sensor

placement for damage detection. Cobb and Liebst [34] discussed one of the first such approaches. That sensor placement technique makes no assumption about damage location and, instead, focuses on a sensitivity analysis to find the degrees of freedom which maximize the changes due to damage in the observable partial eigenstructure. The method does not control which sections of the system will be detectable. Finally, other techniques are based on maximizing the Fischer information matrix to find the optimum sensor placement for damage detection [35, 36].

1.2.3 Sensitivity Enhancement of Resonant Frequencies

The shift in resonant frequencies due to changes in structural parameters has been used in micro and macro scale applications. For instance, at the micro scale, vibrating micro-structures such as micro-cantilevers [37–39] and micro-beams [40] have been used for atomic force microscopes in tapping mode [41] as well as for chemical and biological detection.

At the macro scale, vibration based methods can be used for damage detection and health monitoring for structures such as bridges and aircraft. Many of these vibration based methods use both mode shapes and natural frequencies [42–44]. Methods that are based on the measurement of mode shapes often require the placement of many sensors (in practical applications) and are more sensitive to noise [45] than methods that require the use of only resonant frequencies.

There are three central drawbacks to detection methods that use only resonant frequencies (herein referred to as frequency-shift based methods). The first drawback is the insensitivity of the resonant frequencies to changes in system parameters. Swamidas and Chen [46] showed this on a numerical study of a cracked plate. Their work showed that a surface crack 70% through its depth and 40% through its width only resulted in a max-

imum frequency shift of less than 0.7%. The insensitivity of the resonant frequency was also shown experimentally by Adams et al. [47]. They found less than a 1% change in the first three resonant frequencies of an aluminum bar under axial loading when cut at its center through 30% of its thickness. Ray and Tian [48] proposed sensitivity enhancing control to overcome this lack of sensitivity. They increased the sensitivity of the resonant frequencies of a cantilevered beam using vibration control to place the closed loop poles of the system. Ray et al. [49] experimentally validated sensitivity enhancing control using a cantilevered beam in bending. Juang et al. [50] extended the sensitivity enhancing control from single input to multi input systems. Their work proposed an eigenstructure assignment technique that placed closed loop eigenvectors close to the open loop eigenvectors to minimize control effort, while placing the poles such that they are more sensitive to changes in the system.

The second drawback of frequency-shift based methods is the limited number of resonant frequencies that can be accurately measured. This limited information often leads to an underdetermined problem when trying to solve for multiple simultaneous parameter variations common in damage detection and sensing applications. In the context of damage detection, Nalitolela et al. [51] tried to overcome the lack of frequency information by adding mass and stiffness elements. Although this method can enrich the frequency information, this approach is difficult to implement in practice. Lew and Juang [52] overcame this difficulty by introducing virtual passive controllers. The idea of that approach is that the frequency information can be enriched using controllers rather than physically adding mass or stiffness elements.

To overcome both the lack of frequency information and the insensitivity of the frequencies, Koh and Ray [53] proposed multiple independent controllers, which can each be designed to enhance the sensitivity to different parameters. Jiang et al. [24] extended this

approach by simultaneously placing both the eigenvalues and eigenvectors for multiple controller configurations for sensitivity enhancement. The final unresolved drawback is the inability of frequency-shift based methods to handle nonlinear systems.

1.3 Dissertation Outline

The remaining chapters of this dissertation contain six manuscripts that have been submitted to scientific journals (either in print or in review). Therefore some material in the background and methodology may overlap. The following is a brief overview of the remaining chapters.

Chapter II introduces a method for analyzing a nonlinear system as an augmented linear system. This allows for the much better developed areas of linear modal analysis and linear damage detection to be exploited. A key feature of the augmentation requires the modal analysis technique used to work with a forcing that is known but not prescribed. A MIMO technique such as DSPI [7] that uses natural excitations of the system as forcing is the technique used in this dissertation to identify the modal properties of the augmented system. Next, the modal properties of the augmented system are used in conjunction with a novel generalized minimum rank perturbation theory (GMRPT) to detect the location and extent of damage in nonlinear systems. The proposed GMRPT is designed to account for nonlinearities, and is inspired from a linear damage detection technique employing minimum rank perturbation theory (MRPT) [1, 27–30]. A key characteristic of the proposed augmentation is that the nonlinear damage is manifested in an asymmetrical fashion in the system matrices. A formulation of GMRPT is proposed to handle cases of asymmetric damage and nonlinear systems. The approach is demonstrated by applying the method to several nonlinear mass-spring systems in numerical experiments. Also, the influence of measurement noise and of inaccuracies in modal parameters is analyzed.

Chapter III introduces a theoretical framework for the detection of simultaneous damages in multiple system matrices and several other additions to the damage detection method developed in Chapter II. A subspace selection algorithm is used to reduce the effects of measurement noise. Also, an iterative approach to the solution of the left eigenvectors for simultaneous damage detection is employed. Moreover, an alternate approach is presented for the cases where an incomplete set of right eigenvectors are known. This new approach is based on multiple augmentations of the same nonlinear system. Finally, eigenvector filtering algorithms are discussed to reduce the effects of random measurement noise on the method. These techniques are demonstrated on nonlinear mass-spring systems and nonlinear frame structures. Complex simultaneous damage scenarios are explored and the effectiveness of the methodology for nonlinearities such as cubic springs and Colomb friction are presented. Also, the influence of measurement noise with and without filtering algorithms is demonstrated through numerical simulations.

Chapter IV introduces a reduced order health assessment methodology for detecting damage in the hot spots of linear and nonlinear (augmented) systems with few measurements. The physical measured displacements and forcing of the structure are filtered in the frequency domain to keep only frequencies that are near the frequencies of the eigenmodes used in the projection matrix. Modal information corresponding to the measurement locations can then be extracted. This (partial) modal information can be expanded (to full modal information) by an approach which enforces that damage can only occur in the hot spots of the system. Any number of modal based damage detection methods, such as minimum rank perturbation theory [1, 27–29] (MRPT) or optimal matrix update approaches [25, 26], can be used to calculate the damage. However, to provide additional noise rejection, a novel method called damage identification by hot spot projection (DIHSP) is presented. Also, the methodology for an improved sensor placement is laid

out for linear and nonlinear (augmented) systems. To demonstrate the approach, linear and nonlinear 5-bay frames are used for various tests illustrating the effectiveness of the proposed techniques.

Chapter V introduces nonlinear feedback auxiliary signals for sensitivity enhancement of resonant frequencies in nonlinear systems. An optimization algorithm is used with an eigenstructure assignment technique to place the augmented resonant frequencies and mode shapes of the system to maximize sensitivity, while minimizing control effort. The concept of the optimal augmentation is also introduced for further sensitivity enhancement. A mass-spring system containing cubic nonlinearities is investigated using system augmentation and optimal feedback auxiliary signals. Various numerical studies are presented to demonstrate optimal sensitivity enhancement for damage detection, and the effects of random noise are also discussed.

Chapter VI applies *nonlinear* feedback auxiliary signals that are optimally designed and applied to *linear* systems by means of system augmentation. In addition to the benefits of using nonlinear control to enable the use of system augmentation, the effects of modeling generalized damping in the optimization algorithm are discussed. Also, a more realistic output feedback approach is presented, which allows for the eigenstructure assignment to be carried out with an incomplete set of measurements (where only a few displacements need to be measured). Additionally, the optimal feedback auxiliary signals have been adaptively designed to the expected level of parameter variation using a linearity constraint in the optimization algorithm. The systems explored herein are a linear mass-spring system and a mass-spring-damper system. Numerical simulations are presented, and the effects of random noise are discussed.

Chapter VII builds on the work in Chapters V and VI for the case where there are limited measurements available and a single input actuator for two cantilevered beam sys-

tems. In the first system, the motion of the structure, which must be fed back into the system using the control gain matrix, is known only at 5 locations. In the second system, the motion of the structure is known only at 2 locations. Linear approaches would allow for the placement of only 2 resonant frequencies in the first system and 1 in the second system. In contrast, the use of nonlinear feedback auxiliary signals allows the creation of several augmented variables, which increases the amount of measurement information, and in turn enables the placement of additional frequencies of the augmented system. Additionally, the simultaneous detection of global changes in the system (e.g. due to environmental changes in temperature or humidity) and local changes is explored. Also, the idea of sensitivity enhancement for parameters of interest combined with sensitivity reduction for parameters that are not of interest (due to environmental or operational changes) is developed and explored. A methodology is also presented to accurately extract augmented frequencies from displacement and forcing data corrupted by noise. Various numerical simulations are included to demonstrate the proposed techniques, and to discuss the effects of random noise.

CHAPTER II

Damage Detection in Nonlinear Systems Using System Augmentation and Generalized Minimum Rank Perturbation Theory

2.1 Introduction

Health monitoring and online damage detection of structural systems is of growing importance in many fields. The aerospace industry is one of the fields where these methods are applied. Many current structural damage detection techniques are focused on identifying changes in the linear system behavior [54] and employ linear methods based on changes in the natural frequencies and mode shapes [55]. Also, system identification [56–60] and generic (and not necessarily physical) models such as neural networks [61–63] are used. With the increasing demand for safe space technology, the various structural systems that compose air and space vehicles must be monitored for safety and reliability. Hence, the current most common methods of visual inspection and time-based maintenance will be upgraded to online monitoring of the integrity of the vehicle and condition-based maintenance.

The field of nonlinear experimental modal analysis is an active area of research which plays an important role in nonlinear vibration-based damage detection. Worden and Tomlinson [8] separate the research in this field into three main areas. The first area uses

the basic theory and philosophy of linear modal analysis by characterizing the nonlinear system in a way such that the amplitude invariance is lost. The study of the frequency response functions (FRF) distortion was one of the early studies in this area by Ewins [9]. The second area consists of extending the linear approach of modal analysis to encompass quantities that are amplitude invariants of nonlinear systems. For example, Gifford [10] develops a technique in this area which is based on Volterra series [11] and obtains the linear parameters from a nonlinear optimization step and the nonlinear parameters from a linear least squares analysis of higher order FRFs (HFRF). The third area of the study of nonlinearity in modal analysis requires the discarding of the linear theory and the creation of new theories to address the nonlinearity directly, such as nonlinear normal modes [12–15] and center manifold theory [17, 18].

The field of linear modal analysis is much more developed than its nonlinear counterpart. Linear techniques based on single input single output, single input multiple output, and multiple input multiple output (MIMO) approaches are available. These techniques are developed for both time and frequency domains. The time-based MIMO methods have several different characteristics which were surveyed by Yang et al. [2]. The poly-reference complex exponential [3], eigensystem realization algorithm [4] and Ibrahim time domain [5] methods find the modal properties using impulse or free responses of the system. The auto-regressive moving average vector [6] and direct system parameter identification (DSPI) [7] both use the response of systems forced by natural excitations to determine modal properties.

Using modal analysis to obtain the mode shapes and natural frequencies is the first step in many structural health monitoring approaches. The modal properties are then used in a damage detection algorithm. The linear nondestructive evaluation field has been developed greatly and includes four general categories: optimal matrix updates, sensitivity

methods, eigenstructure assignment techniques, and minimum rank perturbation methods (for a review, see review papers by Ibrahim [19] and Heylen [20]).

In this work an algorithm for analyzing a nonlinear system as an augmented linear system is presented. This allows for the much better developed areas of linear modal analysis and linear damage detection to be exploited. A key feature of the augmentation requires the modal analysis technique used to work with a forcing that is known but not prescribed. A MIMO technique such as DSPI [7] that uses natural excitations of the system as forcing is the technique used in this chapter to identify the modal properties of the augmented system. Nonetheless, other techniques may be used as well. Next, the modal properties of the augmented system are used in conjunction with a novel generalized minimum rank perturbation theory (GMRPT) to detect the location and extent of damage in nonlinear systems. The proposed GMRPT is designed to account for nonlinearities, and is inspired from a linear damage detection technique employing minimum rank perturbation theory (MRPT) [1,27–29]. A key characteristic of the proposed augmentation is that the nonlinear damage is manifested in an asymmetrical fashion in the system matrices. A formulation of GMRPT is proposed to handle cases of asymmetric damage and nonlinear systems.

To demonstrate the proposed approach, the method is applied to several nonlinear mass-spring systems. The effectiveness of the augmentation and the GMRPT are demonstrated by numerical experiments. Also, the influence of measurement noise and of inaccuracies in modal parameters is analyzed.

2.2 General Methodology

In this section, the procedure for detecting the location and extent of damage in nonlinear systems using linear theories is demonstrated. First, the modeling of the nonlinear system by an augmented linear one is introduced. Then, a means to solve the eigenvalue

problem for the augmented system using DSPI [7] is detailed. Next, GMRPT is developed for damage that is not symmetric, which is a characteristic of the augmented system.

2.2.1 System Augmentation for Modeling Nonlinear Systems

In this section, a method to model a nonlinear system by an augmented linear system is presented. Consider a nonlinear system (characterized by a coordinate vector $\mathbf{x}$ and forced by an external excitation $\mathbf{g}(t)$) expressed as

$$\begin{aligned} \mathbf{M}\ddot{\mathbf{x}} + \mathbf{D}\dot{\mathbf{x}} + \mathbf{K}\mathbf{x} + \mathbf{f}(\mathbf{x}, \dot{\mathbf{x}}, \ddot{\mathbf{x}}) &= \mathbf{g}(t), \quad \text{or} \\ \begin{bmatrix} \mathbf{M} & \mathbf{0} \\ \mathbf{0} & \mathbf{I} \end{bmatrix} \begin{bmatrix} \ddot{\mathbf{x}} \\ \dot{\mathbf{x}} \end{bmatrix} + \begin{bmatrix} \mathbf{D} & \mathbf{K} \\ -\mathbf{I} & \mathbf{0} \end{bmatrix} \begin{bmatrix} \dot{\mathbf{x}} \\ \mathbf{x} \end{bmatrix} + \begin{bmatrix} \mathbf{f}(\mathbf{x}, \dot{\mathbf{x}}, \ddot{\mathbf{x}}) \\ \mathbf{0} \end{bmatrix} &= \begin{bmatrix} \mathbf{g}(t) \\ \mathbf{0} \end{bmatrix}, \end{aligned} \tag{2.1}$$

where $\mathbf{M}$, $\mathbf{D}$, and $\mathbf{K}$ are the mass, damping and stiffness matrices and $\mathbf{f}$ is a nonlinear function. Eq. (2.1) can be rewritten as

$$\begin{aligned} \mathbf{M}\ddot{\mathbf{x}} + \mathbf{D}\dot{\mathbf{x}} + \mathbf{K}\mathbf{x} + \mathbf{N}\mathbf{y} &= \mathbf{g}(t), \quad \text{or} \\ \begin{bmatrix} \mathbf{M} & \mathbf{0} & \mathbf{0} \\ \mathbf{0} & \mathbf{I} & \mathbf{0} \\ \mathbf{0} & \mathbf{0} & \mathbf{I} \end{bmatrix} \begin{bmatrix} \ddot{\mathbf{x}} \\ \dot{\mathbf{x}} \\ \ddot{\mathbf{y}} \end{bmatrix} + \begin{bmatrix} \mathbf{D} & \mathbf{K} & \mathbf{N} \\ -\mathbf{I} & \mathbf{0} & \mathbf{0} \\ \mathbf{0} & \mathbf{N}_C & \mathbf{N}_S \end{bmatrix} \begin{bmatrix} \dot{\mathbf{x}} \\ \mathbf{x} \\ \mathbf{y} \end{bmatrix} &= \begin{bmatrix} \mathbf{g}(t) \\ \mathbf{0} \\ \mathbf{h}(t) \end{bmatrix}, \end{aligned} \tag{2.2}$$

where $\mathbf{y}$ contains nonlinear terms of the form $(d^m x_i/dt^m)^p (d^n x_j/dt^n)^q$ (with integer m, n, p, q), and $\mathbf{N}$, $\mathbf{N}_C$ and $\mathbf{N}_S$ are constant matrices. The function $\mathbf{h}(t)$ in Eq. (2.2) is introduced to preserve most of the properties of the matrices in Eq. (2.1). The augmentation is expressed such that it matches the form used in examples later in this chapter. However, the system can be augmented differently to optimally suit various applications. Eq. (2.2) is the augmented linear model of the nonlinear system for which the eigenvalue problem must be solved.

2.2.2 Eigenvalue Problem for Augmented Systems

To use the augmented model given in the previous section, a modal analysis technique which uses an excitation that is known, but not prescribed is needed. An example of a modal analysis technique that meets these requirements is DSPI, and it is also the technique used to generate data for this chapter. DSPI enables one to determine the mode shapes and natural frequencies of the system when the displacement of the degrees of freedom ($\mathbf{x}(t)$ and $\mathbf{y}(t)$) and the forcing ($\mathbf{g}(t)$ and $\mathbf{h}(t)$) are known.

An example of implementation of the proposed approach is to measure the displacement vector $\mathbf{x}(t)$ and the forcing vector $\mathbf{g}(t)$. The vector $\mathbf{y}(t)$ may then be computed from $\mathbf{x}(t)$, and the vector $\mathbf{h}(t)$ may be calculated to satisfy Eq. (2.2). The requirement of the modal analysis technique to use a known but not prescribed forcing stems from the known forcing $\mathbf{h}(t)$.

A consequence of the form of the augmentation is the inability for damage to be modeled in the augmentation. This means that if damage occurs in $\mathbf{N}$ it will only be reflected in the linear portion and not the augmented portion of the system. The end result is that, when using this augmentation, nonlinear damage causes asymmetrical changes in the system matrices.

2.2.3 Generalized Minimum Rank Perturbation Theory

In this section, MRPT is generalized to handle cases where linear and nonlinear damage is present and the damage is not necessarily symmetric. First, the location algorithm is presented, and then the modified extent calculation is formulated.

Identification of damage location

The damage location algorithm for GMRPT follows closely that of MRPT [1, 27–29] except for the addition of several equations that are used in the identification of the damage

extent. It is assumed that a discrete, n-degree of freedom (e.g. finite element) model exists for the healthy system, and may be expressed as

$$\mathbf{M}\ddot{\mathbf{w}} + \mathbf{D}\dot{\mathbf{w}} + \mathbf{K}\mathbf{w} = \mathbf{0}, \tag{2.3}$$

where $\mathbf{M}$, $\mathbf{D}$ and $\mathbf{K}$ are $n \times n$ mass, damping and stiffness matrices, and $\mathbf{w}$ is an $n \times 1$ vector of displacements. The eigenvalue problem of Eq. (2.3) (i.e. λ-equation) can be written in second order form as

$$\begin{aligned} \left(\lambda_{hi}^2\mathbf{M} + \lambda_{hi}\mathbf{D} + \mathbf{K}\right)\mathbf{v}_{hi} &= \mathbf{0}, \\ \mathbf{u}_{hi}^T\left(\lambda_{hi}^2\mathbf{M} + \lambda_{hi}\mathbf{D} + \mathbf{K}\right) &= \mathbf{0}, \end{aligned} \tag{2.4}$$

where λ_{hi}, $\mathbf{v}_{hi}$ and $\mathbf{u}_{hi}$ denote the ith eigenvalue, ith right eigenvector, and ith left eigenvector of the healthy structure. Next, consider that the ith eigenvalue λ_{di}, ith right eigenvector $\mathbf{v}_{di}$, and ith left eigenvector $\mathbf{u}_{di}$ of the damaged structure are measured (e.g. through modal analysis and DSPI). Let $\Delta\mathbf{M}$, $\Delta\mathbf{D}$ and $\Delta\mathbf{K}$ be the exact perturbation matrices that reflect the nature of the structural damage. Thus, the exact perturbation matrices are sparse matrices with the nonzero elements reflecting the presence of the damage. The λ-equation for the damaged structure may be expressed as

$$\begin{aligned} \left[\lambda_{di}^2(\mathbf{M} - \Delta\mathbf{M}) + \lambda_{di}(\mathbf{D} - \Delta\mathbf{D}) + (\mathbf{K} - \Delta\mathbf{K})\right]\mathbf{v}_{di} &= \mathbf{0}, \\ \mathbf{u}_{di}^T\left[\lambda_{di}^2(\mathbf{M} - \Delta\mathbf{M}) + \lambda_{di}(\mathbf{D} - \Delta\mathbf{D}) + (\mathbf{K} - \Delta\mathbf{K})\right] &= \mathbf{0}. \end{aligned} \tag{2.5}$$

Although only p of the n eigenvalues/eigenvectors are assumed measured (with $p << n$), these equations hold for any particular eigenvalue and eigenvector of the damaged structure because the perturbation matrices are assumed to be exact. Grouping all perturbation

matrices on the right hand side defines two damage vectors $\mathbf{d}_i$ and $\mathbf{c}_i$ as

$$\mathbf{d}_i \equiv \mathbf{Z}_{di}\mathbf{v}_{di} = \left(\lambda_{di}^2\Delta\mathbf{M} + \lambda_{di}\Delta\mathbf{D} + \Delta\mathbf{K}\right)\mathbf{v}_{di}, \tag{2.6}$$

$$\mathbf{c}_i^T \equiv \mathbf{u}_{di}^T\mathbf{Z}_{di} = \mathbf{u}_{di}^T\left(\lambda_{di}^2\Delta\mathbf{M} + \lambda_{di}\Delta\mathbf{D} + \Delta\mathbf{K}\right), \tag{2.7}$$

$$\mathbf{Z}_{di} \equiv \lambda_{di}^2\mathbf{M} + \lambda_{di}\mathbf{D} + \mathbf{K}. \tag{2.8}$$

A composite damage vector may be defined from the multiple measured modes as

$$\mathbf{d} = \frac{1}{p}\sum_{i=1}^{p}\frac{\mathbf{d}_i}{\|\mathbf{v}_{di}\|}. \tag{2.9}$$

Also, Zimmerman [1, 27–29] developed an alternative view of the state of damage where Eq. (2.6) can be rewritten as

$$d_i^j \equiv \mathbf{z}_{di}^j\mathbf{v}_{di} = \| \mathbf{z}_{di}^j \| \| \mathbf{v}_{di} \| \cos(\theta_i^j), \tag{2.10}$$

where d_i^j is the jth component (i.e. jth degree of freedom DOF) of the ith damage vector, $\mathbf{z}_{di}^j$ is the jth row of the matrix $\mathbf{Z}_{di}$, and θ_i^j is the angle between the vectors $\mathbf{z}_{di}^j$ and $\mathbf{v}_{di}$. A damage detector α_i^j may be calculated from θ_i^j, where

$$\alpha_i^j = \theta_i^j\left(\frac{180^\circ}{\pi}\right) - 90^\circ. \tag{2.11}$$

A composite damage vector γ may be defined from the multiple measured modes as

$$\gamma_j = \frac{1}{p}\sum_{i=1}^{p}|\alpha_i^j|. \tag{2.12}$$

Identification of damage extent

Often it is of interest to determine the extent of the structural damage in addition to its location. Due to the nature of the augmentation, the perturbation matrices, $\Delta\mathbf{M}$, $\Delta\mathbf{D}$ and $\Delta\mathbf{K}$, may not be symmetric. For simplicity, in the following it is assumed that the structure under consideration is undamped (and that both $\mathbf{M}$ and $\mathbf{K}$ are symmetric). Nonetheless,

the presence of damping can be included with little change to the proposed methodology. Furthermore, it is assumed the effect of the damage on the mass is negligible. Eq. (2.6) and Eq. (2.7) can be rewritten with these assumptions as

$$\begin{aligned} \left(\lambda_{di}^2\mathbf{M}+\mathbf{K}\right)\mathbf{v}_{di} = \Delta\mathbf{K}\mathbf{v}_{di} &\equiv \mathbf{d}_i, \\ \mathbf{u}_{di}^T\left(\lambda_{di}^2\mathbf{M}+\mathbf{K}\right) = \mathbf{u}_{di}^T\Delta\mathbf{K} &\equiv \mathbf{c}_i^T, \end{aligned} \tag{2.13}$$

where $i = 1, \ldots, p$ as it is assumed that only p damaged eigenvalues and eigenvectors are measured. These equations can be rewritten in matrix form as

$$\begin{aligned} \mathbf{M}\mathbf{V}_d\mathbf{\Lambda}_d + \mathbf{K}\mathbf{V}_d = \Delta\mathbf{K}\mathbf{V}_d &\equiv \mathbf{B}, \\ \mathbf{\Lambda}_d\mathbf{U}_d^T\mathbf{M} + \mathbf{U}_d^T\mathbf{K} = \mathbf{U}_d^T\Delta\mathbf{K} &\equiv \mathbf{A}^T, \end{aligned} \tag{2.14}$$

where

$$\begin{aligned} \mathbf{\Lambda}_d &= \mathrm{diag}(\lambda_{d1}^2, \lambda_{d2}^2, \ldots, \lambda_{dp}^2), \\ \mathbf{V}_d &= [\mathbf{v}_{d1}, \mathbf{v}_{d2}, \ldots, \mathbf{v}_{dp}], \\ \mathbf{B} &= [\mathbf{d}_1, \mathbf{d}_2, \ldots, \mathbf{d}_p], \\ \mathbf{U}_d^T &= [\mathbf{u}_{d1}, \mathbf{u}_{d2}, \ldots, \mathbf{u}_{dp}]^T, \\ \mathbf{A}^T &= [\mathbf{c}_1, \mathbf{c}_2, \ldots, \mathbf{c}_p]^T. \end{aligned}$$

The algorithm for identifying the damage extent is mathematically supported by the following. *Proposition*: Suppose that $\mathbf{V}_d \in \Re^{n\times p}$, $\mathbf{B} \in \Re^{n\times p}$ and $\mathbf{A} \in \Re^{n\times p}$ are given, where $p < n$ and $\mathrm{rank}(\mathbf{V}_d) = \mathrm{rank}(\mathbf{B}) = \mathrm{rank}(\mathbf{A}) = p$. Define $\mathcal{K}$ to be the set of matrices $\Delta\mathbf{K}$ in $\Re^{n\times n}$ that satisfies,

$$\Delta\mathbf{K}\mathbf{V}_d = \mathbf{B}, \tag{2.15}$$

$$\mathbf{U}_d^T\Delta\mathbf{K} = \mathbf{A}^T. \tag{2.16}$$

Then

(a) If the set $\mathcal{K}$ is nonempty, then the minimum rank of any matrix $\Delta\mathbf{K}$ in $\mathcal{K}$ is p. Next, define $\mathcal{K}^{\surd}$ to be a subset of $\mathcal{K}$ comprised of all $\Delta\mathbf{K}$ such that $\mathrm{rank}(\Delta\mathbf{K}) = p$.

(b) One member of $\mathcal{K}^p$ is given by

$$\Delta\mathbf{K}^p = \mathbf{B}\mathbf{H}\mathbf{A}^T \quad \text{with} \quad \mathbf{H} = \left(\mathbf{A}^T\mathbf{V}_d\right)^{-1}. \tag{2.17}$$

(c) The matrix defined by Eq. (2.17) is the unique member of $\mathcal{K}^{\surd}$.

To prove *Proposition* (a), note that Eq. (2.15) and Eq. (2.16) are exactly satisfied if and only if $\mathrm{range}(\mathbf{B})$ and $\mathrm{range}(\mathbf{A})$ are included in $\mathrm{range}(\Delta\mathbf{K})$. This implies that $\mathrm{rank}(\mathbf{B}) = \mathrm{rank}(\mathbf{A}) = p \leq \mathrm{rank}(\Delta\mathbf{K})$. Hence, the minimum rank of $\Delta\mathbf{K}$ is p.

To prove *Proposition* (b), assume that the expanded singular value decomposition of member j of $\mathcal{K}^{\surd}$, $\Delta\mathbf{K}^{p,j}$ to be of the form

$$\begin{aligned} \Delta\mathbf{K}^{p,j} &= \mathbf{U}^j\mathbf{\Sigma}^j{\mathbf{V}^j}^T, \\ &\text{where} \\ \mathbf{U}^j &= \left[\mathbf{u}_1^j, \mathbf{u}_2^j, \ldots, \mathbf{u}_p^j\right], \\ \mathbf{\Sigma}^j &= \mathrm{diag}\left(\sigma_1^j, \sigma_2^j, \ldots, \sigma_p^j\right), \\ {\mathbf{V}^j}^T &= \left[\mathbf{v}_1^j, \mathbf{v}_2^j, \ldots, \mathbf{v}_p^j\right]^T, \end{aligned} \tag{2.18}$$

where the superscript j indicates the jth family member, the vectors $\mathbf{u}_i^j$ are the left singular vectors, the vectors $\mathbf{v}_i^j$ are the right singular vectors, and the values σ_i^j are nonzero singular values of $\Delta\mathbf{K}^{p,j}$. In the expanded singular value decomposition, the singular vectors with indexes from $(p+1)$ to n are not shown in the factorization because they all correspond to zero singular values. For Eq. (2.15) and Eq. (2.16) to be satisfied, the range of $\mathbf{B}$ must

equal the range of $\mathbf{U}^j$ and the range of $\mathbf{A}$ must equal the range of $\mathbf{V}^j$. Therefore, the matrices $\mathbf{B}$ and $\mathbf{U}^j$ can be related by an invertible $p \times p$ matrix $\mathbf{Q}^j$ as follows

$$\mathbf{B} = \mathbf{U}^j \mathbf{Q}^j, \quad \text{where} \quad \mathbf{Q}^j = \mathbf{\Sigma}^j {\mathbf{V}^j}^T \mathbf{V}_d. \tag{2.19}$$

Likewise, the matrices $\mathbf{A}$ and $\mathbf{V}^j$ can be related by an invertible $p \times p$ matrix $\mathbf{P}^j$ as follows

$$\mathbf{A} = \mathbf{V}^j \mathbf{P}^j, \quad \text{where} \quad \mathbf{P}^j = \mathbf{\Sigma}^j {\mathbf{U}^j}^T \mathbf{U}_d. \tag{2.20}$$

Substituting Eq. (2.19) and Eq. (2.20) into Eq. (2.18) yields

$$\Delta\mathbf{K}^{p,j} = \mathbf{B}{\mathbf{Q}^j}^{-1} \mathbf{\Sigma}^j {\mathbf{P}^j}^{-T} \mathbf{A}^T = \mathbf{B}\mathbf{H}^j \mathbf{A}^T. \tag{2.21}$$

Thus, each family member is uniquely defined by the factorization of Eq. (2.21). Also, it is evident that $\mathbf{H}^j$ is of full rank because its inverse exists (and it is given by ${\mathbf{P}^j}^T {\mathbf{\Sigma}^j}^{-1} \mathbf{Q}^j$).

Inspection of Eq. (2.21) reveals that the only unknown term in the factorization is $\mathbf{H}^j$. Eq. (2.15) can be rewritten using the factorization of $\Delta\mathbf{K}^{p,j}$ defined by Eq. (2.21), as

$$\mathbf{B} = \Delta\mathbf{K}^{p,j}\mathbf{V}_d = \left(\mathbf{B}\mathbf{H}^j\mathbf{A}^T\right)\mathbf{V}_d = \mathbf{B}\left(\mathbf{H}^j\mathbf{A}^T\mathbf{V}_d\right). \tag{2.22}$$

the equation above is satisfied if and only if $\mathbf{H}^j\mathbf{A}^T\mathbf{V}_d = \mathbf{I}$, where $\mathbf{I}$ is the $p \times p$ identity matrix. This holds because $\mathbf{B}$ is of full column rank. Thus, $\mathbf{H}^j$ is uniquely calculated to be

$$\mathbf{H}^j = \left(\mathbf{A}^T\mathbf{V}_d\right)^{-1}. \tag{2.23}$$

Hence, Eq. (2.17) holds as shown by Eq. (2.21) and Eq. (2.23).

The proof of *Proposition* (c) follows immediately by inspecting the right hand side of Eq. (2.23). Inspection reveals that $\mathbf{H}^j$ is the same for all members of $\mathcal{K}\surd$. This fact, in conjunction with Eq. (2.21) leads to the conclusion that $\Delta\mathbf{K}^{p,j}$ is the unique member of the set $\mathcal{K}\surd$. This (unique) member is given by Eq. (2.17).

The conclusions of the proposition above may be used to determine $\Delta\mathbf{K}$, and thus identify the damage location and extent. Nonetheless, to identify the damage *location*, only right eigenvectors are needed in GMRPT. However, to identify the damage *extent* using GMRPT, p of the n left eigenvectors of the system are needed as well. One way of obtaining the left eigenvectors from the right eigenvectors is to use the mass orthogonality property of the eigenvectors given by

$$\mathbf{U}_d^T\mathbf{M}\mathbf{V}_d = \mathbf{I}, \quad \text{so that} \quad \mathbf{U}_d^T = \mathbf{V}_d^{-1}\mathbf{M}^{-1}. \tag{2.24}$$

An approach based on Eq. (2.24) requires the knowledge of all n right eigenvectors of the system to be known in order to solve for the left ones. In many vibratory problems in structural dynamics and/or fluid-structure interactions, the system of interest is modeled accurately by a system of equations of motion which is large dimensional (i.e. n is very large). Recent techniques for reducing the complexity of these models employs reduced order modeling [64–72] based on approaches such as component mode synthesis and proper orthogonal decomposition. These techniques are applicable to both linear and nonlinear systems and usually provide a transformation from the high-dimensional space of displacements $\mathbf{w}$ (of size n) to a reduced order space $\mathbf{q}$ (of size $r << n$) as $\mathbf{w} = \mathbf{P}\mathbf{q}$, where $\mathbf{P}$ is a $n \times r$ matrix. Next, the equations of motion are expressed in the reduced order space. For example, Eq. (2.3) successively becomes

$$\begin{aligned} \mathbf{M}\mathbf{P}\ddot{\mathbf{q}} + \mathbf{D}\mathbf{P}\dot{\mathbf{q}} + \mathbf{K}\mathbf{P}\mathbf{q} &= \mathbf{0}, \\ \mathbf{P}^T\mathbf{M}\mathbf{P}\ddot{\mathbf{q}} + \mathbf{P}^T\mathbf{D}\mathbf{P}\dot{\mathbf{q}} + \mathbf{P}^T\mathbf{K}\mathbf{P}\mathbf{q} &= \mathbf{0}, \\ \bar{\mathbf{M}}\ddot{\mathbf{q}} + \bar{\mathbf{D}}\dot{\mathbf{q}} + \bar{\mathbf{K}}\mathbf{q} &= \mathbf{0}. \end{aligned} \tag{2.25}$$

The reduced order equation of motion in Eq. (2.25) has a low order r. Hence, its r right eigenvectors may be measured much more easily than the n right eigenvectors of the orig-

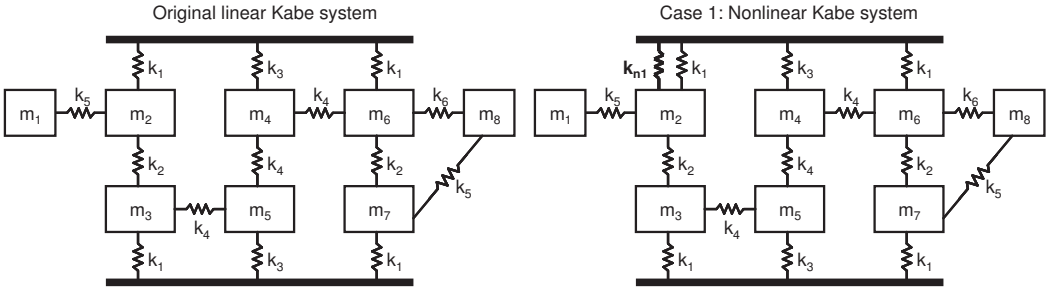

(a) (b)

Figure 2.1: Kabe's problem [1] (a) and with addition of a nonlinear spring between mass two and ground (b)

inal problem. Once the r reduced order right eigenvectors are obtained, the r left eigenvectors $\mathbf{e}_i$ (for $i = 1, \ldots, r$) of the reduced order model may be computed using a relation similar to Eq. (2.24) by using the reduced order mass matrix $\bar{\mathbf{M}}$. Next, the r most dominant full size left eigenvectors are obtained as $\mathbf{u}_{di} = \mathbf{P}\mathbf{e}_i$, for $i = 1, \ldots, r$.

2.3 Examples of Implementation of the Proposed Approach

To demonstrate its characteristics, this methodology was applied to an eight degree of freedom mass-spring system (Kabe system [1, 27–29]), shown in Fig. 2.1(a). The parameter values are $m_1 = 0.001$, $m_8 = 0.002$, $m_j = 1$ for $j = 2, \ldots 7$, $k_1 = 1000$, $k_2 = 10$, $k_3 = 900$, $k_4 = 100$, $k_5 = 1.5$, and $k_6 = 2$. First, the linear system was modeled, and then numerical tests were run using harmonic forcing at each of the masses to validate the GMRPT by comparison with previously published results [1]. Next, three nonlinear mass spring systems based on the Kabe system were created. The methodology was applied to each of the nonlinear systems, and numerical tests were conducted.

Kabe's problem shown in Fig. 2.1(a) is generalized into a nonlinear mass spring system in three cases. In each of the cases, the nonlinear springs are of the form $k_{ni}\Delta x^3$, where

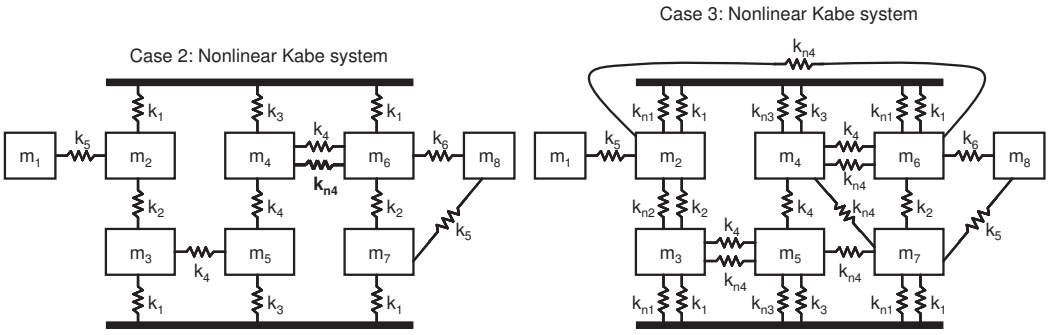

Figure 2.2: Kabe's problem [1] with addition of a nonlinear spring between mass four and mass six (a) and twelve nonlinear springs connecting masses to each other and ground (b)

k_{ni} is the nonlinear spring stiffness, and Δx represents the distance the nonlinear spring is stretched. The first case consists of one nonlinear spring being added between mass two and ground as shown in Fig. 2.1(b) ($k_{n1} = k_1 = 1000$). The second case consists of one nonlinear spring being added between masses four and six as shown in Fig. 2.2(a) ($k_{n4} = k_4 = 100$). The third and last case consists of 12 nonlinear springs added between the masses and ground, as is illustrated in Fig. 2.2(b). The parameter values are $k_{n1} = 1000$, $k_{n2} = 10$, $k_{n3} = 900$, and $k_{n4} = 100$.

2.3.1 Case 1: Methodology

This case consists of one nonlinear spring attached from mass two to ground as shown on the right side of Fig. 2.1(a). The nonlinear system is the same as the linear system with the exception of the added term in the second degree of freedom and the augmented equation.

The added term in the second degree of freedom of the linear equation is $k_{2ng}y$, where k_{2ng} is the nonlinear spring stiffness that connects mass two to ground and $y = x_2^3$ (with x_2 being the displacement of mass two from its equilibrium). The augmented equation may

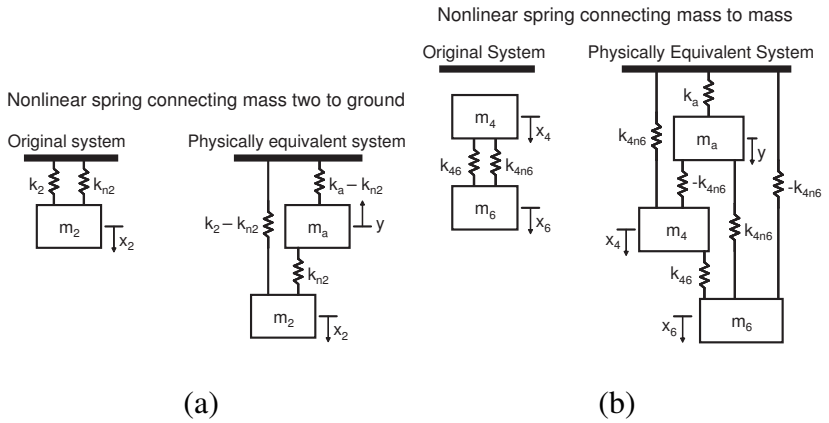

Figure 2.3: Physical equivalence of the augmentation for a nonlinear spring connecting (a) a mass to ground and (b) a mass to another mass

be expressed as

$$\ddot{y} + k_{2ng}x_2 + 2k_{2ng}y = h(t). \tag{2.26}$$

A physical representation of the above system equation is demonstrated in Fig. 2.3(a) which illustrates how the use of an additional mass moving in a specified manner (i.e. $y = x_2^3$) in conjunction with linear springs can be used to account for the nonlinear spring. The additional mass results in an additional degree of freedom, which corresponds to the augmented equation for $h(t)$ given above.

2.3.2 Case 2: Methodology

This case consists of a nonlinear spring attached between masses four and six, which results in a slightly more complicated model then the first (above) as shown in Fig. 2.2(a). The nonlinear system is again similar to the linear system with the exception of the added term to the fourth and sixth degrees of freedom and the augmented equation.

The term $k_{4n6}y$ is added to the fourth degree of freedom equation, and it is subtracted from the sixth degree of freedom equation. The nonlinear spring stiffness is denoted by

k_{4n6}, while the stretching of the nonlinear spring is $y = (x_4 - x_6)^3$. The augmented equation may be expressed as

$$\ddot{y} + k_{4n6}x_4 - k_{4n6}x_6 + 2k_{4n6}y = h(t). \tag{2.27}$$

The physical realization of the above system is demonstrated in Fig. 2.3(b). As in the case where the mass is connected with a nonlinear spring to the ground, the system can be physically represented by adding a mass and several springs to the system.

2.3.3 Case 3: Methodology

This case consists of twelve nonlinear springs being added to the linear mass spring system as shown in Fig. 2.2(b). Each degree of freedom is modified in the same manner as done in the previous two sections. The following augmented equations are obtained

$$\begin{array}{lcllcl}
\ddot{y_1} + k_{2ng}x_2 + 2k_{2ng}y_1, & = & h_1(t) & & y_1 & = & x_2^3, \\
\ddot{y_2} + k_{4n6}x_4 - k_{4n6}x_6 + 2k_{4n6}y_2, & = & h_2(t) & & y_2 & = & (x_4 - x_6)^3, \\
\ddot{y_3} + k_{5n7}x_5 - k_{5n7}x_7 + 2k_{5n7}y_3, & = & h_3(t) & & y_3 & = & (x_5 - x_7)^3, \\
\ddot{y_4} + k_{3ng}x_3 + 2k_{3ng}y_4, & = & h_4(t) & & y_4 & = & x_3^3, \\
\ddot{y_5} + k_{2n3}x_2 - k_{2n3}x_3 + 2k_{2n3}y_5, & = & h_5(t) & & y_5 & = & (x_2 - x_3)^3, \\
\ddot{y_6} + k_{6ng}x_6 + 2k_{6ng}y_6, & = & h_6(t) & \text{where} \quad y_6 & = & x_6^3, \\
\ddot{y_7} + k_{4n7}x_4 - k_{4n7}x_7 + 2k_{4n7}y_7, & = & h_7(t) & & y_7 & = & (x_4 - x_7)^3, \\
\ddot{y_8} + k_{5ng}x_5 + 2k_{5ng}y_8, & = & h_8(t) & & y_8 & = & x_5^3, \\
\ddot{y_9} + k_{4ng}x_4 + 2k_{4ng}y_9, & = & h_9(t) & & y_9 & = & x_4^3, \\
\ddot{y_{10}} + k_{7ng}x_7 + 2k_{7ng}y_{10}, & = & h_{10}(t) & & y_{10} & = & x_7^3, \\
\ddot{y_{11}} + k_{3n5}x_3 - k_{3n5}x_5 + 2k_{3n5}y_{11}, & = & h_{11}(t) & & y_{11} & = & (x_3 - x_5)^3, \\
\ddot{y_{12}} + k_{2n6}x_2 - k_{2n6}x_6 + 2k_{2n6}y_{12}, & = & h_{12}(t) & & y_{12} & = & (x_2 - x_6)^3.
\end{array} \tag{2.28}$$

The stiffnesses of the nonlinear springs are denoted by an n in the subscript (i.e. k_{inj}).

2.4 Numerical Results

To implement the methodology presented, a numerical simulation of the Kabe system was performed. The matrices $\mathbf{M}$, $\mathbf{K}$, $\mathbf{N}$, $\mathbf{N}_C$ and $\mathbf{N}_S$ were obtained for the selected system, and each mass was forced harmonically. The vector of displacements $\mathbf{x}(t)$ was calculated by standard time integration, while $\mathbf{y}(t)$ and $\mathbf{h}(t)$ were calculated based on their relation to $\mathbf{x}(t)$. DSPI was employed for the augmented system to determine the eigenvalues and eigenvectors of the augmented matrices by using the time series for $\mathbf{x}(t)$, $\mathbf{g}(t)$, $\mathbf{y}(t)$ and $\mathbf{h}(t)$. Next, GMRPT was used to determine the damage location and extent by using the modal data provided by DSPI. Reduced order modeling was not needed for this system since it only has eight linear degrees of freedom. Various damage scenarios were investigated using this approach for the three cases considered.

2.4.1 Case 1: Numerical Results

In this section, two key characteristics of the nonlinear damage detection approach are discussed for a system with a nonlinear spring connected to the ground. First, the effect of the augmentation is discussed. Next, the relationship between MRPT and GMRPT is explored.

The effect of the nonlinearity on the healthy system can be seen in Fig. 2.4. The plot shows the damage location obtained using Eq. (2.9) for four different approaches. The first approach (augmented without DSPI) uses an augmented system and a calculation where the *exact* eigenvalues and eigenvectors are used. This accurately predicts that no damage is present in any of the degrees of freedom. The second approach (augmented with DSPI) uses an augmented system and a calculation where DSPI is used to obtain eigenvalues and eigenvectors. These results show a very good estimate, with nearly zero damage predicted by GMRPT (as expected for a healthy system). In contrast, the next

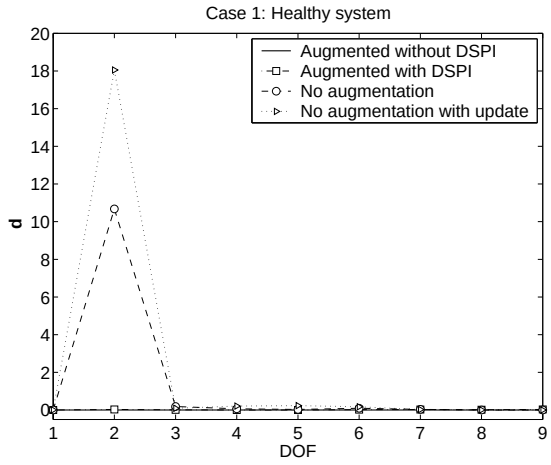

Figure 2.4: Results of the damage location algorithm applied to a healthy un-augmented nonlinear system and a healthy augmented nonlinear system for Case 1

approach (no augmentation) uses DSPI to obtain the eigenvalues and eigenvectors also, but the system is modeled as the original linear system even though there is a nonlinear spring connecting mass two to ground. The results show that damage is erroneously predicted by the linear MRPT in the second degree of freedom, the location of the nonlinear spring.

The erroneous predictions of the linear MRPT are not alleviated by matrix updating. To show that, the stiffness matrix was updated with the damage predicted using MRPT and the forcing $\mathbf{g}(t)$ was slightly altered to simulate a change in forcing with time. The results are shown in Fig. 2.4 where the last approach (no augmentation with update) used DSPI with the updated linear model. This approach shows that the linear model is inaccurate when used to model a nonlinear system, despite matrix updating because damage is still erroneously predicted at the degree of freedom that contains the nonlinearity.

MRPT is a subset of GMRPT, and detects damage in systems with symmetric damage. Hence, when the damage to a system is solely in its linear components, then both GMRPT and MRPT are accurate since the linear damage results in symmetric damage matrices,

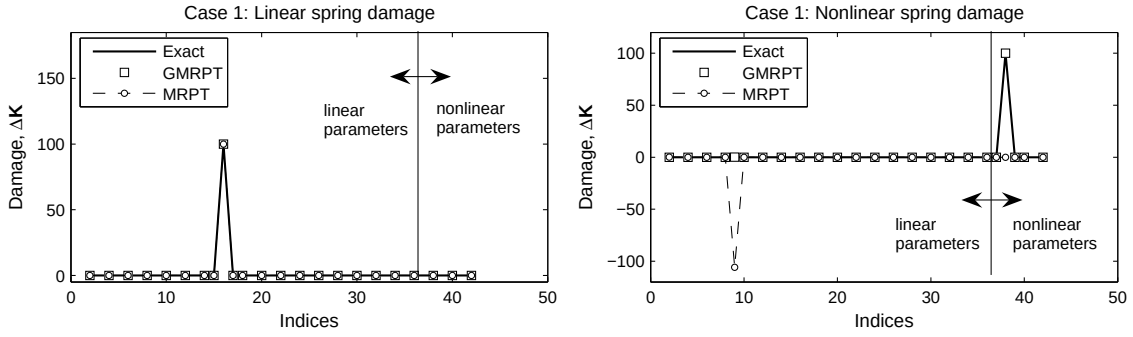

(a) (b)

Figure 2.5: A comparison of results obtained for Case 1 using GMRPT and MRPT for damage in a linear spring (a) and a nonlinear spring (b)

which result in $\mathbf{v}_{di} = \mathbf{u}_{di}$. Fig. 2.5 presents element by element the values of the stiffness perturbation matrices ($\Delta\mathbf{K}$) obtained using MRPT and separately GMRPT (and using exact eigenvalues and eigenvectors of the augmented system). The x-axes in each plot represent the index of a column vector obtained from storing the upper triangular portion of the perturbation stiffness matrix ($\Delta\mathbf{K}$) into a column vector. The linear and nonlinear parameteres of the matrix are demarcated by a line in the figure. The y-axes in the plots represent the entries of the difference between the original and updated stiffness matrices, $\Delta\mathbf{K}$. The plot in Fig. 2.5(a) is the scenario where the linear spring connecting mass three to ground is reduced from a healthy value of 1000 to 900. Since the damage is linear, both MRPT and GMRPT predict accurately the exact damage of 100. The plot in Fig. 2.5(b) is the scenario where the nonlinear spring is reduced from a healthy value of 1000 to 900. GMRPT is able to predict accurately the exact damage of 100, while MRPT incorrectly predicts damage in the linear spring that connects mass two to ground.

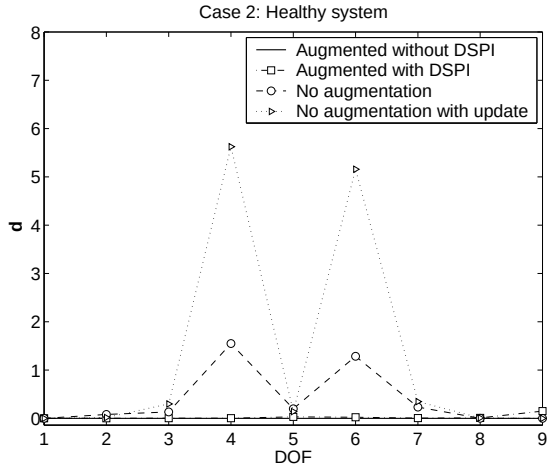

Figure 2.6: Results of the damage location algorithm applied to a healthy un-augmented nonlinear system and a healthy augmented nonlinear system for Case 2

2.4.2 Case 2: Numerical Results

This section explores the same characteristics of the nonlinear damage detection approach as in case 1, except that the nonlinear spring connects two masses here instead of a mass and ground.

The effect of the nonlinearity on the healthy system can be discerned when comparing the approaches presented in Fig. 2.6. The plot shows the damage location obtained using Eq. (2.9) for four different approaches. These four approaches are the same as the ones in Fig. 2.4. The results in Fig. 2.6 show that damage is erroneously predicted by MRPT in both degrees of freedom that the nonlinear spring affects for the approach with no augmentation. Also, the damage continues to be erroneously predicted by MRPT despite updating the stiffness matrix. In contrast, for the approach with the augmentation and exact eigenvalues and eigenvectors, zero damage is again accurately predicted by the proposed technique. Finally, the approach with the augmentation coupled with DSPI predicts low damage. This damage is negligible and due to small inaccuracies in solving the eigenvalue

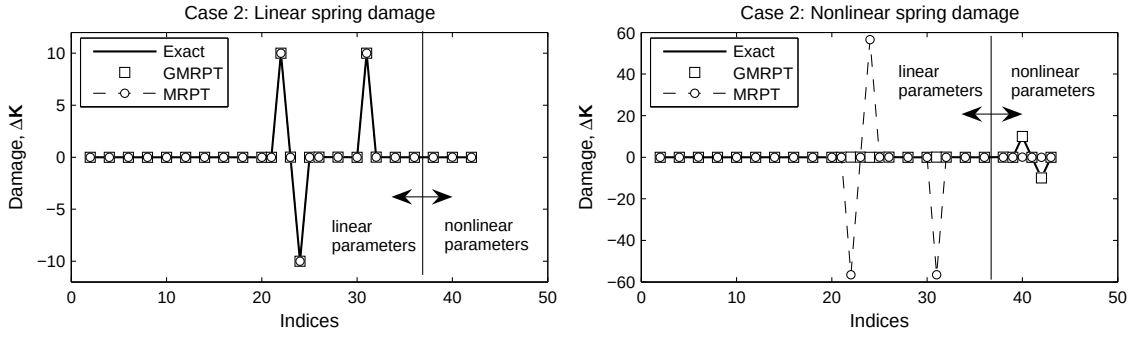

(a) (b)

Figure 2.7: A comparison of results obtained for Case 2 using GMRPT and MRPT for damage in a linear spring (a) and a nonlinear spring (b)

problem by DSPI.

Fig. 2.7 shows results which further explore the relationship between MRPT and GMRPT. An element by element plot of the stiffness perturbation matrices ($\Delta\mathbf{K}$) obtained using MRPT and separately GMRPT are shown. The plot in Fig. 2.7(a) is the scenario where the linear spring connecting mass four to mass six is reduced from a healthy value of 100 to 90. Since the damage is linear, both MRPT and GMRPT predict accurately the exact damage of 10. The plot in Fig. 2.7(b) is the scenario where the nonlinear spring is reduced from a healthy value of 100 to 90. GMRPT is able to predict accurately the exact damage of 10, while MRPT incorrectly predicts damage in the linear spring that connects mass four and mass six.

2.4.3 Case 3: Numerical Results

In this section, the characteristics of the proposed approach are demonstrated, and a discussion of the influence of noise is presented.

The effects of the nonlinearity on the healthy system can be discerned by comparing the cases presented in Fig. 2.8. The plot shows the damage location obtained by using

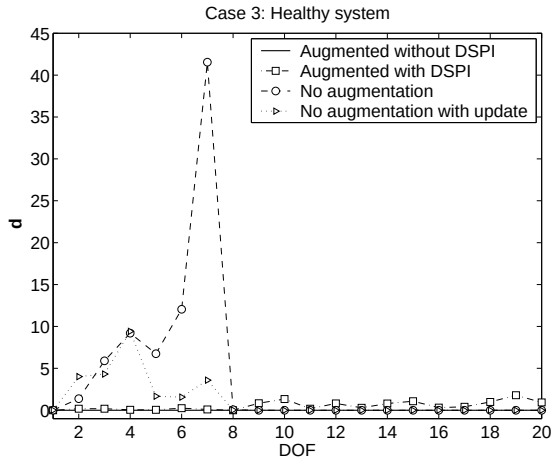

Figure 2.8: Results of the damage location algorithm applied to a healthy un-augmented nonlinear system and a healthy augmented nonlinear system for Case 3

Eq. (2.9) for four different approaches. These four approaches are the same as the ones in Fig. 2.4 and Fig. 2.6. The results in Fig. 2.8 show that damage is erroneously predicted by MRPT in all the linear degrees of freedom, except for one and eight (which are the two masses that do not have nonlinear springs attached to them). After updating, the erroneous damage does happen to be reduced, but there is still a significant extent of damage being inaccurately predicted by MRPT. For the approach where the augmentation is used with exact eigenvalues and eigenvectors, zero damage is accurately predicted by GMRPT. Finally, the approach with the augmentation coupled with DSPI predicts low damage, mainly in the augmented degrees of freedom, due to small inaccuracies in solving the eigenvalue problem by DSPI.

Next, one may further explore the relationship between MRPT and GMRPT. Fig. 2.9 presents an element by element plot of the stiffness perturbation matrices obtained using MRPT and separately GMRPT. In this calculation, 1% random eigenvector noise and 0.1% random eigenvalue noise was added. The average damage values were calculated for each

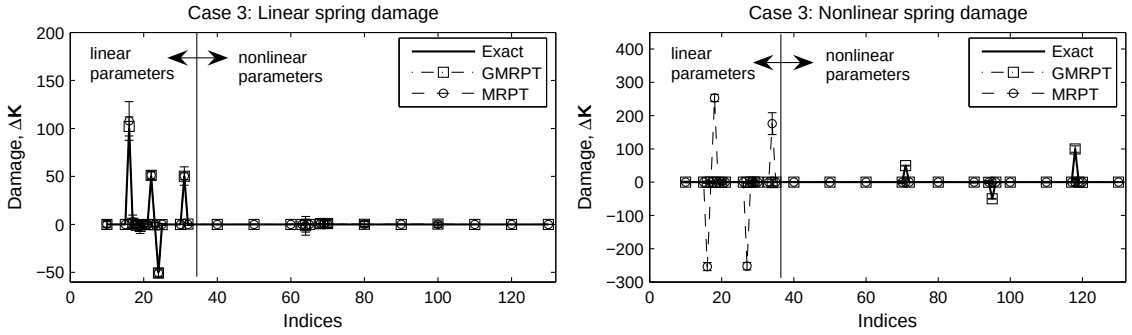

(a) (b)

Figure 2.9: A comparison of results obtained for Case 3 using GMRPT and MRPT for simultaneous damage in several linear springs (a) and several nonlinear springs (b) with 1% random eigenvector noise and 0.1% random eigenvalue noise

index, and standard deviation error bars are plotted for 100 separate calculations. The plot in Fig. 2.9(a) is the scenario where the linear spring connecting mass four to mass six is reduced from a healthy value of 100 to 50, and the linear spring connecting mass three to ground is reduced from 1000 to 900. Since the damage is linear, both MRPT and GMRPT predict similar values with average values within 7% and 3%, respectively, of the exact damages. The plot in Fig. 2.9(b) is the scenario where the nonlinear spring connecting mass three to five is reduced from a healthy value of 100 to 50, and the nonlinear spring connecting mass seven to ground is reduced from a healthy value of 1000 to 900. GMRPT is able to predict the damage within 1% of the exact damages, while MRPT incorrectly predicts that damage is present in the linear springs that connect mass three to mass five, and mass seven to ground.

To examine further the sensitivity of the proposed method to measurement noise, three scenarios are explored: (*i*) a scenario with no random noise, (*ii*) a scenario where noise is present in the measured eigenvectors and eigenvalues, and (*iii*) a scenario where noise is present in the measurements of $\mathbf{x}(t)$ (which is used by DSPI). An examination of the

matrix $\Delta\mathbf{K}$ for a healthy system is shown in Fig. 2.10. Surely, the exact value of $\Delta\mathbf{K}$ is precisely zero since there is no damage. The plot in Fig. 2.10(a) shows that the proposed method predicts the exact damage for the scenario of no noise. The other two plots represent scenarios with random measurement noise. The average damage values were calculated for each index, and standard deviation error bars are plotted for 100 separate calculations. The plot in Fig. 2.10(b) shows damage predicted for 1% random eigenvector noise and 0.1% random eigenvalue noise. The average value for all indexes is close to zero as it should be for a healthy system. The plot in Fig. 2.10(c) presents the results for a scenario where ± 0.0001 random noise was added to $\mathbf{x}(t)$, which was used by DSPI. The average values of the damages obtained in this case are larger than in the previous case, but they have much smaller standard deviations.

Fig. 2.11 shows a scenario where a 10% damage is applied to a linear and a nonlinear spring. The linear spring connecting mass three to ground is reduced from 1000 to 900, and the nonlinear spring connecting mass four to ground is reduced from 900 to 810. The three plots are similar to Fig. 2.10, but here damage is present in the system. The plot in Fig. 2.11(a) shows the exact damage being accurately predicted by GMRPT for the noise-free scenario. The plot in Fig. 2.11(b) shows that the proposed approach can predict the damage extent within approximately 10% for the scenario with 1% eigenvector noise. Similarly, the plot in Fig. 2.11(c) shows that the proposed approach can predict the damage extent within approximately 15% for the scenario with ± 0.0001 measurement noise.

Fig. 2.12 shows a scenario where a 50% damage is applied to a linear and a nonlinear spring. The linear spring connecting mass three to ground is reduced from 1000 to 500, and the nonlinear spring connecting mass four to ground is reduced from 900 to 450. The three plots show results similar to Fig. 2.10 and Fig. 2.11, but here the damage applied is larger. The plot in Fig. 2.12(a) shows the exact damage being predicted accurately by GMRPT

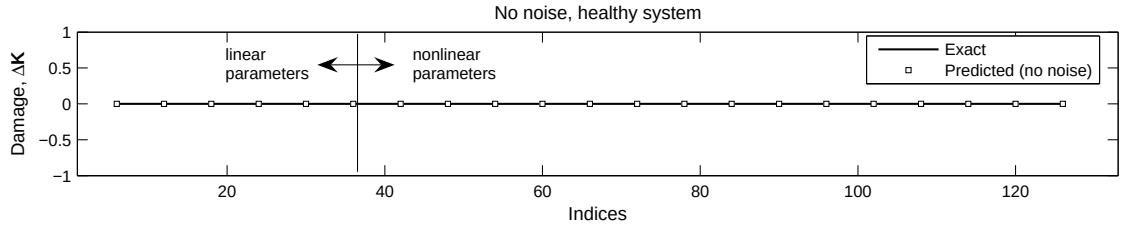

(a)

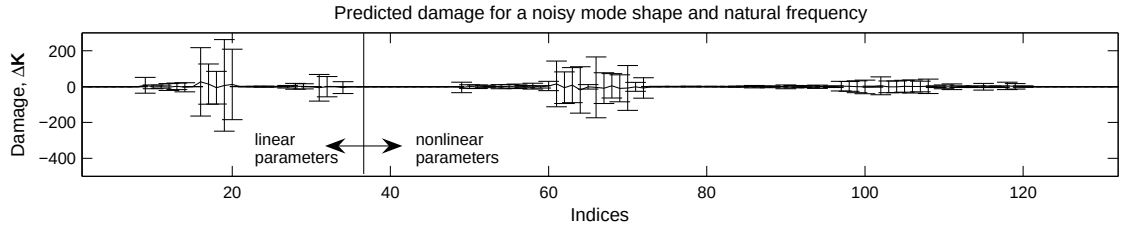

(b)

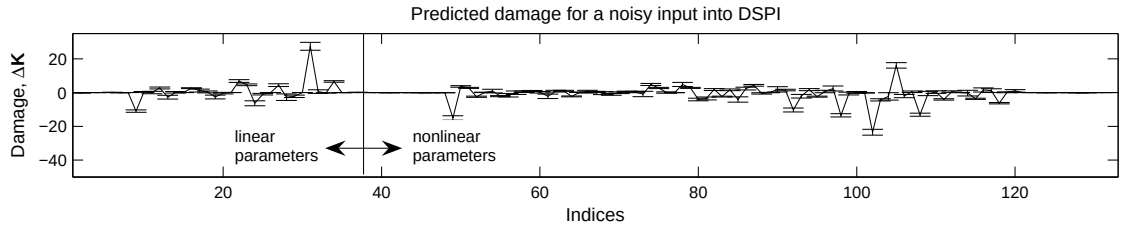

(c)

Figure 2.10: Predicted damage in healthy system for a case of no noise (a), 1% random eigenvector noise and 0.1% random eigenvalue noise (b), and ± 0.0001 random noise input into DSPI (c)

for the noise-free scenario. The plot in Fig. 2.12(b), with a level of 5% eigenvector noise, the average predicted value of the damage is within 1% of the actual damage. Finally, the plot in Fig. 2.12(c) shows that, in the scenario where ± 0.002 random noise is present in the measurements, damage can be predicted within approximately 8% by the proposed technique.

The accuracy of GMRPT agrees well with results presented in the literature for MRPT [1]. In those studies, a much larger relative damage was applied (e.g. k_{78} was reduced by over 93%, from 1.5 to 0.1) and, as a result, MRPT was shown to be able to predict

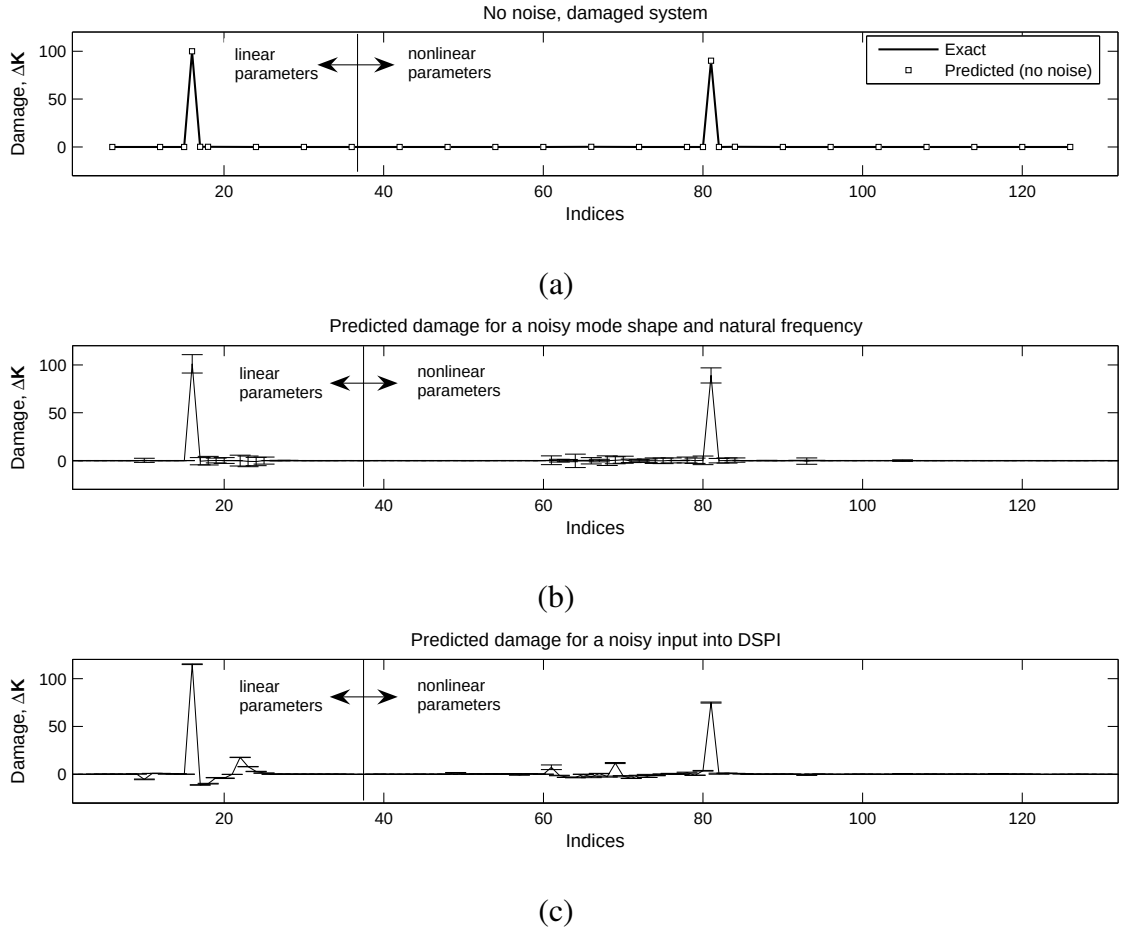

Figure 2.11: Predicted damage in a system with 10% damage in a linear and a nonlinear spring for a case of no noise (a), 1% random eigenvector noise and 0.1% random eigenvalue noise (b), and ± 0.0001 random noise input into DSPI (c)

damage in the linear Kabe's problem with 5% eigenvector noise. The examples discussed here show that much smaller relative damages (of only 10% compared to 93.3%) can be detected if there is a lower eigenvector noise (of 1%).

2.5 Conclusions

A method to model nonlinear systems employing augmentation was presented, and a damage detection method was proposed. The proposed approach requires a discrete (e.g. finite element) model for the system. The nature of the augmentation requires the use

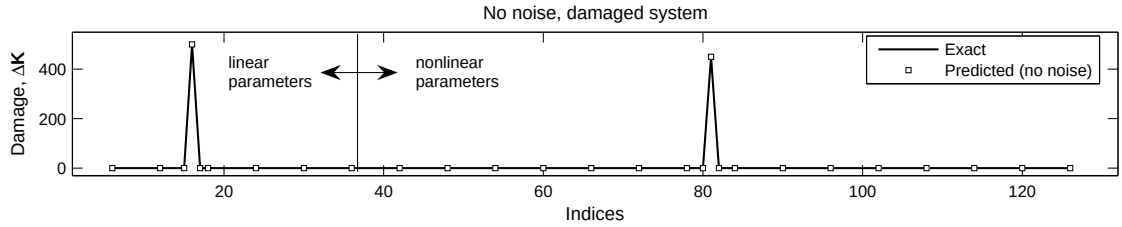

(a)

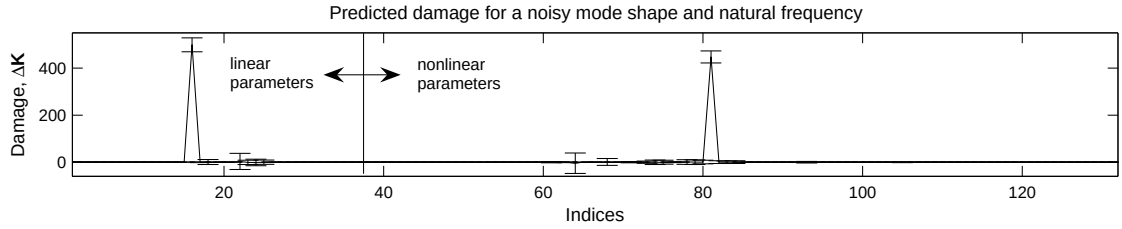

(b)

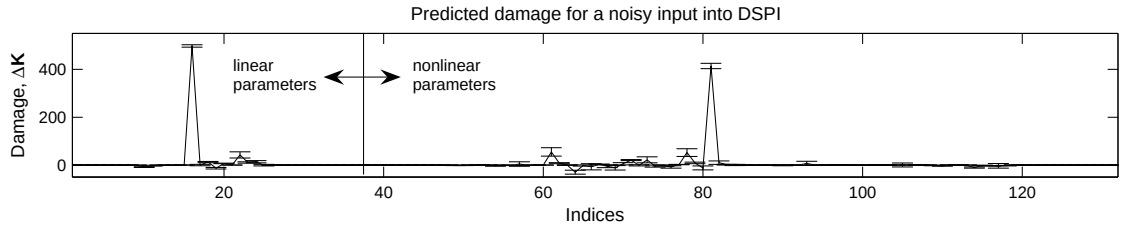

(c)

Figure 2.12: Predicted damage in a system with 50% damage in a linear and a nonlinear spring for a case of no noise (a), 5% random eigenvector noise and 1% random eigenvalue noise (b), and ± 0.002 random noise input into DSPI (c)

of a modal analysis technique that has known but not prescribed forcing, such as DSPI. Once the eigenvalue problem was solved, the proposed approach was shown to predict accurately both the location as well as the extent of damage. A generalized minimal rank perturbation theory was presented. This method is able to address the issue of asymmetric damage caused by nonlinearities (and the augmentation).

The algorithms proposed have been demonstrated numerically for several different nonlinear mass-spring systems. The effectiveness of the proposed method was demonstrated, and the effects of measurement errors were presented.

CHAPTER III

Multiple Augmentations of Nonlinear Systems and Generalized Minimum Rank Perturbations for Damage Detection

3.1 Introduction

Due to the increasing need for air and space technologies that are capable of operating in extreme environments for extended periods of time, there is a need for online damage detection and structural health monitoring techniques. Although there has been a great deal of research focused on structural health monitoring, most of the current methods ignore the effects of nonlinearities on the system dynamics, and use purely linear approaches. This is motivated in part by the fact that linear methods are more developed than nonlinear ones. Nonlinearities, however, are important in many structures and fluid-structural systems. Hence, methodologies that account for the effects of nonlinearities are needed.

Typically, damage detection methodologies use information about both the healthy and damaged systems. This information is in various forms, including a discrete or continuous model of the system, or modal properties of the (linearized) system. Most current methodologies then extract system features such as natural frequencies or mode shapes (for the linearized system) from measurements to detect damages. These (linear) features are obtained by using well established linear modal analysis techniques in either the time

or frequency domain. These techniques are usually based on single input single output or multiple input multiple output approaches. A review of time-based multiple input multiple output approaches and their main characteristics was presented by Yang et al. [2]. Such current available techniques include free and impulse response methods such as the poly-reference complex exponential [3], eigensystem realization algorithms [4] and Ibrahim time domain methods [5]. Also, forced response methods are available, such as auto-regressive moving average vector [6] and direct system parameter identification [7], which use the forcing from natural excitations to determine modal properties. The use of natural excitations makes these latter methods well-suited for online damage detection. Complementary to these linear methods, *nonlinear* experimental analyses are now under development. For example, nonlinear normal modes can be obtained by the harmonic balance method, invariant manifolds technique, method of multiple time scales, and asymptotic methods [16].

In a model based approach, model parameters are identified first, and then used for structural health monitoring. Ibrahim [19] and Heylen [20] provide a review of the four general categories of linear nondestructive evaluation. The first category is sensitivity methods, which use the modal sensitivity to parameter changes to identify damage. In this area, recently Leung [21] proposed a more accurate solution technique for inverse sensitivity equations for asymmetric systems. The second is eigenstructure assignment techniques, which place eigenvalues and/or eigenvectors of the closed loop system. A good review of different eigenstructure assignment techniques can be found in the work by Andry et al. [22]. Lim [23] developed a constrained eigenstructure assignment for damage detection that formed a direct relation between the feedback control and structural parameter changes, while Jiang et al. [24] developed optimal controllers for sensitivity enhancement by eigenstructure assignment. The third category includes optimal matrix

update methods [25, 26], which can be used for both system identification and damage detection. These methods update the system model using a set of constraints (e.g. maintaining the sparsity pattern of the original finite element model) for a given cost function (e.g. the minimum Frobenius norm for the update). The fourth and last category includes minimum rank perturbation methods [1, 27–30], which solve for damage as the minimum rank solution to perturbation equations for the system. The key idea of minimum rank perturbation approaches is to exploit the fact that, for most physical models, there is a direct and simple relation between properties at one location in the system and the location of the corresponding entries of the matrices of the discrete system model. Hence, a localized damage corresponds to a localized change in system matrices. Thus, the change/perturbation of the system matrices is sparse and has low rank.

In this work, an algorithm that uses a system augmentation and a Generalized Minimum Rank Perturbation Theory (GMRPT) [73, 74] for nonlinear systems is developed and demonstrated to handle multiple simultaneous damages in linear and nonlinear parameters. The augmentation was shown to work for systems with cubic spring nonlinearities, and can be extended to any system where the functional form of the nonlinearity is known as a function of the state vector of the system and its derivatives. Control theory also uses a type of augmentation in the area of linear [75] and nonlinear [76, 77] observers. However, the primary purpose of these observers is for state estimation coupled with state feedback to control the system. This differs significantly from the augmentation in this chapter. The augmentation herein is used to generate an augmented (fictitious) linear system that follows a *single* trajectory of the real nonlinear system. This augmentation is not used to control the system, rather it is defined such that the augmented linear system follows (in a given subspace) a given trajectory of the nonlinear system while allowing for the use of linear theories for system identification and damage detection.

The augmentation requires that the forcing of the system be known but not prescribed. Hence, a technique such as direct system parameter identification [7] can be employed to perform the modal analysis (for the augmented system) to determine the modal properties of the augmented system since it uses as forcing the external excitations of the system. The augmented modal properties are then used by GMRPT [73], to determine damage location and extent. GMRPT was developed to handle the asymmetric damage scenarios that result from damage in the nonlinear portion of the system which, in turn, are due to the specialized nature of the augmentation.

A theoretical framework for the detection of simultaneous damages is developed herein, and several additions to the damage detection method proposed previously [73,74] are presented. A subspace selection algorithm is used to reduce the effects of measurement noise. Also, an iterative approach to the solution of the left eigenvectors for simultaneous damage detection is employed. Moreover, an alternate approach is presented for the cases where an incomplete set of right eigenvectors are known. This new approach is based on multiple augmentations of the same nonlinear system. Finally, eigenvector filtering algorithms are discussed to reduce the effects of random measurement noise on damage detection. These techniques are demonstrated on nonlinear mass-spring systems and nonlinear frame structures. Complex simultaneous damage scenarios are explored and the effectiveness of the methodology for nonlinearities such as cubic springs and Colomb friction are presented. Also, the influence of measurement noise with and without filtering algorithms is demonstrated through numerical simulations.

3.2 General Methodology

In this section, the methodology for determining damage in nonlinear systems using system augmentation and generalized minimum rank perturbation theory (GMRPT) [73]

is presented. First, the augmentation procedure is described. Then, the procedure for detecting damage location and extent by GMRPT is extended for the case of simultaneous damages in the mass, damping and stiffness parameters. Additionally, the damage detection methodology is extended by using multiple augmentations to determine damages in the nonlinear parameters in order to handle the cases where only an incomplete set of right eigenvectors are known. Finally, eigenvector filtering algorithms, which reduce the effects of noise, are detailed.

The work in this chapter builds on three key papers which introduce and discuss MRPT [1,30] and GMRPT and system augmentation [73]. Although the following presentation of the methodology is self contained, these three papers [1,30,73] provide additional detailed background on many of the approaches explicated herein.

3.2.1 System Augmentation for Modeling Nonlinear Systems

In this subsection, a method to model a single trajectory of a nonlinear system as a projection of the trajectory of an augmented linear system (of higher dimension) is presented. Consider a nonlinear system (characterized by a coordinate vector $\mathbf{x}$ and forced by an external excitation $\mathbf{g}(t)$) expressed as

$$\begin{bmatrix} \mathbf{M}_O & \mathbf{0} \\ \mathbf{0} & \mathbf{I} \end{bmatrix} \begin{bmatrix} \ddot{\mathbf{x}} \\ \dot{\mathbf{x}} \end{bmatrix} + \begin{bmatrix} \mathbf{D}_O & \mathbf{K}_O \\ -\mathbf{I} & \mathbf{0} \end{bmatrix} \begin{bmatrix} \dot{\mathbf{x}} \\ \mathbf{x} \end{bmatrix} + \begin{bmatrix} \mathbf{f}(\mathbf{x}, \dot{\mathbf{x}}, \ddot{\mathbf{x}}) \\ \mathbf{0} \end{bmatrix} = \begin{bmatrix} \mathbf{g}(t) \\ \mathbf{0} \end{bmatrix}, \quad (3.1)$$

where $\mathbf{M}_O$, $\mathbf{D}_O$, and $\mathbf{K}_O$ are the mass, damping and stiffness matrices of the linearized system, and $\mathbf{f}$ is a nonlinear function. For a large category of nonlinearities, Eq. (3.1) can be rewritten as [73]

$$\mathbf{M}_O\ddot{\mathbf{x}} + \mathbf{D}_O\dot{\mathbf{x}} + \mathbf{K}_O\mathbf{x} + \mathbf{N}_I\ddot{\mathbf{y}} + \mathbf{N}_D\dot{\mathbf{y}} + \mathbf{N}_S\mathbf{y} = \mathbf{g}(t),$$

which in first order matrix form becomes

$$\begin{bmatrix} \mathbf{M}_O & \mathbf{0} & \mathbf{N}_I & \mathbf{0} \\ \mathbf{0} & \mathbf{I} & \mathbf{0} & \mathbf{0} \\ \mathbf{0} & \mathbf{0} & \mathbf{N}_{AI} & \mathbf{0} \\ \mathbf{0} & \mathbf{0} & \mathbf{0} & \mathbf{I} \end{bmatrix} \begin{bmatrix} \ddot{\mathbf{x}} \\ \dot{\mathbf{x}} \\ \ddot{\mathbf{y}} \\ \dot{\mathbf{y}} \end{bmatrix} + \begin{bmatrix} \mathbf{D}_O & \mathbf{K}_O & \mathbf{N}_D & \mathbf{N}_S \\ -\mathbf{I} & \mathbf{0} & \mathbf{0} & \mathbf{0} \\ \mathbf{0} & \mathbf{N}_{CS} & \mathbf{N}_{AD} & \mathbf{N}_{AS} \\ \mathbf{0} & \mathbf{0} & -\mathbf{I} & \mathbf{0} \end{bmatrix} \begin{bmatrix} \dot{\mathbf{x}} \\ \mathbf{x} \\ \dot{\mathbf{y}} \\ \mathbf{y} \end{bmatrix} = \begin{bmatrix} \mathbf{g}(t) \\ \mathbf{0} \\ \mathbf{h}(t) \\ \mathbf{0} \end{bmatrix}, \tag{3.2}$$

where $\mathbf{N}_I$, $\mathbf{N}_{AI}$, $\mathbf{N}_D$, $\mathbf{N}_{AD}$, $\mathbf{N}_S$, $\mathbf{N}_{AS}$ and $\mathbf{N}_{CS}$ are constant matrices (more details are presented in the following), and $\mathbf{y}$ contains nonlinear terms. Eq. (3.2) may be written as a standard linear system as

$$\begin{bmatrix} \mathbf{M}_O & \mathbf{N}_I \\ \mathbf{0} & \mathbf{N}_{AI} \end{bmatrix} \begin{bmatrix} \ddot{\mathbf{x}} \\ \ddot{\mathbf{y}} \end{bmatrix} + \begin{bmatrix} \mathbf{D}_O & \mathbf{N}_D \\ \mathbf{0} & \mathbf{N}_{AD} \end{bmatrix} \begin{bmatrix} \dot{\mathbf{x}} \\ \dot{\mathbf{y}} \end{bmatrix} + \begin{bmatrix} \mathbf{K}_O & \mathbf{N}_S \\ \mathbf{N}_{CS} & \mathbf{N}_{AS} \end{bmatrix} \begin{bmatrix} \mathbf{x} \\ \mathbf{y} \end{bmatrix} = \begin{bmatrix} \mathbf{g}(t) \\ \mathbf{h}(t) \end{bmatrix}, \tag{3.3}$$

$$\mathbf{M} \begin{bmatrix} \ddot{\mathbf{x}} \\ \ddot{\mathbf{y}} \end{bmatrix} + \mathbf{D} \begin{bmatrix} \dot{\mathbf{x}} \\ \dot{\mathbf{y}} \end{bmatrix} + \mathbf{K} \begin{bmatrix} \mathbf{x} \\ \mathbf{y} \end{bmatrix} = \begin{bmatrix} \mathbf{g}(t) \\ \mathbf{h}(t) \end{bmatrix},$$

where $\mathbf{M}$, $\mathbf{D}$, and $\mathbf{K}$ are the mass, damping and stiffness matrices of the augmented (linear) system. The function $\mathbf{h}(t)$ (in Eqs. (3.2) and (3.3)) is introduced to preserve most of the properties of the matrices in Eq. (3.1). The augmentation is expressed such that it matches the form of the nonlinearities in the systems of interest. One may note that the system can be augmented in several ways (by choosing $\mathbf{N}_{AI}$, $\mathbf{N}_{AD}$, $\mathbf{N}_{AS}$, and $\mathbf{N}_{CS}$) as to optimally suit various applications. Eq. (3.3) is the augmented linear model of the nonlinear system for which the eigenvalue problem must be solved.

Examples of augmentation

The specific form of the augmentation used is of crucial importance for the accuracy and robustness of the modal analysis technique used (e.g. direct system parameter identification). Hence, as discussed in the next subsection, the augmentation is done in a physical way [73]. Next, two examples of the augmentation for nonlinear one degree of freedom systems are presented. The first example illustrates how the augmentation is carried out for a cubic spring nonlinearity. The second example demonstrates how the augmentation is done for a Colomb friction nonlinearity.

Consider an example of a one degree of freedom system with a mass connected to ground by a linear and a nonlinear (cubic) spring. The equation of motion of this simple nonlinear system can be written as

$$m\ddot{x} + kx + k_n x^3 = g(t), \tag{3.4}$$

where m is the mass, k is the linear spring stiffness, and k_n is the nonlinear spring stiffness. Using a physically consistent augmentation developed previously [73] the new augmented system is represented by the following

$$\begin{aligned} m\ddot{x} + kx + N_S y &= g(t), \\ N_{AI}\ddot{y} + N_{AD}\dot{y} + N_{CS}x + N_{AS}y &= h(t). \end{aligned} \tag{3.5}$$

In this case, N_S and N_{CS} are both simply k_n, and y is x^3, while N_{AI}, N_{AD}, and N_{AS} are constants of our choosing. In this chapter, N_{AI} was set to values of order of magnitude similar to the mass, N_{AS} was chosen to be multiples of k_n, and N_{AD} was set to zero. Finally, comparing Eqs. (3.2) and (3.4), one may note that N_I and N_D are zero.

The augmentation for Colomb friction is distinct because Colomb friction forces are discontinuous. The following is an example of how the augmentation is applied to a one

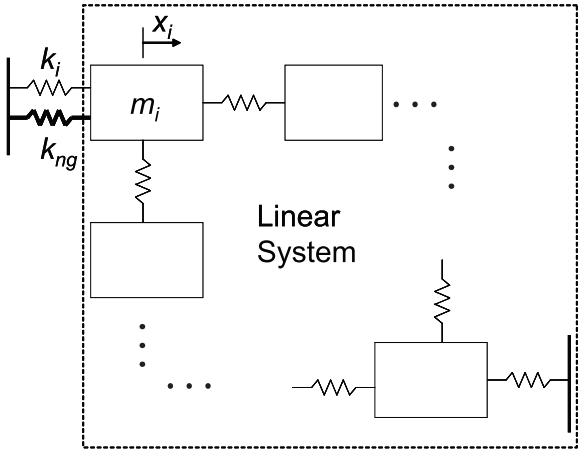

Figure 3.1: Conceptual sketch of an n degree of freedom system with mass i connected to ground by a nonlinear spring

degree of freedom mass connected to the ground by a linear spring and also rubbing against the ground. The equation of motion for this nonlinear system can be written as

$$m\ddot{x} + kx + \mu \text{sign}(\dot{x}) = g(t), \tag{3.6}$$

where μ is the coefficient of Colomb friction. The augmentation described in this chapter is represented by the following system

$$\begin{aligned} m\ddot{x} + kx + N_I\ddot{y} &= g(t), \\ N_{AI}\ddot{y} + N_{AD}\dot{y} + N_{CS}x + N_{AS}y &= h(t). \end{aligned} \tag{3.7}$$

In this case, $\ddot{y} = \text{sign}(\dot{x})$ and N_I is μ, while N_D and N_S are zero, and N_{AI}, N_{AD}, N_{CS} and N_{AS} are constants of our choosing. In this chpater, μ was chosen for N_{AI}, zero was chosen for N_{AD}, and a constant was chosen for N_{AS}, while N_{CS} was simply set to the negative of N_{AS}.

Physical augmentation

Although there is a great amount of flexibility in choosing an augmentation for a system, most modal analysis techniques take advantage of certain physical properties of the systems they are identifying. In particular, most modal analysis techniques require the system matrices to be positive definite because these techniques are defined for vibration about a stable equilibrium. Next, an example of a brief proof of the positive definiteness of the augmented system matrices (such as the one in Eq. (3.5)) is given for a cubic spring connecting a mass to the ground. Consider an n degree of freedom system with a cubic spring connecting mass i to ground as shown in Fig. 3.1. The displacement of the system is given by $\mathbf{x}$, the nonlinear spring stiffness is k_{ng}, the augmented variable is $y = x_i^3$, and a is a parameter ($a \geq 0$) which characterizes the amount of damage in the nonlinear spring stiffness (e.g. $0 \leq a < 1$ for softening damage). The parameter b (which corresponds to the $\mathbf{N}_{CS}$) term equals one, while the parameter c (which corresponds to the $\mathbf{N}_{AS}$) term is greater than one. The mass matrix of the augmented system is diagonal with all positive entries, and is therefore positive definite. The augmented stiffness matrix is shown to be positive definite by showing that the following expression is positive for $\|\mathbf{x}\| + |y| \neq 0$, i.e.

$$[x_1 \dots x_i \dots x_n \; y] \begin{bmatrix} k_{1,1} & \dots & k_{1,i} & \dots & k_{1,n} & 0 \\ \vdots & \ddots & \vdots & & \vdots & \mathbf{0} \\ k_{i,1} & \dots & k_{i,i} & \dots & k_{i,n} & ak_{ng} \\ \vdots & & \vdots & \ddots & \vdots & \mathbf{0} \\ k_{n,1} & \dots & k_{n,i} & \dots & k_{n,n} & 0 \\ 0 & \mathbf{0} & bk_{ng} & \mathbf{0} & 0 & ck_{ng} \end{bmatrix} \begin{bmatrix} x_1 \\ \vdots \\ x_i \\ \vdots \\ x_n \\ y \end{bmatrix} = \begin{array}{l} \Pi \\ +(b+a)k_{ng}x_i y \\ +ck_{ng}y^2 \geq 0. \end{array} \tag{3.8}$$

Since $y^2 = x_i^6 \geq 0$, $x_i y = x_i^4 \geq 0$, and Π is the value from just the linear portion of the system, which is itself greater than zero, the only way the expression above can be equal

to zero is when $\mathbf{x} = \mathbf{0}$ and $y = 0$. Similar proofs showing the positive definiteness can be obtained for a cubic spring connecting a mass to another mass and for the case of Colomb friction, but they are omitted here for the sake of brevity.

Extraction of augmented modal properties

The extraction of modal properties from an augmented system requires a modal analysis technique which uses an excitation that is known, but not prescribed because the forcing term $\mathbf{h}(t)$ cannot be prescribed. Direct system parameter identification is a technique that resembles auto-regressive moving average vector and enables one to determine the mode shapes and natural frequencies of the system when the displacement of the degrees of freedom ($\mathbf{x}(t)$ and $\mathbf{y}(t)$) and the forcing ($\mathbf{g}(t)$ and $\mathbf{h}(t)$) are known. The requirement of the modal analysis technique to use a known but not prescribed forcing stems from the known but constrained forcing $\mathbf{h}(t)$. An example of implementation of the proposed approach is to measure the displacement vector $\mathbf{x}(t)$ and the forcing vector $\mathbf{g}(t)$. The vector $\mathbf{y}(t)$ is then computed from $\mathbf{x}(t)$, and the vector $\mathbf{h}(t)$ is calculated to satisfy Eq. (3.2).

A consequence of the manner in which the augmentation is done is the inability for damage to appear in the augmented parameters. This means that damage occurring in $\mathbf{N}_S$, $\mathbf{N}_D$ or $\mathbf{N}_I$ will only be reflected in the linear portion, and not the augmented portion of the system. The end result is that damage in nonlinear parameters causes asymmetrical changes in the system matrices when using augmentation.

3.2.2 Iterative GMRPT for Simultaneous Damages

In this subsection, GMRPT is extended to handle certain simultaneous damages in the mass, damping and stiffness parameters. The work closely follows Kaouk et al. [30]. First, the damage location algorithm is presented. Then, the damage extent algorithm for simultaneous damages is detailed. Finally, the iterative nature of the algorithm, caused by

the approach employed for the calculation of the left eigenvectors, is presented.

Identification of damage location

To provide GMRPT [73, 74] with the degrees of freedom where damages are located, an algorithm which follows closely that of minimum rank perturbation theory (MRPT) [1] is used. In particular, it is assumed that a discrete, n-degree of freedom (e.g. finite element) model exists for the healthy augmented system, such that $\mathbf{M}$, $\mathbf{D}$ and $\mathbf{K}$ are the augmented $n \times n$ mass, (proportional) damping and stiffness matrices. Hence, damage vectors $\mathbf{d}_i$ and $\mathbf{c}_i$ can be defined as

$$\begin{aligned} \mathbf{d}_i &\equiv \mathbf{Z}_{di}\mathbf{v}_{di} = \left(\lambda_{di}^2\Delta\mathbf{M} + \lambda_{di}\Delta\mathbf{D} + \Delta\mathbf{K}\right)\mathbf{v}_{di}, \\ \mathbf{c}_i^T &\equiv \mathbf{u}_{di}^T\mathbf{Z}_{di} = \mathbf{u}_{di}^T\left(\lambda_{di}^2\Delta\mathbf{M} + \lambda_{di}\Delta\mathbf{D} + \Delta\mathbf{K}\right), \quad \text{with} \\ \mathbf{Z}_{di} &\equiv \lambda_{di}^2\mathbf{M} + \lambda_{di}\mathbf{D} + \mathbf{K}, \end{aligned} \tag{3.9}$$

where the ith eigenvalue λ_{di}, ith right eigenvector $\mathbf{v}_{di}$, and ith left eigenvector $\mathbf{u}_{di}$ are of the damaged structure, and $\Delta\mathbf{M}$, $\Delta\mathbf{D}$ and $\Delta\mathbf{K}$ are the exact perturbation matrices (that reflect the nature of the structural damage).

A composite damage vector may be defined from (all or just a few) multiple measured modes as

$$\mathbf{d} = \frac{1}{q}\sum_{i=1}^{q}\frac{\mathbf{d}_i}{\|\mathbf{v}_{di}\|}, \tag{3.10}$$

where q is the number of measured modes.

Also, Zimmerman and Kaouk [1] developed an alternative view of the state of damage where Eq. (3.9) can be rewritten as

$$d_i^j \equiv \mathbf{z}_{di}^j\mathbf{v}_{di} = \| \mathbf{z}_{di}^j \| \| \mathbf{v}_{di} \| \cos(\theta_i^j), \tag{3.11}$$

where d_i^j is the jth component (i.e. jth degree of freedom) of the ith damage vector, $\mathbf{z}_{di}^j$ is the jth row of the matrix $\mathbf{Z}_{di}$, and θ_i^j is the angle between the vectors $\mathbf{z}_{di}^j$ and $\mathbf{v}_{di}$. A

damage detector α_i^j may be calculated from θ_i^j as

$$\alpha_i^j = \theta_i^j \left(\frac{180^\circ}{\pi} \right) - 90^\circ. \tag{3.12}$$

Finally, a composite damage vector γ may be defined from the multiple measured modes as

$$\gamma_j = \frac{1}{q} \sum_{i=1}^{q} |\alpha_i^j|. \tag{3.13}$$

The indexes j where d_i^j, α_i^j or γ_j are large are the identified locations of damage. We denote by p the number of such locations.

Damage isolation

Once the damage location is known, the next step in assessing structural health is to determine the damage extent by isolating which system matrices are affected by damage. Following closely the work developed in MRPT [30], we extended the previous approach for the case of asymmetric damage scenarios. This section uses the cross-orthogonality properties of the modes to the system matrices and a specialized pseudo-inverse developed in [30]. Using the information garnered from the damage location algorithm, damage location matrices, $\mathbf{B}$ and $\mathbf{A}$ can be defined as

$$\begin{aligned} \mathbf{M}\mathbf{V}_d\mathbf{\Lambda}_d^2 + \mathbf{D}\mathbf{V}_d\mathbf{\Lambda}_d + \mathbf{K}\mathbf{V}_d = \Delta\mathbf{M}\mathbf{V}_d\mathbf{\Lambda}_d^2 + \Delta\mathbf{D}\mathbf{V}_d\mathbf{\Lambda}_d + \Delta\mathbf{K}\mathbf{V}_d &\equiv \mathbf{B}, \\ \mathbf{\Lambda}_d^2\mathbf{U}_d^T\mathbf{M} + \mathbf{\Lambda}_d\mathbf{U}_d^T\mathbf{D} + \mathbf{U}_d^T\mathbf{K} = \mathbf{\Lambda}_d^2\mathbf{U}_d^T\Delta\mathbf{M} + \mathbf{\Lambda}_d\mathbf{U}_d^T\Delta\mathbf{D} + \mathbf{U}_d^T\Delta\mathbf{K} &\equiv \mathbf{A}^T, \end{aligned} \tag{3.14}$$

where

$$\begin{aligned}
\mathbf{\Lambda}_d &= \mathrm{diag}(\lambda_{d1}, \lambda_{d2} \ldots \lambda_{dq}), \\
\mathbf{V}_d &= [\mathbf{v}_{d1}, \mathbf{v}_{d2} \ldots \mathbf{v}_{dq}], \\
\mathbf{B} &= [\mathbf{d}_1, \mathbf{d}_2 \ldots \mathbf{d}_q], \\
\mathbf{U}_d^T &= [\mathbf{u}_{d1}, \mathbf{u}_{d2} \ldots \mathbf{u}_{dq}]^T, \\
\mathbf{A}^T &= [\mathbf{c}_1, \mathbf{c}_2 \ldots \mathbf{c}_q]^T.
\end{aligned}$$

Note that $\mathbf{B}$ and $\mathbf{A}$ can be determined from the original system matrices ($\mathbf{M}$, $\mathbf{D}$, $\mathbf{K}$) and only p of the measured damaged eigenvalues and eigenvectors. However, using the subspace selection algorithm for GMRPT (presented below), all q measured modes ($q > p$) can be used to define $\mathbf{B}$ and $\mathbf{A}$ to obtain more accurate results.

Matrices $\mathbf{B}$ and $\mathbf{A}$ contain contributions of force imbalances due to the damage in the mass, damping and stiffness parameters. The matrix $\mathbf{B}$ is precisely that used by Kaouk et al. [30]. This force imbalance can be written as

$$\mathbf{B} = \mathbf{B}_M \mathbf{\Lambda}_d^2 + \mathbf{B}_D \mathbf{\Lambda}_d + \mathbf{B}_K, \tag{3.15}$$

where

$$\mathbf{B}_M = \Delta\mathbf{M}\mathbf{V}_d, \qquad \mathbf{B}_D = \Delta\mathbf{D}\mathbf{V}_d, \qquad \mathbf{B}_K = \Delta\mathbf{K}\mathbf{V}_d, \tag{3.16}$$

and

$$\mathbf{A} = \mathbf{A}_M \mathbf{\Lambda}_d^2 + \mathbf{A}_D \mathbf{\Lambda}_d + \mathbf{A}_K, \tag{3.17}$$

where

$$\mathbf{A}_M = \Delta\mathbf{M}^T\mathbf{U}_d, \qquad \mathbf{A}_D = \Delta\mathbf{D}^T\mathbf{U}_d, \qquad \mathbf{A}_K = \Delta\mathbf{K}^T\mathbf{U}_d. \tag{3.18}$$

The motivation for expressing $\mathbf{B}$ and $\mathbf{A}$ as in Eqs. (3.15) and (3.17), is that force imbalances due to the mass, damping, and stiffness matrices are separated according to their

respective matrix. The matrices $\mathbf{B}_M$, $\mathbf{B}_D$, $\mathbf{B}_K$, $\mathbf{A}_M$, $\mathbf{A}_D$ and $\mathbf{A}_K$ can be determined using the cross-orthogonality relations that arise from the proportional damping assumption. By extracting mass normalized right and left eigenvectors, the cross-orthogonality relations of the damaged system can be expressed as

$$\begin{aligned} \mathbf{U}_d^T(\mathbf{M}-\Delta\mathbf{M})\mathbf{V}_d &= \mathbf{I}_{q\times q}, \\ \mathbf{U}_d^T\left(\mathbf{D}-\Delta\mathbf{D}\right)\mathbf{V}_d = \mathrm{diag}(2\zeta_{d1}\lambda_{d1}\ldots 2\zeta_{dq}\lambda_{dq}) &= \mathbf{\Sigma}_d, \\ \mathbf{U}_d^T\left(\mathbf{K}-\Delta\mathbf{K}\right)\mathbf{V}_d = \mathrm{diag}(\lambda_{d1}^2\ldots\lambda_{dq}^2) &= \mathbf{\Lambda}_d^2, \end{aligned} \tag{3.19}$$

where ζ_{di} is the damping ratio for the ith mode of the damaged structure. Rearranging Eq. (3.19) yields

$$\begin{aligned} \mathbf{U}_d^T\Delta\mathbf{M}\mathbf{V}_d &= \mathbf{U}_d^T\mathbf{M}\mathbf{V}_d-\mathbf{I}_{q\times q} \equiv \mathbf{U}_d^T\mathbf{B}_M, \\ \mathbf{U}_d^T\Delta\mathbf{D}\mathbf{V}_d &= \mathbf{U}_d^T\mathbf{D}\mathbf{V}_d-\mathbf{\Sigma}_d \equiv \mathbf{U}_d^T\mathbf{B}_D, \\ \mathbf{U}_d^T\Delta\mathbf{K}\mathbf{V}_d &= \mathbf{U}_d^T\mathbf{K}\mathbf{V}_d-\mathbf{\Lambda}_d^2 \equiv \mathbf{U}_d^T\mathbf{B}_K. \end{aligned} \tag{3.20}$$

Similarly, Eq. (3.19) can be rearranged to yield relations for the force imbalances in the A matrices to obtain

$$\begin{aligned} \mathbf{V}_d^T\mathbf{A}_M &\equiv \mathbf{V}_d^T\mathbf{M}^T\mathbf{U}_d-\mathbf{I}_{q\times q}, \\ \mathbf{V}_d^T\mathbf{A}_D &\equiv \mathbf{V}_d^T\mathbf{D}^T\mathbf{U}_d-\mathbf{\Sigma}_d, \\ \mathbf{V}_d^T\mathbf{A}_K &\equiv \mathbf{V}_d^T\mathbf{K}^T\mathbf{U}_d-\mathbf{\Lambda}_d^2. \end{aligned} \tag{3.21}$$

All the damage location matrices, $\mathbf{B}_M$, $\mathbf{B}_D$, $\mathbf{B}_K$, $\mathbf{A}_M$, $\mathbf{A}_D$ and $\mathbf{A}_K$, can be calculated from Eq. (3.20) and Eq. (3.21). In the case where the number of measured modes equals the number of degrees of freedom in the model (i.e. $q = n$), these matrices can be computed by using the inverses of $\mathbf{V}_d$ and $\mathbf{U}_d$. However, often the number of measured modes is much less than the size of the model ($q << n$). For this case, the use of the Moore-Penrose pseudo-inverse of the matrices $\mathbf{V}_d$ and $\mathbf{U}_d$ comes to mind. Unfortunately, the

sparsity of $\mathbf{B}$ and $\mathbf{A}$ would not be reflected in $\mathbf{B}_M$, $\mathbf{B}_D$, $\mathbf{B}_K$, $\mathbf{A}_M$, $\mathbf{A}_D$ and $\mathbf{A}_K$. Hence, the minimality of the rank of the variation in the mass, damping and stiffness matrices cannot be capitalized upon. Nonetheless, this problem can be overcome by defining a pseudo-inverse that preserves the sparsity of the damage location matrices $\mathbf{B}$ and $\mathbf{A}$. For matrix $\mathbf{B}$, this has been proposed by Kaouk et al. [30]. This approach results in solving for the $n \times q$ real matrices $\mathbf{P}_B$ and $\mathbf{P}_A$ as follows

$$\begin{array}{rclcrcl} \mathbf{P}_B\left(\mathbf{U}_d^T\mathbf{B}\right) & = & \mathbf{B}, & & \mathbf{P}_B & = & \mathbf{B}\left(\mathbf{U}_d^T\mathbf{B}\right)^{-1}, \\ \mathbf{P}_A\left(\mathbf{V}_d^T\mathbf{A}\right) & = & \mathbf{A}, & \text{so that} & \mathbf{P}_A & = & \mathbf{A}\left(\mathbf{V}_d^T\mathbf{A}\right)^{-1}. \end{array} \tag{3.22}$$

Once $\mathbf{P}_B$ and $\mathbf{P}_A$ are computed, $\mathbf{B}_M$, $\mathbf{B}_D$, $\mathbf{B}_K$, $\mathbf{A}_M$, $\mathbf{A}_D$ and $\mathbf{A}_K$ can be calculated using Eqs. (3.20) and (3.21) as

$$\begin{array}{rclcrcl} \mathbf{B}_M & = & \mathbf{P}_B\left(\mathbf{U}_d^T\mathbf{M}\mathbf{V}_d - \mathbf{I}_{q\times q}\right), & & \mathbf{A}_M & = & \mathbf{P}_A\left(\mathbf{V}_d^T\mathbf{M}^T\mathbf{U}_d - \mathbf{I}_{q\times q}\right), \\ \mathbf{B}_D & = & \mathbf{P}_B\left(\mathbf{U}_d^T\mathbf{D}\mathbf{V}_d - \mathbf{\Sigma}_d\right), & \text{and} & \mathbf{A}_D & = & \mathbf{P}_A\left(\mathbf{V}_d^T\mathbf{D}^T\mathbf{U}_d - \mathbf{\Sigma}_d\right), \\ \mathbf{B}_K & = & \mathbf{P}_B\left(\mathbf{U}_d^T\mathbf{K}\mathbf{V}_d - \mathbf{\Lambda}_d^2\right), & & \mathbf{A}_K & = & \mathbf{P}_A\left(\mathbf{V}_d^T\mathbf{K}^T\mathbf{U}_d - \mathbf{\Lambda}_d^2\right). \end{array} \tag{3.23}$$

From Eq. (3.22) it is clear that $\mathbf{P}_B$ and $\mathbf{P}_A$ have the same sparsity pattern as matrices $\mathbf{B}$ and $\mathbf{A}$, respectively. Therefore, matrices $\mathbf{B}_M$, $\mathbf{B}_D$, $\mathbf{B}_K$ will also reflect the sparsity pattern of $\mathbf{B}$, while $\mathbf{A}_M$, $\mathbf{A}_D$ and $\mathbf{A}_K$ will reflect the sparsity pattern of $\mathbf{A}$.

Equations of GMRPT

In this section, the equations of GMRPT are only outlined. For a more complete proof the reader is referred to [73]. The work presented in [73] discusses minimal rank solutions for asymmetric damage cases, and is a generalization of symmetric damage cases developed in [1]. This section provides the unique solution to the unknown perturbation matrices from Eqs. (3.24) and (3.25) that is minimum rank. For clarity, the following discussion is for the case where $q = p$. Nonetheless, the GMRPT subspace selection algorithm directly extends these results for the case where $q > p$. The only unknowns in

Eq. (3.16) and Eq. (3.18) are the damage perturbation matrices. Each of the three equations in Eq. (3.16) can be expressed as

$$\mathbf{C}\mathbf{X}_B = \mathbf{Y}_B, \tag{3.24}$$

where matrices $\mathbf{X}_B$ and $\mathbf{Y}_B$ are known (e.g. $\mathbf{X}_B = \mathbf{V}_d$ and $\mathbf{Y}_B = \mathbf{B}_M$), and matrix $\mathbf{C}$ is unknown (e.g. $\mathbf{C} = \Delta\mathbf{M}$). Also, each of the three equations in Eq. (3.18) can be expressed as

$$\mathbf{C}^T\mathbf{X}_A = \mathbf{Y}_A, \tag{3.25}$$

where matrices $\mathbf{X}_A$ and $\mathbf{Y}_A$ are known (e.g. $\mathbf{X}_A = \mathbf{U}_d$ and $\mathbf{Y}_A = \mathbf{A}_M$). The minimum rank solution $\mathbf{C}$ of Eqs. (3.24) and (3.25) is unique and can be expressed as

$$\mathbf{C} = \mathbf{Y}_B\mathbf{H}\mathbf{Y}_A^T, \quad \text{with} \quad \mathbf{H} = \left(\mathbf{Y}_A^T\mathbf{X}_B\right)^{-1}. \tag{3.26}$$

This solution given by GMRPT [73] is unique and of rank p, where $\mathbf{X}_B$, $\mathbf{X}_A$, $\mathbf{Y}_B$, and $\mathbf{Y}_A \in \Re^{n\times p}$ are given, with $p < n$ and $\text{rank}(\mathbf{C}) = \text{rank}(\mathbf{X}_B) = \text{rank}(\mathbf{X}_A) = \text{rank}(\mathbf{Y}_B) = \text{rank}(\mathbf{Y}_A) = p$.

GMRPT subspace selection

Experimental modal data is always affected by measurement and eigenvector/eigenvalue extraction noise. In this section, a subspace selection algorithm, which reduces the influence of noise, is presented. This algorithm is the same as the one developed by Kaouk et al. [30] for MRPT, but it has been extended for GMRPT. This section uses a singular value decomposition of the force imbalance matrices (e.g. $\mathbf{B}_m$) to filter out noise. The subspace selection algorithm is defined as the numerically well conditioned search for two matrices $\mathbf{Z}_B \in \Re^{q\times\hat{p}_B}$ and $\mathbf{Z}_A \in \Re^{q\times\hat{p}_A}$ such that

$$\mathbf{C}\mathbf{X}_B\mathbf{Z}_B = \mathbf{Y}_B\mathbf{Z}_B, \quad \text{and} \quad \mathbf{C}^T\mathbf{X}_A\mathbf{Z}_A = \mathbf{Y}_A\mathbf{Z}_A. \tag{3.27}$$

The unknowns are $\hat{p}_B$ and $\hat{p}_A$, i.e. the numerical rank of $\mathbf{Y}_B$, $\mathbf{Y}_A$, and $\mathbf{Z}_B$, $\mathbf{Z}_A$. Note that $\hat{p}_B < q$ and $\hat{p}_A < q$. Consider the singular value decomposition of $\mathbf{Y}_B$ and $\mathbf{Y}_A$ defined as

$$\begin{aligned} \mathbf{Y}_B &= [\mathbf{U}_{B1}\mathbf{U}_{B2}] \begin{bmatrix} \mathbf{\Sigma}_B & \mathbf{0} \\ \mathbf{0} & \mathbf{\Sigma}_{\varepsilon B} \end{bmatrix} [\mathbf{V}_{B1}\mathbf{V}_{B2}]^T, \\ \mathbf{Y}_A &= [\mathbf{U}_{A1}\mathbf{U}_{A2}] \begin{bmatrix} \mathbf{\Sigma}_A & \mathbf{0} \\ \mathbf{0} & \mathbf{\Sigma}_{\varepsilon A} \end{bmatrix} [\mathbf{V}_{A1}\mathbf{V}_{A2}]^T, \end{aligned} \tag{3.28}$$

where $\mathbf{\Sigma}_B$ and $\mathbf{\Sigma}_A$ include singular values larger than ε, while $\mathbf{\Sigma}_{\varepsilon B}$ and $\mathbf{\Sigma}_{\varepsilon A}$ include singular values smaller than ε (where ε is a small positive constant which approximates zero). Also, $\mathbf{U}_B$, $\mathbf{V}_B$ and $\mathbf{U}_A$, $\mathbf{V}_A$ are the left and right singular vectors in partitioned form for $\mathbf{Y}_B$ and $\mathbf{Y}_A$. When $\mathbf{Y}_B$ is rank deficient, the range of $\mathbf{Y}_B$ is spanned by the $\hat{p}_B$ columns of $\mathbf{U}_{B1}$. Therefore, the goal is to find matrices $\mathbf{Z}_B$ and $\mathbf{Z}_A$ such that

$$\mathbf{Y}_B\mathbf{Z}_B = \mathbf{U}_{B1}, \quad \text{and} \quad \mathbf{Y}_A\mathbf{Z}_A = \mathbf{U}_{A1}. \tag{3.29}$$

The matrices $\mathbf{Z}_B$ and $\mathbf{Z}_A$ can be calculated from Eq. (3.29) by employing the pseudo-inverse $\mathbf{Y}_B^+$ of $\mathbf{Y}_B$ and $\mathbf{Y}_A^+$ of $\mathbf{Y}_A$, and by neglecting $\mathbf{\Sigma}_{\varepsilon B}$ and $\mathbf{\Sigma}_{\varepsilon A}$ (for small ε) to obtain

$$\begin{aligned} \mathbf{Z}_B &= \mathbf{Y}_B^+\mathbf{U}_{B1} \equiv \mathbf{V}_{B1}\mathbf{\Sigma}_B\mathbf{U}_{B1}^T\mathbf{U}_{B1} = \mathbf{V}_{B1}\mathbf{\Sigma}_B, \\ \mathbf{Z}_A &= \mathbf{Y}_A^+\mathbf{U}_{A1} \equiv \mathbf{V}_{A1}\mathbf{\Sigma}_A\mathbf{U}_{A1}^T\mathbf{U}_{A1} = \mathbf{V}_{A1}\mathbf{\Sigma}_A. \end{aligned}$$

The solution of Eq. (3.27) is then given by

$$\mathbf{C} = \mathbf{Y}_B\mathbf{Z}_B \left(\mathbf{Z}_A^T\mathbf{Y}_A^T\mathbf{X}_B\mathbf{Z}_B\right)^{-1} \mathbf{Z}_A^T\mathbf{Y}_A^T. \tag{3.30}$$

The final form of the solution using GMRPT with the subspace selection algorithm and simultaneous damages can be written as

$$\begin{aligned} \Delta\mathbf{M} &= \mathbf{B}_M\mathbf{Z}_{BM} \left(\mathbf{Z}_{AM}^T\mathbf{A}_M^T\mathbf{V}_d\mathbf{Z}_{BM}\right)^{-1} \mathbf{Z}_{AM}^T\mathbf{A}_M^T, \\ \Delta\mathbf{D} &= \mathbf{B}_D\mathbf{Z}_{BD} \left(\mathbf{Z}_{AD}^T\mathbf{A}_D^T\mathbf{V}_d\mathbf{Z}_{BD}\right)^{-1} \mathbf{Z}_{AD}^T\mathbf{A}_D^T, \\ \Delta\mathbf{K} &= \mathbf{B}_K\mathbf{Z}_{BK} \left(\mathbf{Z}_{AK}^T\mathbf{A}_K^T\mathbf{V}_d\mathbf{Z}_{BK}\right)^{-1} \mathbf{Z}_{AK}^T\mathbf{A}_K^T, \end{aligned} \tag{3.31}$$

where matrices $\mathbf{Z}_{BM}$, $\mathbf{Z}_{BD}$, $\mathbf{Z}_{BK}$, and $\mathbf{Z}_{AM}$, $\mathbf{Z}_{AD}$, $\mathbf{Z}_{AK}$ from Eq. (3.31) are found for their respective $\mathbf{X}_B$, $\mathbf{Y}_B$, and $\mathbf{X}_A$, $\mathbf{Y}_A$ (used in Eqs. (3.24) and (3.25)).

The theory above has been developed for (proportionally) damped structures. This can easily be contracted for the case where the model does not include proportional damping by simply setting $\mathbf{D}$, $\Delta\mathbf{D}$, $\mathbf{B}_d$ and $\mathbf{A}_d$ to zero in the formulation. For simplicity, the systems explored in this chapter include no proportional damping. Instead a more challenging form of (nonlinear) damping, caused by Colomb friction is investigated.

Determination of left eigenvectors

The determination of the left eigenvectors of the system is an essential element of GMRPT as revealed by Eq. (3.31). This section uses the cross-orthogonality properties of the modes to the system matrices to help extract the left eigenvectors. In previous work [73], the orthogonality properties of the eigenvectors of the system to the mass matrix were capitalized upon. For example, assuming that no damage occurs in the mass matrix (i.e. $\Delta\mathbf{M} = \mathbf{0}$), the following equation was used to determine the needed left eigenvectors

$$\mathbf{U}_d^T\mathbf{M}\mathbf{V}_d = \mathbf{I}, \quad \text{so that} \quad \mathbf{U}_d^T = \mathbf{V}_d^{-1}\mathbf{M}^{-1}. \tag{3.32}$$

For the case of damage in the mass matrix, Eq. (3.32) cannot be used. However, assuming that no damage occurs in the stiffness matrix (i.e. $\Delta\mathbf{K} = \mathbf{0}$), the following equation was used to determine the needed left eigenvectors

$$\mathbf{U}_d^T\mathbf{K}\mathbf{V}_d = \mathbf{\Lambda}_d^2, \quad \text{so that} \quad \mathbf{U}_d^T = \mathbf{\Lambda}_d^2\mathbf{V}_d^{-1}\mathbf{K}^{-1}. \tag{3.33}$$

For the case of simultaneous damages in the mass, damping and stiffness parameters, an iterative update approach can be used to determine the left eigenvectors and the damaged state of the system. This approach is referred to as the *iterative* GMRPT method. The first step in this approach is to apply the procedure as if the mass matrix is healthy.

Namely, use the orthogonality property given by Eq. (3.32) to determine a set of left eigenvectors. Then, use Eq. (3.31) to determine the $\Delta\mathbf{K}$ matrix and update the $\mathbf{K}$ matrix. The next step is to use the updated $\mathbf{K}$ matrix as if it is healthy. For example, use the orthogonality property given by Eq. (3.33). Then, use Eq. (3.31) to determine the $\Delta\mathbf{M}$ and update the $\mathbf{M}$ matrix. These two steps are then repeated with the most recently updated $\mathbf{M}$ and $\mathbf{K}$ matrices until the process converges. It was found that this procedure only takes a few iterations to reach convergence. The converged solution satisfies the following equation

$$\mathbf{\Gamma M}\dot{\mathbf{s}} + \mathbf{\Gamma K}\mathbf{s} = \mathbf{\Gamma}\xi,$$

where the matrices $\mathbf{\Gamma M}$ and $\mathbf{\Gamma K}$ are the converged matrices (denoted by $\underline{\mathbf{M}}$ and $\underline{\mathbf{K}}$), $\mathbf{s}$ is the full (linear, augmented) state vector of the forced system $\mathbf{s} = [\dot{\mathbf{x}}\ \mathbf{x}\ \dot{\mathbf{y}}\ \mathbf{y}]^T$, and ξ is the full forcing vector. The matrix $\mathbf{\Gamma}$ is a constant and unknown matrix. The matrix $\mathbf{\Gamma}$ can be determined by collecting snapshots of ξ in time. Denote ξ_i (for $i = 1, \ldots, r$, with $r > n$) a set of r such snapshots obtained at r time instances. At those instances the augmented state vectors are denoted by $\mathbf{s}_i$. After convergence, the matrices $\mathbf{\Gamma M}$ and $\mathbf{\Gamma K}$ are known. Hence, a set of vectors ψ_i can be computed as

$$\psi_i = \mathbf{\Gamma M}\dot{\mathbf{s}}_i + \mathbf{\Gamma K}\mathbf{s}_i$$

Grouping the vectors ψ_i and the snapshots ξ_i as columns, (and using $\psi_i = \mathbf{\Gamma}\xi_i$), the matrix $\mathbf{\Gamma}$ can be determined as $\mathbf{\Gamma} = [\psi_1 \ldots \psi_i \ldots \psi_r]\,[\xi_1 \ldots \xi_i \ldots \xi_r]^+$, where the superscript $+$ denotes the pseudo-inverse. Finally, the mass and stiffness matrices of the damaged augmented system can be calculated by multiplying the converged $\mathbf{\Gamma M}$ and $\mathbf{\Gamma K}$ matrices by $\mathbf{\Gamma}^{-1}$.

3.2.3 Multiple Augmentations GMRPT for Damage Detection

As an alternative to the approach presented in the previous subsection, in this subsection a damage detection methodology that uses *multiple augmentations* to determine

damages in nonlinear parameters is developed for the case where only an *incomplete* set of eigenvectors is available, since in practice all modes and frequencies of the system would be very difficult to obtain accurately. This still requires all finite element model degrees of freedom to be measured. This approach is referred to as multiple augmentations GMRPT. This section exploits the fact that multiple augmented system models can be used to follow the same nonlinear trajectory in order to determine the damage in the nonlinear parameters. The first step of the methodology is to identify the degrees of freedom where damage is located, similar to the previous subsection, by using Eqs. (3.10) to (3.13). Next, information from the damage location equations and multiple augmentations is used to detect the damage in the nonlinear parameters. Finally, MRPT is used to detect damage in the linear portion of the system after the system matrices are updated and the system is augmented (once more) in a symmetric form.

Consider a system with cubic spring nonlinearities, and which, for simplicity, has no damping. Also for simplicity, assume that damage only occurs in the linear and nonlinear stiffness terms. The augmented system matrices have the following form

$$\mathbf{M} = \begin{bmatrix} \mathbf{M}_O & \mathbf{0} \\ \mathbf{0} & \mathbf{N}_{AI} \end{bmatrix} \quad \text{and} \quad \mathbf{K} = \begin{bmatrix} \mathbf{K}_d & \mathbf{N}_{Sd} \\ \mathbf{N}_{CS} & \mathbf{N}_{AS} \end{bmatrix}, \tag{3.34}$$

where $\mathbf{M}$ and $\mathbf{K}$ are the augmented mass and stiffness matrices, $\mathbf{K}_d$ is the damaged linear stiffness matrix, $\mathbf{N}_{Sd}$ is the damaged matrix that contains the nonlinear parameters, and $\mathbf{M}_O$, $\mathbf{N}_{AI}$, $\mathbf{N}_{CS}$ and $\mathbf{N}_{AS}$ are as previously defined. The resulting eigenvalue problem can be written as

$$-\lambda_{ik}^2 \begin{bmatrix} \mathbf{M}_O & \mathbf{0} \\ \mathbf{0} & \mathbf{N}_{AI} \end{bmatrix} \begin{bmatrix} \mathbf{v}_{Lik} \\ \mathbf{v}_{Aik} \end{bmatrix} = \begin{bmatrix} \mathbf{K}_d & \mathbf{N}_{Sd} \\ \mathbf{N}_{CS} & \mathbf{N}_{ASi} \end{bmatrix} \begin{bmatrix} \mathbf{v}_{Lik} \\ \mathbf{v}_{Aik} \end{bmatrix}, \tag{3.35}$$

where λ_{ik} is the kth eigenvalue of the ith augmentation of the system, with $\mathbf{v}_{Lik}$ being the linear part (upper portion) of the corresponding eigenvector and $\mathbf{v}_{Aik}$ being the augmented

part (lower portion) of the corresponding eigenvector.

The top part of Eq. (3.35) (corresponding to the actual linearized system equations alone) for two different augmentations i and j and eigenvectors numbered k and l gives the following equations

$$\mathbf{K}_d\mathbf{v}_{Lik} + \mathbf{N}_{Sd}\mathbf{v}_{Aik} = -\lambda_{ik}^2\mathbf{M}_O\mathbf{v}_{Lik}, \tag{3.36}$$

$$\mathbf{K}_d\mathbf{v}_{Ljl} + \mathbf{N}_{Sd}\mathbf{v}_{Ajl} = -\lambda_{jl}^2\mathbf{M}_O\mathbf{v}_{Ljl}. \tag{3.37}$$

Premultiplying Eq. (3.36) by $\mathbf{v}_{Ljl}^T$ and Eq. (3.37) by $\mathbf{v}_{Lik}^T$ yields

$$\mathbf{v}_{Ljl}^T\mathbf{K}_d\mathbf{v}_{Lik} + \mathbf{v}_{Ljl}^T\mathbf{N}_{Sd}\mathbf{v}_{Aik} = -\lambda_{ik}^2\mathbf{v}_{Ljl}^T\mathbf{M}_O\mathbf{v}_{Lik}, \tag{3.38}$$

$$\mathbf{v}_{Lik}^T\mathbf{K}_d\mathbf{v}_{Ljl} + \mathbf{v}_{Lik}^T\mathbf{N}_{Sd}\mathbf{v}_{Ajl} = -\lambda_{jl}^2\mathbf{v}_{Lik}^T\mathbf{M}_O\mathbf{v}_{Ljl}. \tag{3.39}$$

Subtracting Eq. (3.39) from Eq. (3.38), using $\mathbf{K}_d = \mathbf{K}_d^T$, substituting $\mathbf{N}_{Sd} = \mathbf{N}_S - \Delta\mathbf{N}$, and solving for $\Delta\mathbf{N}$ yields

$$\begin{aligned}\mathbf{v}_{Ljl}^T\Delta\mathbf{N}\mathbf{v}_{Aik} - \mathbf{v}_{Lik}^T\Delta\mathbf{N}\mathbf{v}_{Ajl} = \;& \mathbf{v}_{Ljl}^T\mathbf{N}_S\mathbf{v}_{Aik} - \mathbf{v}_{Lik}^T\mathbf{N}_S\mathbf{v}_{Ajl} \\ &+ (\lambda_{ik}^2 - \lambda_{jl}^2)\mathbf{v}_{Ljl}^T\mathbf{M}_O\mathbf{v}_{Lik}.\end{aligned} \tag{3.40}$$

The result is a scalar equation for each pair (i, j), with the unknowns in the $\Delta\mathbf{N}$ matrix, which correspond to nonlinear parameters in the degrees of freedom containing damage found from Eqs. (3.10) to (3.13). A separate equation can be written for each combination of different augmentations and eigenvectors. The equations obtained for each pair (i, j) can be combined and rearranged as to form

$$\begin{bmatrix} \rho_1^1 & \rho_2^1 & \cdots & \rho_p^1 \\ \rho_1^2 & \rho_2^2 & \cdots & \rho_p^2 \\ \vdots & \vdots & \ddots & \vdots \\ \rho_1^m & \rho_2^m & \cdots & \rho_p^m \end{bmatrix} \begin{bmatrix} \Delta_1 \\ \Delta_2 \\ \vdots \\ \Delta_p \end{bmatrix} = \begin{bmatrix} \beta_1 \\ \beta_2 \\ \vdots \\ \beta_m \end{bmatrix}, \tag{3.41}$$

where the constants ρ_r^s (for $r = 1, \ldots, p$, and $s = 1, \ldots, m$) come from combinations of entries from $\mathbf{v}_{Ljl}^T$, $\mathbf{v}_{Lik}^T$, $\mathbf{v}_{Aik}$, and $\mathbf{v}_{Ajl}$. The unknowns Δ_r come from elements of $\Delta\mathbf{N}$, and can be greater or less than zero. The constants β_s are computed directly from the right hand side of Eq. (3.40). For the case of zero measurement error, the number of equations m has to be at least equal to the number of unknowns p. More realistic scenarios, with measurement errors, require $m > p$, as discussed in the results (below).

After the damages in nonlinear parameters has been calculated, the system matrices can be updated. A new augmentation can then be generated so that it corresponds to a symmetric augmented system. The damage location algorithm can then be employed once more to determine where the damage in linear parameters resides, and finally MRPT can be used to determine the extent of the damage in linear parameters.

3.2.4 Eigenvector Filtering Algorithms

The measurement and eigenvector/eigenvalue extraction noise which affects eigenanalyses performed experimentally can be alleviated by the following two filtering algorithms.

The first filtering algorithm exploits the fact that no damage can occur in the augmented equations of the system, and was previously proposed [78]. The filtering algorithm uses the fact that no damage can occur in the augmented equations, which implies that asymmetric damage scenarios may occur. The algorithm filters all q measured eigenvectors of the system by placing them into Eq. (3.9). Then, for each eigenvector one enforces that no damage can occur in the elements of $\mathbf{d}_i$ corresponding to the augmented degrees of freedom. This is done by calculating new entries for the eigenvector in the augmented degrees of freedom corresponding to zero damage. This calculation is done by balancing each eigenvector component exactly with the eigenvector components that couple with it (the degrees of freedom that contain the nonlinearity). Since there should never be any dam-

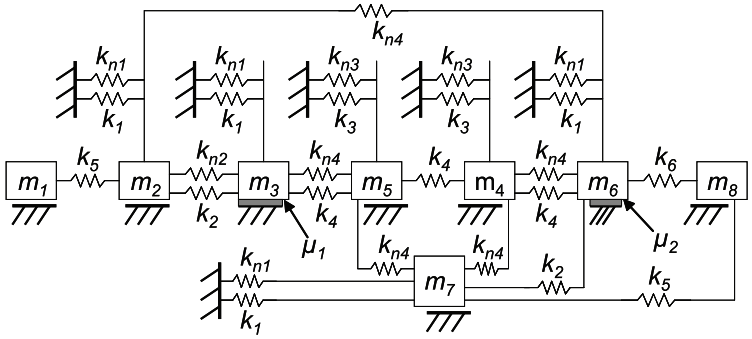

Figure 3.2: A nonlinear Kabe-type problem, which also includes 12 cubic springs and Colomb friction at two locations

age in the augmented equations, this filtering algorithm can be applied *before* the damage location is determined.

The second filtering algorithm, which was developed by Zimmerman and Kaouk [1], is also useful in reducing the effects of noise. This filtering algorithm is used *after* the damage location is determined. It is assumed that the nonzero elements of the vector $\mathbf{d}_i$ associated with undamaged degrees of freedom are due to eigenvector errors, and can be set to zero. The result is a filtered (and augmented) damage vector $\mathbf{d}_{fi}$, which can then be used to obtain the ith filtered eigenvector $\mathbf{v}_{dfi}$ using

$$\left(\lambda_{di}^2\mathbf{M} + \mathbf{K}\right)\mathbf{v}_{dfi} = \mathbf{d}_{fi}.$$

3.3 Results

To demonstrate the proposed method, numerical simulations on nonlinear systems of the type shown in Figs. 3.2, 3.3 and 3.4 are performed. Matrices $\mathbf{M}_O$, $\mathbf{K}_O$, $\mathbf{N}_I$, $\mathbf{N}_S$, $\mathbf{N}_{AI}$, $\mathbf{N}_{AD}$, $\mathbf{N}_{AS}$ and $\mathbf{N}_{CS}$ were generated for each of the systems. Next, the damage detection methods discussed were implemented for each of the systems. Random measurement noise was also included to determine the sensitivity of the approaches and to estimate the

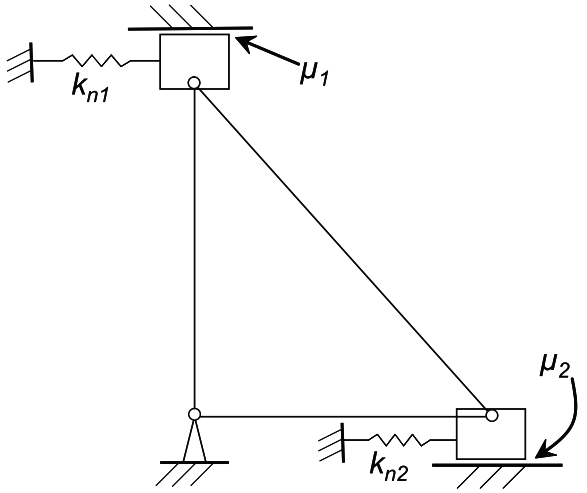

Figure 3.3: Truss structure with two cubic springs and and Colomb friction at two locations

effectiveness of the filtering algorithms.

3.3.1 Case 1: Nonlinear Kabe System

The nonlinear Kabe system shown in Fig. 3.2 is based on a linear Kabe system which was investigated previously by Zimmerman and Kaouk [1]. With knowledge of the linear and augmented system matrices, numerical simulations were conducted. Each mass was forced harmonically. The vector of displacements $\mathbf{x}(t)$ was calculated by standard time integration, while $\mathbf{y}(t)$ and $\mathbf{h}(t)$ were calculated based on their relation to $\mathbf{x}(t)$. The eigenvalues and eigenvectors of the augmented matrices can be obtained by using the time series for $\mathbf{x}(t)$, $\mathbf{g}(t)$, $\mathbf{y}(t)$ and $\mathbf{h}(t)$. Next, the iterative generalized minimum rank perturbation theory (GMRPT) technique was used to determine the damage location and extent by using the modal data. The iterative GMRPT technique required the full set of the right eigenvectors to be measured to be used. Trials were conducted to show the effectiveness of calculating simultaneous damages in the mass and stiffness parameters and the effect of random noise.

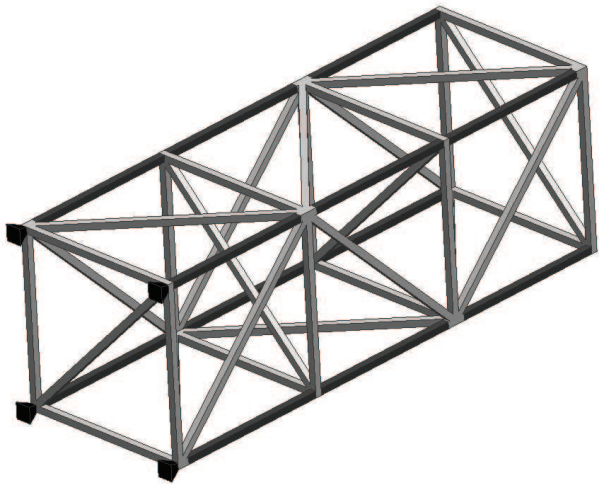

Figure 3.4: Linear 3-bay structure with 4 cubic springs connecting joints to ground and 8 cubic springs connecting joints to other joints (the dark colored elements represent nonlinear beams, while the light colored elements represent linear beams)

To determine the effectiveness of the iterative GMRPT method (presented in Sec. 3.2.2), a case where two linear and two nonlinear springs were damaged (in the stiffness matrix), and the Colomb friction increased at both locations was investigated using the exact eigenvalues and right eigenvectors of the system and using noisy right eigenvectors. Fig. 3.5 presents element by element the values of the mass and stiffness perturbation matrices ($\Delta\mathbf{M}$ and $\Delta\mathbf{K}$) obtained using GMRPT. The x-axes in each plot represent the index of a column vector obtained from storing the upper triangular portion of the perturbation matrix into a column vector. In order to better visualize the results every tenth index is plotted unless the absolute value of the average value of damage predicted is greater than 0.05 for (a) and 10 for (b). The y-axes in the plots represent the entries of the difference between the original and updated matrices for (a) $\Delta\mathbf{M}$ and for (b) $\Delta\mathbf{K}$. In each plot, a line demarcates the section of linear and nonlinear parameters.

The figure illustrates how the method predicts the exact damage in both the mass and

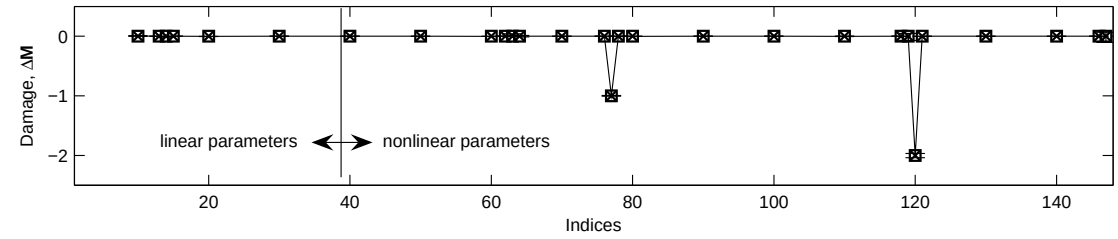

(a)

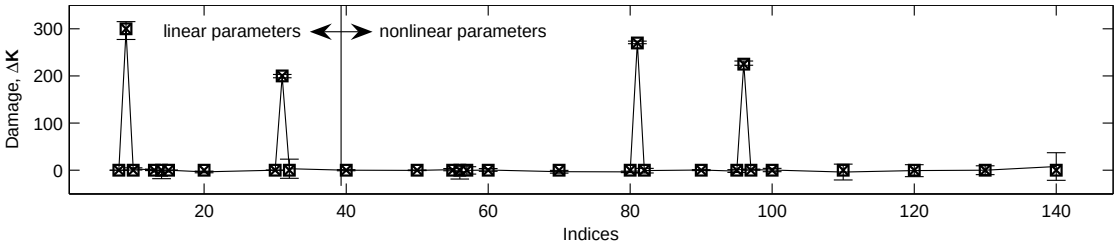

(b)

Figure 3.5: Case 1: Predicted damage in the nonlinear Kabe system with damage associated with an increase in Colomb friction (a) and a reduction of stiffness in two linear and two nonlinear springs (b) ($\square$ exact damage; $\times$ predicted damage for no noise; $-$ predicted damage for 5% random eigenvector noise)

stiffness parameters when using exact eigenvalues and right eigenvectors of the system. For the case where 5% random noise was added to the right eigenvectors the average damage values for 100 separate calculations were obtained, and standard deviation error bars are plotted. The figure shows that the average value of the predicted damage is close to the exact damage. The maximum standard deviation in the damaged parameters is approximately 6% of the actual damage in that parameter.

3.3.2 Case 2: Nonlinear Truss Structure

The iterative GMRPT method (presented in Sec. 3.2.2) is explored in this case for a more complex structure, shown schematically in Fig. 3.3. The method was used to determine the damage location and extent. Trials were conducted to show the effectiveness of calculating simultaneous damages in the mass and stiffness parameters and the effect of

random measurement noise.

Using the exact eigenvalues and right eigenvectors of the system, the effectiveness of the algorithm is demonstrated for a case with two damaged springs, one linear and one nonlinear (in the stiffness matrix), and an increase in Colomb friction at one location. The results shown in Fig. 3.6 illustrate that the method predicts the exact damage in both the mass and stiffness parameters. Additionally, to determine the sensitivity of the iterative GMRPT method to random measurement noise, a 10% random eigenvector and 1% random eigenvalue perturbation was added to the simulated measurements for the same case. The average damage values for 100 separate calculations were obtained and standard deviation error bars are plotted. The figure shows that the average value of the predicted damage is close to the exact damage. The maximum standard deviation in the damaged parameters is approximately 25% of the actual damage in that parameter.

3.3.3 Case 3: Nonlinear 3-bay Structure

To demonstrate the multiple augmentations GMRPT technique (with an incomplete set of right eigenvectors, as presented in Sec. 3.2.3), a numerical investigation of a nonlinear system of the type shown in Fig. 3.4 was performed. The *nonlinear* 3-bay structure is based on a linear structure. The linear 3-bay structure consists of 44 steel beams connected at 16 nodes, 4 of which are pinned to the ground. In addition to that, the nonlinear frame also has 4 cubic springs connecting nodes to ground, as well as 8 cubic spring nonlinearities connecting nodes to each other and to the linear beams.

Augmented linear systems were created from the nonlinear system by obtaining the matrices $\mathbf{M}_O$, $\mathbf{K}_O$, $\mathbf{N}_I$, $\mathbf{N}_D$, $\mathbf{N}_S$, $\mathbf{N}_{AI}$, $\mathbf{N}_{AD}$, $\mathbf{N}_{AS}$ and $\mathbf{N}_{CS}$. The $\mathbf{N}_S$ matrix is composed of cubic spring stiffnesses, while $\mathbf{N}_I$ and $\mathbf{N}_D$ are zero. The matrix $\mathbf{N}_{AI}$ is a diagonal matrix containing the augmented masses. The augmented masses are chosen of the same

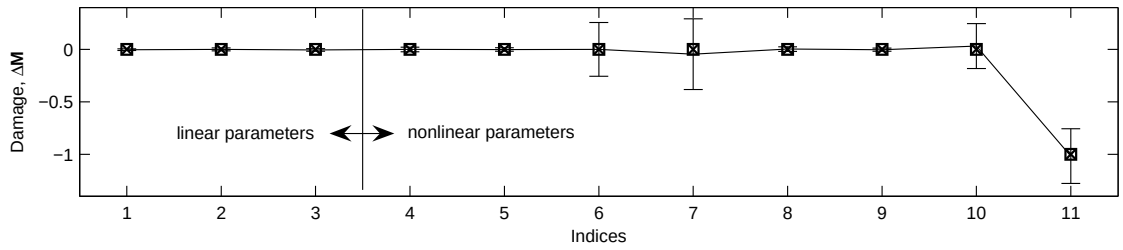

(a)

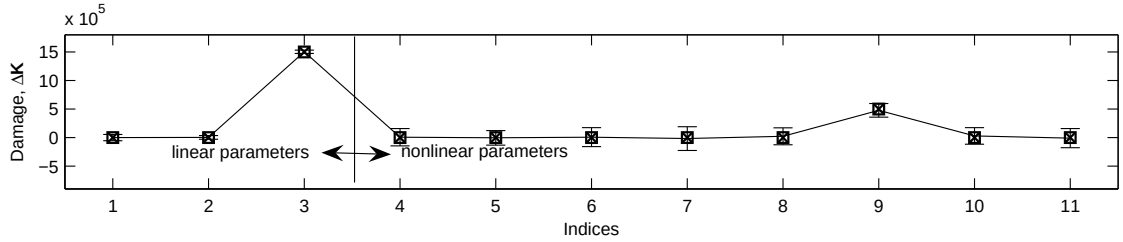

(b)

Figure 3.6: Case 2: Predicted damage in the nonlinear truss system with an increase in Colomb friction (a) and a reduction of stiffness in one linear and one nonlinear spring (b) (□ exact damage; × predicted damage for no noise; − predicted damage for 10% random eigenvector noise and 1% eigenvalue noise)

order of magnitude as the linear masses that they are coupled to. The matrix $\mathbf{N}_{CS}$ is chosen to keep the system symmetric, i.e. the entries are the cubic spring stiffnesses. The matrix $\mathbf{N}_{AS}$ is a diagonal matrix containing augmented spring stiffnesses that were varied for different augmentations. Finally, $\mathbf{N}_{AD}$ is zero. For the 15 different augmentations that were performed for each scenario, the augmented spring stiffnesses k_a, were varied as follows

$$\begin{aligned} k_{aji} &= i \cdot k_{nj}, \quad \text{for } i = 2, \ldots, 15, \\ k_{aj1} &= 1.5 \cdot k_{nj}, \end{aligned} \tag{3.42}$$

where k_{nj} is the cubic spring stiffness for the jth nonlinear degree of freedom, and k_{aji} is the corresponding augmented spring stiffness for the ith augmentation.

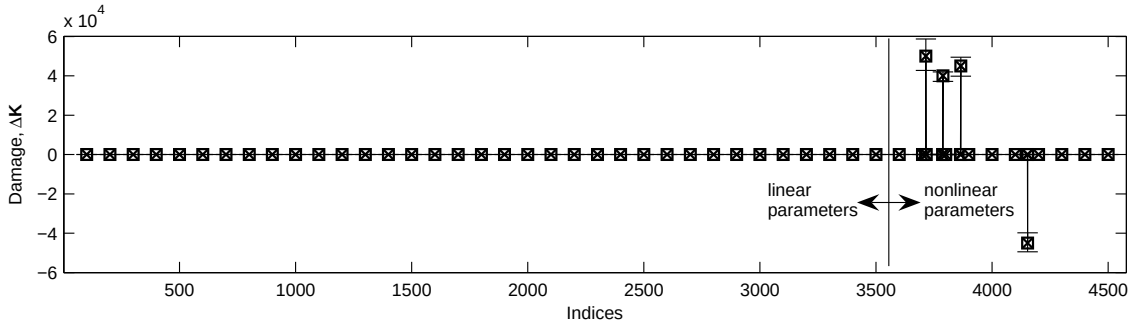

Figure 3.7: Case 3: Predicted damage in a nonlinear 3-bay structure when 3 cubic springs are damaged (□ exact damage; × predicted damage for no noise; − predicted damage for 5% random eigenvector noise)

Augmented modal properties of each of these augmented systems were then used to determine damage location and extent. The number of modes used is restricted to the first 10 out of a total of 96. All 10 measured modes were used in the updating for each case by using the subspace selection algorithm (discussed in Sec. 3.2.2). Numerical simulations were performed to show the effectiveness of the method for incomplete measurements for various damage scenarios. Finally, different levels of noise were added to the eigenvectors for different damage levels to determine the sensitivity of the method to noise and to the amount of damage.

3.3.4 Case 3: Scenario 1: Damage in Nonlinear Parameters

The first scenario explored for case 3 is damage in purely nonlinear parameters. The multiple augmentations GMRPT damage detection method (presented in Sec. 3.2.3) is applied in the following manner. First, the degrees of freedom affected by damage are isolated using Eq. (3.10) and Eq. (3.13). Then, using the augmented modal properties from multiple augmentations, Eq. (3.41) is solved for the damage in nonlinear parameters. Next, the damage in nonlinear parameters is incorporated, and a symmetric augmentation

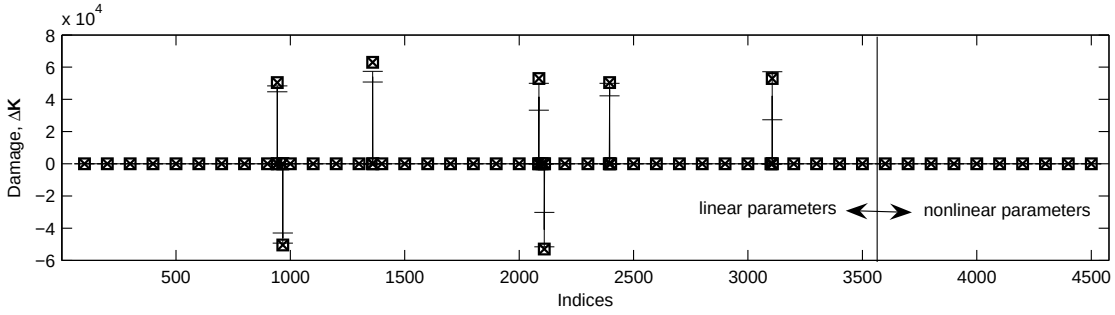

Figure 3.8: Case 3: Predicted damage in a nonlinear 3-bay structure when 3 beams are damaged (□ exact damage; × predicted damage for no noise; − predicted damage for 5% random eigenvector noise)

is produced. Finally, the degrees of freedom affected by damage are solved for again (and, as expected, no damage is found).

Results for numerical simulations where 3 cubic springs lose some of their stiffness is plotted in Fig. 3.7. Two of the damaged cubic springs connect nodes to ground, and one connects two nodes to each other. The percent of damages (relative to the healthy spring) in the cubic spring stiffnesses range from 40% to 50%. The plot presents element by element the values of the identified stiffness perturbation matrix $\Delta\mathbf{K}$. In order to better visualize the results every 100th index is plotted unless the absolute value of the average value of damage predicted is greater than 10. Shown are the exact value of the damage, the damage predicted using the exact eigenvectors of the system, and the damage predicted when there is 5% noise in the eigenvectors of the system. For the case of noisy data, 100 separate calculations were performed, and average and standard deviation error bars are plotted. Fig. 3.7 shows that, when exact eigenvectors of the system are used, damage in nonlinear parameters can be assessed exactly. Also, the average prediction is still quite accurate when there is as much as 5% random noise. The maximum standard deviation in the damaged parameters is approximately 16% of the actual damage in that parameter.

3.3.5 Case 3: Scenario 2: Damage in Linear Parameters

The second scenario examined for case 3 is damage purely in linear parameters. The methodology is carried out similarly to the scenario of damage in nonlinear parameters. However, little or no damage is predicted in the nonlinear parameters (in the presence of noise). As expected, damage is predicted when the damage location algorithm is employed a second time. Finally, GMRPT is carried out using Eq. (3.31) to identify the damage in linear parameters.

Results for numerical simulations where the stiffness of 3 beams is reduced are plotted in Fig. 3.8. One of the damaged beams connects a node to ground, and two connect two nodes to each other. The percent of damages (relative to the healthy beam) in the beam stiffnesses range from 40% to 50%. The data is plotted in the same way as Fig. 3.7, with 100 separate calculations performed for the case of 5% noise.

The results in Fig. 3.8 show that, when exact eigenvectors of the system are provided, damage (in this case linear) can be assessed exactly. Also, when there is 5% random noise, the average prediction is still quite accurate, although it deviates somewhat more than the damage in nonlinear parameters (shown in Fig. 3.7). The maximum standard deviation in the damaged parameters is approximately 28% of the actual damage in that parameter.

3.3.6 Case 3: Scenario 3: Simultaneous Damage in Linear & Nonlinear Parameters

The third scenario examined for case 3 is combined damage in linear and nonlinear parameters. Similarly to the first two scenarios, after the damaged degrees of freedom are isolated using Eqs. (3.10) and (3.13), damage to the nonlinear parameters is determined using Eq. (3.41). Then, the system is updated (and made symmetric). Next, the damage location is identified, and finally the damage in linear parameters is determined using Eq. (3.31).

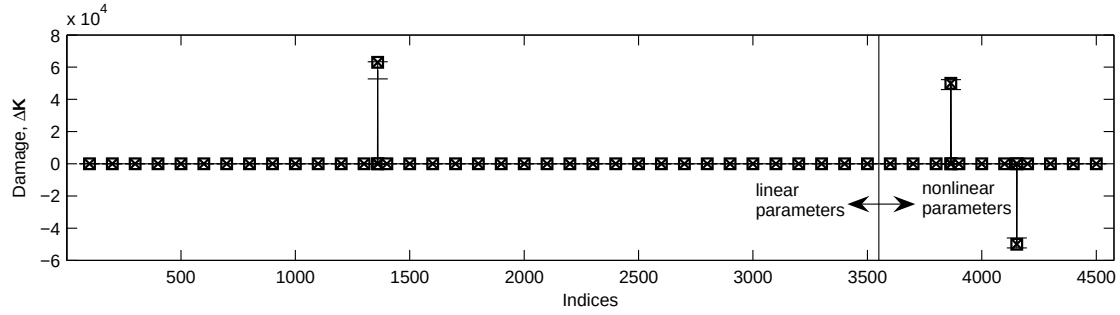

Figure 3.9: Case 3: Predicted damage in a nonlinear 3-bay structure when one cubic spring and one beam are damaged (□ exact damage; × predicted damage for no noise; − predicted damage for 5% random eigenvector noise).

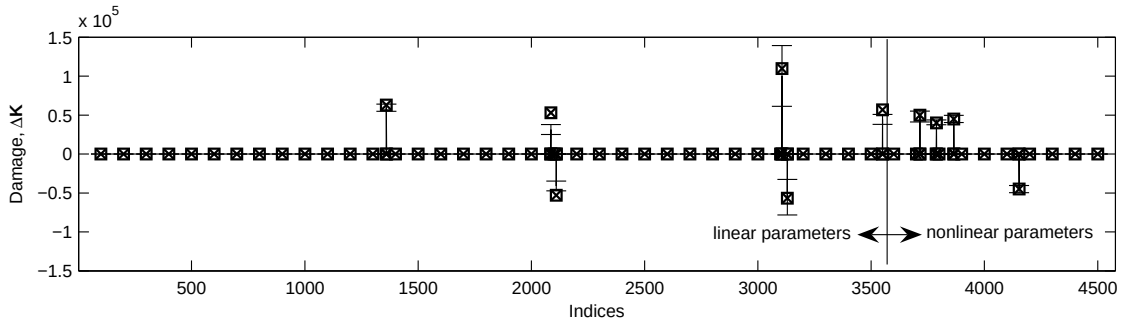

Figure 3.10: Case 3: Predicted damage in a nonlinear 3-bay structure when 3 cubic springs and 3 beams are damaged (□ exact damage; × predicted damage for no noise; − predicted damage for 5% random eigenvector noise)

Results for numerical simulations where the stiffness of one beam and one cubic spring is reduced are plotted in Fig. 3.9. The damaged cubic spring connects two nodes to each other, and has its stiffness reduced by 45%. The damaged beam connects a node to ground, and has its stiffness reduced by 50%. The data is plotted as in Fig. 3.7, with 100 separate calculations performed for the case of 5% noise.

The results in Fig. 3.9 show that damage in both linear and nonlinear parameters can be assessed exactly when exact eigenvectors of the system are provided. Also, when there is

Exact Percent Damage	Element Type	Random Noise %			
		1	3	5	10
		Prediction Error %			
10	linear	6.9	12.4	-	-
	nonlinear	0.4	1.6	-	-
50	linear	2.3	5.9	7.8	16.1
	nonlinear	0.1	0.3	1.6	1.5

Table 3.1: Percent error in the average predicted damage from 100 separate calculations. The symbol $-$ indicates that the algorithm is unable work because it could not identify the damaged degrees of freedom.

5% random measurement noise, the average prediction is still quite accurate. The standard deviation in the linear damaged parameter is approximately 8% of the actual damage, while the standard deviation in the nonlinear damaged parameter is approximately 6% of the actual damage.

Results for numerical simulations where the stiffnesses of 3 beams and 3 cubic springs are reduced are plotted in Fig. 3.10. One of the damaged beams connects a node to ground, and two connect two nodes to each other. Two of the damaged cubic springs connect nodes to ground, and one connects two nodes to each other. The percent of damages (relative to the healthy case) ranges from 40% to 50% stiffness loss. The results are for 100 separate calculations performed for the case of 5% noise. This plot shows that, even with more complicated damage cases, the methodology works precisely when there is no noise, and it is quite accurate with as much as 5% measurement noise. The maximum standard deviation in the linear damaged parameters is approximately 35% of the actual damage, while the maximum standard deviation in the nonlinear damaged parameters is approximately 14% of the actual damage.

3.3.7 Case 3: Effects of Noise and Amount of Damage

To better understand the effects of noise and of the amount of damage on the multiple augmentations GMRPT method (presented in Sec. 3.2.3), several additional cases were examined. The results are summarized in Tab. 3.1, and consist of 10% and 50% damage to the same two elements damaged (as shown in Fig. 3.9) for 1%, 3%, 5%, and 10% noise. In each case, the percent error in the average predicted damage from 100 separate calculations is reported.

As expected, Tab. 3.1 shows that, in general, as the amount of noise is increased, the percent of error in the average predicted damage value is increased for both linear and nonlinear elements. Also, it is clear that the error percentage drops as the amount of damage in the elements are increased from 10% to 50%. For low noise (less than 3%) the methodology can predict damage as low as 10%. When noise is increased however, the damage location methodology fails to isolate the damaged degrees of freedom, which makes the methodology unable to predict damage. A final note is that the damage in nonlinear parameters is predicted significantly more accurately then the damage in linear parameters for the cases examined.

3.3.8 Effects of the Eigenvector Filtering Algorithms on Measurement Noise

The effectiveness of the filtering algorithms are demonstrated in several numerical simulations. The results are summarized in Tabs. 3.2 to 3.4. Tab. 3.2 shows the results obtained by using the iterative GMRPT method (presented in Sec. 3.2.2) for the nonlinear Kabe system (shown in Fig. 3.2) with 1%, 3%, and 5% random measurement noise, and for 100 separate numerical simulations. The linear spring connecting mass 2 to ground has a 10% reduction in stiffness, the nonlinear spring connecting mass 4 to ground has a 20% reduction in stiffness and the Colomb friction between mass 6 and ground has a 35% rise

Filters	Exact Percent Damage	Random Noise %		
		1	3	5
		Predicted % Damage		
No filter	10	9.9	9.8	-
	20	20.0	19.8	-
	35	28.0	24.3	-
Filter 1	10	10.0	9.9	-
	20	20.0	19.8	-
	35	28.7	23.5	-
Filter 1 and 2	10	10.0	10.0	9.9
	20	20.1	20.1	20.2
	35	35.1	34.7	30.5

Table 3.2: Identified percent damage and the effect of the eigenvector filtering algorithms on reducing noise in the Kabe System. Filter 1 was proposed by Zimmerman and Filter 2 is the new filtering algorithm proposed herein. The symbol $-$ indicates that the methodology was not used because the damage location could not be identified.

in friction Three cases were investigated, including a case where no filtering algorithms is used, a case where Zimmerman and Kaouk's filtering algorithm [1] is used alone, and a case where Zimmerman and Kaouk's filtering algorithm is used in conjunction with the new filtering algorithm proposed herein. The results in Tab. 3.2 show that the additional filtering algorithm helps reduce the effects of noise, and leads to average predicted damages closer to their exact values. In addition, since the new filtering algorithm is applied *before* the damage location algorithm is used, it helps the damage location algorithm as well, which allows the iterative GMRPT method to work for larger amounts of noise.

Similar to Tab. 3.2, Tab. 3.3 also shows results obtained by using the iterative GMRPT method, but for the nonlinear truss structure (shown in Fig. 3.3) with 2%, 5%, and 10% random measurement noise, and for 100 separate numerical simulations. The linear stiff-

Filters	Exact Percent Damage	Random Noise %		
		2	5	10
		Predicted % Damage		
No filter	10	10.7	-	-
	20	19.9	-	-
	35	28.0	-	-
Filter 1	10	9.8	-	-
	20	20.0	-	-
	35	30.3	-	-
Filter 1 and 2	10	10.0	9.9	10.4
	20	20.0	20.0	19.9
	35	30.0	30.3	28.3

Table 3.3: Identified percent damage and the effect of the eigenvector filtering algorithms on reducing noise in the 2 degree of freedom truss system. Filter 1 was proposed by Zimmerman and Filter 2 is the new filtering algorithm proposed herein. The symbol $-$ indicates that the methodology was not used because the damage location could not be identified.

ness connecting mass 2 to ground has 20% damage, the nonlinear spring connecting mass 2 to ground has 10% damage, and the Colomb friction at the second degree of freedom is increased by 30%. Each of these cases were performed for the same filtering scenarios as in Tab. 3.2. It is demonstrated that the additional filtering algorithm helps obtain a better estimate of the state of damage. Additionally, it enables the iterative GMRPT method to work for 5% and even 10% random measurement noise.

Tab. 3.4 shows the results obtained using the multiple augmentations GMRPT method (presented in Sec. 3.2.3) for the nonlinear 3-bay structure with 1%, 3%, and 5% random measurement noise, and for 100 separate numerical simulations. The linear beam connecting the 19th degree of freedom to ground is reduced by 10%, the nonlinear spring connecting the 13th degree of freedom to ground is reduced by 35%, and the nonlinear spring connecting the 25th degree of freedom to the 49th is reduced by 20%. The same filtering cases were performed as in Tab. 3.2. The additional filtering algorithm, generally alleviates the effects of noise and allows the multiple augmentations GMRPT method to

Filters	Exact Percent Damage	Random Noise %		
		1	3	5
		Predicted % Damage		
No filter	10	8.6	7.9	-
	20	20.0	19.2	-
	35	35.0	34.3	-
Filter 1	10	9.3	7.8	-
	20	20.0	19.4	-
	35	35.0	34.5	-
Filter 1 and 2	10	9.2	8.3	7.8
	20	19.9	19.9	19.8
	35	34.7	34.8	33.8

Table 3.4: Identified percent damage and the effect of the eigenvector filtering algorithms on reducing noise in the 3-bay structure. Filter 1 was proposed by Zimmerman and Filter 2 is the new filtering algorithm proposed herein. The symbol $-$ indicates that the methodology was not used because the damage location could not be identified.

operate well for larger amounts of random measurement noise.

3.4 Conclusions

In this chapter, a generalized damage detection methodology which is applicable to both linear and nonlinear systems was presented. The methodology uses a specially designed augmentation to model the nonlinear system, and a generalized minimum rank perturbation theory (GMRPT) to detect damage in the augmented system. The types of nonlinearities demonstrated herein include Colomb friction and cubic springs. An iterative GMRPT method was used to detect simultaneous damages in mass and stiffness parameters for lower-dimensional systems. Also, multiple augmentations GMRPT was used to determine damage in linear and nonlinear parameters when an incomplete set of right eigenvectors is available (and) for high-dimensional systems. Finally, two eigenvector filtering algorithms were presented that reduce the effects of random measurement noise on the accuracy of both damage detection methods. The new filtering algorithm enables these

methodologies to discern the damage location when the level of noise is larger, thus allowing damage to be detected accurately when the measurement data is more corrupted by noise. The algorithms proposed have been demonstrated numerically for several different nonlinear systems. The effectiveness of the proposed methods were demonstrated, and the effects of measurement errors were presented.

CHAPTER IV

Sensor Placement for Damage Detection in Nonlinear Systems using System Augmentations

4.1 Introduction

Large and complex air and space structures are being placed in new and extreme conditions for extended periods of time. As a result, the need for robust and accurate health monitoring techniques continues to grow. Ideally, these health monitoring techniques would have unrestricted access to sensor information from all the degrees of freedom of a finite element model used for monitoring the integrity of the structure. Practically, however, only a limited number of locations can be instrumented due to cost, weight and accessibility issues.

Most current sensor placement methodologies are focused on maximizing the controllability and observability of the healthy structure. For example, Cherng [31] identified the optimal placement of sensors and actuators for controllability and observability. That method examines the whole structure and selects sensor locations to maximize the signal to noise ratio in the system. Other approaches examine ways to minimize the information entropy norm, which is a measure of the uncertainty in parameter estimates. For example, Yuen et al. [32] proposed a sensor placement method designed for system identification and based on reducing entropy. That method requires choosing a number of damage-

able areas (each with an associated parameter) and placing an equal number of sensors to minimize the uncertainty in parameter estimates. Another technique, called the effective independence distribution vector (EIDV) method [33], selects sensor locations that make the measured partial eigenstructure as linearly independent as possible while capturing as much information as possible from the measured data. This method is based on capturing the dynamics of the healthy system.

Recently, several other techniques have been proposed, which are focused on sensor placement for damage detection. Cobb and Liebst [34] discussed one of the first such approaches. Their sensor placement technique makes no assumption about damage location but focuses instead on a sensitivity analysis to find the degrees of freedom which maximize the changes due to damage in the observable partial eigenstructure. The method does not control which damaged components of the system are detectable. Finally, other techniques are based on maximizing the Fischer information matrix to find the optimum sensor placement for damage detection [35, 36]. These methods make no assumption about the location of the damage; instead they localize the damage to particular scenarios using the Multiple Damage Location Assurance Criterion [79] before determining the extent of the damage.

The method herein uses a novel reduced order modeling method combined with an eigenvector sensitivity analysis to find which eigenvectors are most sensitive to the damageable regions of interest. These damageable regions of interest are defined based on knowledge that certain regions of the system are the most likely points of damage (hot spots). This differs significantly from classical reduced order modeling (ROM) techniques [64–70] that model the dynamics of the system and, therefore, are interested in the first few modes of the system. Instead, herein a reduced order health assessment (ROHA) methodology is developed to capture *changes* in the dynamics, which lead to different

modes being of interest.

This work develops a novel sensor placement methodology specifically designed for damage detection. It places sensors at the hot spots of the system. If additional sensors need to be placed, or if certain characteristics of the hot spots of the system make placing sensors difficult or impossible, then a generalized EIDV can be formulated to place the remaining sensors.

The physical measured displacements and forcing of the structure are filtered in the frequency domain to keep only frequencies that are near the frequencies of the eigenmodes used in the projection matrix. Modal information corresponding to the measurement locations can then be extracted. This (partial) modal information can be expanded (to full modal information) by an approach which enforces that damage can only occur in the hot spots of the system. Any number of modal based damage detection methods, such as minimum rank perturbation theory [1, 27–29] (MRPT) or optimal matrix update approaches [25, 26], can be used to calculate the damage. However, to provide additional noise rejection, a novel method called damage identification by hot spot projection (DIHSP) is presented in this chapter.

One of the advantages of the integrated sensor placement and damage detection methodology demonstrated herein is that it can be applied to both linear and nonlinear systems if the nonlinear system can be modeled by augmented systems previously proposed [73, 80]. These augmented systems are of higher dimension than their corresponding nonlinear systems. If the augmented systems are projected into the lower dimension space of the nonlinear system, they will follow a single trajectory of the nonlinear system. Linear modal extraction methods can be used with augmented systems if the identification method uses a forcing that is known but not prescribed such as direct system parameter identification [7] (DSPI) or vector backward auto-regressive with exogenous modeling [81]. A linear dam-

age detection methodology called generalized MRPT (GMRPT) has been previously developed for these augmented systems [73, 80].

In this work, the ROHA methodology is detailed for detecting damage in the hot spots of linear and nonlinear (augmented) systems with few measurements. Next, the methodology for an improved sensor placement is laid out for linear and nonlinear (augmented) systems. Then, the MRPT and DIHSP damage detection methodologies are explained. Finally, linear and nonlinear 5-bay frames are used for various tests illustrating the effectiveness of the proposed techniques.

4.2 Methodology

In this section, system augmentation for nonlinear systems is reviewed. Next, a novel reduced order health assessment (ROHA) methodology for determining the full mode shape of linear and nonlinear (augmented) systems from partial measurement data is explained. Additionally, an improved sensor placement algorithm is introduced for linear and nonlinear systems when ROHA is employed. A damage detection technique based on minimum rank perturbation theory (MRPT) is overviewed, and then damage identification by hot spot projection (DIHSP) is presented. Finally, filtering algorithms to reduce the effects of noise are discussed.

4.2.1 System Augmentation

A detailed explanation of system augmentation for nonlinear systems can be found in previous work [73, 80]. In this section, a brief overview of system augmentation is explored through a simple example of a two degree of freedom nonlinear system.

Consider a two degree of freedom mass-spring system with one cubic nonlinearity

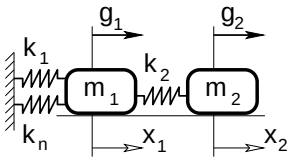

Figure 4.1: Two degree of freedom nonlinear mass-spring system

(shown in Fig. 4.1). This system can be characterized by the following equations of motion

$$\begin{aligned} m_1\ddot{x}_1 + (k_1+k_2)x_1 - k_2x_2 + k_nx_1^3 &= g_1(t), \\ m_2\ddot{x}_2 - k_2x_1 + k_2x_2 &= g_2(t), \end{aligned} \tag{4.1}$$

where m_i, k_i, k_n, $g_i(t)$ and x_i correspond to mass, linear spring stiffness, cubic spring stiffness, linear forcing, and displacement of the system, respectively.

The system augmentation approach consists of constructing a higher dimensional (augmented) system that follows a single trajectory of the nonlinear system when projected down onto the lower dimensional (physical) space. The augmented system is constructed by creating augmented variables y_i for each nonlinearity in the system. For the system characterized by Eq. (4.1), only one augmented variable $y = x_1^3$ is created. Each augmented variable corresponds to one degree of freedom added to the system, and therefore one added equation of motion. The augmented equations of motion for Eq. (4.1) are

$$\begin{aligned} m_1\ddot{x}_1 + (k_1+k_2)x_1 - k_2x_2 + k_{n1}y &= g_1(t), \\ m_2\ddot{x}_2 - k_2x_1 + k_2x_2 &= g_2(t), \\ m_a\ddot{y} + k_cx_1 + k_ay &= h(t), \end{aligned} \tag{4.2}$$

where m_a, k_a, k_c, and $h(t)$ correspond to the augmented mass, augmented stiffness, coupled stiffness, and augmented forcing, respectively. The parameters m_a, k_a, and k_c are not

unique and are chosen by the user to optimally suit their needs. The augmented forcing $h(t)$ is computed directly from the left side of Eq. (4.2), since m_a, k_a, and k_c are chosen by the user, x_1 is measured, and y is calculated by its dependence on x_1 (i.e. $y = x_1^3$).

The construction of the specific augmented forcing is what constrains the augmented linear system to exactly follow the nonlinear system when projected onto the lower dimensional space (spanned by x_1, x_2, $\dot{x}_1$, and $\dot{x}_2$). A consequence of the augmented forcing is that modal analysis techniques that are used with augmented systems must be input-output approaches (as opposed to output only approaches). DSPI is a multi-input multi-output, time-based modal analysis approach that has been used successfully with augmented linear systems [73, 80]. An additional consequence of the system augmentation approach is that the degrees of freedom that contain the nonlinearity must be measured to construct the augmented variable. For example, in the system given by Eq. (4.1), x_1 has to be measured to construct the augmented variable $y = x_1^3$.

4.2.2 Reduced Order Health Assessment

In this section, the procedure for extracting the full mode shapes that are most sensitive to damage in the hot spots of the system is outlined.

Modal based damage detection techniques are only effective when the modes that are used are sensitive to the damages. Reduced order health assessment (ROHA) is therefore formulated to determine the full mode shapes (that are most sensitive to changes in the hot spots of the system) from limited sensor information. These damages are chosen on the basis that, in many structures, the hot spot locations are known. A sensitivity rating $\mathbf{r}$ of the eigenvectors to the s different damage scenarios is evaluated as

$$r_i = \sum_{j=1}^{s} \mathbf{v}_{hi}^T \mathbf{M} \mathbf{v}_{dij}, \tag{4.3}$$

where i denotes the eigenvector number, j denotes the damage scenario, and $\mathbf{v}_h$ and $\mathbf{v}_d$

are the (augmented) eigenvectors for the healthy and damaged systems, respectively. A projection matrix that consists of the n eigenvectors with the highest sensitivity (lowest r_i) is denoted by $\mathbf{P}$. The dimensions of $\mathbf{P}$ are $N \times n$, where N is the size of the full system, and $n << N$.

To accurately extract the partial modes of the system corresponding to the sensitive eigenvectors, the measured forcing and positions of the system must be filtered appropriately. Consider the case where p sensors measure the degrees of freedom $\mathbf{x}_m$ of the full model. The remaining unmeasured degrees of freedom are denoted by $\mathbf{x}_u$. The forcing $\mathbf{F}$ is measured. In the nonlinear case, $\mathbf{x}_m$ contains all the augmented variables, and $\mathbf{F}$ contains the augmented forcing. The indices of the degrees of freedom of the system are re-ordered such that the measured degrees of freedom of the system are the first. Then, the full coordinates of the system, $\mathbf{x}$ can be written as

$$\mathbf{x} = \begin{bmatrix} \mathbf{x}_m \\ \\ \mathbf{x}_u \end{bmatrix}. \tag{4.4}$$

The modal content of $\mathbf{x}_m$ and $\mathbf{F}$ can be filtered by taking a Fourier transform of $\mathbf{x}_m$ and $\mathbf{F}$, and filtering out all frequencies except the ones near the healthy natural frequencies of the desired reduced modes. The bandwidth of the frequency filter depends on the system of interest. In particular, the changes in the frequencies due to changes in the hot spots of the system are the determining factors in the bandwidth. Due to the filtering algorithm, it is preferable to extract grouped frequencies over a specified range, rather than isolated frequencies. The filtered frequency domain data can then be returned to the time domain via an inverse Fourier transform, yielding $\mathbf{x}_{mf}$ and $\mathbf{F}_f$ corresponding to a filtered $\mathbf{x}_m$ and $\mathbf{F}$, respectively. The input data of a modal analysis approach, such as DSPI, is the filtered measurements $\mathbf{x}_{mf}$ and $\mathbf{F}_f$. DSPI is invariant to possible phase distortions caused by the inverse Fourier transform if the filtering is done similarly to both displacements and

forcing. That leads to phase distortions occurring in the same manner in both the input and output used by DSPI, and as a result the features extracted (frequencies and partial mode shapes) are unaffected by the distortions.

The coordinates of the system can be transformed into modal coordinates as follows

$$\mathbf{x} = \begin{bmatrix} \mathbf{x}_m \\ \\ \mathbf{x}_u \end{bmatrix} = \sum_{i=1}^{n} c_i(t)\mathbf{v}_{ki} + \sum_{j=n+1}^{N} c_j(t)\mathbf{v}_{rj}, \tag{4.5}$$

where $\mathbf{v}_k$ corresponds to the kept modes of the damaged system, $\mathbf{v}_r$ corresponds to the removed modes of the damaged system, and $c_i(t)$ are time varying coefficients. The filtering process that produces $\mathbf{x}_{mf}$ and $\mathbf{F}_f$ forces $c_j(t)$ to be zero for $j = n+1 \ldots N$, which gives the following filtered response in modal coordinates

$$\mathbf{x}_f = \begin{bmatrix} \mathbf{x}_{mf} \\ \\ \mathbf{x}_{uf} \end{bmatrix} = \sum_{i=1}^{n} c_i(t)\mathbf{v}_{ki} = \mathbf{P}_d\mathbf{c}, \tag{4.6}$$

where

$$\begin{aligned} \mathbf{P}_d &= \begin{bmatrix} \mathbf{v}_{k1} & \mathbf{v}_{k2} \ldots \mathbf{v}_{kn} \end{bmatrix}, \\ \mathbf{c} &= \begin{bmatrix} c_1(t) & c_2(t) \ldots c_n(t) \end{bmatrix}^T. \end{aligned}$$

The output from a modal analysis approach such as DSPI is a matrix $\mathbf{P}_{dm}$ which contains partial modal information, as indicated by the subscript m (that corresponds to the degrees of freedom that relate to the measured ones in $\mathbf{x}$).

Next, one may expand each partial mode shape from $\mathbf{P}_{dm}$ to the full space using the fact that damage is limited to the hot spots of the system. A damage location vector $\mathbf{d}_i$ used in MRPT [1], can be defined as follows (when, for example, damage only occurs in the stiffness matrix of an undamped system)

$$\mathbf{d}_i \equiv \left(\lambda_{di}^2\mathbf{M} + \mathbf{K}\right)\mathbf{v}_{di} = \Delta\mathbf{K}\mathbf{v}_{di}, \tag{4.7}$$

where $\mathbf{d}_i$ is the perturbation vector for the i^{th} eigenvector $\mathbf{v}_{di}$ and natural frequency λ_{di}. Matrices $\mathbf{M}$ and $\mathbf{K}$ are the (known) healthy mass and stiffness matrices, and $\Delta\mathbf{K}$ is the change in the healthy stiffness matrix.

The entries in $\mathbf{d}_i$ that correspond to degrees of freedom in the system that are undamageable (not in the hot spots) are known to be exactly zero. Therefore, if the number of measured degrees of freedom p is equal to or greater than the number q of degrees of freedom that are damageable, then there are at least as many equations (from Eq. (4.7)) as unknowns, and the inverse problem can be solved to obtain a unique solution. Two matrices $\mathbf{\Phi}_i$ (of size $(N-q)\times p$) and $\mathbf{\Psi}_i$ (of size $(N-q)\times(N-p)$) can be defined such that

$$[\mathbf{\Phi}_i \quad \mathbf{\Psi}_i] = \lambda_{di}^2\tilde{\mathbf{M}} + \tilde{\mathbf{K}} = \mathbf{A}_i, \tag{4.8}$$

where $\tilde{\mathbf{M}}$ and $\tilde{\mathbf{K}}$ are matrices of size $(N-q)\times N$ that are composed only of the rows of $\mathbf{M}$ and $\mathbf{K}$ that correspond to the undamageable degrees of freedom. If the system is nonlinear, then the augmented degrees of freedom are not contained in $\tilde{\mathbf{M}}$ and $\tilde{\mathbf{K}}$ (even though they are undamageable). Combining Eqs. (4.7) and (4.8), one obtains

$$\begin{aligned}
\mathbf{0} &= [\mathbf{\Phi}_i \quad \mathbf{\Psi}_i]\begin{bmatrix}\mathbf{v}_{mi}\\ \\ \mathbf{v}_{ui}\end{bmatrix},\\
\mathbf{0} &= \mathbf{\Phi}_i\mathbf{v}_{mi} + \mathbf{\Psi}_i\mathbf{v}_{ui},\\
\mathbf{v}_{ui} &= -\mathbf{\Psi}_i^{+}\mathbf{\Phi}_i\mathbf{v}_{mi},
\end{aligned} \tag{4.9}$$

where $\mathbf{v}_{mi}$ is the i^{th} column of $\mathbf{P}_{dm}$ and represents the measured portion of the i^{th} eigenvector given by the modal analysis technique, while $\mathbf{v}_{ui}$ is the corresponding unmeasured portion of that eigenvector, and $\mathbf{\Psi}_i^{+}$ is the pseudo-inverse of $\mathbf{\Psi}_i$. The system is well conditioned if the number of measured degrees of freedom is equal to or greater than the number of degrees of freedom that are damageable, and $\mathbf{\Psi}_i$ is full rank. One way to ensure that $\mathbf{\Psi}_i$

is full rank is to properly choose the sensor locations, which is discussed next.

4.2.3 Sensor Placement

In this section, the sensor placement methodology is explained for linear and nonlinear systems. Of course, in the very few cases where there is exactly the same number of sensors as degrees of freedom, and the sensors can be placed anywhere, they are placed at the hot spots. For the nonlinear case, sensors must be placed at the degrees of freedom that contain nonlinearities. Often however, additional sensors may be used to reduce the effects of measurement noise. Also, some hot spots may not allow the placement of sensors nearby. In either of these cases, a generalized EIDV [33] method can be used to place the remaining sensors, as described next.

The goal of the generalized EIDV sensor placement methodology is to find the locations of sensors that lead to the largest minimum singular values of $\mathbf{\Psi}_i$ for all i, where $\mathbf{\Psi}_i$ contains $N - p$ columns of $\mathbf{A}_i$ in Eq. (4.8). Hence, EIDV [33] can be used on $\mathbf{A}_i$ to determine which columns of $\mathbf{A}_i$ contribute the least to the rank of $\mathbf{A}_i$, and then remove them. The procedure for EIDV is to form the matrix $\mathbf{E}_i$ given by [33]

$$\mathbf{E}_i = \mathbf{A}_i^T(\mathbf{A}_i\mathbf{A}_i^T)^{-1}\mathbf{A}_i. \tag{4.10}$$

Matrix $\mathbf{E}_i$ is an idempotent matrix with the property that its trace equals its rank. The lowest entry along the diagonal of $\mathbf{E}_i$ corresponds to the smallest contribution to the rank, and hence, the corresponding column can be removed. Matrix $\mathbf{A}_i$ is then recalculated without the removed column, and the process is repeated.

Since there are n matrices $\mathbf{A}_i$ to be optimized at each step, the generalized EIDV requires n matrices $\mathbf{E}_i$ to be formed simultaneously. Then, the entries of the diagonals of each $\mathbf{E}_i$ are squared. Finally, the diagonals are summed, the column corresponding to the minimum value is removed, and the process is repeated. When there are more sensors than

hot spots, $\mathbf{A}_i$ is replaced with $\mathbf{A}_i^T$ in Eq. (4.10) to yield

$$\mathbf{E}_i = \mathbf{A}_i(\mathbf{A}_i^T\mathbf{A}_i)^{-1}\mathbf{A}_i^T. \tag{4.11}$$

With this small adjustment, the rest of the search process is the same.

Note that the damaged natural frequencies are not known until after damage occurs. Therefore, healthy natural frequencies must be used in Eq. (4.8) in order to calculate $\mathbf{A}_i$ for sensor placement.

The procedure is similar for nonlinear systems modeled through augmentation. The only difference is that columns associated with the augmented degrees of freedom and the linear degrees of freedom that contain the nonlinearity are removed from $\mathbf{A}_i$ at the beginning of the procedure along with the sensors that can be placed at the hot spots. This is because those degrees of freedom have to be measured to form the augmented system [73].

4.2.4 Damage Detection Methodology: MRPT

A variety of modal based damage detection methods can use the modes given by Eq. (4.9) to identify damage. In this section, minimum rank perturbation theory (MRPT) [1] is discussed.

MRPT was developed on the basis that damage often occurs first at localized regions of the system. Therefore, a minimum rank solution to the perturbation equations can be used. For example, for a system with damage in stiffness only (and no damping), the perturbation equations are defined in Eq. (4.7). The minimum rank solution to the perturbation equations for $\Delta\mathbf{K}$ (using MRPT and a subspace selection algorithm) is given by [1]

$$\Delta\mathbf{K} = \mathbf{B}\mathbf{Z}\left(\mathbf{Z}^T\mathbf{B}^T\mathbf{P}_d\mathbf{Z}\right)^{-1}\mathbf{Z}^T\mathbf{B}^T, \tag{4.12}$$

where $\mathbf{B} = [\mathbf{d}_1 \quad \mathbf{d}_2 \dots \mathbf{d}_n]$, $\mathbf{Z} = \mathbf{V}\mathbf{\Sigma}_\epsilon$, $\mathbf{B} = \mathbf{U}\mathbf{\Sigma}\mathbf{V}^T$, and $\mathbf{U}$, $\mathbf{\Sigma}$, and $\mathbf{V}$ form the standard singular value decomposition of matrix $\mathbf{B}$, while $\mathbf{\Sigma}_\epsilon$ contains the singular values that are greater than a tolerance level ϵ.

If the system is an augmented one, damage is first calculated in the nonlinear parameters using the multiple augmentations approach previously developed [80].

4.2.5 Damage Detection Methodology: DIHSP

This section introduces an alternate damage detection methodology (to MRPT) called damage identification by hot spot projection (DIHSP). This approach has been developed on the basis that damage is constrained to a linear combination of s possible damage scenarios (or hot spots).

The eigenvalue problem for n modes of the damaged system can be written as

$$\mathbf{M}\mathbf{P}_d\mathbf{\Lambda}_d^2 + \mathbf{K}\mathbf{P}_d = \Delta\mathbf{K}\mathbf{P}_d, \tag{4.13}$$

where $\mathbf{\Lambda}_d = \mathrm{diag}\,[\lambda_{d1} \quad \lambda_{d2} \dots \lambda_{dn}]$. Eq. (4.13) can be projected onto a reduced space by premultiplying it by $\mathbf{P}_d^T$ to obtain reduced order matrices $\Delta\bar{\mathbf{K}}$ as

$$\mathbf{P}_d^T\mathbf{M}\mathbf{P}_d\mathbf{\Lambda}_d^2 + \mathbf{P}_d^T\mathbf{K}\mathbf{P}_d = \mathbf{P}_d^T\Delta\mathbf{K}\mathbf{P}_d = \Delta\bar{\mathbf{K}}. \tag{4.14}$$

Using the knowledge that only certain regions of the system are damageable, different $\Delta\bar{\mathbf{K}}_i'$ can be generated as a set of basis matrices for damage in the reduced space. A requirement of these basis matrices is that they are linearly independent. These basis matrices are calculated by transforming the physical damage scenarios to the reduced ones using the following relation

$$\mathbf{P}_d^T\Delta\mathbf{K}_i\mathbf{P}_d = \Delta\bar{\mathbf{K}}_i', \tag{4.15}$$

where $\Delta\mathbf{K}_i$ is the damage in the stiffness matrix in the full (augmented) space, and $i =$

$1 \ldots s$ corresponds to the damage scenario. The damage predicted can then be written as

$$\Delta\bar{\mathbf{K}} = \sum_{i=1}^{s} \Delta\bar{\mathbf{K}}_i' \alpha_i, \tag{4.16}$$

where α_i corresponds to the level of damage corresponding to the i^{th} damage scenario.

If the matrices $\Delta\bar{\mathbf{K}}_i'$ from Eq. (4.16) are transformed into column vectors by stacking the columns of each matrix on top of each other, vectors of size n^2 will result. When $n^2 > s$ and the $\Delta\bar{\mathbf{K}}_i'$ matrices are independent, an over determined set of equations results for calculating the damage, and α_i can be obtained from Eq. (4.16) (from the computed $\Delta\bar{\mathbf{K}}_i'$ and measured $\Delta\bar{\mathbf{K}}$).

4.2.6 Filtering Algorithms

There are two filtering algorithms that can be used with the DIHSP and MRPT methodologies to reduce the effects of noise. The first filtering algorithm uses the fact that different damage scenarios affect the natural frequencies of the system differently. This filtering can be implemented by first determining which natural frequencies are changed significantly by each damage scenario (in the damage range of interest). After damage occurs, the natural frequencies can be inspected to identify which ones were affected. Finally, any damage scenario that would cause a change in a natural frequency of the system that remains unaffected is eliminated as a possible damage scenario. This information can be used in Eq. (4.15). Essentially, basis matrices $\Delta\bar{\mathbf{K}}_i'$ do not have to be computed for the eliminated damage scenarios, which filters out any damage that would be erroneously predicted in that space (due to measurement noise). This filtering algorithm is particularly powerful for cases where damages occur in only a few damage scenarios.

The second filtering algorithm is based on the fact that the minimum singular values of the different $\mathbf{\Psi}_i$ matrices can be different in scale. A threshold value can be used such that if the minimum singular value for a given i is lower than the threshold, then that $\mathbf{\Psi}_i$

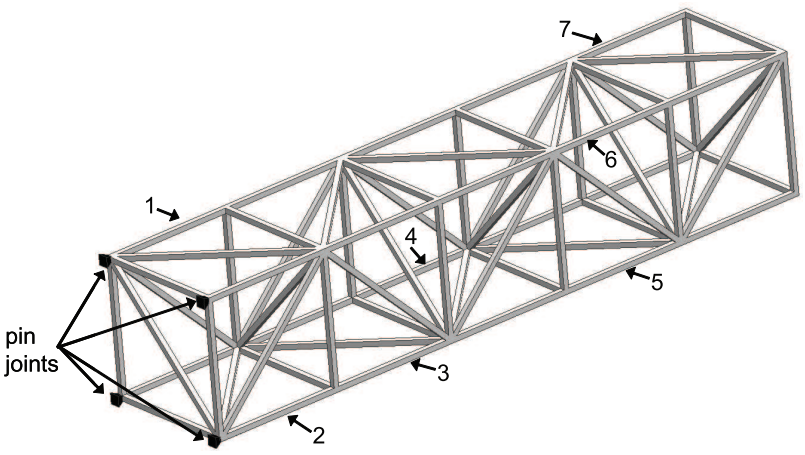

Figure 4.2: A linear 5-bay frame structure

would not be used (in turn, the eigenvector it corresponds to would not be calculated). This filtering algorithm is important because the singular values of $\mathbf{\Psi}_i$ are not known until after damage occurs (and the natural frequencies of the damaged system can be measured).

4.3 Numerical Results

To demonstrate the proposed methodology, a numerical analysis of linear and non-linear frame structures was implemented. The linear frame structure shown in Fig. 4.2 consists of 70 steel beams connected at 24 nodes, 4 of which are pinned to the ground. The elastic modulus of the steel used is $200GPa$ and its density is $7845kg/m^3$. The length of the entire structure is $2.5m$, while the width and height of the entire structure are $0.5m$. The cross section of each individual beam is a $30mm$ wide, hollow square with a $1mm$ wall thickness. The damageable portions of the linear system were chosen as the transverse (bending) stiffnesses of the 20 longitudinal beams. A finite element model for the structure was constructed using 5 beam elements to discretize each of the beams that are not aligned in the longitudinal (horizontal) direction, for a total of 1332 degrees of

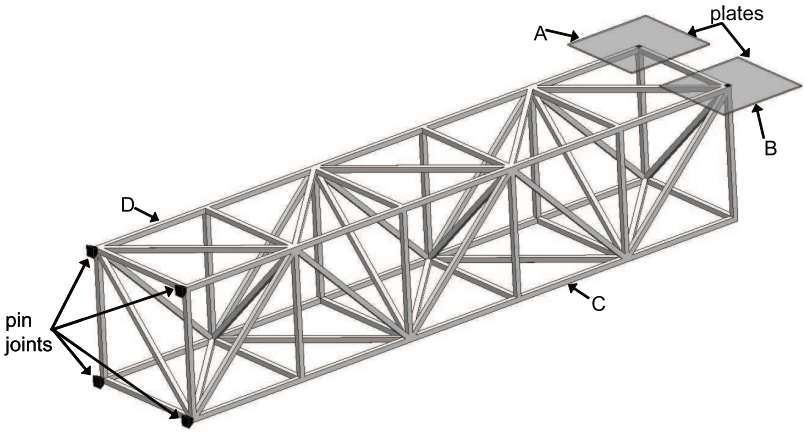

Figure 4.3: A linear 5-bay structure with 2 plates which introduce cubic stiffness nonlinearities

freedom. To verify that this discretization is converged, the frequencies and mode shapes for this model were compared to those given by a much more refined model, where 20 beam elements were used to discretize each and every beam in the structure. The first 50 frequencies and mode shapes for the two models were in very good agreement.

The nonlinear frame structure shown in Fig. 4.3 consists of the same linear frame structure as in Fig. 4.2 with the addition of two plates connected to the frame at their center. These plates are pinned to the ground at their perimeter. Hence, they exhibit stretching induced by bending. Using a one mode Galerkin approximation for each plate, a linear and cubic stiffness is introduced to the frame structure at the point of attachment. The characteristics of the plates are such that the stiffness of the cubic spring nonlinearity added to the system by each plate is $60MN/m^3$. The damageable portions of the nonlinear system were chosen as the transverse stiffness of the 20 longitudinal beams and the two plates. The full augmented linear system has a total of 1334 degrees of freedom.

In the following sections, several important aspects of the novel methodology are highlighted. First, the differences between ROM and ROHA are explored. Second, a compari-

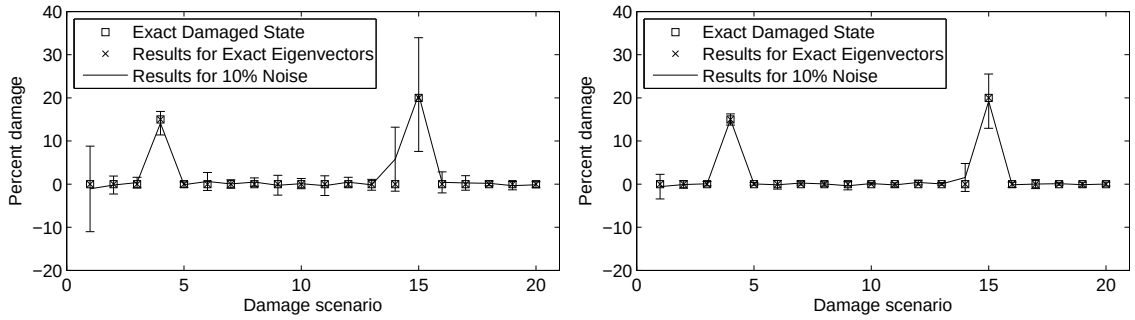

(a) ROM (b) ROHA

Figure 4.4: Predicted damage in the linear 5-bay frame with damage at 2 locations and 10% random eigenvector noise using the first 20 modes of the system (a) and using 20 sensitive modes to damage in the hot spots (b)

son case is setup for MRPT and DIHSP. Then, the robustness of the algorithm for damage outside of the hot spots is explored. Next, the effects of the filtering algorithms and the placement of additional sensors are illustrated. Finally, damage cases for the nonlinear frame system are examined.

Sensors were placed at the hot spots for all the results obtained. In the linear system, that implies that the sensors measure the transverse displacement of the 20 longitudinal beams. The nonlinear system has the same 20 sensors as the linear system.

4.3.1 ROHA vs. ROM

This section highlights the differences between a ROM type method and ROHA. ROM is designed to predict the system dynamics. In contrast, ROHA is designed to predict *changes* in the system dynamics. ROM uses the first (dominant) several modes of the system to capture the dynamics of the system. This fundamentally differs from ROHA which uses the eigenvectors sensitive to changes in the hot spots of the system. In contrast to a usual ROM, in this work, the modes chosen for ROHA were the 11^{th} through 30^{th}.

Fig. 4.4 illustrates the difference in applying the ROM method and using the first 20

modes as opposed to more sensitive modes obtained by using ROHA and Eq. (4.3). The case plotted in Fig. 4.4 is for a 15% loss of transverse stiffness in beam 2, and a 20% loss of transverse stiffness in beam 6, where these beam numbers are shown in Fig. 4.2. Standard deviation error bars are plotted for the 100 separate numerical simulations in which 10% random eigenvector noise was added. The noise was added into the partial eigenstructure. The x-axis in each plot represents the 20 damage scenarios (i.e. the 20 transverse stiffnesses of the 20 longitudinal beams). The y-axis in each plot represents the percent damage for each scenario. No filtering algorithm was applied for this case, and 20 sensors were used. DIHSP was the damage methodology used to obtain the results. Fig. 4.4(a) shows results obtained using the dominant modes of the system, while Fig. 4.4(b) shows results obtained using the sensitive modes of the system. In both plots it is shown that for the case of zero noise, damage is predicted exactly. For 10% noise, the actual damage is also predicted accurately. However, the results in Fig. 4.4(a) show that the deviation in the damage locations is significantly larger and there are damages predicted by ROM in two other damage scenarios where there is no damage.

4.3.2 DIHSP vs. MRPT

In this section, the differences between DIHSP and MRPT are explored. The results for both methodologies in a case with a 15% loss of stiffness in beam 4, 30% loss in beam 5, and 20% loss in beam 7 are plotted in Fig. 4.5. For 5% random eigenvector noise, 100 separate numerical simulations were performed and standard deviation error bars are plotted. The x-axis in each plot represents the index of a column vector obtained from storing the upper triangular portion of the perturbation stiffness matrix ($\Delta\mathbf{K}$) into a column vector. The y-axis in the plots represents the entries of the difference $\Delta\mathbf{K}$ between the original and updated stiffness matrices. In both cases the filtering method that eliminates

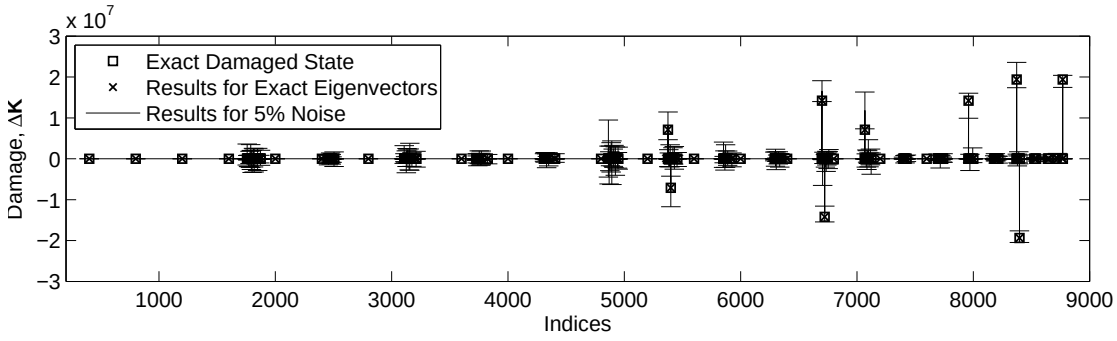

(a) MRPT

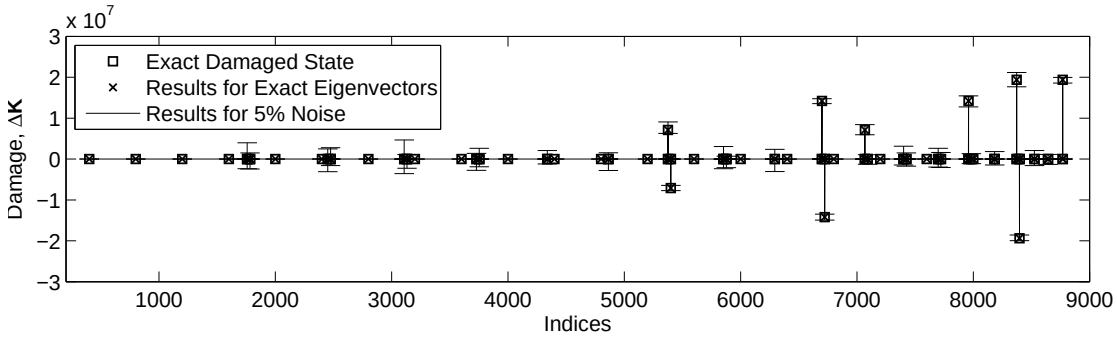

(b) DIHSP

Figure 4.5: Predicted damage in the linear 5-bay frame with damage at 3 locations and 5% random eigenvector noise using 20 sensors to find damage using MRPT (a) and using DIHSP (b)

damage scenarios based on the shift in frequencies was used.

Fig. 4.5(a) shows results for the case where MRPT was used to predict damage, while Fig. 4.5(b) shows results for the case where DIHSP was used. Damage is predicted exactly by each methodology when the noise is zero. For 5% noise, the results in Fig. 4.5 show that DIHSP predicts damage more accurately than MRPT. Also, DIHSP predicts fewer false damages elsewhere in the system.

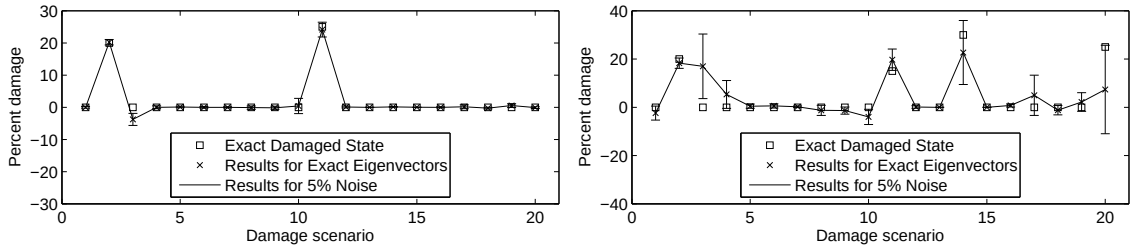

(a) (b)

Figure 4.6: Predicted damage in the linear 5-bay frame with damage in 2 hot spots and 1 other location (a) and with damage in 4 hot spots and 2 other locations (b) with 5% random eigenvector noise using 20 sensors

4.3.3 Robustness

In this section, the robustness of the methodology to damages outside of the hot spots is explored. Fig. 4.6(a) contains results for a 20% loss of transverse stiffness in beam 1, and a 25% loss of transverse stiffness in beam 4, where these beam numbers are shown in Fig. 4.2. Additionally, there is 25% loss of longitudinal stiffness in beam 7. The last damage was not part of the 20 allowable damage scenarios for the linear system. The plot in Fig. 4.6(a) is structured in the same way as in Fig. 4.4. Standard deviation error bars are plotted for 100 separate numerical simulations in which 5% random eigenvector noise was added.

Fig. 4.6(a) shows that, when there is zero noise, exact damage is not predicted because there are damages that are occurring in the system at locations assumed undamageable. Although the damages to the system in and out of the hot spots are of a similar level, the method predicts the damage in the hot spots within about 2% of the actual damage (and DIHSP does not predict any damage outside of the hot spots). Also, very little false damage is predicted in the other damage scenarios. For 5% random eigenvector noise, the damage is still predicted well with the largest deviation of about 2% occurring at the 3$^{\text{rd}}$

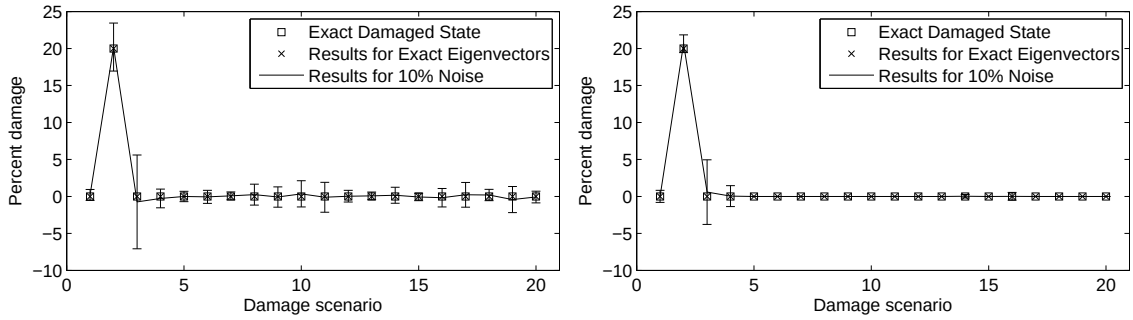

(a) Filter off (b) Filter on

Figure 4.7: Predicted damage in the linear 5-bay frame with damage at one location and 10% random eigenvector noise using 20 sensors without the frequency shift filter (a) and with the frequency shift filter (b)

damage scenario.

Fig. 4.6(b) shows results for a 20% loss of transverse stiffness in beam 1, a 15% loss in beam 4, a 30% loss in beam 5, and a 25% loss in beam 7 where these beam numbers are shown in Fig. 4.2. Additionally, there is 20% loss of longitudinal stiffness in beam 1, and a 10% loss of longitudinal stiffness in beam 3. The latter two damages were not part of the 20 allowable damage scenarios for the linear system. The plot in Fig. 4.6(b) is structured in the same way as in Fig. 4.4. Standard deviation error bars are plotted for 100 separate numerical simulations in which 5% random eigenvector noise was added.

Fig. 4.6(b) shows that, when there is zero noise, exact damage is not predicted because there are damages that are occurring in the system at locations outside of the assumed hot spots. In this case, the results are not as good as those in Fig. 4.6(a) due to the large number of damages that are occurring simultaneously. Although the damage at locations where there is actual damage is predicted relatively accurately in all cases except one, there is a significant amount of false damage predicted in the 3^{rd}, 4^{th} and 17^{th} damage scenarios in particular.

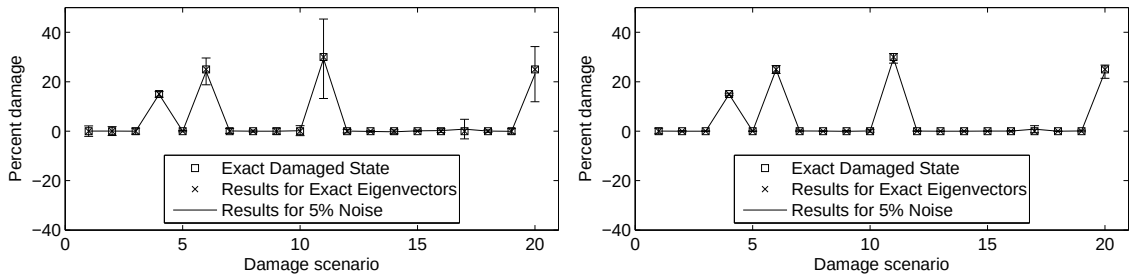

(a) Results for 20 sensors

(b) Results for 21 sensors

Figure 4.8: Predicted damage in the linear 5-bay frame with damage at 4 locations and 5% random eigenvector noise using 20 sensors (a) and using 21 sensors (b)

4.3.4 Filtering

In this section, the benefit of the filtering algorithm, which eliminates damage scenarios based on the shift in frequencies, is demonstrated.

Fig. 4.7 shows results for a case with a 20% loss of stiffness in beam 1. The plots in Fig. 4.7 are structured in the same way as in Fig. 4.4. Standard deviation error bars are plotted for 100 separate numerical simulations in which 10% random eigenvector noise was added. Fig. 4.7(a) shows results for the case without filtering, and Fig. 4.7(b) shows results for the case with filtering. When there is zero noise, both cases predict damage exactly. For 10% noise, both cases predict the damage to a similar level of accuracy, but the results obtained using filtering (Fig. 4.7(b)) exhibit less noise in the other damage scenarios (where there is no damage).

4.3.5 Effect of Additional Sensors

In this section, the benefit of using additional sensors is illustrated. Fig. 4.8 shows results for a case with a 15% loss of stiffness in beam 2, 25% loss in beam 3, 30% loss in beam 4, and 25% loss in beam 7. The plots in Fig. 4.8 are structured in the same way as in Fig. 4.4. For 5% random eigenvector noise, 100 separate numerical simulations were

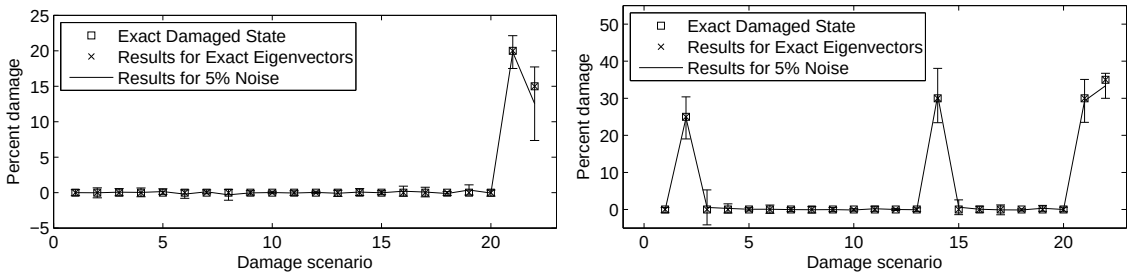

(a) (b)

Figure 4.9: Predicted damage in the nonlinear 5-bay frame with damage in both cubic stiffnesses (a) and with damage in both cubic stiffnesses and 2 linear hot spots (b) with 5% random eigenvector noise using 20 sensors

performed and standard deviation error bars are plotted. Fig. 4.8(a) shows results for the case where 20 sensors are used, and Fig. 4.8(b) shows results for the case where 21 sensors are used. The one sensor added to the 20 located at the hot spots was placed using the generalized EIDV method. When there is zero noise, both sensor placements predict damage exactly. For 5% noise, the 21 sensors (Fig. 4.8(b)) predict the damage significantly better in the scenarios with damage, and predict significantly fewer false damages compared to the results obtained using 20 sensors (Fig. 4.8(a)).

4.3.6 Nonlinear 5-Bay Structure

In this section, the use of ROHA and DIHSP is demonstrated for determining damage in linear and nonlinear elements of the nonlinear structure shown in Fig. 4.3.

Fig. 4.9(a) shows results for a case with a 15% loss of stiffness in plate A, and 20% loss in plate B (see Fig. 4.3). The plot in Fig. 4.9(a) is structured in the same way as in Fig. 4.4. Standard deviation error bars are plotted for 100 separate numerical simulations in which 5% random eigenvector noise was added. When there is zero noise, exact damage is predicted. For 5% noise, the actual damage is predicted very accurately.

Fig. 4.9(b) shows the results for a case with a 35% loss of stiffness in plate A, 30%

loss in plate B, 30% loss in beam C, and 25% loss in beam D (see Fig. 4.3). The plot in Fig. 4.9(b) is structured in the same way as in Fig. 4.4. Standard deviation error bars are plotted for 100 separate numerical simulations in which 5% random eigenvector noise was added. When there is zero noise, exact damage is predicted. For 5% noise, the actual damage is predicted very accurately, with little false damage predicted in other scenarios.

4.4 Discussion

Several new ideas are incorporated into this integrated sensor placement and damage detection methodology. A major aspect of the methodology is ROHA. ROHA differs fundamentally from ROM techniques in its goal. ROM techniques are utilized to capture the dynamics of the system. Therefore, they use the dominant modes of the system, which tend to be the modes corresponding to the lowest frequencies of the system. In contrast, ROHA is used to characterize changes in the dynamics, and as a result employs the modes that are sensitive to changes in the hot spots of the system. ROHA uses a frequency filtering algorithm to remove frequency content of the modes outside the selected modes so that the partial eigenstructure obtained corresponds to the desired modes. The partial modes are then expanded to the full space using information about the possible damage locations. Other algorithms that expand the modes within the small dimensional space of a set of the healthy eigenvectors fail because damages cause the eigenvectors to vary/rotate into the space of a large number of eigenvectors of the original healthy system.

Another major aspect of the methodology is the improved sensor placement. For the case where the number of sensors equals the number of damageable degrees of freedom, and the hot spots of the system are accessible, the sensors are placed at the hot spots of the system. If additional sensors can be used, a generalized EIDV method can be applied to place these sensors (especially when some hot spots are inaccessible for sensor placement).

EIDV is inherently a quasi-optimal method in that it finds the optimal sensor choice at each step, but all the choices together do not necessarily lead to the global optimum sensor placement. However, using EIDV to place the remaining sensors is effective since EIDV searches for the optimal locations of the remaining sensors only.

The DIHSP technique is another important component of the methodology. The key advantage DIHSP has over other modal based techniques is that it filters out all damages except the desired damage scenarios. That is also why DIHSP is only truly useful when the damage scenarios are known in advance.

The final novel aspect of the methodology herein is that it was extended to nonlinear (augmented) systems. When applied to nonlinear systems, the methodology as a whole is essentially the same as for linear systems. The only difference is that using nonlinear ROHA/DIHSP requires the measurement of the degrees of freedom that contain nonlinearities. This is necessary in order to form the augmented equations of motion.

4.5 Conclusions

A method to place sensors for damage detection in linear and nonlinear systems has been presented. The sensor placement approach is based on determining the eigenvectors most sensitive to changes in damageable hot spots in the system. The full modes are extracted from partial measurements by using a novel reduced order health assessment technique. Damage can then be assessed using any number of modal based approaches or by damage identification by hot spot projection. Nonlinear systems can be handled using this methodology by exploiting the features of augmented linear systems. The algorithms proposed have been explored numerically for linear and nonlinear structures. The effectiveness of the proposed methods were demonstrated, and the effects of measurement errors were presented.

CHAPTER V

Damage Detection in Nonlinear Systems Using Optimal Feedback Auxiliary Signals and System Augmentations

5.1 Introduction

Structural health monitoring that is reliable and efficient is very important for cost effective maintenance of large structures such as space and aircraft. One class of monitoring techniques use vibration-based damage detection methods. They exploit the fact that localized changes in system parameters have an effect on vibration frequencies and mode shapes. Matrix update algorithms such as minimum rank perturbation methods [1] and optimal matrix update methods [25] use both frequency and mode shape information to identify updates to the system model. One advantage in using mode shapes (together with frequencies) is the additional detailed information that they provide for damage detection. The disadvantages of using mode shapes are that they tend to be sensitive to measurement error and noise [82], and they require a larger number of sensors.

Thus, damage detection methods using only the vibration frequencies of the system (which herein are referred to as frequency-shift based approaches) have been developed. Although these approaches are less sensitive to noise [45], they have several drawbacks. One of the most important drawbacks is due to the limited number of frequencies that can be measured accurately, which makes the identification of damage an underdetermined

problem [83, 84]. To handle this problem, several techniques have been proposed. For example, the use of "twin" structures (where an additional structure is attached to the tested structure to generate additional modal information) was proposed by Trivailo et al. [85]. Nalitolela et al. [51] investigated the feasibility of adding mass/stiffness to obtain additional vibration frequencies. Practically, however, it is often very difficult to attach these mechanical elements to the tested structure. Lew and Juang [52] overcame these issues by introducing the concept of a virtual passive controller. Instead of using the physical mass and stiffness attachments to the structure, they used output and feedback controllers to generate additional closed loop vibration frequencies.

Another drawback of frequency-based methods is that the sensitivity of vibration frequencies to damage is often low, which was shown both numerically [46] and experimentally [47]. Ray and Tian [48] proposed a sensitivity enhancement technique which uses feedback control laws to place the poles of the system at desired locations. These closed loop vibration frequencies were chosen to increase their sensitivity to mass and stiffness damages. The method was investigated through numerical simulations of a cantilevered beam. Ray et al. [49] extended the work by experimentally validating a sensitivity enhancing control technique for a cantilevered beam under bending. Ray and Marini [86] explored the optimality of the closed loop pole locations for mass and stiffness damage determined by sensitivity enhancing control for fixed actuator locations and minimizing the control effort. Juang et al. [50] explored multi-input control for pole placement. They used the open loop eigenvectors as candidates for the desired closed loop eigenvectors, which results in minimum control gains and therefore minimum control effort. Koh and Ray [53] extended the work by using several independent closed loop systems to increase the frequency data set and ultimately improve the frequency-shift based damage detection performance. Jiang et al. [24] considered the optimal placement of the closed loop eigen-

vectors, and they developed an optimization algorithm that minimizes the control effort while maximizing the sensitivity of the frequencies by placing both the frequencies and the eigenvectors.

All these currently known techniques have been developed using linear theories for linear systems only. This chapter extends these results to *nonlinear* systems. This extension is done by forming higher dimensional augmented systems [73, 80, 87] that follow a single trajectory of the nonlinear system. The system augmentation approach allows for particular linear methods to be used with nonlinear systems. Previously, these augmented systems have been used to detect damage in systems with Colomb friction [80] and cubic stiffness nonlinearities [73, 80, 87] using modal based damage detection methodologies.

In this chapter, a mass-spring system containing cubic nonlinearities is investigated using system augmentation and optimal feedback auxiliary signals. The concept of the optimal augmentation is introduced for further sensitivity enhancement. Various numerical studies are presented to demonstrate optimal sensitivity enhancement for damage detection. The effects of random noise are also discussed.

5.2 Methodology

In this section, the procedure for designing optimal feedback auxiliary signals and system augmentation for damage detection in nonlinear systems is presented. First, an overview of the augmentation is provided. Next, a frequency-shift based damage detection method is discussed. After that, the eigenstructure assignment technique is explained. Finally, the optimization algorithm, used to determine the feedback auxiliary signals and augmentation parameters, is presented.

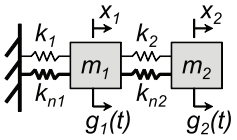

Figure 5.1: Two degree of freedom nonlinear system containing cubic springs.

5.2.1 System Augmentation

A detailed explanation of system augmentation can be found in previous work [73, 80, 87]. These augmented models have a specific forcing in the augmented degrees of freedom. The specific forcing ensures that the augmented systems follow the trajectory of the nonlinear system when projected onto the (original) physical space. Due to the specialized nature of the augmentation, the modal extraction technique used must be an input-output approach as opposed to an output-only approach. This requirement is particularly well suited for use in conjunction with feedback auxiliary signals (such as sensitivity enhancing feedback control) since there the input excitation is known (as the controller output is easily measured). For example, consider the equations of motion corresponding to a mass connected to the ground and to another mass by linear and cubic springs (Fig. 5.1) expressed as

$$\begin{aligned} m_1\ddot{x}_1 + (k_1+k_2)x_1 - k_2x_2 + k_{n1}x_1^3 + k_{n2}(x_1-x_2)^3 &= g_1(t), \\ m_2\ddot{x}_2 - k_2x_1 + k_2x_2 - k_{n2}(x_1-x_2)^3 &= g_2(t), \end{aligned} \tag{5.1}$$

where m_i, k_i, k_{ni}, $g_i(t)$ and x_i correspond to mass, linear spring stiffness, cubic spring stiffness, linear forcing, and displacement of the system, respectively. The augmented equations of motion for this nonlinear system correspond to a four degree of freedom system (two for the linear degrees of freedom, and one for each cubic spring nonlinearity).

The augmented equations of motion are given by

$$\begin{aligned} m_1\ddot{x}_1 + (k_1+k_2)x_1 - k_2x_2 + k_{n1}y_1 + k_{n2}y_2 &= g_1(t), \\ m_2\ddot{x}_2 - k_2x_1 + k_2x_2 - k_{n2}y_2 &= g_2(t), \\ m_{a1}\ddot{y}_1 + k_{c1}x_1 + k_{a1}y_1 &= h_1(t), \\ m_{a2}\ddot{y}_2 + k_{c2}x_1 - k_{c2}x_2 + k_{a2}y_2 &= h_2(t), \end{aligned} \tag{5.2}$$

where $y_1 = x_1^3$, and $y_2 = (x_1 - x_2)^3$, with m_{ai}, k_{ai}, k_{ci}, $h_i(t)$, and y_i corresponding to the augmented mass, augmented stiffness, coupled stiffness, augmented forcing, and augmented variables, respectively.

Complex nonlinearities can be handled accurately. The limit on the level of complexity of these nonlinearities is mainly due to the system augmentation approach (where the definitions of the augmented variables y_i are the key). Any nonlinearity that is a function of only the state vector is well suited for the system augmentation approach (provided that those states are measured).

The values of the parameters m_{ai} and k_{ai} can be chosen by the user to optimally suit their needs, while y_i can be directly computed as $y_1 = x_1^3$ and $y_2 = (x_1 - x_2)^3$. Finally, $h_i(t)$ can be computed from the left hand side of Eq. (5.2). Parameters m_{ai}, k_{ci}, and k_{ai} are not unique. That implies that multiple augmentations exist for the same nonlinear system. Previously, these multiple augmentations have been exploited for damage detection [80]. In this work, the values of augmented parameters m_{ai} and k_{ai} are calculated for optimal sensitivity enhancement. More details are provided in subsequent sections.

The design of a controller for an augmented system has several features that distinguish it from controllers designed for a linear system. The following is a general controller

designed for a nonlinear (physical) system modeled via an augmented system:

$$\begin{bmatrix} \mathbf{M} & \mathbf{N}_I \\ \mathbf{N}_{CI} & \mathbf{N}_{AI} \end{bmatrix} \begin{bmatrix} \ddot{\mathbf{x}} \\ \ddot{\mathbf{y}} \end{bmatrix} + \begin{bmatrix} \mathbf{D} & \mathbf{N}_D \\ \mathbf{N}_{CD} & \mathbf{N}_{AD} \end{bmatrix} \begin{bmatrix} \dot{\mathbf{x}} \\ \dot{\mathbf{y}} \end{bmatrix} + \begin{bmatrix} \mathbf{K} & \mathbf{N}_S \\ \mathbf{N}_{CS} & \mathbf{N}_{AS} \end{bmatrix} \begin{bmatrix} \mathbf{x} \\ \mathbf{y} \end{bmatrix} + \mathbf{B} \begin{bmatrix} \mathbf{K}_{CL} & \mathbf{K}_{CN} \\ \mathbf{K}_{CLA} & \mathbf{K}_{CNA} \end{bmatrix} \begin{bmatrix} \mathbf{x} \\ \mathbf{y} \end{bmatrix} = \begin{bmatrix} \mathbf{g} \\ \mathbf{h} \end{bmatrix}, \tag{5.3}$$

where $\mathbf{M}$, $\mathbf{D}$, $\mathbf{K}$ are the linear mass, damping and stiffness matrices of the physical system; $\mathbf{N}_I$, $\mathbf{N}_D$, $\mathbf{N}_S$ are nonlinear parameter matrices which contain terms such as the cubic spring stiffness k_n; $\mathbf{N}_{CI}$, $\mathbf{N}_{CD}$, $\mathbf{N}_{CS}$ are the coupled parameter matrices which are often used in system augmentation to maintain symmetry of the augmented system matrices for the healthy structure; and $\mathbf{N}_{AI}$, $\mathbf{N}_{AD}$, $\mathbf{N}_{AS}$ are the augmented matrices which contain parameters of the augmentation such as m_{ai} and k_{ai}. The matrix $\mathbf{K}_{CL}$ corresponds to the linear portion of the gain matrix $\mathbf{K}_C$, while $\mathbf{K}_{CN}$ (which multiplies $\mathbf{y}$) is the nonlinear portion of the gain matrix, and $\mathbf{K}_{CLA}$ and $\mathbf{K}_{CNA}$ are the augmented portions of the gain matrix. When designing the controller, if a linear controller is desired, then $\mathbf{K}_{CN}$ must be constrained to zero. In the actual implementation of the augmented portion of the controller, no physical actuation is applied since those equations are fictitious. Rather, the calculated actuation is used in the computation of the augmented forcing $\mathbf{h}$. Note that, although nonlinear control is being used on nonlinear systems, linear analysis tools can be used because of the system augmentation approach.

Next, a mass connected to ground by a linear and a cubic spring and controlled by a single point actuator is presented as an illustrative example (the augmented variable is $y = x^3$). The augmented equations of motion are

$$\begin{aligned} m\ddot{x} + kx + k_n y + K_{CL}x + K_{CN}y &= g(t), \\ m_a\ddot{y} + k_c x + k_a y + K_{CLA}x + K_{CNA}y &= h(t). \end{aligned} \tag{5.4}$$

This controlled augmented system corresponds to a physical system expressed as

$$m\ddot{x} + kx + k_n x^3 + K_{CL}x + K_{CN}x^3 = g(t), \tag{5.5}$$

where the nonlinear controller that acts on the system is given by $K_{CN}y = K_{CN}x^3$. Since k_c and k_a are constants chosen by the user, the augmented control gains can be grouped to obtain the resulting augmented equation of motion

$$m_a\ddot{y} + k_c'x + k_a'y = h(t), \tag{5.6}$$

where $k_c' = k_c + K_{CLA}$ and $k_a' = k_a + K_{CNA}$. In this manner, the user has complete control over the augmented equations, and can adjust them for increased sensitivity with no additional actuation effort.

5.2.2 Damage Detection by Frequency-Shift Based Method

In this work, a first order perturbation method is used to calculate the damage [24, 53]. Perturbations $\Delta\mathbf{p}$ to a damageable set of parameters grouped in a vector $\mathbf{p}$, which contains variables that relate to the mass, damping or stiffness properties, and the changes in the frequencies of the system grouped in a vector $\Delta\omega$ are defined as

$$\Delta\mathbf{p} = \mathbf{p}_h - \mathbf{p}_d \quad \text{and} \quad \Delta\omega = \omega_h - \omega_d, \tag{5.7}$$

where $\mathbf{p}_h$ corresponds to the known healthy parameters, $\mathbf{p}_d$ corresponds to the unknown damaged parameters, and vectors ω_h and ω_d contain the measured frequencies of the healthy and damaged structure.

In general a nonlinear relation exists between $\Delta\mathbf{p}$ and $\Delta\omega$. However, for small damages, this relation can be approximated as first order perturbations expressed as [24, 53]

$$\Delta\omega = \mathbf{S}\Delta\mathbf{p}, \tag{5.8}$$

where $\mathbf{S}$ is the first order sensitivity matrix expressed as

$$\mathbf{S} = \begin{bmatrix} \frac{\partial \omega_1}{\partial p_1} & \frac{\partial \omega_1}{\partial p_2} & \cdots & \frac{\partial \omega_1}{\partial p_r} \\ \frac{\partial \omega_2}{\partial p_1} & \frac{\partial \omega_2}{\partial p_2} & \cdots & \frac{\partial \omega_2}{\partial p_r} \\ \vdots & \vdots & \ddots & \vdots \\ \frac{\partial \omega_q}{\partial p_1} & \frac{\partial \omega_q}{\partial p_2} & \cdots & \frac{\partial \omega_q}{\partial p_r} \end{bmatrix} \approx \begin{bmatrix} \frac{\Delta \omega_1}{\Delta p_1} & \frac{\Delta \omega_1}{\Delta p_2} & \cdots & \frac{\Delta \omega_1}{\Delta p_r} \\ \frac{\Delta \omega_2}{\Delta p_1} & \frac{\Delta \omega_2}{\Delta p_2} & \cdots & \frac{\Delta \omega_2}{\Delta p_r} \\ \vdots & \vdots & \ddots & \vdots \\ \frac{\Delta \omega_q}{\Delta p_1} & \frac{\Delta \omega_q}{\Delta p_2} & \cdots & \frac{\Delta \omega_q}{\Delta p_r} \end{bmatrix}.$$

The index r represents the number of damageable parameters p_i. The index q represents the number of measured frequencies ω_j. From Eq. (5.8) it is clear that the vector of r unknowns $\Delta\mathbf{p}$ can be solved for by taking the pseudo-inverse of $\mathbf{S}$ to obtain

$$\Delta\mathbf{p} = \mathbf{S}^{+}\Delta\omega. \tag{5.9}$$

The goal of the sensitivity enhancement by means of nonlinear feedback auxiliary signals is to increase the values of a closed loop sensitivity matrix $\mathbf{S}^{ci}$ with respect to the open loop sensitivity matrix $\mathbf{S}^{o}$. Since the number r of parameters to be determined is often larger than the number q of measurable frequencies, Eq. (5.8) is underdetermined. To overcome this problem, multiple closed loop systems can be designed by using distinct combinations of control inputs to obtain

$$\mathbf{S} = \begin{bmatrix} \mathbf{S}^{c1} \\ \mathbf{S}^{c2} \\ \vdots \\ \mathbf{S}^{ct} \end{bmatrix}, \tag{5.10}$$

where t corresponds to the number of distinct controller combinations used. If $q * t > r$, an overdetermined set of equations can be used to solve for the unknown parameters $\Delta\mathbf{p}$ using Eq. (5.9). Implicit to this approach is that the distinct controllers are chosen such that $\mathbf{S}$ is of full rank.

5.2.3 Eigenstructure Assignment

Eigenstructure assignment via SVD (singular value decomposition) has been explored extensively for linear systems [88–92]. This section follows closely the work of Jiang et al. [24] and is included to provide a brief overview of the SVD-based eigenstructure assignment and to present the new subtleties associated with its use in conjunction with augmented systems. Just as in the case of eigenstructure assignment for linear systems, a model of the healthy augmented (nonlinear) system is required for eigenstructure assignment via SVD.

Expanding the work of Jiang et al. [24] to augmented systems, the equations of motion for a (nonlinear) system without damping can be written as

$$\mathbf{M}_A\ddot{\mathbf{z}} + (\mathbf{K}_A + \mathbf{B}\mathbf{K}_C)\mathbf{z} = \mathbf{F}, \tag{5.11}$$

where

$$\mathbf{z} = \begin{bmatrix} \mathbf{x} \\ \\ \mathbf{y} \end{bmatrix}, \quad \text{and} \quad \mathbf{F} = \begin{bmatrix} \mathbf{g} \\ \\ \mathbf{h} \end{bmatrix},$$

and where $\mathbf{M}_A$ and $\mathbf{K}_A$ are $N_o \times N_o$ augmented mass and stiffness matrices, $\mathbf{B}$ is the $N_o \times c$ control input matrix, $\mathbf{K}_c$ is the $c \times N_o$ control gain matrix, $\mathbf{x}$ is the $N \times 1$ coordinate vector, $\mathbf{y}$ is the $n \times 1$ augmented variable vector, $\mathbf{g}$ is the $N \times 1$ physical forcing, and $\mathbf{h}$ is the $n \times 1$ augmented forcing.

The eigenvalue problem for the augmented closed loop system can be written as

$$(\mathbf{K}_A + \mathbf{B}\mathbf{K}_C)\phi_j = \omega_{cj}^2 \mathbf{M}_A \phi_j, \tag{5.12}$$

where ϕ_j represents the j^{th} eigenvector and ω_{cj} is the j^{th} (complex) frequency of the closed loop system. Eq. (5.12) can alternatively be written as

$$\left[\mathbf{K}_A - \omega_{cj}^2 \mathbf{M}_A | \mathbf{B}\right] \begin{bmatrix} \phi_j \\ \\ \mathbf{K}_C \phi_j \end{bmatrix} = \mathbf{0}, \tag{5.13}$$

which means that the null space of the matrix $\left[\mathbf{K}_A - \omega_{cj}^2 \mathbf{M}_A | \mathbf{B}\right]$ must contain the vector $[\phi_j \ \mathbf{K}_C \phi_j]^T$. The symbol | indicates a partition in the matrix, e.g. the matrix is composed of two matrices side by side. Next, define $\mathbf{S}_{wcj} = \left[\mathbf{K}_A - \omega_{cj}^2 \mathbf{M}_A | \mathbf{B}\right]$, and perform an SVD of $\mathbf{S}_{wcj}$ to obtain

$$\mathbf{S}_{wcj} = \left[\mathbf{K}_A - \omega_{cj}^2 \mathbf{M}_A | \mathbf{B}\right] = \mathbf{U}_j \left[\mathbf{D}_j | \mathbf{0}_{N_o \times c}\right] \mathbf{V}_j^*, \tag{5.14}$$

where $\mathbf{U}_j$ and $\mathbf{V}_j$ correspond to the orthonormal left and right singular vectors, respectively, and $\mathbf{D}_j$ is a diagonal matrix that contains the singular values. The right singular matrix can be divided into 4 sub-matrices as follows

$$\mathbf{V}_j = \begin{bmatrix} \mathbf{V}_{11}^{(j)} & \mathbf{V}_{12}^{(j)} \\ \mathbf{V}_{21}^{(j)} & \mathbf{V}_{22}^{(j)} \end{bmatrix}, \tag{5.15}$$

where $\mathbf{V}_{11}^{(j)}$ is $N_o \times N_o$, $\mathbf{V}_{12}^{(j)}$ is $N_o \times c$, $\mathbf{V}_{21}^{(j)}$ is $c \times N_o$, and $\mathbf{V}_{22}^{(j)}$ is $c \times c$.

Using the orthogonality property of the singular vectors, one can post multiply Eq. (5.14) by $\left[\mathbf{V}_{12}^{(j)} \ \mathbf{V}_{22}^{(j)}\right]^T$ to obtain

$$\left[\mathbf{K}_A - \omega_{cj}^2 \mathbf{M}_A | \mathbf{B}\right] \begin{bmatrix} \mathbf{V}_{12}^{(j)} \\ \mathbf{V}_{22}^{(j)} \end{bmatrix} = \mathbf{0}. \tag{5.16}$$

Consequently, all achievable eigenvectors must be in the span of $\mathbf{V}_{12}^{(j)}$. Therefore, a coefficient vector $\mathbf{f}_j$ can be used to assign the eigenvector j within the admissible subspace (e.g. $\mathbf{V}_{12}^{(j)}$). Hence, the assigned right eigenvector ϕ_j^a can be expressed as

$$\phi_j^a = \mathbf{V}_{12}^{(j)} \mathbf{f}_j, \tag{5.17}$$

and the following relation holds

$$\mathbf{K}_C \phi_j^a = \mathbf{V}_{22}^{(j)} \mathbf{f}_j. \tag{5.18}$$

By gathering all N_o eigen-solutions from Eq. (5.18), one can write

$$\mathbf{K}_C \Phi^a = \mathbf{W}, \tag{5.19}$$

where $\Phi^a = \left[\phi_1^a\ \phi_2^a\ \ldots\ \phi_{N_o}^a\right]$, $\phi_j^a = \mathbf{V}_{12}^{(j)}\mathbf{f}_j$, and $\mathbf{W} = [\mathbf{w}_1\ \mathbf{w}_2\ \ldots\ \mathbf{w}_{N_o}]$, with $\mathbf{w}_j = \mathbf{V}_{22}^{(j)}\mathbf{f}_j$. Inverting Φ^a in Eq. (5.19), one can solve for the gain matrix as

$$\mathbf{K}_C = \mathbf{W}\left(\Phi^a\right)^{-1}. \tag{5.20}$$

5.2.4 Optimization for Optimal Controller Design

The basic idea behind sensitivity enhancing feedback control for single degree of freedom systems is that decreasing the stiffness enhances the sensitivity of the frequencies to stiffness changes, while increasing the stiffness enhances the sensitivity of the frequencies to mass changes. Extending this idea to multi-degree of freedom systems is more complicated. The sensitivity of the modal frequencies to changes in mass and stiffness parameters is given by a function that includes the mass, damping, and stiffness matrices along with their derivatives, and the closed loop eigenvalues along with the right and left eigenvectors [24]. As a result, no simple relation exists for designing controllers. However, an optimization algorithm can be used to design the controller. In this section, a constrained optimization algorithm is discussed for optimal placement of the modal frequencies and right eigenvectors of the augmented system to maximize the sensitivity to parameter variations while minimizing the control effort. This optimization algorithm extends the work of Jiang et al. [24] to augmented systems.

There are three types of parameters that need to be optimized to obtain the optimal feedback control. The first type of parameters affects the desired closed loop frequencies, which are close to the open loop frequencies. These parameters consist of q coefficients γ_j that represent percentages of the q measurable open loop frequencies ω_{oj}. Therefore, all the closed loop frequencies can be expressed as

$$\omega_{cj} = \begin{cases} \gamma_j\omega_{oj}, & j = 1, 2, \ldots, q \\ \omega_{oj}, & j = q+1, q+2, \ldots, N_o \end{cases}. \tag{5.21}$$

The second type of parameters are the coefficient vectors $\mathbf{f}_j$ that are used to assign the right eigenvectors of the system within the admissible space. All the closed loop eigenvectors ϕ_j^c can be expressed as

$$\phi_j^c = \begin{cases} \mathbf{V}_{12}^{(j)}\mathbf{f}_j, & j = 1, 2, \ldots, q \\ \mathbf{V}_{12}^{(j)}\tilde{\mathbf{f}}_j, & j = q+1, q+2, \ldots, N_o \end{cases}, \tag{5.22}$$

where $\mathbf{f}_j$ corresponds to the unknown parameters being optimized (for $j = 1, 2, \ldots, q$) and $\tilde{\mathbf{f}}_j$ are coefficient vectors that are chosen as close to the open loop eigenvectors ϕ_j^o as possible to minimize the controller effort (for $j = q+1, q+2, \ldots, N_o$). The coefficient vectors $\tilde{\mathbf{f}}_j$ can therefore be determined by minimizing the Euclidean norm $\left\| \phi_j^o - \mathbf{V}_{12}^{(j)}\tilde{\mathbf{f}}_j \right\|$ as well as $\left\| \tilde{\mathbf{f}}_j \right\|$. Using the pseudo-inverse, one obtains

$$\tilde{\mathbf{f}}_j = \left(\mathbf{V}_{12}^{(j)*}\mathbf{V}_{12}^{(j)} \right)^{-1} \mathbf{V}_{12}^{(j)*}\phi_j^o, \qquad \text{where} \quad j = q+1, q+2, \ldots, N_o, \tag{5.23}$$

and the closest achievable eigenvector is given by

$$\phi_j^c = \mathbf{V}_{12}^{(j)} \left(\mathbf{V}_{12}^{(j)*}\mathbf{V}_{12}^{(j)} \right)^{-1} \mathbf{V}_{12}^{(j)*}\phi_j^o, \qquad \text{where} \quad j = q+1, q+2, \ldots N_o. \tag{5.24}$$

The augmented equations of a system are not unique for a given nonlinear system. One way to optimize the augmentation is to determine the stiffnesses of the augmented equations that maximize the sensitivity enhancement (by determining the optimal rows in $\mathbf{K}_C$ that correspond to the augmented equations, as discussed in Sec. 5.2.1). Additionally, the augmented mass parameters m_{ai} can also be optimized. Traditionally, parameters m_{ai} have been set to values similar to the masses of the degrees of freedom that contain the nonlinearity [73, 80, 87]. In this work, those ad hoc values for m_{ai} are optimized to obtain m_{ai}^o. The optimal values m_{ai}^o are used to define the coefficients Γ_i by the relation $m_{ai}^o = \Gamma_i m_{ai}$. Parameters Γ_i are the third type of parameters of the augmentation that can be optimized (for $i = 1, 2, \ldots, n$).

There are two parts of the optimization function. The first part is the sensitivity enhancement variable SE which needs to be maximized. SE is an average of the element by element ratios of the closed loop sensitivity matrix $\mathbf{S}^c$ to the open loop sensitivity matrix $\mathbf{S}^o$. Hence, SE is given by

$$SE = \frac{\sum_{j=1}^{q} \sum_{i=1}^{r} |\frac{\mathbf{S}^c(j,i)}{\mathbf{S}^o(j,i)}|}{q\ r}. \tag{5.25}$$

The second part of the optimization function is the controller effort which needs to be minimized. In this work, the controller effort CE was chosen as the absolute value of the largest entry in any row of $\mathbf{K}_C$ except ones corresponding to the augmented equations. The augmented rows of $\mathbf{K}_C$ are excluded because there is no physical controller acting on these augmented equations, and hence there is no *physical* controller effort associated with these parameters.

Using its two parts, the optimization function is written as

$$J(\gamma_1,\ \gamma_2,\ \ldots,\ \gamma_q,\ \mathbf{f}_1,\ \mathbf{f}_2,\ \ldots,\ \mathbf{f}_q,\ \Gamma_1,\ \Gamma_2,\ \ldots,\ \Gamma_n) = \frac{C_1}{SE} + C_2 CE, \tag{5.26}$$

where C_1 and C_2 are constants chosen to weight the importance of SE relative to CE. Of course, J is a function of all controller design variables.

A very important aspect of the design of feedback auxiliary signals is the requirement that the system be stable during its interrogation. Hence, the optimization function is also subject to stability constraints. In general, the stability of the linearized physical system is the important issue, while the augmented linear system does not have to be stable. The augmented linear system does not necessarily need to be stable because it is a fictitious system, and it is only subjected to a specific excitation. For example, an unstable augmented system can be constructed for a *stable* physical (nonlinear) system. Nonetheless, the linearized physical system must be stable both when it is healthy and

after each damage scenario. Therefore, Eq. (5.26) is subject to the following constraints

$$\begin{aligned} -\Im(\omega_{cj}^{L}) &\leq 0, \;\; j = 1, 2, \ldots, N, \text{ and} \\ -\Im(\omega_{dcji}^{L}) &\leq 0, \;\; j = 1, 2, \ldots, N, \text{ and } i = 1, 2, \ldots, r, \end{aligned}$$

where $\Im$ indicates the imaginary part, ω_{cj}^{L} are the (complex) frequencies of the linearized closed loop healthy system, and ω_{dcji}^{L} are the frequencies of the linearized closed loop damaged system for the i^{th} damage scenario. These constraints must be satisfied for a damage level that is the maximum allowable damage for all r scenarios.

In this work, for several of the results, a stricter stability requirement is enforced, namely the stability of the augmented linear system. Although increased sensitivity can be achieved when the augmented system becomes unstable, care must be taken to ensure the linearity approximation in Eq. (5.8) holds. If the system is allowed to vary unrestricted into unstable regimes the system may become hyper-sensitive, and the linear assumption of Eq. (5.8) can be inaccurate. The sensitivity (and the range of linearity) can be controlled by using the following constraints on the optimal controller design

$$\begin{aligned} -\Im(\omega_{cj}^{A}) &\leq \epsilon, \;\; j = 1, 2, \ldots, N_o, \text{ and} \\ -\Im(\omega_{dcji}^{A}) &\leq \epsilon, \;\; j = 1, 2, \ldots, N_o, \text{ and } i = 1, 2, \ldots, r, \end{aligned}$$

where ω_{cj}^{A} are the (complex) frequencies of the augmented closed loop healthy system, ω_{dcji}^{A} are the frequencies of the augmented closed loop damaged system, and ϵ is a positive parameter that constrains the level of instability allowed into the *augmented* system.

5.3 Results

To demonstrate the proposed method, a numerical investigation of a nonlinear system of the type shown in Fig. 5.2 was performed. The nonlinear mass-spring system has 5

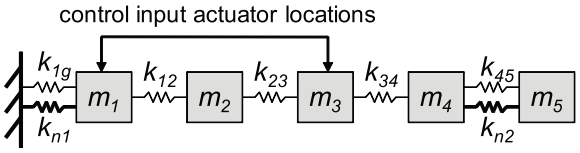

Figure 5.2: Nonlinear mass spring system that contains two cubic spring nonlinearities denoted by the cubic stiffness k_{n1} and k_{n2} ($m_i = 1$, $i = 1 \ldots 5$, $k_{1g} = k_{34} = 10000$, $k_{12} = k_{23} = 15000$, $k_{45} = 20000$, $k_{n1} = k_{n2} = 10000$).

degrees of freedom. The system contains 5 linear springs and 2 cubic springs, which are the damageable elements and are denoted by $p_1 = k_{1g}$, $p_2 = k_{12}$, $p_3 = k_{23}$, $p_4 = k_{34}$, $p_5 = k_{45}$, $p_6 = k_{n1}$, and $p_7 = k_{n2}$. Augmented linear systems were created from the nonlinear system by generating the matrices $\mathbf{M}$, $\mathbf{K}$, $\mathbf{N}_I$, $\mathbf{N}_S$, $\mathbf{N}_{AI}$, $\mathbf{N}_{AS}$ and $\mathbf{N}_{CS}$ in Eq. (5.3). In particular, the nonzero entries of the $\mathbf{N}_S$ matrix are composed of cubic spring stiffnesses. The matrix $\mathbf{N}_{AI}$ is a diagonal matrix containing the augmented masses, which are chosen as the same values as the physical masses that the augmented variables physically interact with. The matrix $\mathbf{N}_{CS}$ is chosen to maintain certain physical characteristics of the augmented system [73]. In particular, the nonzero entries of $\mathbf{N}_{CS}$ are the cubic spring stiffnesses. The matrix $\mathbf{N}_{AS}$ is a diagonal matrix that contains the terms k_{ai} chosen as $k_{ai} = 2k_{ni}$. The values of the weighting factors between SE and CE were chosen as $C_1 = 10^3$ and $C_2 = 10^{-4}$. Four controllers ($CL1 - 4$) were designed to maximize the sensitivity of the first 3 frequencies of the system to changes in the 7 (damageable) elements. Since only the first 3 frequencies were measured and there are 7 damageable parameters, multiple controllers must be designed so that Eq. (5.9) is overdetermined. A minimum of 3 controllers are needed, but 4 were used in this work ($CL1 - 4$) to better the conditioning of the matrix $\mathbf{S}$. The different combinations of feedback auxiliary signals are given by locations as follows: $CL1$ - [1, 3, 6, 7]; $CL2$ - [1, 6, 7]; $CL3$ - [3, 6, 7];

System	Actuator locations	Optimal closed loop augmented mass parameters	Optimal closed-loop eigenvalues	Coefficient vectors of optimal closed-loop eigenvectors
Optimal Augmentation				
CL-1	1,3,6,7	$m^o_{a1}=6.08m_{a1}$ $m^o_{a2}=3.44m_{a2}$	$\omega_{c1}=0.81\omega_{o1}$ $\omega_{c2}=0.90\omega_{o2}$ $\omega_{c3}=0.97\omega_{o3}$	$\mathbf{f}_1$=[-2.08, 2.36, -0.00, -34.56] $\mathbf{f}_2$=[-0.16, -0.45, -0.38, 1.62] $\mathbf{f}_3$=[-4.08, 9.60, 3.27, -0.65]
CL-2	1,6,7	$m^o_{a1}=1.11m_{a1}$ $m^o_{a2}=0.49m_{a2}$	$\omega_{c1}=0.75\omega_{o1}$ $\omega_{c2}=0.98\omega_{o2}$ $\omega_{c3}=0.13\omega_{o3}$	$\mathbf{f}_1$=[-3.37, -7.68, -4.22] $\mathbf{f}_2$=[-7.28, -1.72, 5.50] $\mathbf{f}_3$=[-1.88, 0.41, 2.61]
CL-3	3,6,7	$m^o_{a1}=1.29m_{a1}$ $m^o_{a2}=1.13m_{a2}$	$\omega_{c1}=0.48\omega_{o1}$ $\omega_{c2}=0.30\omega_{o2}$ $\omega_{c3}=0.71\omega_{o3}$	$\mathbf{f}_1$=[-0.95, -1.65, -5.38] $\mathbf{f}_2$=[0.72, -0.86, 0.57] $\mathbf{f}_3$=[-1.15, -0.25, 5.83]
CL-4	6,7	$m^o_{a1}=0.98m_{a1}$ $m^o_{a2}=0.96m_{a2}$	$\omega_{c1}=0.23\omega_{o1}$ $\omega_{c2}=1.00\omega_{o2}$ $\omega_{c3}=0.41\omega_{o3}$	$\mathbf{f}_1$=[-0.14, -4.08] $\mathbf{f}_2$=[2.35, 4.72] $\mathbf{f}_3$=[-1.37, 4.56]
Ad hoc Augmentation				
CL-1	1,3,6,7	$m^o_{a1}=m_{a1}$ $m^o_{a2}=m_{a2}$	$\omega_{c1}=0.15\omega_{o1}$ $\omega_{c2}=0.91\omega_{o2}$ $\omega_{c3}=1.00\omega_{o3}$	$\mathbf{f}_1$=[-2.93, 3.18, 1.89, -34.14] $\mathbf{f}_2$=[-0.59, 0.36, -0.08, 0.56] $\mathbf{f}_3$=[1.81, 6.09, 0.23, -1.44]
CL-2	1,6,7	$m^o_{a1}=m_{a1}$ $m^o_{a2}=m_{a2}$	$\omega_{c1}=0.11\omega_{o1}$ $\omega_{c2}=0.96\omega_{o2}$ $\omega_{c3}=0.54\omega_{o3}$	$\mathbf{f}_1$=[-3.78, -8.11, -0.96] $\mathbf{f}_2$=[-1.50, -2.64, 0.63] $\mathbf{f}_3$=[-0.95, 1.52, 2.31]
CL-3	3,6,7	$m^o_{a1}=m_{a1}$ $m^o_{a2}=m_{a2}$	$\omega_{c1}=0.22\omega_{o1}$ $\omega_{c2}=0.44\omega_{o2}$ $\omega_{c3}=0.50\omega_{o3}$	$\mathbf{f}_1$=[-0.63, 0.56, -2.00] $\mathbf{f}_2$=[0.35, -0.83, -0.17] $\mathbf{f}_3$=[-0.98, -1.44, 5.80]
CL-4	6,7	$m^o_{a1}=m_{a1}$ $m^o_{a2}=m_{a2}$	$\omega_{c1}=1.00\omega_{o1}$ $\omega_{c2}=0.12\omega_{o2}$ $\omega_{c3}=0.36\omega_{o3}$	$\mathbf{f}_1$=[-0.67, -7.22] $\mathbf{f}_2$=[-0.94, 4.77] $\mathbf{f}_3$=[0.64, -3.07]

Table 5.1: Design parameters for multiple sensitivity enhancing feedback controllers for an optimal augmentation and an ad hoc augmentation.

and $CL4$ - [6, 7]. Locations 6 and 7 correspond to the augmented degrees of freedom, so $CL4$ corresponds to purely augmented gain control, which requires no actual actuation, but only signal processing.

The constrained optimization function was solved by using the `fmincon` function in MATLAB [93]. We found that the global optimum was not always obtained because different initial guesses could lead to different solutions by the optimizer. To be consistent, we used the open loop system as the starting point for the optimization for all the fully

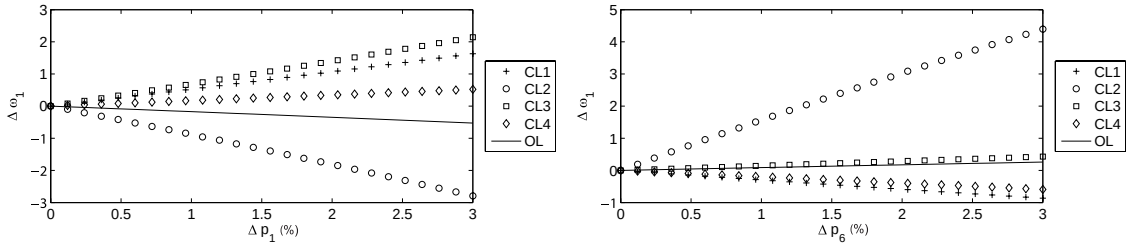

(a) Linear parameter (b) Nonlinear parameter

Figure 5.3: Sensitivity of the first resonant frequency to a change in a linear spring (a) and a cubic spring (b) for the open loop (OL) and 4 fully stable, closed loop systems ($CL1-4$).

stable systems.

5.3.1 Optimal Augmentation

In this section, the effectiveness of using the nonlinear feedback auxiliary signals to interrogate a nonlinear system using system augmentation is demonstrated. As discussed in the system augmentation section of the methodology, augmented systems are not unique for a given nonlinear system. The optimization of the augmented portion of the gain matrix $\mathbf{K}_C$ optimally enhances the sensitivity to the stiffness portion of the augmentation. When the augmented mass is also optimized using the design variable Γ_i, the augmentation is designated as an *optimal augmentation*. Otherwise it is referred to as an *ad hoc augmentation*.

The design variables γ_1, γ_2, γ_3, $\mathbf{f}_1$, $\mathbf{f}_2$, $\mathbf{f}_3$, Γ_1, and Γ_2 are given in Tab. 5.1 for each closed loop system ($CL1-4$). Two sets of closed loop systems ($CL1-4$) are given. The first corresponds to the case where, in addition to determining the optimal controller configuration, the optimal augmentation is determined by finding the design parameters Γ_1 and Γ_2. The second set of closed loop systems does not optimize the augmented mass. Instead, the nominal ad hoc values are used for the augmented masses (that is, $\Gamma_1 = \Gamma_2 =$

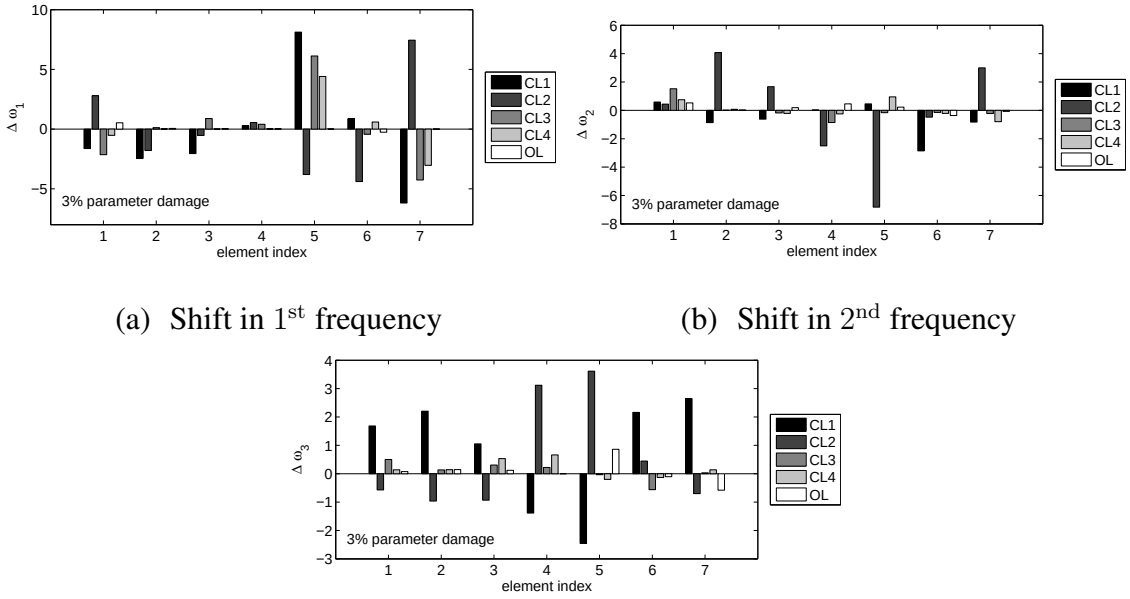

(a) Shift in 1^{st} frequency

(b) Shift in 2^{nd} frequency

(c) Shift in 3^{rd} frequency

Figure 5.4: Comparison of the frequency shift due to a 3% loss of stiffness in each parameter for the open loop (OL) and 4 fully stable, closed loop systems ($CL1-4$) for the optimally augmented system for the 1^{st} (a), 2^{nd} (b), 3^{rd} (c) frequencies.

1). In both cases, the closed loop systems are designed to be *fully stable* (i.e. $\epsilon = 0$).

The results in Fig. 5.3 show the change in the first frequency in one linear and one nonlinear parameter for the open loop and each of the optimally augmented closed loop systems ($CL1-4$). The x-axis in each plot corresponds to the change in the parameter, while the y-axis in each plot corresponds to the change in the first frequency. It is clear from the plots that the changes in each of the closed loop frequencies is equal to or greater than the change in the open loop frequency. Also, the dependence of $\Delta\omega_1$ upon Δp_1 and Δp_6 is linear across the range of 3% parameter variation. Similar results can be obtained for the other 2 frequencies and 5 parameters, but they are omitted here for the sake of brevity. These results validate/demonstrate the linearity approximation used in Eq. (5.8).

The results in Fig. 5.4 show the shifts $\Delta\omega_1$, $\Delta\omega_2$, $\Delta\omega_3$ in the first 3 frequencies due to

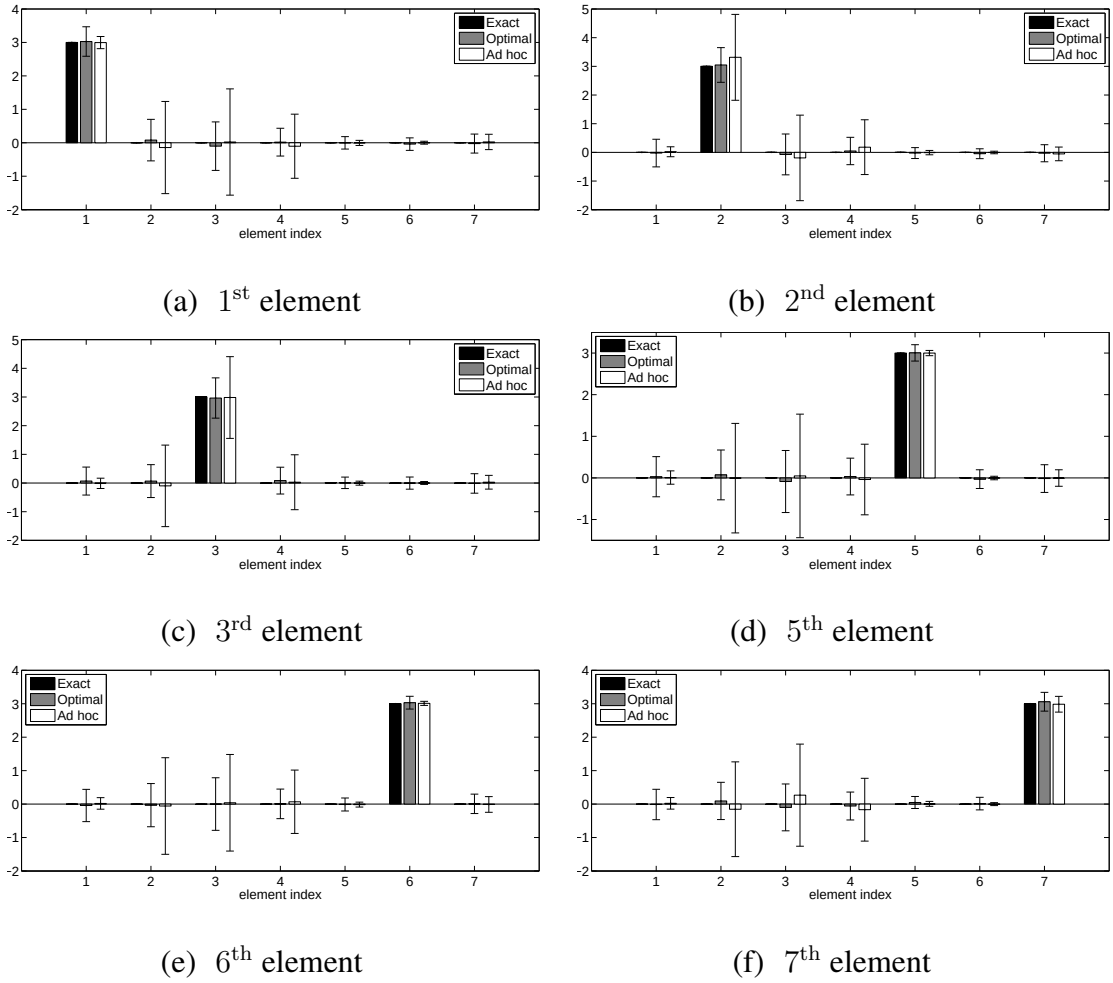

(a) 1^{st} element (b) 2^{nd} element

(c) 3^{rd} element (d) 5^{th} element

(e) 6^{th} element (f) 7^{th} element

Figure 5.5: Damage detection results for frequencies contaminated with 1% random noise for the optimal and ad hoc augmented systems for the 1^{st} (a), 2^{nd} (b), 3^{rd} (c), 5^{th} (d), 6^{th} (e), and 7^{th} (f) elements.

3% damage in each of the 7 (damageable) elements. The 4 closed loop systems ($CL1-4$) correspond to the optimally augmented systems with design parameters given in Tab. 5.1. The x-axis in each plot corresponds to the damaged element, while the y-axis in each plot corresponds to the change in frequency due to damage. The first 5 elements correspond to the 5 linear stiffnesses, while elements 6 and 7 correspond to the cubic stiffnesses. The plots show that the sensitivity of the 4 closed loop systems is from 200 to 1300 times higher compared to the open loop system (SE varies from 200 to 1300 for the different closed

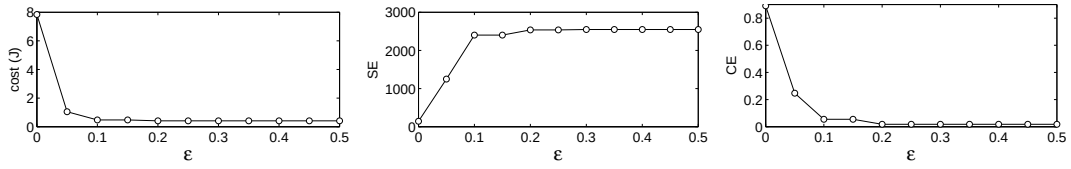

(a) (b) (c)

Figure 5.6: Change in function cost (a), sensitivity enhancement (b), and control effort (c) with increase in ϵ.

loop systems).

The results in Fig. 5.5 show the excellent performance of the approach for 6 different damage scenarios. The x-axis in each plot corresponds to the damaged elements, while the y-axis in each plot corresponds to the percent damage. Each plot shows the exact value of the damage, and the average predicted damage for the optimal and ad hoc augmented systems. One hundred separate calculations were performed for the case of 1% random eigenvalue noise applied to the frequencies of the damaged system. Standard deviation error bars are plotted. For the case of zero noise, both the optimal and ad hoc augmentation predict the exact damage. For the noisy case, the average predicted value is very close for both the optimal and ad hoc augmentation. However, the deviations tend to be larger for the ad hoc augmentation.

5.3.2 Physical Stability

In this section, certain issues related to the stability of the system are explored. Results are presented for a closed loop system where the augmented linear system is allowed to become unstable (although the linearized physical system is still enforced to be stable, i.e. $\epsilon > 0$). That case is designated as *physically stable*. Also, results for a case where no instability is allowed even in the augmented system (i.e. $\epsilon = 0$) are presented. That case is designated as *fully stable*.

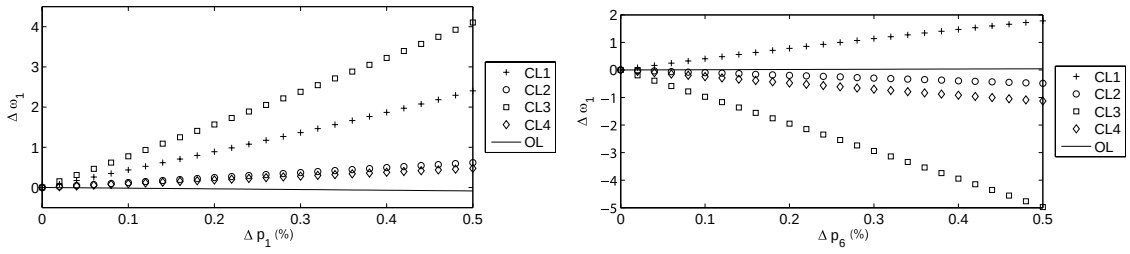

(a) Linear parameter (b) Nonlinear parameter

Figure 5.7: Sensitivity of the first resonant frequency to a change in a linear spring (a) and a cubic spring (b) for the open loop (OL) and 4 physically stable, closed loop systems ($CL1-4$).

The results in Fig. 5.6 show how the cost J, sensitivity enhancement SE, and control effort CE change as ϵ is increased from zero for the $CL2$ system. For each optimal controller, the initial starting point chosen for the optimizer was the final point from the lower value of ϵ. The plots show how the cost and CE decrease and SE increases as ϵ is increased. Although it appears as though ϵ could be arbitrarily large, care must be taken in setting a maximum allowed value. If ϵ is allowed to be too large, then the linear relation between the change in the parameters and frequencies begins to break down, and the linearity approximation used in Eq. (5.8) is not accurate. In the results in this section, the maximum value of ϵ was 0.5 for $CL1-4$.

The results in Fig. 5.7 show the changes in the first frequency for damages in one linear and one nonlinear parameter for the open loop and each of the physically stable closed loop systems ($CL1-4$). The plots are laid out in the same manner as in Fig. 5.3. Over the range of 0.5% parameter variation, the dependence of $\Delta\omega_1$ upon Δp_1 and Δp_6 is linear. Similar results can be obtained for the other 2 frequencies and 5 parameters, but are omitted here for the sake of brevity.

Similar to Fig. 5.4, the results in Fig. 5.8 show the shift in the first 3 frequencies due to

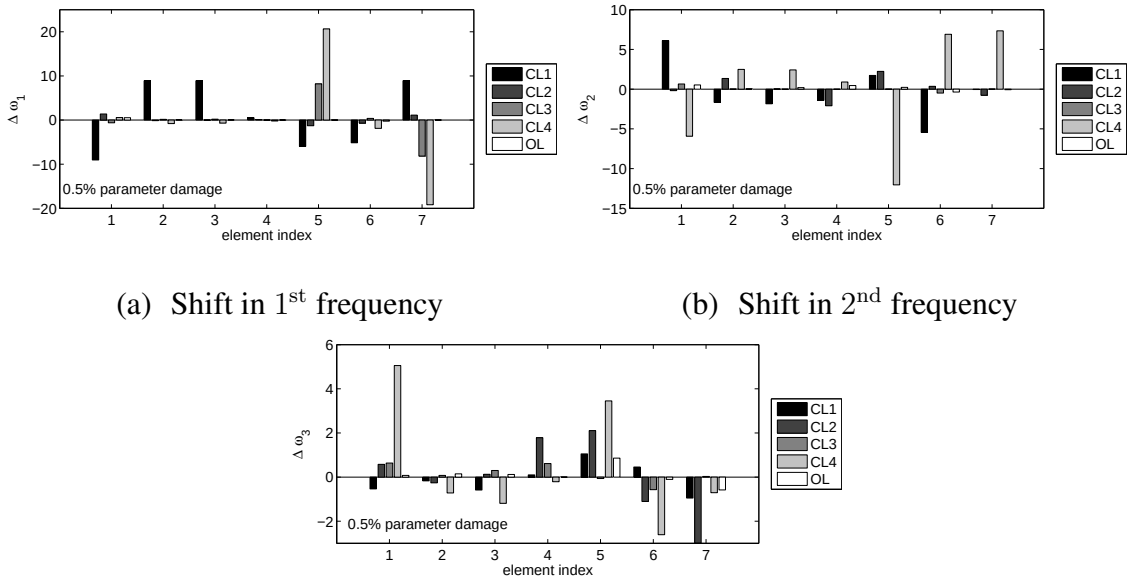

(a) Shift in 1^{st} frequency

(b) Shift in 2^{nd} frequency

(c) Shift in 3^{rd} frequency

Figure 5.8: Comparison of the frequency shift due to a 0.5% loss of stiffness in each parameter for the open loop (OL) and 4 physically stable, closed loop systems ($CL1-4$) for the optimally augmented system for the 1^{st} (a), 2^{nd} (b), 3^{rd} (c) frequencies.

0.5% damage in each of the 7 (damageable) elements. In Fig. 5.8, there are 4 closed loop systems ($CL1-4$) which are compared against the open loop system. The plots show that the sensitivity of the 4 closed loop systems ranges from 900 to 4700 times higher compared to the open loop system (SE varies from 900 to 4700 for the different closed loop systems).

The results in Fig. 5.9 show the excellent performance of the approach for 6 different damage scenarios. The plots are laid out in the same manner as Fig. 5.5. Each plot shows the exact value of damage, and the average predicted damage for the fully stable and physically stable augmented systems. One hundred separate calculations were performed for the case of 0.5% random eigenvalue noise applied to the frequencies of the damaged system. Standard deviation error bars are plotted. For the case of zero noise, both the

fully stable and the physically stable augmented systems predict the exact damage. In the presence of noise, however, the physically stable system predicts the damage better, as evidenced by the significantly smaller error bars.

5.4 Conclusions and Discussion

A novel approach for sensitivity enhancement for nonlinear systems via nonlinear feedback auxiliary signals and optimal system augmentations was presented. In addition to the advantage that linear approaches such as modal analysis can be used to extract features of nonlinear systems (by the use of the augmented linear systems), there are several other features of the augmented system that can be used as well. One of these is the ability to use a nonlinear controller, while still having the benefit of being able to use linear methods such as modal analysis.

Another key feature is the nonuniqueness of the augmentation. Although all augmentations of a system are designed such that they follow a single trajectory of the nonlinear system, some perform better than others for sensitivity enhancement. In this work, an optimal augmentation for sensitivity enhancement was designed and found to perform significantly better in the presence of noise than previous (intuitively designed) augmentations.

Another feature is the ability to apply control in the augmented equations. Although this does not require any physical actuation, it can increase the sensitivity of the overall damage detection. Furthermore, a key related benefit is the availability of additional controller configurations that are possible due to the additional controller input locations (at all the augmented degrees of freedom) at no additional cost.

The final important feature of the augmented system is related to the constraint on the stability of the controlled system. The requirement of stability of the system applies only

to the linear parameters and linear portion of the controller. The actual augmented system does not have to be stable. This stability requirement is very important especially when the damage to be detected is small. In this work, it was shown that the relaxation of the stability in the augmented system allowed the detection of damage of lower levels, where a fully stable system would perform poorly in the presence of the same amount of noise. Nonetheless, care must still be taken in determining the allowable level of instability in the augmented system because the damage detection method assumes a linear relation between changes in parameters and frequencies.

The sensitivity enhancement and damage detection approach using system augmentations and feedback auxiliary signals was shown to work for a nonlinear mass-spring system containing cubic spring nonlinearities, and sensitivity increases of up to more than 3 orders of magnitude were obtained. The effects of measurement noise were also discussed.

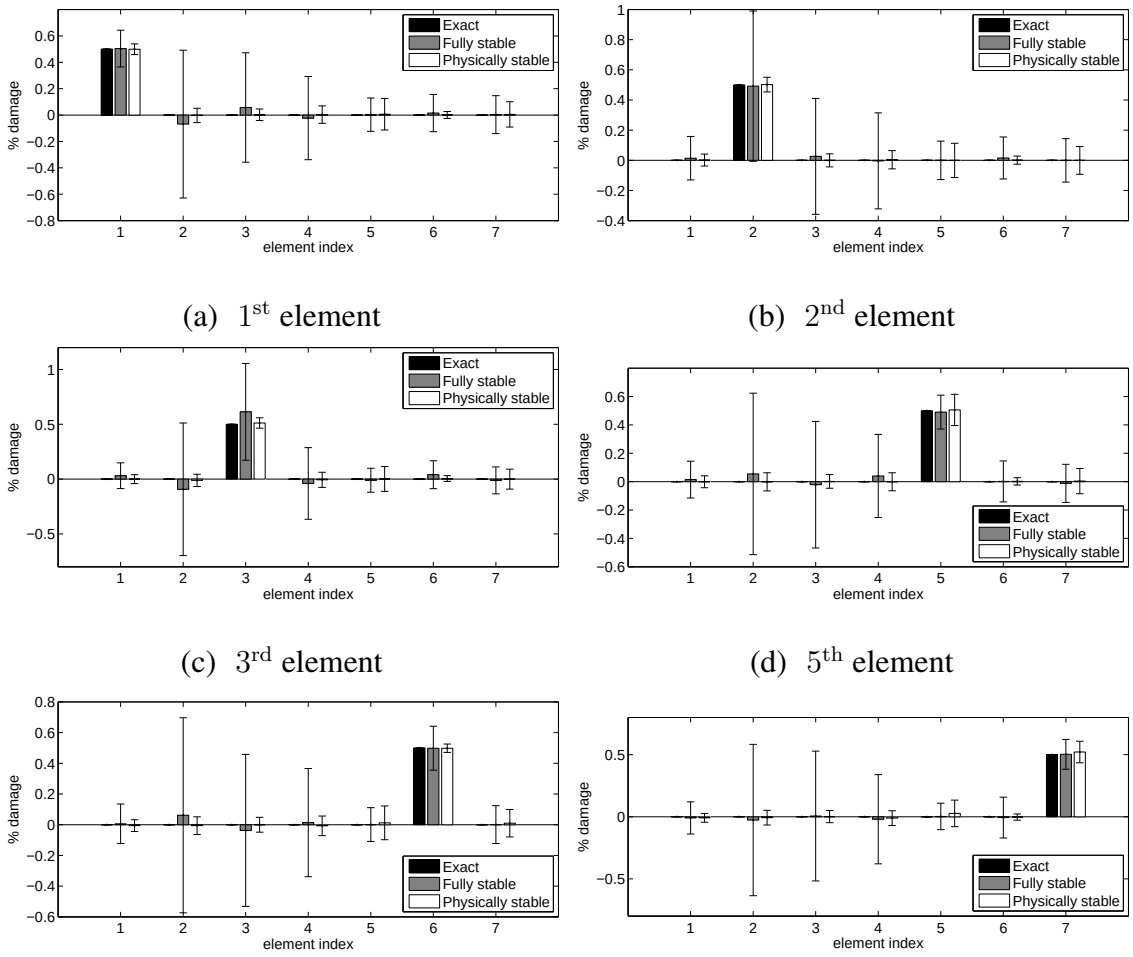

(a) 1^{st} element

(b) 2^{nd} element

(c) 3^{rd} element

(d) 5^{th} element

(e) 6^{th} element

(f) 7^{th} element

Figure 5.9: Damage detection results for frequencies contaminated with 0.5% random noise for the fully stable and physically stable augmented systems for the 1^{st} (a), 2^{nd} (b), 3^{rd} (c), 5^{th} (d), 6^{th} (e), and 7^{th} (f) elements.

CHAPTER VI

Nonlinear Feedback Auxiliary Signals for System Interrogation and Damage Detection

6.1 Introduction

Recently, methods that use measured resonant frequencies for applications involving model updating in structural dynamics have received increased attention. These methods (herein referred to as frequency-shift based methods) have several advantages over other approaches such as the ones which use mode shapes, for instance. First, measuring mode shapes requires the use of many sensors, which is difficult to implement in practical structures. Second, mode shapes are more sensitive to noise and measurement error than resonant frequencies [82].

However, there are several drawbacks to using classical frequency-shift based methods. The first key drawback is the limited number of frequencies that can be extracted accurately, which leads to an under-determined problem when solving for parameter variations [83,84]. Several approaches have been suggested to handle this problem. Trivailo et al. [85] proposed attaching an additional ("twin") structure to the tested structure to obtain additional frequency information. However, attaching these "twin" structures is difficult in practice. To overcome this issue, a virtual passive controller was proposed by Lew and Juang [52]. They obtained additional frequencies by using output and feedback controllers

instead of physically adding mass and stiffness elements to the interrogated structure.

The second key drawback of classical frequency-shift based model updating methods is that often the sensitivity of the resonant frequencies to parameter variations is low, which has been shown both numerically [46] and experimentally [47]. To overcome this drawback, Ray and Tian [48] proposed to enhance the sensitivity of the resonant frequencies through feedback control. They used feedback control to increase the sensitivity of the poles of a system to changes in mass or stiffness. Their approach has been demonstrated on a cantilevered beam both numerically [48] and experimentally [49]. For fixed actuator locations and minimized control effort, Ray and Marini [86] explored the optimality of the sensitivity of the closed loop frequencies to mass or stiffness changes. Juang et al. [50] explored the use of eigenstructure assignment techniques for the multi-input case. They assigned the closed loop eigenvectors close to the open loop eigenvectors to minimize the control gains (and hence the control effort). Koh and Ray [53] enriched the frequency information and increased the sensitivity of the resonant frequencies by using multiple independent closed loop systems. Jiang et al. [24] formulated an optimization algorithm for eigenstructure assignment in the multi-input case. Their algorithm minimizes the control effort while maximizing the sensitivity enhancement by optimally placing both the closed loop frequencies and the eigenvectors of the system.

The third key drawback of existent frequency-shift based methods for model updating and system interrogation is their inability to handle nonlinearities. Nonlinearities, however, can be particularly beneficial for system interrogation. Recently, augmented linear systems were proposed to handle discrete nonlinearities [73, 80, 87, 94]. These augmented (fictitious) systems are of higher dimension than the corresponding nonlinear (physical) system, and are designed to follow a single trajectory of the nonlinear system when projected onto the original (physical) space. The augmentation has been used together with

approaches that use mode shape information [73, 80, 87], and frequency-shift based approaches [94]. When handling nonlinear systems using optimal feedback auxiliary signals, several benefits were discovered for system augmentation combined with optimal feedback auxiliary signals beyond handling nonlinear systems. For instance, nonlinear feedback auxiliary signals provide the ability to control the augmented (fictitious) degrees of freedom without changing the input actuation. Also, the system augmentation approach provides the ability to use unstable augmented (fictitious) systems to enhance sensitivity (while maintaining the stability of the physical linearized system). These features are key enablers for the approach proposed herein, where optimal *nonlinear* feedback auxiliary signals are designed and used for identifying parameter variations in *linear* systems. This work is distinct from (and complements) other results where nonlinearity (with given functional form and characteristics) was already present in the interrogated system, and where that nonlinearity was tailored though feedback controllers [94].

In this work, *nonlinear* feedback auxiliary signals are optimally designed and applied to *linear* systems by means of system augmentation. The nonlinear feedback signal design developed herein is a strong solution to a very challenging problem [95] in the vibration-based identification of changes in structural parameters (which is currently used in a wide variety of technologies). In particular, two areas, sensing and damage detection, focus closely on identifying parameter variations such as mass and stiffness by exploiting variations in resonant frequencies. For example, recent sensing techniques for chemical and biological detection as well as atomic force microscopes in tapping mode [41] use the vibration of micro-structures such as micro-channel resonators [96, 97], micro-beams [40] and micro-cantilevers [37–39, 98, 99]. These sensing and detection methods based on frequency shifts [100] have recently become of increasing interest. They have been developed because frequency extraction can be done robustly for both micro- and large-scale appli-

cations. Embedding (nonlinear) controllers within the interrogated system also enables additional applications of nonlinear feedback auxiliary signals such as vibration confinement [91] and vibration suppression [49].

As an application for the approach herein, damage detection is discussed in Section 6.3. An overview of damage detection (and structural health monitoring applied to civil infrastructure) is provided by Brownjohn [101]. Currently, many existent damage detection approaches are model based [102–104]. These approaches use a model of the healthy structure along with various features of the damaged structure (e.g. mode shapes, mode shape curvature, natural frequencies) to assess changes in structural properties. Here, the results focus on this application because a general, powerful approach to interrogate the monitored system is essential to the success of damage detection.

The systems explored in this chapter are a linear mass-spring system and a mass-spring-damper system. In addition to the benefits of using nonlinear control to enable the use of system augmentation, the effects of modeling generalized damping in the optimization algorithm are discussed. Also, a more realistic output feedback approach is presented, which allows for the eigenstructure assignment to be carried out with an incomplete set of measurements (where only a few displacements need to be measured). Additionally, the optimal feedback auxiliary signals have been adaptively designed to the expected level of parameter variation using a linearity constraint in the optimization algorithm. Numerical simulations are presented, and the effects of random noise are discussed.

6.2 Methodology

In this section, the procedure for using system augmentation and optimal nonlinear feedback auxiliary signals for linear systems is explained. First, the implementation of system augmentation to linear systems is discussed. Next, a frequency-shift based method

for identifying parameter variations is reviewed. Then, the eigenstructure assignment technique is detailed. Finally, the optimization algorithm that determines the parameters of the optimal nonlinear feedback auxiliary signals and system augmentation is presented.

6.2.1 System Augmentation for Linear Systems using Nonlinear Feedback Auxiliary Signals

A detailed explanation of system augmentation for nonlinear systems can be found in previous work [73, 80, 87, 94]. A key attribute of all augmented systems is that they have a higher dimension than their corresponding nonlinear system. Also, each augmented system is designed to follow a single trajectory of the nonlinear system when projected onto the original (physical) subspace.

As a simple example, consider a single degree of freedom linear mass-spring-damper system excited by a forcing $g(t)$. The equation of motion of the linear system is given by

$$m\ddot{x} + d\dot{x} + kx = g(t), \tag{6.1}$$

where m, d, k and x correspond to the mass, damping, stiffness and position, respectively, and t is time. Fig. 6.1(a) depicts this linear system with a nonlinear controller given by $N(x) = K_{CL}x + K_{CN}x^3$, where K_{CL} is the linear control gain and K_{CN} is the nonlinear (cubic) control gain. The nonlinear equation of motion of the closed loop system is

$$m\ddot{x} + d\dot{x} + (k + K_{CL})x + K_{CN}x^3 = g(t). \tag{6.2}$$

Since the closed loop system is nonlinear, the usual linear methods do not apply. However, system augmentation can be applied. Fig. 6.1(b) depicts an augmented system that can be created for Eq. (6.2), with the following equations of motion

$$\begin{aligned} m\ddot{x} + d\dot{x} + k'x + K_{CN}y &= g(t), \\ m_a\ddot{y} + k_c x + k_a y &= h(t), \end{aligned} \tag{6.3}$$

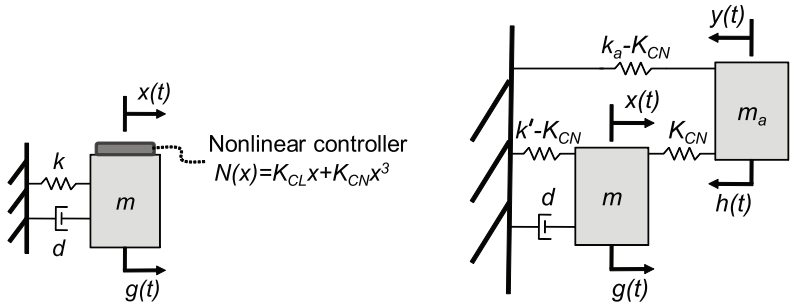

(a) (b)

Figure 6.1: One degree of freedom linear system with a nonlinear controller (a), and corresponding (higher dimensional) augmented system (b).

where m_a, k_c, k_a, y and $h(t)$ are the augmented mass, coupled stiffness, augmented stiffness, augmented variable and augmented forcing, respectively, and $k' = k + K_{CL}$. The constants m_a, k_c and k_a are chosen to provide sensitivity enhancement, and their optimization is discussed below, in subsections (6.2.3) and (6.2.4). The augmented variable is chosen as the nonlinearity, i.e. $y = x^3$. The augmented forcing $h(t)$ is calculated directly from the left hand side of Eq. (6.3) since m_a, k_c and k_a are known (chosen), $x(t)$ is measured and $y(t)$ is calculated from its (known) dependence on $x(t)$.

The augmented forcing $h(t)$ constrains the higher dimensional (augmented) system to follow a single trajectory of the nonlinear system when projected onto the lower dimension (physical) space. The use of this augmented forcing is also the reason why frequency extraction or modal analysis techniques that are used with augmented systems must be input-output approaches (as opposed to output only approaches). For example, a multi-input multi-output approach called DSPI [7] has been used successfully with augmented systems to extract both natural frequencies and mode shapes [73, 80].

Designing optimal nonlinear feedback auxiliary signals by means of system augmentation has several advantages over standard linear feedback excitation. Consider a general

multiple degree of freedom linear system that is actuated upon by a multi-input nonlinear controller. The equations of motion can be expressed as

$$\begin{bmatrix} \mathbf{M} & \mathbf{0} \\ \mathbf{0} & \mathbf{N}_{AI} \end{bmatrix} \begin{bmatrix} \ddot{\mathbf{x}} \\ \ddot{\mathbf{y}} \end{bmatrix} + \begin{bmatrix} \mathbf{D} & \mathbf{0} \\ \mathbf{0} & \mathbf{N}_{AD} \end{bmatrix} \begin{bmatrix} \dot{\mathbf{x}} \\ \dot{\mathbf{y}} \end{bmatrix} + \begin{bmatrix} \mathbf{K} + \mathbf{K}_{CL} & \mathbf{K}_{CN} \\ \mathbf{N}_{CS} & \mathbf{N}_{AS} \end{bmatrix} \begin{bmatrix} \mathbf{x} \\ \mathbf{y} \end{bmatrix} = \begin{bmatrix} \mathbf{g} \\ \mathbf{h} \end{bmatrix}, \tag{6.4}$$

where $\mathbf{M}$, $\mathbf{D}$ and $\mathbf{K}$ are the linear mass, damping and stiffness matrices of the physical system; $\mathbf{N}_{AI}$, $\mathbf{N}_{AD}$, $\mathbf{N}_{AS}$ are the augmented matrices which contain parameters of the augmentation (such as m_a and k_a); $\mathbf{N}_{CS}$ is the coupled stiffness matrix (which can be used to maintain the symmetry of the augmented system matrices for the healthy structure); and $\mathbf{K}_{CL}$ and $\mathbf{K}_{CN}$ are the linear and nonlinear control gain matrices. In contrast to Eq. (6.4), a linear system with standard linear feedback excitation would have the following equation of motion

$$\mathbf{M}\ddot{\mathbf{x}} + \mathbf{D}\dot{\mathbf{x}} + (\mathbf{K} + \mathbf{K}_{CL})\mathbf{x} = \mathbf{g}(t). \tag{6.5}$$

There are several advantages of using a system characterized by Eq. (6.4) rather than Eq. (6.5). First, the additional inputs in Eq. (6.4) (all the augmented degrees of freedom $\mathbf{y}$) allow for additional controller configurations. That can significantly increase the amount of frequency information, which in turn helps identifying more types of parameters (which may vary simultaneously). Second, having displacement information and control over additional degrees of freedom (all the augmented degrees of freedom $\mathbf{y}$) helps significantly when performing eigenstructure assignment without full state feedback. Also, the placement of $\mathbf{N}_{AI}$, $\mathbf{N}_{AD}$, $\mathbf{N}_{CS}$ and $\mathbf{N}_{AS}$ requires no actuation energy because those matrices affect only the signals used to calculate the augmented forcing $\mathbf{h}$. Finally, the system that must be stable during interrogation is the physical linearized system, while the fictitious

augmented system in Eq. (6.4) does not have to be stable. That can greatly increase the performance of the interrogation.

Note that a physical linearized system is readily extractable from the augmented system by setting the nonlinear terms to zero and removing the augmented equations.

6.2.2 First Order Frequency-Shift Based Methods

In this work, parameter variations are identified using a first order frequency-shift based method. This method has been used in the literature with sensitivity enhancing feedback control [24, 53] and optimal nonlinear feedback auxiliary signals [94]. A summary of this approach is presented next. In general, perturbations $\Delta\mathbf{p}$ to parameters lead to changes $\Delta\omega$ in the resonant frequencies, which can be expressed as

$$\Delta\omega = \mathbf{S}\Delta\mathbf{p} + \mathbf{N}(\Delta\mathbf{p}) \approx \mathbf{S}\Delta\mathbf{p} \tag{6.6}$$

where $\mathbf{S}$ is the first order sensitivity matrix, and $\mathbf{N}(\Delta\mathbf{p})$ is a nonlinear function of the change $\Delta\mathbf{p}$ in parameters. The first order perturbation approach neglects the nonlinear term $\mathbf{N}$. The entries of matrix $\mathbf{S}$ are expressed as $S_{ij} = \frac{\partial\omega_i}{\partial p_j} \approx \frac{\Delta\omega_i}{\Delta p_j}$, where $i = 1, \ldots, q$ and $j = 1, \ldots, r$, while r represents the number of variable parameters p_i, and q represents the number of measurable frequencies ω_j. Thus, $\Delta\mathbf{p}$ is a vector of dimension r while $\Delta\omega$ is a vector of dimension q. The first order perturbation approximation is expected to be valid for small parameter variations. In this work, a linearity constraint is added to the optimization function to ensure the validity of Eq. (6.6) up to the desired/expected level of parameter variation. Assuming that the matrix $\mathbf{S}$ has full rank, one may use the pseudo-inverse of $\mathbf{S}$ to solve Eq. (6.6) for the unknown vector of parameter variations as $\Delta\mathbf{p} = \mathbf{S}^{+}\Delta\omega$.

Designing optimal nonlinear feedback auxiliary signals for linear systems has two goals. The first goal is to create multiple independent closed loop systems to increase

the amount of measured frequency information. This is particularly important when the number of variable parameters r is greater than the number of measured frequencies q. The independent closed loop sensitivity matrices (denoted by $\mathbf{S}^{ci}$) can be combined to form the overall sensitivity matrix expressed as $\mathbf{S} = \left[\mathbf{S}^{c1\ \mathrm{T}}\ \mathbf{S}^{c2\ \mathrm{T}} \ldots \mathbf{S}^{cu\ \mathrm{T}}\right]^{\mathrm{T}}$, where u is the number of unique controller configurations used, and superscript T indicates a transpose. When $\mathbf{S}$ is full rank and $q \cdot u > r$, then an overdetermined set of equations exist, and $\Delta\mathbf{p}$ can be obtained as $\Delta\mathbf{p} = \mathbf{S}^{+}\Delta\omega$. The second goal is to increase the sensitivity of the closed loop sensitivity matrices (denoted by $\mathbf{S}^{ci}$) compared to the open loop sensitivity matrix.

6.2.3 Eigenstructure Assignment via Singular Value Decomposition

Eigenstructure assignment via singular value decomposition has been studied extensively for linear systems [88–92]. The following is a brief overview of eigenstructure assignment that follows closely the work presented by Jiang et al. [24], but it is extended for augmented systems and includes the option for the direct output feedback of Juang et al. [50] (as opposed to full state feedback). Consider Eq. (6.4) transformed into state space. The augmented equations of motion in state space form are

$$\begin{bmatrix} \mathbf{M}_A & \mathbf{0} \\ \mathbf{0} & \mathbf{I} \end{bmatrix} \begin{bmatrix} \ddot{\mathbf{z}} \\ \dot{\mathbf{z}} \end{bmatrix} + \begin{bmatrix} \mathbf{D}_A & \mathbf{K}_A \\ -\mathbf{I} & \mathbf{0} \end{bmatrix} \begin{bmatrix} \dot{\mathbf{z}} \\ \mathbf{z} \end{bmatrix} + (\mathbf{BCH}) \begin{bmatrix} \dot{\mathbf{z}} \\ \mathbf{z} \end{bmatrix} = \begin{bmatrix} \mathbf{f} \\ \mathbf{0} \end{bmatrix}, \qquad (6.7)$$

where

$$\mathbf{z} = \begin{bmatrix} \mathbf{x} \\ \mathbf{y} \end{bmatrix}, \quad \text{and} \quad \mathbf{f} = \begin{bmatrix} \mathbf{g} \\ \mathbf{h} \end{bmatrix},$$

and where $\mathbf{M}_A$, $\mathbf{D}_A$ and $\mathbf{K}_A$ are $N_o \times N_o$ augmented mass, damping and stiffness matrices; $\mathbf{x}$ and $\mathbf{y}$ are the $N \times 1$ coordinate vector and $n \times 1$ augmented variable vector; $\mathbf{g}$ and $\mathbf{h}$ are the $N \times 1$ physical forcing and $n \times 1$ augmented forcing; and $\mathbf{B}$, $\mathbf{C}$ and $\mathbf{H}$ are the $2N_o \times c$ controller input matrix, $c \times s$ control matrix and $s \times 2N_o$ sensor matrix. Here, c is the

number of actuators, and s is the number of sensors used. Note that $N_o = N + n$, and the control gain matrix is defined as $\mathbf{K}_C = \mathbf{CH}$. Also, the bottom N_o rows of the controller input matrix $\mathbf{B}$ are always zero. Eq. (6.7) can be written as

$$\mathbf{M}_{ss}\dot{\mathbf{z}}_{ss} + (\mathbf{A} + \mathbf{BCH})\mathbf{z}_{ss} = \mathbf{F}, \tag{6.8}$$

where

$$\mathbf{M}_{ss} = \begin{bmatrix} \mathbf{M}_A & \mathbf{0} \\ \mathbf{0} & \mathbf{I} \end{bmatrix}, \quad \mathbf{A} = \begin{bmatrix} \mathbf{D}_A & \mathbf{K}_A \\ -\mathbf{I} & \mathbf{0} \end{bmatrix}, \quad \mathbf{F} = \begin{bmatrix} \mathbf{f} \\ \mathbf{0} \end{bmatrix}, \quad \text{and} \quad \mathbf{z}_{ss} = \begin{bmatrix} \dot{\mathbf{z}} \\ \mathbf{z} \end{bmatrix}.$$

The eigenvalue problem for the augmented closed loop system can be expressed as

$$-(\mathbf{A} + \mathbf{BCH})\phi_j = \omega_{cj}\mathbf{M}_{ss}\phi_j, \tag{6.9}$$

where ω_{cj} is the j^{th} closed loop eigenvalue and ϕ_j is the corresponding eigenvector. Eq. (6.9) can alternatively be written as

$$[\mathbf{A} + \omega_{cj}\mathbf{M}_{ss}|\mathbf{B}] \begin{bmatrix} \phi_j \\ \mathbf{CH}\phi_j \end{bmatrix} = \mathbf{0}, \tag{6.10}$$

which means that $\left[\phi_j^{\mathrm{T}}\ \mathbf{CH}\phi_j^{\mathrm{T}}\right]^{\mathrm{T}}$ must fall into the null space of $[\mathbf{A} + \omega_{cj}\mathbf{M}_{ss}|\mathbf{B}]$. The symbol $|$ indicates a partition in the matrix, e.g. the matrix is composed of two matrices side by side.

Next, perform a singular value decomposition of $[\mathbf{A} + \omega_{cj}\mathbf{M}_{ss}|\mathbf{B}]$ to obtain

$$[\mathbf{A} + \omega_{cj}\mathbf{M}_{ss}|\mathbf{B}] = \mathbf{U}_j[\mathbf{D}_j|\mathbf{0}_{2N_o \times c}]\mathbf{V}_j^*, \tag{6.11}$$

where $\mathbf{U}_j$ and $\mathbf{V}_j$ correspond to the left and right singular matrices, respectively, and $\mathbf{D}_j$ is a diagonal matrix that contains the singular values. The superscript $*$ indicates a complex conjugate. The right singular matrix can be partitioned into 4 sub-matrices

$$\mathbf{V}_j = \begin{bmatrix} \mathbf{V}_{11}^j & \mathbf{V}_{12}^j \\ \mathbf{V}_{21}^j & \mathbf{V}_{22}^j \end{bmatrix}, \tag{6.12}$$

where $\mathbf{V}_{11}^j$ is $2N_o \times 2N_o$, $\mathbf{V}_{12}^j$ is $2N_o \times c$, $\mathbf{V}_{21}^j$ is $c \times 2N_o$, and $\mathbf{V}_{22}^j$ is $c \times c$.

To exploit the orthogonality property of the singular value decomposition, one can multiply Eq. (6.11) by $\left[\mathbf{V}_{12}^{j\,\mathrm{T}}\ \mathbf{V}_{22}^{j\,\mathrm{T}}\right]^{\mathrm{T}}$ to obtain

$$[\mathbf{A} + \omega_{cj}\mathbf{M}_{ss}|\mathbf{B}] \begin{bmatrix} \mathbf{V}_{12}^j \\ \\ \mathbf{V}_{22}^j \end{bmatrix} = \mathbf{0}. \tag{6.13}$$

Next, a coefficient vector $\mathbf{f}_j$ can be defined for the j^{th} eigenvector in its admissible subspace. That subspace is the span of $\mathbf{V}_{12}^j$, as shown by Eq. (6.13). Hence, the assigned eigenvector ϕ_j^a can be expressed as $\phi_j^a = \mathbf{V}_{12}^j \mathbf{f}_j$, while $\mathbf{CH}\phi_j^a = \mathbf{V}_{22}^j \mathbf{f}_j$. Next, gather all $2N_o$ eigen-solutions for all j to obtain $\mathbf{CH}\mathbf{\Phi}^a = \mathbf{W}$, where $\mathbf{\Phi}^a = \left[\phi_1^a\ \phi_2^a\ \ldots\ \phi_{2N_o}^a\right]$, $\phi_j^a = \mathbf{V}_{12}^j \mathbf{f}_j$, and $\mathbf{W} = [\mathbf{w}_1\ \mathbf{w}_2\ \ldots\ \mathbf{w}_{2N_o}]$, $\mathbf{w}_j = \mathbf{V}_{22}^j \mathbf{f}_j$. Then, invert $\mathbf{H}\mathbf{\Phi}^a$ to solve for the control matrix as $\mathbf{C} = \mathbf{W}\left(\mathbf{H}\mathbf{\Phi}^a\right)^+$, where superscript $+$ indicates the pseudo-inverse. Finally, the control gain matrix $\mathbf{K}_C$ can then be calculated as $\mathbf{K}_C = \mathbf{CH}$.

The number of frequencies that can be placed by this technique is limited for the case where full state feedback is not employed (i.e. when $s < 2N_o$). The number of assignable frequencies q was given by Juang et al. [50] as $2q \leq \max(c, s)$.

6.2.4 Optimization Algorithm for Sensitivity Enhancement

The relationship between eigenvectors and resonant frequencies (with sensitivity enhancement) on one side and control effort on the other side is complex in the multiple degree of freedom case [24]. As a result, optimization algorithms are used to design $\mathbf{K}_C$ to place the frequencies and eigenvectors optimally by maximizing sensitivity while minimizing control effort. In this work, a linearity constraint is also included in the optimization algorithm to enforce the linearity needed when using Eq. (6.6). The optimization algorithm follows closely the algorithm presented previously [24, 94], which maximizes the sensitivity while minimizing the control effort.

The parameters optimized are the coefficient vectors $\mathbf{f}_j$, the frequencies ω_{cj} of the q measurable frequencies, and the n augmented masses m_{ai}^o (where one assumes that the augmented mass matrix is diagonal). Primarily for computational reasons, the latter two sets of these parameters are defined relative to their open loop or nominal values. Hence, the optimization is applied to parameters γ_j and Γ_i, defined by $\omega_{cj} = \gamma_j \omega_{oj}$, and $m_{ai}^o = \Gamma_i m_{ai}$, where ω_{oj} are the open loop eigenvalues of the system, m_{ai} are nominal values for the augmented masses (values chosen by the user are typically close to the value of the mass at the degree of freedom the nonlinearity originates from), and $j = 1, 2, \ldots, q$, $i = 1, 2, \ldots n$. Note that, in general the augmented equations are not unique for a given nonlinear system, in fact multiple augmentations of a single nonlinear system have been exploited for damage detection [80]. Also, note that the stiffness portion of the augmentation is already being optimized via the calculation of the rows in the gain matrix that correspond to the augmented equations.

The assigned closed loop eigenvectors can be expressed as $\phi_j^c = \mathbf{V}_{12}^j \mathbf{f}_j$ for $j = 1, 2, \ldots, q$. The remainder of the eigenvectors (for $j = q+1, q+2, \ldots, N_o$) have to be placed as close as possible to the open loop eigenvectors ϕ_j^o to minimize the control effort. Hence, one searches for the coefficient vectors $\tilde{\mathbf{f}}_j$ so that ϕ_j^c is as close as possible to $\mathbf{V}_{12}^j \tilde{\mathbf{f}}_j$. The coefficient vectors $\tilde{\mathbf{f}}_j$ can be found by minimizing $\left\| \phi_j^o - \mathbf{V}_{12}^j \tilde{\mathbf{f}}_j \right\|$ (and $\left\| \tilde{\mathbf{f}}_j \right\|$). The coefficient vectors are obtained as $\tilde{\mathbf{f}}_j = \left(\mathbf{V}_{12}^{j*} \mathbf{V}_{12}^j \right)^{-1} \mathbf{V}_{12}^{j*} \phi_j^o$. Finally, the closest achievable eigenvector is given by $\phi_j^c = \mathbf{V}_{12}^j \left(\mathbf{V}_{12}^{j*} \mathbf{V}_{12}^j \right)^{-1} \mathbf{V}_{12}^{j*} \phi_j^o$, where $j = q+1, q+2, \ldots, N_o$.

The optimization cost function (which is maximized) includes the level of sensitivity enhancement. This level is defined as the sum of the (absolute values of the) element by element ratios of the closed loop sensitivity matrices $\mathbf{S}^{ci}$ to the open loop sensitivity matrix, divided by the number of elements. Also, the singular values of $\mathbf{S}$ are maximized (particularly the minimum singular value). This is important when noisy data are used,

and in cases where very few measurements are taken.

The control effort for the nonlinear feedback actuation is optimized by minimizing the absolute value of the maximum entry in the controller gain matrix $\mathbf{K}_C$. The rows of the gain matrix that correspond to the augmented equations are not included in the controller effort because the augmented degrees of freedom do not require any physical actuation (but just signal processing). The relative importance of these components of the optimization is taken into account by weighting the sensitivity enhancement with a coefficient c_1 and the control effort with a coefficient c_2.

The optimization is subject to stability constraints because the physical system cannot be unstable during its interrogation.

Note that the stability of the physical linearized system is (related to but) independent of the stability of the augmented system. The important issue is the stability of the physical linearized system. That is ensured by a constraint in the optimization algorithm. Note that the instability in the augmented system is due to the augmentation and not the physics. Hence, it is possible for an augmented system to be unstable while the physical system is stable. The reason why the augmented system can be unstable while the response of the physical system remains stable is the specialized augmented forcing which limits the growth of the motion of the augmented system.

Thus, the important issue is ensuring the stability of the linearized physical system, whereas the augmented linear system does not have to be stable. The linearized physical system must be stable both when it is healthy and after each damage scenario. Thus, the optimization is subject to the following constraints

$$\begin{aligned} \Re(\omega_{cj}^L) &\leq 0, \quad j = 1, 2, \ldots, N, \\ \Re(\omega_{dcji}^L) &\leq 0, \quad j = 1, 2, \ldots, N; \;\; i = 1, 2, \ldots, r, \end{aligned}$$

where ω_{cj}^L are the linearized closed loop eigenvalues of the baseline system, and ω_{dcji}^L

are the linearized closed loop eigenvalues of the system with changed parameters. These constraints must be satisfied for the maximum allowable (expected) level of parameter variations for all r scenarios of parameter variations.

Furthermore, in order for Eq. (6.6) to hold, a relationship close to linear must exist between $\Delta\omega$ and $\Delta\mathbf{p}$. A linearity constraint can be included into the optimization algorithm to enforce this relationship. In this work, cost was added proportional to $\left|\frac{\partial\omega_i}{\partial p_j} - \frac{\Delta\omega_i}{\Delta p_j}\right|$. Here, $\frac{\partial\omega_i}{\partial p_j}$ is obtained for a small change in parameter p_j, and $\frac{\Delta\omega_i}{\Delta p_j}$ is obtained for the maximum allowable damage level for parameter p_j.

An important aspect of any frequency-based method is ensuring that the sensitivity matrix used for parameter reconstruction is full rank. Hence, the optimization process can include maximizing the sensitivity matrices $\mathbf{S}^{ci}$ (which compose $\mathbf{S}$) while also maximizing the minimum singular value of $\mathbf{S}$. Maximizing the minimum singular value of $\mathbf{S}$ in the optimization process ensures that this overall sensitivity matrix is full rank (when the minimum singular value is large). Hence, the independence of the sensitivities of the closed loop systems is ensured as closely as possible. However, given the limited measurements and control input actuators, it is possible that only a subset of the parameters is identifiable, and variations in the unidentifiable parameters have to be detected by other means.

6.3 Results

To demonstrate the proposed methods, numerical simulations were performed for the systems shown in Figs. 6.2 and 6.3. The system in Fig. 6.2 is a 6 degree of freedom linear mass-spring system. Considering the parameter identification as a damage detection problem, the damageable elements consist of the 6 linear springs with stiffnesses denoted as $p_1 = k_{1g}$, $p_2 = k_{12}$, $p_3 = k_{23}$, $p_4 = k_{34}$, $p_5 = k_{45}$ and $p_6 = k_{56}$. The controller input actuators were located at the 1^{st} and 6^{th} masses. The system in Fig. 6.3 is similar to

the one in Fig. 6.2, with 6 dampers placed between the masses and ground. Augmented linear systems were created by generating matrices $\mathbf{M}$, $\mathbf{D}$, $\mathbf{K}$, $\mathbf{K}_{CL}$, $\mathbf{K}_{CN}$, $\mathbf{N}_{AI}$, $\mathbf{N}_{AD}$, $\mathbf{N}_{AS}$ and $\mathbf{N}_{CS}$ in Eq. (6.4). The nonzero entries of the $\mathbf{K}_{CN}$ matrix consist of cubic nonlinearities that are generated using nonlinear feedback control. The matrix $\mathbf{N}_{AI}$ consists of the augmented masses. The nominal values for the augmented masses are chosen to have the same values as the (physical) masses they are coupled to. The matrix $\mathbf{N}_{CS}$ is constructed to create a symmetric augmentation for the nominal (healthy) system. The matrix $\mathbf{N}_{AS}$ is a diagonal matrix that contains the terms k_a chosen as $k_a = 2k_n$. The matrix $\mathbf{N}_{AD}$ is a zero matrix. The matrices $\mathbf{M}$, $\mathbf{D}$, and $\mathbf{K}$ have been constructed for the physical uncontrolled system using the parameters given in Figs. 6.2 and 6.3. The entries in the matrices $\mathbf{K}_{CL}$, $\mathbf{K}_{CN}$, $\mathbf{N}_{AI}$, $\mathbf{N}_{CS}$ and $\mathbf{N}_{AS}$ are then all optimized. The constrained optimization problem was solved using the `fmincon` function in MATLAB [93]. Note that the global optimum was not always found because of the initial guesses used. Three controllers ($NFAS1-3$) were designed to maximize the sensitivity of the first 3 frequencies of the system to changes in the 6 (damageable) elements. The different combinations of feedback auxiliary signals are given by actuation locations as follows: $NFAS1$ - [1, 6, 7, 8]; $NFAS2$ - [1, 7, 8]; and $NFAS3$ - [6, 7, 8]. Note that locations 7 and 8 correspond to the augmented degrees of freedom, which require no actual actuation, but only signal processing. Additionally, 3 different combinations of linear feedback controllers were also used: $LF1$ - [1, 6]; $LF2$ - [1]; and $LF3$ - [6].

6.3.1 Frequency Extraction for Unstable Augmented System

In this section, an example of how the frequencies of an augmented system can be extracted using DSPI [7], a time-based multi-input multi-output modal analysis technique, is demonstrated. In particular, the system explored was physically stable during its inter-

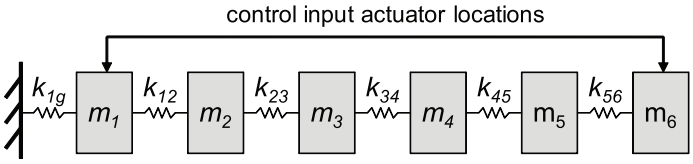

Figure 6.2: Linear mass-spring system that has nonlinear control applied at 2 locations with parameters $m_i = 1, i = 1, 2, \ldots 6$, $k_{1g} = k_{34} = 10^4$, $k_{12} = k_{23} = 1.5 \cdot 10^4$, $k_{45} = 2 \cdot 10^4$, and $k_{56} = 2.5 \cdot 10^4$.

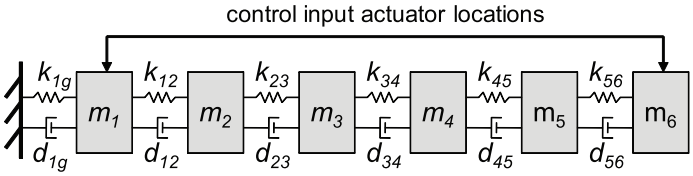

Figure 6.3: Linear mass-spring-damper system that has nonlinear control applied at 2 locations (with the same mass and stiffness parameters as in Fig. 6.2) and $d_{1g} = 30$, $d_{12} = 35$, $d_{23} = 40$, $d_{34} = 18$, $d_{45} = 27$ and $d_{56} = 53$.

rogation. However, the augmented system was unstable. An unstable augmented system can be physically stable because the augmented system is a fictitious system excited by a specific augmented forcing. In the case of the unstable augmented system, the augmented forcing actually stabilizes the response of the augmented system such that the response is bounded.

Tab. 6.1 shows the eigenvalues of a physically stable system characterized by an unstable augmented system. These eigenvalues are those of a 6 degree of freedom mass-spring system (shown in Fig. 6.2) with nonlinear feedback auxiliary signals applied to the 1^{st} and 6^{th} masses. The first column of Tab. 6.1 consists of the eigenvalues of the linearized system. There are 6 eigenvalues because there are 6 physical degrees of freedom. The second column of Tab. 6.1 consists of the exact eigenvalues of the augmented system. There are 8 eigenvalues for the augmented system: 6 for the physical degrees of freedom,

Eigenvalues of Physical Linearized System	Exact Eigenvalues of Augmented System	Eigenvalues of Augmented System Computed by DSPI
	0.5042 + 12.9049i	0.4862 + 12.9045i
	0.5042 - 12.9049i	0.4862 - 12.9045i
5.6881i	54.5368i	54.5368i
75.8141i	82.97i	82.9699i
144.43i	145.7084i	145.7087i
179.3784i	179.779i	179.779i
222.2159i	222.3982i	222.3981i
264.0378i	264.0428i	264.0428i

Table 6.1: Eigenvalues of a physically stable system with an unstable augmented system.

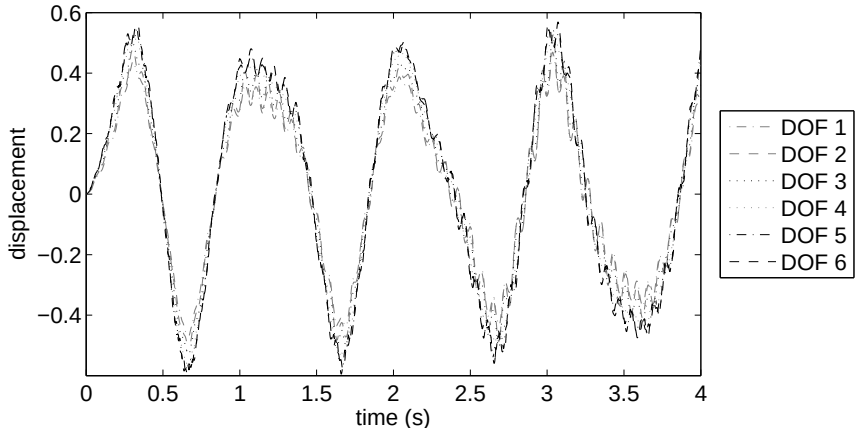

Figure 6.4: Response of the 6 physical degrees of freedom (DOF) of a physically stable system with an unstable augmented system.

and 2 for the augmented degrees of freedom (one for each nonlinearity). The last column of Tab. 6.1 consists of the eigenvalues extracted using DSPI, when the physical system is forced by harmonic excitation at all 6 physical degrees of freedom. Comparing the 2^{nd} and 3^{rd} columns of Tab. 6.1, it is clear that DSPI can accurately extract the eigenvalues of an unstable augmented system. Fig. 6.4 shows the response of the 6 physical degrees of freedom of the system to the harmonic excitation used.

System	Actuator locations	Control Effort	Optimal closed loop augmented mass parameters	Optimal closed-loop eigenvalues	Coefficient vectors of optimal closed-loop eigenvectors
Linear Feedback					
LF-1	1,6	1.29	-	$\omega_{c1}=1.00\omega_{o1}$ $\omega_{c2}=0.34\omega_{o2}$ $\omega_{c3}=0.16\omega_{o3}$	f_1=[38.48, -10.09] f_2=[-1.17, -1.01] f_3=[17.01, 14.05]
LF-2	1	2.31	-	$\omega_{c1}=0.71\omega_{o1}$ $\omega_{c2}=0.25\omega_{o2}$ $\omega_{c3}=0.15\omega_{o3}$	f_1=[2.30] f_2=[-1.41] f_3=[0.95]
LF-3	6	1.46	-	$\omega_{c1}=0.19\omega_{o1}$ $\omega_{c2}=0.10\omega_{o2}$ $\omega_{c3}=0.73\omega_{o3}$	f_1=[-0.99] f_2=[0.98] f_3=[1.00]
Nonlinear Optimal Feedback Auxiliary Signals					
NFAS-1	1,6,7,8	0.32	$m^o_{a1}=0.10m_{a1}$ $m^o_{a2}=0.16m_{a2}$	$\omega_{c1}=0.10\omega_{o1}$ $\omega_{c2}=0.16\omega_{o2}$ $\omega_{c3}=1.00\omega_{o3}$	f_1=[-8.62, 9.27, 5.43, -4.48] f_2=[1.97, -1.44, 1.85, -7.22] f_3=[-2.26, -2.11, 1.14, -3.05]
NFAS-2	1,7,8	0.2	$m^o_{a1}=1.23m_{a1}$ $m^o_{a2}=1.07m_{a2}$	$\omega_{c1}=0.81\omega_{o1}$ $\omega_{c2}=0.30\omega_{o2}$ $\omega_{c3}=0.24\omega_{o3}$	f_1=[11.08, 37.81, -5.24] f_2=[2.89, 5.60, -1.87] f_3=[0.09, 8.46, 3.07]
NFAS-3	6,7,8	0.3	$m^o_{a1}=0.22m_{a1}$ $m^o_{a2}=1.86m_{a2}$	$\omega_{c1}=1.00\omega_{o1}$ $\omega_{c2}=0.82\omega_{o2}$ $\omega_{c3}=0.54\omega_{o3}$	f_1=[0.38, -3.15, 1.47] f_2=[-1.01, 4.91, -8.60] f_3=[-1.24, -3.89, 20.91]

Table 6.2: Design parameters for multiple (sensitivity enhancing) linear feedback excitations and nonlinear feedback auxiliary signals.

6.3.2 Linear Feedback vs. Optimal Nonlinear Feedback Auxiliary Signals

In this section, a comparison of linear feedback excitation and optimal nonlinear feedback auxiliary signals is provided. In these results, the measurements collected are the positions of the 6 linear degrees of freedom (the velocities of the masses are not measured). The weighting factors were chosen as $c_1 = 10^3$ and $c_2 = 10^{-4}$.

The design variables (γ_1, γ_2, γ_3, $\mathbf{f}_1$, $\mathbf{f}_2$, $\mathbf{f}_3$, Γ_1, and Γ_2) for the linear feedback controller and the nonlinear feedback auxiliary signals are shown in Tab. 6.2. The optimal closed loop augmented mass parameters are not listed in the linear feedback section of the table since no augmentation is created for the case of linear feedback applied to a linear system.

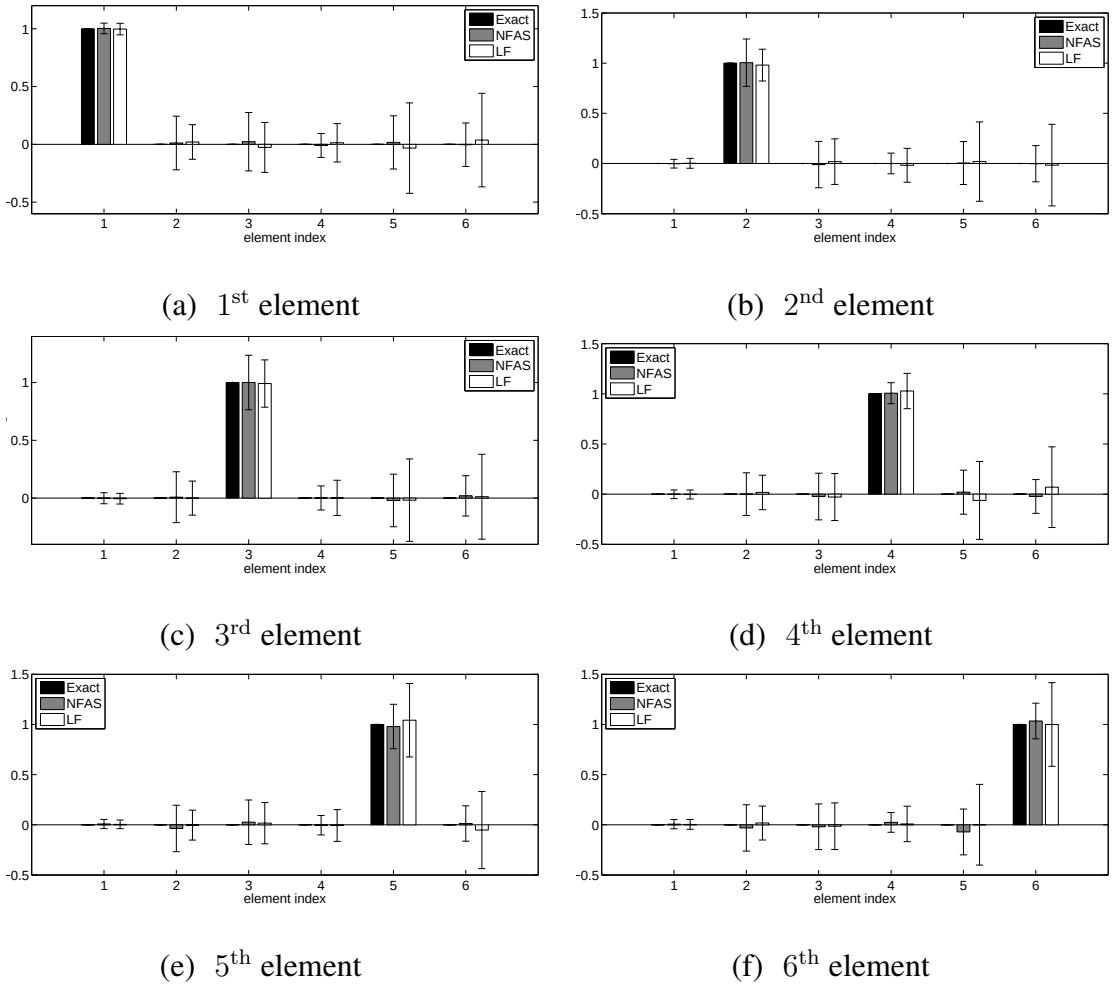

(a) 1^{st} element

(b) 2^{nd} element

(c) 3^{rd} element

(d) 4^{th} element

(e) 5^{th} element

(f) 6^{th} element

Figure 6.5: Damage detection results for resonant frequencies contaminated with ± 0.25 random noise for linear feedback (LF) and nonlinear feedback auxiliary signals (NFAS) for the 1^{st} (a), 2^{nd} (b), 3^{rd} (c), 4^{th} (d), 5^{th} (e), and 6^{th} (f) elements.

It should be noted that the control effort is considerably $(4 - 10$ times) larger for the cases where linear feedback is used.

The results in Fig. 6.5 show the increased performance when using nonlinear feedback auxiliary signals and system augmentation versus using just linear feedback excitation for the 6 damage scenarios. The x-axis in each plot corresponds to the damaged elements, while the y-axis in each plot corresponds to the percent damage. Each plot shows the exact value of the damage, and the average predicted damage for linear feedback and nonlinear

feedback auxiliary signals. One hundred separate calculations were performed for the case of ± 0.25 ($\sim 1\%$ of the lowest frequency) random noise applied to the frequencies of the damaged system. Standard deviation error bars are plotted. Note that elements 4, 5 and 6 have smaller error bars when nonlinear feedback auxiliary signals are used instead of standard linear feedback.

Also, elements 2 and 3 have slightly decreased performance, but that is a small issue compared to the significant improvement at elements 4, 5 and 6, and the fact that the control effort required when using the nonlinear feedback is 4 to 10 times smaller than that required by the linear feedback.

6.3.3 Linearity and Sensitivity

In this section, the relationships between the linearity constraint, the sensitivity to noise and the damage level are explored. Two sets of controllers were designed to maximize the sensitivity of frequencies. The first set of controllers $0.1NFAS1-3$ were designed to maximize the sensitivity of the first 3 frequencies to a 0.1% change in parameters. The second set of controllers $5.0NFAS1-3$ were designed to maximize the sensitivity of the first 3 frequencies to a 5% change in parameters. In each case, the positions of the 6 masses were used for feedback.

The relationship between sensitivity and linearity of each set of controllers is shown in Fig. 6.6. The plots show the changes in the 1^{st} frequency for damages in one linear spring for the open loop and each set of closed loop systems (i.e. $0.1NFAS1-3$ and $5.0NFAS1-3$). The x-axis in each plot corresponds to the change in parameter p_1, while the y-axis in each plot corresponds to the change in the 1^{st} frequency ω_1. Fig. 6.6(a) and Fig. 6.6(b) correspond to a parameter change of up to 0.1%, while Fig. 6.6(c) and Fig. 6.6(d) correspond to a parameter change of up to 5%. Fig. 6.6(a) and Fig. 6.6(b)

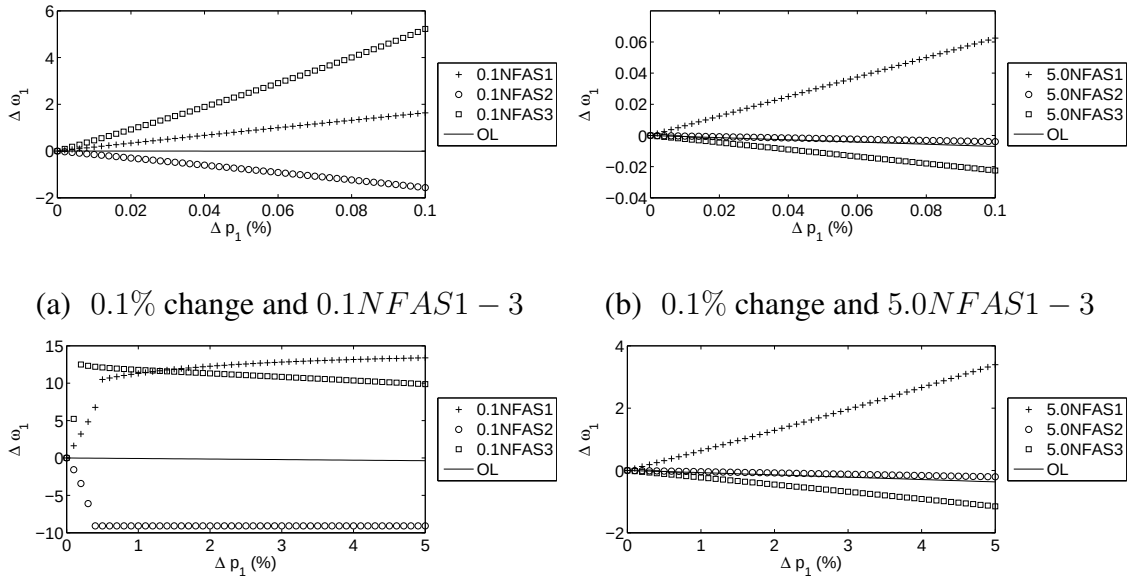

(a) 0.1% change and $0.1NFAS1-3$ (b) 0.1% change and $5.0NFAS1-3$

(c) 5% change and $0.1NFAS1-3$ (d) 5% change and $5.0NFAS1-3$

Figure 6.6: Sensitivity of the 1^{st} resonant frequency to a 0.1% change in a linear spring using $0.1NFAS1-3$ (a) and $5.0NFAS1-3$ (b), and to a 5% change using $0.1NFAS1-3$ (c) and $5.0NFAS1-3$ (d).

show the linear relationship between the change in frequency and the change in parameter required by Eq. (6.6). These results also show that the sensitivity of the controllers designed for a 0.1% parameter change ($0.1NFAS1-3$) is much larger than the sensitivity of the controllers designed for a 5% parameter change ($5.0NFAS1-3$). Fig. 6.6(c) and Fig. 6.6(d) show that the controllers designed for a 0.1% parameter change do not have a linear relationship between the change in frequency and the change in parameter p_1 over the 5% range, while the linear relationship does exist for $5.0NFAS1-3$. Similar results can be obtained for the other 2 frequencies and 5 parameters, but are omitted here for the sake of brevity.

The results in Fig. 6.7 show the excellent performance of the nonlinear approach for two different cases. The first case consists of a 0.1% damage using the $0.1NFAS1-3$ controllers. One hundred separate calculations were performed for the case of ± 0.1

random noise in the measured frequencies. The second case consists of 5% damage using the $5.0FAS1-3$ controllers with ± 1.0 random noise applied to the measured frequencies. The plots are laid out in a similar manner to Fig. 6.5. The y-axis consists of a normalized damage (the damage for each case is divided by the maximum damage) instead of a percent damage. Standard deviation error bars are plotted for both noisy cases.

6.3.4 Modeling Generalized Damping

In this section, the effects of modeling damping in the optimization process are considered. The mass-spring-damper system explored is shown in Fig. 6.3. The form of damping included in the system is a generalized linear damping. The more challenging case of generalized damping is investigated instead of the common proportional damping. Note that the modes of a system with generalized damping are not the same as the ones for the undamped system. In contrast, the modes of a proportionally damped system are the same with or without proportional damping.

The results in Fig. 6.8 compare the performance of the approach for two different control optimizations. The first corresponds to a case where the generalized damping is not modeled in the optimization algorithm. The second corresponds to a case where the generalized damping is modeled in the optimization algorithm. In both cases the only measured locations are the positions of the 1^{st} and 6^{th} degrees of freedom. In addition to these linear degrees of freedom, the positions of the two augmented degrees of freedom are also known (by their relation to the positions of the 1^{st} and 6^{th} degrees of freedom). Due to the eigenvector assignment constraint $2q \leq \max(c, s)$, the maximum number of frequencies and mode shapes q that can be assigned when $s = 4$ and $c = 4$ is $q = 2$. Note that, if a purely linear control were used, s and c would be equal to 2 and the maximum number of frequencies and mode shapes that could be placed would be one, which would

lead to poor damage detection performance.

For these results, the optimization algorithm included the maximization of the minimum singular value of the sensitivity matrix. However, given the limited measurements and control input actuators (sensors and actuators only at the 1^{st} and 6^{th} mass), only 5 parameters of the 6 were identifiable. That indicates that the changes in the 2 frequencies for the 3 control configurations could not create a matrix $\mathbf{S}$ of full rank for all 6 parameters. Therefore, the parameter p_6 was removed as a damageable parameter. One hundred separate calculations were performed for the case of ± 0.12 random noise (which corresponds to $\sim 2\%$ noise in the lowest resonant frequency) in the frequencies of the damaged system. The plots are laid out in the same manner as Fig. 6.5. Standard deviation error bars are plotted for both noisy cases.

6.4 Conclusions and Discussion

A novel approach for improving the sensitivity enhancement for linear systems using optimal *nonlinear* feedback auxiliary signals and system augmentation was presented. The nonlinear feedback auxiliary signals apply linear and nonlinear feedback to the structure. The nonlinearity is handled with system augmentation, which consists of higher dimensional linear models for a trajectory of the physical nonlinear system.

The optimal nonlinear feedback auxiliary signals have been adaptively designed to the level of parameter variation expected. In general, some feedback signals work better for larger parameter variations, when the needed level of sensitivity enhancement is low. However, those signals are not effective for cases where very small parameter variations are expected. There, a hyper-enhancement of sensitivity is needed, and that can be accomplished only by distinct feedback signals. If one naively applies the hyper-sensitive signals to large parameter variations, failures occur in the interrogation because the assumption of

linearity of the frequency shifts with respect to parameter variations is no longer accurate. The adaptive design of the feedback signals is done by a linearity constraint built into the optimization algorithm. That constraint ensures the linearity for any level of parameter variation below the expected values (and it also alleviates other limits on the frequencies of the augmented system).

The eigenstructure assignment used in the design of the feedback signals was done using only partial measurements (of an augmented model). This is an important advantage over other techniques because in many practical implementations only a few degrees of freedom can be measured.

The optimal nonlinear feedback auxiliary signals have been applied to linear systems. Hence, the benefits of nonlinearities compared to traditional linear sensitivity enhancing approaches can be clearly identified. These benefits include a reduced number of actuator points, and a reduced number of sensor locations needed.

The nonlinear feedback auxiliary signals and the system augmentation approach also have the benefit of allowing for physically stable systems to be characterized by unstable augmented systems. Although the augmented system is unstable, the response of this system is still bounded because the linearized physical system is actually stable. The response of the augmented system is bounded because the specified augmented forcing stabilizes the response of the system. Furthermore, the frequencies of these systems can be found using linear multi-input multi-output approaches such as DSPI.

The ability to place the augmented degrees of freedom arbitrarily without extra controller effort is an additional benefit of the proposed approach. This allows for additional controller configurations to diversify the frequency information. Moreover, the added "control" helps when there are limited numbers of sensors and actuators. The eigenvector assignment procedure allows for the placement of q frequencies and modes, where $2q$ is

less than or equal to the number of actuators or sensors.

The benefits of modeling generalized damping in the optimization algorithm was shown. A state space formulation of the equations of motion is required for the optimization algorithm when generalized damping is present. However, the benefits for damage detection are significant. When damping is ignored in the optimization algorithm, the optimizer places the poles and modes optimally for the wrong system, which leads to a lower performance.

To demonstrate the use of nonlinear feedback auxiliary signals and system augmentation for sensitivity enhancement, a damage detection problem has been studied for linear mass-spring and mass-spring-damper systems. The effects of the level of damage and measurement noise were also discussed.

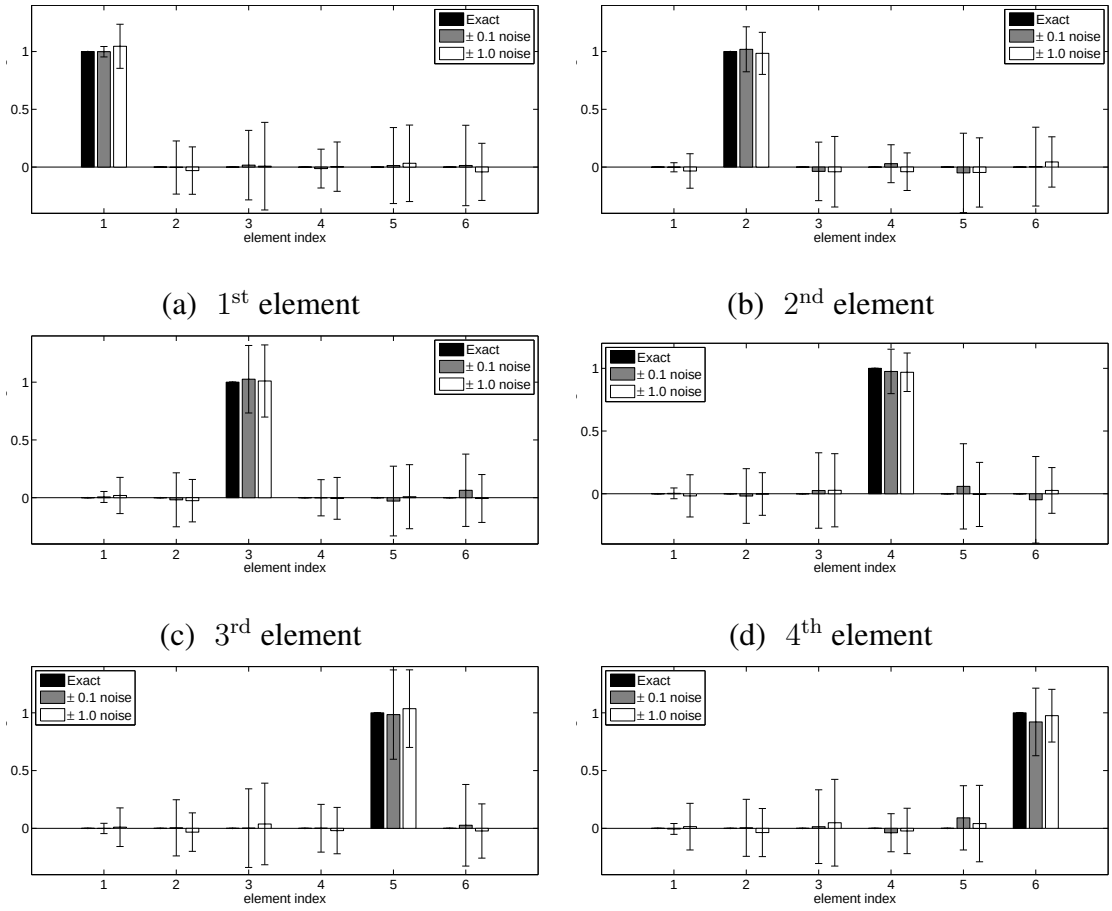

(a) 1^{st} element

(b) 2^{nd} element

(c) 3^{rd} element

(d) 4^{th} element

(e) 5^{th} element

(f) 6^{th} element

Figure 6.7: Damage detection results for resonant frequencies contaminated with ± 0.1 and ± 1.0 random noise for $0.1NFAS1-3$ and $5.0NFAS1-3$ for 0.1% and 5% damage, respectively, for the 1^{st} (a), 2^{nd} (b), 3^{rd} (c), 4^{th} (d), 5^{th} (e), and 6^{th} (f) elements. The damage for each case is normalized by dividing it by the maximum damage.

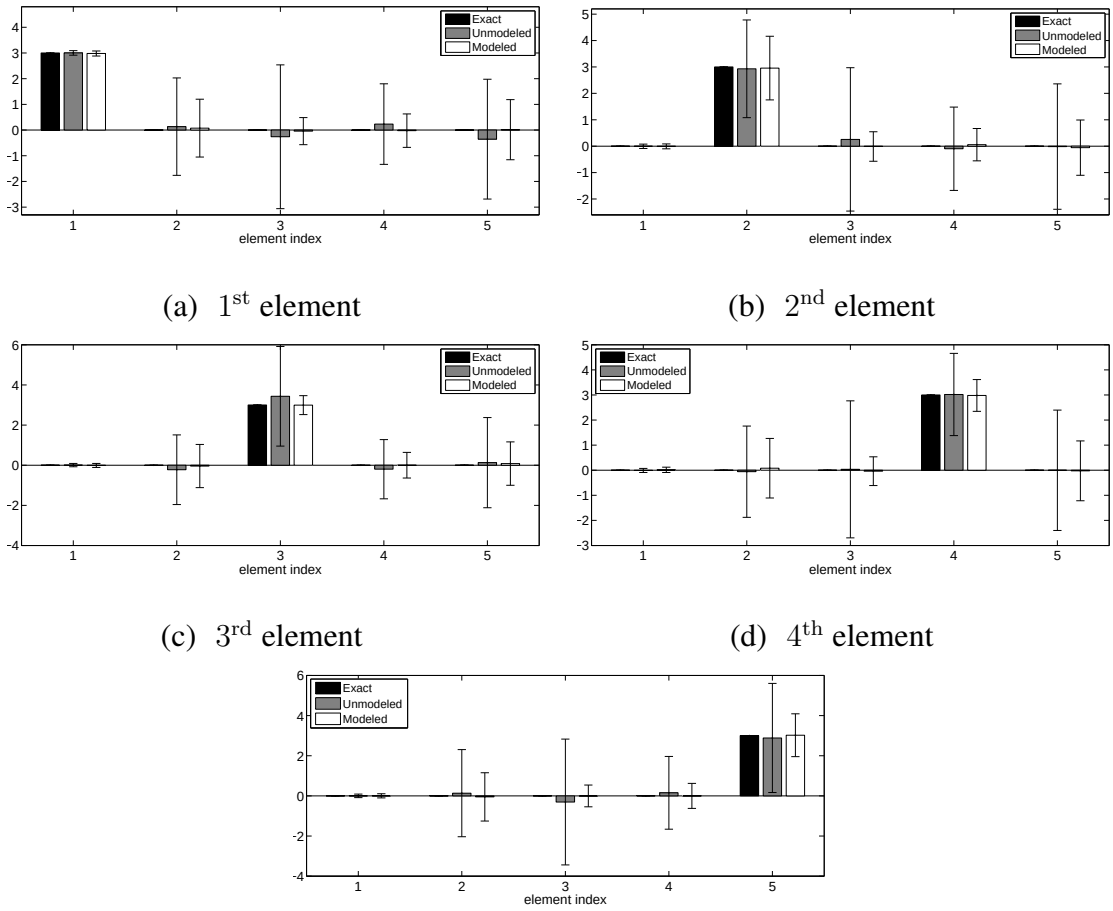

(a) 1^{st} element

(b) 2^{nd} element

(c) 3^{rd} element

(d) 4^{th} element

(e) 5^{th} element

Figure 6.8: Damage detection results for resonant frequencies contaminated with ± 0.12 random noise for a system with damping modeled and damping unmodeled in the optimization algorithm for the 1^{st} (a), 2^{nd} (b), 3^{rd} (c), 4^{th} (d), and 5^{th} (e) elements.

CHAPTER VII

Detection of Global and Local Parameter Variations Using Nonlinear Feedback Auxiliary Signals and System Augmentation

7.1 Introduction

Vibration-based identification of changes in structural parameters is currently used in a wide variety of technologies. In particular, two areas, sensing and damage detection, focus closely on identifying parameter variations such as mass and stiffness by exploiting variations in resonant frequencies. For example, recent sensing techniques for chemical and biological detection as well as atomic force microscopes in tapping mode [41] use the vibration of micro-structures such as micro-beams [40] and micro-cantilevers [37–39].

Resonant frequencies are used not only for micro-scale systems but also for monitoring large-scale structures such as bridges, space and aircraft. Similar to sensing, vibration-based damage detection [42–44] uses changes in the systems modal properties to identify parameter variations indicative of damage. Some of these damage detection techniques use both mode shapes and natural frequencies, although measuring mode shapes is more sensitive to noise [45] than measuring frequencies, and requires more measurements.

Sensing and detection methods that use only the frequencies of the system (which herein are referred to as frequency-shift based methods [100]) have recently become of

increasing interest. They have been developed because frequency extraction can be done robustly for both micro- and large-scale applications.

There are two central drawbacks to frequency-shift based methods. The first drawback is that only a limited number of frequencies can be measured accurately, which leads to an under-determined problem when solving for multiple different parameter variations (e.g. damage scenarios [83, 84], or sensor outputs). To overcome this problem, in the context of damage detection, Cha and Gu [105] and Nalitolela et al. [51] proposed to extract additional modal frequencies by adding mass or stiffness to the structure. However, in practice, the physical addition of mass or stiffness is difficult to implement. This difficulty was overcome by Lew and Juang [52] by introducing virtual passive controllers. They used controllers to generate additional vibration frequencies in the closed loop system instead of attaching physical mass or stiffness elements to the structure. Additionally, Jiang et al. [106] has recently proposed a way to increase frequency measurements using tunable piezoelectric transducer circuitry.

The second drawback of frequency-shift based methods is that the sensitivity of the lowest frequencies to parameter variations is often quite low. Therefore, in sensing applications, the sensitivity of the sensors can be too low; and in damage detection applications, the lowest damage that can be identified is exceedingly large. For example, Swamidas and Chen [46] showed this in a finite element study of a cracked plate. In their study, a surface crack 40% the width of the plate and 70% through its depth had a maximum frequency shift of less than 0.7%. Adams et al. [47] demonstrated this low sensitivity experimentally using an aluminum bar under axial loading. They found less than a 1% change in the first three frequencies when they made a cut through 30% of the surface area of the beam near its center.

To overcome the insensitivity of the frequencies to parameter variations, Ray and

Tian [48] proposed sensitivity enhancing feedback control. They applied closed loop vibration control for pole placement in smart structures with the objective of increasing the sensitivity of resonant frequencies to changes in the system. That method was demonstrated through numerical simulations of a cantilevered beam. Experimental validation of sensitivity enhancing feedback control was conducted by Ray et al. [49] on a cantilevered beam in bending. Ray and Marini [86] developed an optimization method to minimize the control effort while maximizing frequency sensitivity for a single fixed actuator location. Juang et al. [50] proposed an eigenstructure assignment technique that is useful in extending sensitivity enhancing control from single input to multi-input systems. Since in the multi-input case there are an infinite number of placement options for the modal frequencies, they chose the output feedback with the lowest control effort. They achieve this by using the open loop eigenvectors as the desired values of the closed loop eigenvectors, which leads to minimum control gains and minimum control effort. To address the limited frequency information drawback, Koh and Ray [53] proposed the use of multiple independent closed loop systems. Jiang et al. [24] developed an optimizing algorithm for placement of the frequencies and eigenvectors to maximize frequency sensitivity and minimize the control effort in the multi-input case.

One of the frontiers for the development of sensors and the advancement of damage detection technologies is tackling nonlinear systems. In these technologies, nonlinearities are often unavoidable during the regular vibration of the system, and hence, they have to be accounted for. Furthermore, they can be exploited for enhancing sensitivity. For example, recently sensitivity enhancing control has been proposed for nonlinear systems [94, 107]. The nonlinear systems were handled by forming higher dimensional augmented linear systems [73, 80, 87, 94, 107], which are designed to follow a single trajectory of the nonlinear system. The idea of optimal augmentations has also been introduced [94]. The

types of nonlinearities explored have included cubic spring nonlinearities [73, 80, 87, 94, 107] and Colomb friction [80].

In this work, two cantilevered beams are explored using optimal system augmentations and nonlinear feedback auxiliary signals. The objective here is to build on previous work [94, 107] for the case where there are only limited measurements available and a single input actuator. In the first system, the motion of the structure, which must be fed back into the system using the control gain matrix, is known only at 5 locations. In the second system, the motion of the structure is known only at 2 locations. Linear approaches would allow for the placement of only 2 resonant frequencies in the first system and 1 in the second system. In contrast, the use of nonlinear feedback auxiliary signals allows the creation of several augmented variables, which increases the amount of measurement information, and in turn enables the placement of additional frequencies of the augmented system. Additionally, the simultaneous detection of global changes in the system (e.g. due to environmental changes in temperature or humidity) and local is explored. Also, the idea of sensitivity enhancement for parameters of interest combined with sensitivity reduction for parameters that are not of interest (due to environmental or operational changes) is developed and explored. A methodology is also presented to accurately extract augmented frequencies from displacement and forcing data corrupted by noise. Various numerical simulations are included to demonstrate the proposed techniques, and to discuss the effects of random noise.

7.2 Methodology

In this section, the procedure for sensitivity enhancement using nonlinear feedback auxiliary signals in linear systems is presented. First, an overview of system augmentation with feedback auxiliary signals is provided. Second, the frequency-shift based detection

procedure is outlined. Next, the optimization algorithm employed for controller design is discussed briefly. Finally, the augmented frequency extraction procedure is detailed.

7.2.1 System Augmentation

In this section, a brief overview of system augmentation is provided. First, an example of a one degree of freedom system containing 2 nonlinearities is discussed. Then, the general form of the augmented equations are presented for a controlled system. Finally, an example of a simple controlled system is included. More details on system augmentation can be found in previous work [73, 80, 87, 94, 107].

Consider a mass connected to the ground by a linear, cubic and quintic spring. The equation of motion for this nonlinear system is given by

$$m\ddot{x} + kx + k_{n1}x^3 + k_{n2}x^5 = g(t), \tag{7.1}$$

where x is the position of the mass m, $g(t)$ is the external excitation, and k, k_{n1}, and k_{n2} are the linear, cubic and quintic spring stiffnesses, respectively.

The fundamental idea behind the augmentation is that higher dimensional augmented linear systems can be designed to follow a single trajectory of a nonlinear system. For the nonlinear system in Eq. (7.1), a higher dimensional augmented linear system can be formed by adding an additional degree of freedom for each nonlinearity to obtain augmented equations of motion as

$$\begin{aligned} m\ddot{x} + kx + k_{n1}y_1 + k_{n2}y_2 &= g(t), \\ m_{a1}\ddot{y}_1 + k_{c1}x + k_{a1}y_1 &= h_1(t), \\ m_{a2}\ddot{y}_2 + k_{c2}x + k_{a2}y_2 &= h_2(t), \end{aligned} \tag{7.2}$$

where $y_1 = x^3$ and $y_2 = x^5$, with m_{ai}, k_{ai}, k_{ci}, $h_i(t)$, and y_i corresponding to the augmented mass, augmented stiffness, coupled stiffness, augmented forcing, and augmented

variable, respectively.

Typically, the parameters k_{ci} are chosen to maintain the symmetry of the system ($k_{c1} = k_{n1}$ and $k_{c2} = k_{n2}$), m_{ai} are chosen similar to the mass at the degree of freedom they are coupled to ($m_{a1} = m_{a2} = m$), and k_{ai} are chosen to be low multiples of the nonlinear spring stiffness ($k_{a1} = \xi_1 k_{n1}$ and $k_{a2} = \xi_2 k_{n2}$ with constants ξ_1 and ξ_2 of values of about 2). However, one can choose these parameters to optimally suit their needs. An optimization of the augmentation for sensitivity enhancement has been established [94, 107]. It uses the typical values of the augmentation as the starting point, and then optimizes the parameters k_{ci} and k_{ai} by finding the optimal control gains in the augmented equations. Additionally, a separate parameter is included in the optimization to adjust the augmented mass.

The augmented variables y_i can be computed directly from x ($y_1 = x^3$ and $y_2 = x^5$), and the augmented forcing $h_i(t)$ can be computed directly from the left hand side in Eq. (7.2). The specific form of the augmented forcing is a key feature in the augmentation because it ensures that, if the trajectory of the augmented linear system is projected onto the original (physical) space, it will follow the trajectory of the nonlinear system. Due to the required augmented forcing, the modal extraction technique used must be an input/output technique (as opposed to an output only approach).

There are several features of an augmented system that differ from a typical linear system and have to be considered when designing a controller for system interrogation. Consider the general equations of motion of an augmented system with a controller ex-

pressed as

$$\begin{bmatrix} \mathbf{M} & \mathbf{N}_I \\ \mathbf{N}_{CI} & \mathbf{N}_{AI} \end{bmatrix} \begin{bmatrix} \ddot{\mathbf{x}} \\ \ddot{\mathbf{y}} \end{bmatrix} + \begin{bmatrix} \mathbf{D} & \mathbf{N}_D \\ \mathbf{N}_{CD} & \mathbf{N}_{AD} \end{bmatrix} \begin{bmatrix} \dot{\mathbf{x}} \\ \dot{\mathbf{y}} \end{bmatrix} + \begin{bmatrix} \mathbf{K} & \mathbf{N}_S \\ \mathbf{N}_{CS} & \mathbf{N}_{AS} \end{bmatrix} \begin{bmatrix} \mathbf{x} \\ \mathbf{y} \end{bmatrix} + \mathbf{B} \begin{bmatrix} \mathbf{K}_{CL} & \mathbf{K}_{CN} \\ \mathbf{K}_{CLA} & \mathbf{K}_{CNA} \end{bmatrix} \begin{bmatrix} \mathbf{x} \\ \mathbf{y} \end{bmatrix} = \begin{bmatrix} \mathbf{g} \\ \mathbf{h} \end{bmatrix}, \tag{7.3}$$

where $\mathbf{M}$, $\mathbf{D}$ and $\mathbf{K}$ are the linear mass, damping and stiffness matrices; $\mathbf{N}_I$, $\mathbf{N}_D$, and $\mathbf{N}_S$ are nonlinear parameter matrices which contain terms such as the cubic and quintic stiffness terms; $\mathbf{N}_{CI}$, $\mathbf{N}_{CD}$, and $\mathbf{N}_{CS}$ are the coupled inertia, damping and stiffness matrices, which traditionally have been used to maintain the symmetry of the system; and $\mathbf{N}_{AI}$, $\mathbf{N}_{AD}$, and $\mathbf{N}_{AS}$ are the augmented parameter matrices, which contain terms such as m_{ai} and k_{ai}. $\mathbf{B}$ is the control input matrix, which has nonzero values in rows where there are input actuators that can excite the system.

An interesting advantage of augmented systems is that all the rows of the augmentation can have nonzero entries in $\mathbf{B}$ because they do not require any physical actuation. Also, the gain matrix $\mathbf{K}_C$ has been split into four parts in Eq. (7.3). The purely linear portion of the controller is given by $\mathbf{K}_{CL}$. The nonlinear portion of the controller is given by $\mathbf{K}_{CN}$. If a linear controller is desired $\mathbf{K}_{CN}$ must be set to zero. Finally, $\mathbf{K}_{CLA}$ and $\mathbf{K}_{CNA}$ are the augmented portions of the gain matrix. Note that no actual physical actuation is required in the augmented portion of the controller. Rather, the calculated actuation is used in the computation of the augmented forcing $\mathbf{h}$.

Next, consider the augmented system discussed in Eq. (7.2) controlled by a single point

actuator

$$\begin{aligned} m\ddot{x} + kx + k_{n1}y_1 + k_{n2}y_2 + K_{CL}x + K_{CN1}y_1 + K_{CN2}y_2 &= g(t), \\ m_{a1}\ddot{y}_1 + k_{c1}x + k_{a1}y_1 + K_{CLA1}x + K_{CNA1}y_1 &= h_1(t), \\ m_{a2}\ddot{y}_2 + k_{c2}x + k_{a2}y_2 + K_{CLA2}x + K_{CNA2}y_2 &= h_2(t). \end{aligned} \tag{7.4}$$

The nonlinear actuation applied to the physical system is given by $K_{CN1}y_1$ and $K_{CN2}y_2$. Since augmented parameters (such as k_{ci} and k_{ai}) are chosen by the user, they can incorporate the augmented controller gains to obtain the following augmented equations of motion

$$\begin{aligned} m_{a1}\ddot{y}_1 + k'_{c1}x + k'_{a1}y_1 &= h_1(t), \\ m_{a2}\ddot{y}_2 + k'_{c2}x + k'_{a2}y_2 &= h_2(t), \end{aligned} \tag{7.5}$$

where $k'_{c1} = k_{c1}+K_{CLA1}$, $k'_{a1} = k_{a1}+K_{CNA1}$, $k'_{c2} = k_{c2}+K_{CLA2}$, and $k'_{a2} = k_{a2}+K_{CNA2}$.

The procedure for calculating the gain matrix $\mathbf{K}_C$ (containing linear and nonlinear control gains) consists of following an optimization algorithm previously established for augmented systems [94, 107] and linear systems [24]. The procedure uses an eigenstructure assignment technique to place the eigenvectors and resonant frequencies of the augmented system, and is discussed in the subsequent sections.

7.2.2 Frequency-Shift Based Detection Method

In this section, the frequency-shift based detection method used in this work is outlined. The method is a first order perturbation method, and has been used previously with sensitivity enhancing control [24,53,94]. Essentially, the idea is to relate the changes in the modal frequencies $\delta\omega$ to the changes in certain parameters $\delta\mathbf{p}$ (e.g. stiffness, mass, damping parameters). Generally, the relationship between $\delta\mathbf{p}$ and $\delta\omega$ is nonlinear. However, it

can be linearized to a first order perturbation form as

$$\delta\omega = \mathbf{S}\delta\mathbf{p}, \tag{7.6}$$

where

$$\mathbf{S} = \begin{bmatrix} \frac{\partial\omega_1}{\partial p_1} & \frac{\partial\omega_1}{\partial p_2} & \cdots & \frac{\partial\omega_1}{\partial p_r} \\ \frac{\partial\omega_2}{\partial p_1} & \frac{\partial\omega_2}{\partial p_2} & \cdots & \frac{\partial\omega_2}{\partial p_r} \\ \vdots & \vdots & \ddots & \vdots \\ \frac{\partial\omega_q}{\partial p_1} & \frac{\partial\omega_q}{\partial p_2} & \cdots & \frac{\partial\omega_q}{\partial p_r} \end{bmatrix} \approx \begin{bmatrix} \frac{\Delta\omega_1}{\Delta p_1} & \frac{\Delta\omega_1}{\Delta p_2} & \cdots & \frac{\Delta\omega_1}{\Delta p_r} \\ \frac{\Delta\omega_2}{\Delta p_1} & \frac{\Delta\omega_2}{\Delta p_2} & \cdots & \frac{\Delta\omega_2}{\Delta p_r} \\ \vdots & \vdots & \ddots & \vdots \\ \frac{\Delta\omega_q}{\Delta p_1} & \frac{\Delta\omega_q}{\Delta p_2} & \cdots & \frac{\Delta\omega_q}{\Delta p_r} \end{bmatrix},$$

and the r index represents the number of parameters $\mathbf{p}$ that can change, the q index represents the number of measurable frequencies, and $\mathbf{S}$ is the sensitivity matrix. To determine the unknown changes in parameters from the known changes in frequencies, a pseudo-inverse of $\mathbf{S}$ in Eq. (7.6) can be used to yield

$$\delta\mathbf{p} = \mathbf{S}^{+}\delta\omega. \tag{7.7}$$

When feedback interrogation is used, one sensitivity matrix $\mathbf{S}$ is obtained for each controller. For a controller of index i, the corresponding matrix is denoted by $\mathbf{S}^{ci}$. Also, the sensitivity matrix obtained when no controller is used (i.e. open loop) is denoted by $\mathbf{S}^{o}$.

The goal of sensitivity enhancement is to increase the entries in the closed loop sensitivity matrix $\mathbf{S}^{ci}$ with respect to the open loop sensitivity matrix $\mathbf{S}^{o}$. For a single closed loop system or for the open loop system, the solution of Eq. (7.7) is typically not very accurate because the number of changeable parameters r is likely greater than the number of measurable frequencies q, which results in an under-determined problem. Koh and Ray [53] overcame this problem by using multiple independent closed loop systems and unique combinations of actuator locations. Each closed loop system (of index i) corre-

sponds to a unique sensitivity matrix $\mathbf{S}^{ci}$, which means that a complete closed loop sensitivity matrix can be expressed as

$$\mathbf{S}^{c} = \begin{bmatrix} \mathbf{S}^{c1} \\ \mathbf{S}^{c2} \\ \vdots \\ \mathbf{S}^{cz} \end{bmatrix}, \tag{7.8}$$

where z corresponds to the number of unique controller configurations used. Therefore, if $z \cdot q > r$ then Eq. (7.7) becomes an over-determined set of equations for the unknowns $\delta\mathbf{p}$.

7.2.3 Optimization Algorithm

The optimization algorithm used in this work is designed to determine the best control gains (linear and nonlinear) to enhance the sensitivity of the resonant frequencies of the augmented system to changes in particular structural parameters, while being subject to several constraints. The algorithm follows closely the work previously established for augmented systems [94, 107] and linear systems [24], and uses an eigenstructure assignment technique to place the eigenvectors and resonant frequencies of the augmented system.

Two forms of the optimization algorithm are used in this work. The first was used in previous works [94, 107] and has the form

$$J(\tau) = C_1/SE + C_2 CE, \tag{7.9}$$

where J is the cost function that is minimized, τ are the parameters being optimized, C_1 and C_2 are weighting coefficients, SE is the overall sensitivity enhancement that is maximized, and CE is the control effort that is minimized. The parameters τ relate to the placement of the closed loop augmented eigenvalues and eigenvectors of the system, which can be used to determine the linear and nonlinear gain parameters (e.g. corresponding to the K_{CLi}, K_{CNi}, k_{ci} and k_{ai} terms from Sec. 7.2.1).

The control effort CE is defined as the absolute value of the maximum value in the controller gain matrix, not including the rows corresponding to the augmented degrees of freedom. The "control" of the rows corresponding to the augmented degrees of freedom does not require any physical actuation, just signal processing. This complete control authority with no physical actuation (for the augmented degrees of freedom) is one of the key advantages that nonlinear feedback auxiliary signals has over traditional sensitivity enhancing linear feedback.

The sensitivity enhancement SE is defined as the sum of the element by element ratio of the closed loop sensitivity matrices $\mathbf{S}^{ci}$ to the open loop sensitivity matrix $\mathbf{S}^{o}$ divided by the number of elements, i.e.

$$SE = \frac{\sum_{i=1}^{z}\sum_{j=1}^{q}\sum_{k=1}^{r}|\frac{\mathbf{S}_{j,k}^{ci}}{\mathbf{S}_{j,k}^{o}}|}{z \cdot q \cdot r}. \tag{7.10}$$

Eq. (7.7) is used to determine $\delta\mathbf{p}$ from $\delta\omega$. Hence, in addition to purely sensitivity enhancement, it is important to also maximize the singular values (particularly the minimum singular value) of the sensitivity matrix $\mathbf{S}^{c}$ to increase the robustness of the method to noise.

The second optimization algorithm used in this work allows for simultaneous sensitivity enhancement for particular structural changes while also providing sensitivity reduction for other structural changes. Such combination of enhancement and reduction is needed in many applications where it is desirable to sense/detect variations in a parameter while being insensitive to other parameters (usually related to environmental or operational conditions). The corresponding cost function is given as

$$J(\tau) = C_1/SE + C_2CE + C_3SR, \tag{7.11}$$

where C_3 is a weighting coefficient, and SR is a sensitivity reduction term.

Reducing the sensitivity for particular scenarios can be particularly useful for rejecting certain environmental or structural changes that are not of interest. For instance, a uniform change in stiffness that occurs in a beam due to temperature changes or fatigue may not be a change of interest, but can have a significant effect on the system. By reducing the sensitivity to these structural changes, the overall method becomes more robust to a larger array of environmental conditions. That is accomplished by minimizing SR (defined in a similar manner to the sensitivity enhancement term) given by the following expression

$$SR = \frac{\sum_{i=1}^{z}\sum_{j=1}^{q}\sum_{k=1}^{w}|\frac{\mathbf{Sr}_{j,k}^{ci}}{\mathbf{S}_{j,k}^{o'}}|}{z \cdot q \cdot w}, \tag{7.12}$$

where w is the number of parameters for which sensitivity is reduced, $\mathbf{Sr}^{ci}$ is the closed loop sensitivity matrix that is being minimized, and $\mathbf{S}^{o'}$ is the open loop sensitivity matrix for structural changes which are not of interest. Note that, in general, $\mathbf{S}^{o'}$ is distinct from $\mathbf{S}^{o}$ because $\mathbf{S}^{o'}$ includes only sensitivities to parameters that are not of interest.

Both optimization algorithms have certain built-in constraints. The first constraint requires that the physical linearized system be stable. However, the (fictitious) augmented system can be unstable. The linearized system must be stable for the healthy case and also for the maximum changes in each of its parameters. The second constraint enforces a linear relationship between each parameter change and the resonant frequencies. This constraint enables the use of the first order frequency-shift based method explained in the previous section.

7.2.4 Frequency Extraction for Augmented Systems

In this section, a procedure is presented for the extraction of augmented resonant frequencies from a system with few measurement locations and noisy data. The procedure is specially designed for augmented linear systems. However, with a few modifications, it can be used for standard linear systems also.

The first step in the procedure is to excite the system at a single frequency within the frequency range of interest. This frequency range corresponds to the (placed) frequencies of the closed loop augmented system. The response of the system and the physical excitation are stored. Multiple measurements can be performed (at the same frequency), and the measured response and excitation can be averaged at each phase of the dynamics. Hence, noise can be largely filtered out. That is particularly useful when the response of the system is periodic. Next, the harmonic excitation is repeated for additional frequencies until enough frequency information has been extracted from the system. Note that the ability to perform this noise filtering is a key consequence of the fact that the augmented system is linear.

The rest of the procedure deals with post processing and the actual extraction of the resonant frequencies. First, the augmented variables and the augmented forcing are constructed using the filtered data. The augmented variable $\mathbf{y}$ is computed directly from its nonlinear relation to $\mathbf{x}$, while $\ddot{\mathbf{y}}$ is calculated by finite differencing $\mathbf{y}$, and $\mathbf{h}$ is calculated directly from the left hand side of Eq. (7.3). Next, the full responses of the system ($\mathbf{x}$ and $\mathbf{y}$) and full forcing ($\mathbf{g}$ and $\mathbf{h}$) can be summed for all excitation frequencies to form a single (complex) excitation and response data set. The input ($\mathbf{g}$ and $\mathbf{h}$) and output ($\mathbf{x}$ and $\mathbf{y}$) can then be fed into DSPI [7], and the augmented frequencies can be extracted. Note that summing the response of the augmented systems over all frequencies is a key consequence of the fact that the augmented system is linear.

A specialized nonlinearity was designed for use in the nonlinear controller. It had the form $y = x^3 \exp\left(-x^2/C\right)$. A plot of this function for $C = 1$ is shown in Fig. 7.1. The constant C is a scaling term that can be used to adjust the maximum amplitude and width of the nonlinearity. There are several key features that make this nonlinearity desirable. First, this is a smooth nonlinearity, and its second derivative can be calculated accurately

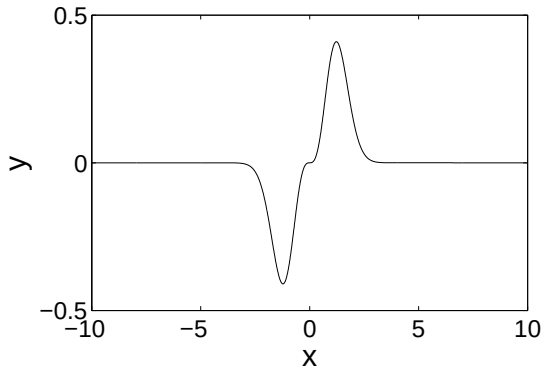

Figure 7.1: Nonlinearity used in the nonlinear controllers.

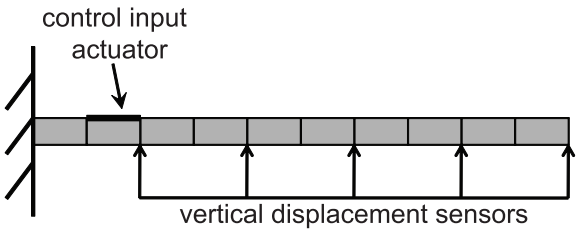

Figure 7.2: Linear beam excited by one piezoelectric patch using nonlinear feedback auxiliary signals from 5 sensors.

using finite differencing. Second, the peak amplitude of the variable y can be tailored to be close to the amplitude of the linear degrees of freedom (by choosing an adequate value for C). Finally, the last key feature is that the nonlinear response tends to zero for large amplitudes in the system. This feature is important in making sure that the system response remains bounded during its interrogation. Since the nonlinearity exponentially tends to zero at large x, and since the open loop (physical) linear system is stable, the closed loop system returns toward the origin when the response becomes large.

7.3 Numerical Results

In this section, numerical simulations were performed on two cantilevered beam systems. First, the system shown in Fig. 7.2 was investigated. In particular, the frequency extraction method was investigated to determine how sensitive to noise the extraction process is. Also, a comparison of nonlinear feedback auxiliary signals, linear feedback, and an uncontrolled system was conducted under various conditions. Next, the system in Fig. 7.3 was investigated. Due to the reduced measurements, linear feedback was not feasible and nonlinear feedback auxiliary signals were directly compared with the open loop system. In particular, two sets of nonlinear feedback auxiliary signals were designed (1) to detect variations in both global and local parameters, and (2) to detect local changes while being insensitive to global changes. The local changes are variations of the mass of the beam in the vicinity of its tip and midspan (which correspond to sensing scenarios). The global changes are proportional variations in the entire mass or stiffness of the physical system. The uniform change in mass scenario could result from a change in humidity, while the uniform change in stiffness scenario could result from a change in temperature. The ability to distinguish the effects of humidity and temperature from the changes due to local additions of mass is critical for practical uses of this method for sensing and damage detection.

7.3.1 Case 1

To demonstrate the augmented frequency extraction and the benefits of nonlinear feedback auxiliary signals over linear feedback, a numerical investigation was performed on a linear cantilevered beam shown in Fig. 7.2. The properties of the system are the same as the system investigated by Jiang et al. [24]. The density and Young's modulus of the beam are $2410\ kg/m^3$ and $6.6 \cdot 10^{10}\ N/m^2$, respectively. The length, thickness, and width of the

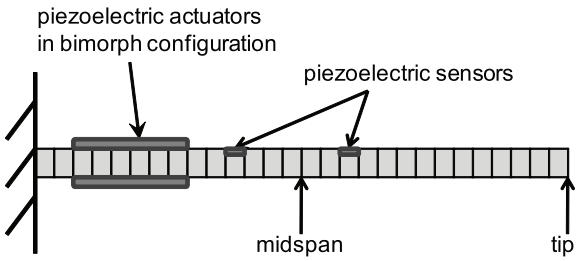

Figure 7.3: Linear beam excited by piezo-actuators using nonlinear feedback auxiliary signals and two piezo-sensors.

beam are $400\ mm$, $3.4\ mm$, and $26\ mm$. The density and Young's modulus of the piezoelectric material are $7600\ kg/m^3$ and $5.9 \cdot 10^{10}\ N/m^2$, respectively. The length, thickness, and width of the piezoelectric patch are $40\ mm$, $0.3\ mm$, and $20\ mm$. The piezoelectric constant is $d_{31} = -276 \cdot 10^{-12}\ m/V$. The beam was discretized into 10 elements with the control and forcing input to the system applied through a moment induced by the piezoelectric patch on the second element of the beam. A light proportional damping of the form $\alpha\mathbf{M} + \beta\mathbf{K}$ was also added to the beam, where $\alpha = 10^2$ and $\beta = 10^{-5}$. Five position measurements (out of a possible 20 degrees of freedom for the system model) were taken along the beam, as indicated in Fig. 7.2.

In addition to the 5 physical measurements, 5 augmented variables were created for the system. The augmented variables are $y_i = x_i^3 \exp\left(-x_i^2/C\right)$, where x_i are the 5 measured signals. Only these nonlinearities are used in the controller. The augmented system was created by generating $\mathbf{M}$, $\mathbf{K}$, $\mathbf{N}_I$, $\mathbf{N}_S$, $\mathbf{N}_{AI}$, $\mathbf{N}_{AD}$, $\mathbf{N}_{AS}$ and $\mathbf{N}_{CS}$ as discussed in the system augmentation section. The augmented matrices and control gains were optimized using the `fmincon` function in MATLAB [93].

In general, the user has complete control over the 5 augmented degrees of freedom corresponding to the 5 augmented variables. Hence, multiple independent closed loop

configurations are possible (even though there is only one physical controller). In this work, the only controller configuration that was used corresponds to control at the physical degrees of freedom affected by the piezoelectric patch and the 5 augmented degrees of freedom.

The first 5 resonant frequencies of the system were optimally placed to maximize the sensitivity and linear independence for 4 scenarios. The first scenario corresponds to added mass at the tip of the beam. The second scenario corresponds to added mass at the midspan of the beam. The third scenario corresponds to a uniform change in mass of the physical system (e.g. a change in humidity of the environment). The fourth scenario corresponds to a uniform change in stiffness of the physical system (e.g. a change in temperature of the environment).

Two controllers were designed to enhance the sensitivity of the resonant frequencies. The first one was based on traditional linear feedback. Due to the fact that only two frequencies could be placed, this controller was created to detect only the local changes in mass at the tip and midspan (and was not designed to detect uniform changes in the mass and stiffness). The second controller is based on nonlinear feedback auxiliary signals. Due to the added control and sensing, five frequencies could be placed. Hence, both the local and the global variations can be detected.

To demonstrate the frequency extraction method, the eigenvalues of the healthy augmented system were extracted by DSPI for the case of zero noise and for the case of noise with a Gaussian distribution having zero mean and a standard deviation of about 0.5% of the the response (and excitation) of the system. The results are shown in Tab. 7.1. The first column consists of the first seven exact eigenvalues. The second column consists of the eigenvalues extracted by DSPI for the noise free case. The third column contains the average values of the eigenvalues obtained from 100 separate numerical simulations for

Exact Augmented Eigenvalues	Augmented Eigenvalues Extracted by DSPI (no noise)	Average Augmented Eigenvalues Extracted by DSPI (noisy measurements)	Standard Deviation of Augmented Frequencies Extracted by DSPI
-50.449 + 320.8487i	-50.4304 + 320.845i	-56.0636 + 320.6479i	2.4056
-51.1395 + 1887.875i	-51.2038 + 1887.8741i	-51.7111 + 1887.4735i	0.3035
-59.0027 + 2031.5986i	-58.9349 + 2031.5773i	-60.7222 + 2033.4844i	0.625
-135.8709 + 3658.8146i	-135.7516 + 3658.7827i	-135.8077 + 3659.1526i	0.4331
-260.9331 + 5581.6613i	-261.0341 + 5581.6112i	-260.8428 + 5581.6889i	0.558
-510.741 + 9425.9538i	-510.6796 + 9426.1458i	-511.3594 + 9426.7778i	1.1731
-959.1626 + 13960.3522i	-958.6539 + 13960.5427i	-959.5121 + 13960.5772i	3.216

Table 7.1: First 7 eigenvalues of a baseline (nominal) closed loop system.

the noisy case. The fourth (and last) column consists of the standard deviations obtained for the identified frequencies. Comparing the first two columns one may note that DSPI can very accurately extract the augmented eigenvalues of the system for zero noise. In the presence of noise, the method still works quite well with the average value very close to the exact eigenvalue with small deviations.

For the following results, the exact frequencies were calculated for the system, and a noise with a Gaussian distribution having zero mean was added to the eigenvalues of the system. The standard deviation for the noise distribution was approximately equal to the standard deviations for the frequencies given in Tab. 7.1.

The results in Fig. 7.4 show the changes predicted for a variety of different cases. The plots on the left correspond to a case where a mass of 0.1% of the beam is placed at the tip of the beam. The plots in the center corresponds to the case where a mass of 0.1% of the beam is placed at the midspan of the beam. The plots on the right corresponds to the case where there are masses each of 0.1% of the beam placed at both the tip and at the midspan of the beam. The top row of plots corresponds to a case where there are no uniform mass or stiffness changes. The second row of plots corresponds to the case where there is a uniform mass change, while the third row of plots corresponds to a uniform

stiffness change. The fourth (and final) row of plots corresponds to a uniform change in both mass and stiffness. There are 4 bars plotted for each plot. The first bar is the exact change in the system. The rest of the bars have standard deviation error bars for the noisy cases. The second bar is the value predicted by an open loop system. The sensitivity matrix of the open loop system would be rank deficient if it was taking into account uniform mass and stiffness changes. Therefore, a sensitivity matrix based solely on added mass at the tip and midspan was created for the open loop case (in the same way as for linear feedback). The third bar is the change predicted when enhancing sensitivity using traditional linear feedback. The fourth (and final) bar is the change predicted when enhancing sensitivity through nonlinear feedback auxiliary signals. For the case when there are no uniform changes in mass or stiffness, the linear feedback gives a significant improvement over the uncontrolled system, and nonlinear feedback auxiliary signals provides an even greater improvement. When there are uniform changes in mass and/or stiffness, both the uncontrolled and linear feedback perform very poorly because they are not able to distinguish the additional (global) changes, while nonlinear feedback auxiliary signals is able to detect simultaneously all of the changes in parameters.

7.3.2 Case 2

To demonstrate several of the additional advantages of nonlinear feedback auxiliary signals over linear feedback, and in particular their ability to enhance or reduce global changes, numerical simulations were performed on a linear cantilevered beam shown in Fig. 7.3. The beam is made of aluminum with a density and Young's modulus of $2660\ kg/m^3$ and $68.9\ GPa$, respectively. The length, width, and thickness of the beam are $280\ mm$, $15\ mm$, and $1.27\ mm$, respectively. The piezo-actuator patches are placed in a bimorph configuration $20\ mm$ from the root. The density, Young's modulus, and

piezoelectric constant are $7800\ kg/m^3$, $62\ GPa$, and $d_{31} = -300 \cdot 10^{-12}\ m/V$, respectively. The length, width, and thickness of each piezoelectric patch is $60\ mm$, $15\ mm$, and $1\ mm$, respectively. The beam was discretized into 28 elements with two degrees of freedom per node. The linear beam model had a total of 56 degrees of freedom. The piezo-sensors placed $100\ mm$ and $160\ mm$ from the root of the beam were assumed to have a negligible impact on the properties of the system. The excitation of the beam by the piezo-actuators was modeled as an induced moment due to an applied voltage. The sensor information used as feedback was a voltage from each sensor that was related to the curvature of the beam, which in turn can be related to the rate of change in the slope of the beam at the location of the sensor. In addition to the two physical measurements, two augmented variables were created for the system.

In general, the user has complete control over the two augmented degrees of freedom corresponding to the two augmented variables. Hence, multiple independent closed loop controllers are possible (even though there is only one physical controller). Hence, note that in this work the only controller configuration that was used corresponds to control applied at the physical degrees of freedom affected by the piezo-actuator and the two augmented degrees of freedom.

Detecting local and global changes

The first set of results consist of designing nonlinear feedback auxiliary signals for sensitivity enhancement for four different scenarios. The four scenarios are the same as the ones in the previous section where the first two scenarios correspond to local changes in the mass of the system, and the last two scenarios correspond to global mass and stiffness changes.

Due to the limited sensor information and control authority, only the first two resonant

frequencies of the system could be placed using nonlinear feedback auxiliary signals. This is an improvement over purely linear feedback which would only be able to place a single frequency. Since there are four scenarios and only two frequencies, the optimization is carried out twice to obtain two distinct sets of nonlinear feedback auxiliary signals. These nonlinear feedback auxiliary signals were optimized for both sensitivity enhancement and linear independence between the nonlinear feedback auxiliary signals such that the global sensitivity matrix is full rank.

For the following results, the exact frequencies were calculated for the system, and a zero mean white noise was added to the eigenvalues of the system. The noise level was approximately $\pm 0.2\%$ of the lowest frequency. The results in Fig. 7.5 show the changes predicted for a variety of different cases. The plots are laid out in the same manner as in Fig. 7.4. In each plot there are three bars plotted, where the first bar is the exact change in the system. The other two bars have standard deviation error bars for the noisy cases. The second bar is the average value predicted by the open loop linear system. The sensitivity matrix of the open loop system would be rank deficient if it were taking into account uniform mass and stiffness changes, and that would lead to completely wrong results. Therefore, a sensitivity matrix based solely on added mass at the tip and midspan was created for the open loop results. The third bar is the average change predicted by nonlinear feedback auxiliary signals. The improvement of the nonlinear feedback auxiliary signals over the open loop predictions are significant even for this limited case of one controller and two sensors. Especially note the reduction in noise effects.

Detecting local changes and ignoring global changes

The next group of results consist of designing a new set of feedback auxiliary signals that are sensitive to local changes in the mass placed at the tip and midspan, but insensitive

to global (uniform) changes in the mass and stiffness.

Similar to the results above, two resonant frequencies of the system were placed using nonlinear feedback auxiliary signals, but since there are only two scenarios being detected, only one set of nonlinear feedback auxiliary signals was used. The plots in Fig. 7.6 are laid out in a similar manner to Fig. 7.5. However, only the local changes are plotted (scenarios 1 and 2) since the effects of the global changes are not of interest (and have been minimized). For the following results, the exact frequencies were calculated for the system, and a zero mean white noise was added to the eigenvalues of the system. The noise was approximately $\pm 0.3\%$ of the lowest frequency. Note that the noise used in this case is larger than in the previous case. Nonetheless, the standard deviation error bars are smaller for the nonlinear feedback auxiliary signals than in the previous case, highlighting the better performance of the nonlinear approach. The system using nonlinear feedback auxiliary signals shows improvement over the open loop predictions in this case for both the average values as well as the effects of noise. These plots show that lowering the influence of unwanted environmental changes or operational conditions on frequency shifts can be achieved through sensitivity reduction (in combination with sensitivity enhancement for the desired parameters).

The final set of results are based on setting up two sets of nonlinear feedback auxiliary signals, which create a sensitivity matrix, which is overdetermined with respect to the two scenarios of interest. The results are shown in Fig. 7.7, where the plots are laid out in the same manner as in Fig. 7.6. A zero mean white noise was added to the eigenvalues of the system. The noise was approximately $\pm 0.5\%$ of the lowest frequency. Note that this noise level is significantly greater than the previous two cases. Even with the greater noise, the error bars on the nonlinear feedback auxiliary signals are comparable to the previous cases, and overall there is an improved prediction of the changes in mass. These results

show that the use of an overdetermined sensitivity matrix (which allows for variation of the global parameters in an unobserved subspace) improves the local detection of mass variations.

7.4 Conclusions and Discussion

A novel approach for sensitivity enhancement for linear and nonlinear systems via optimal augmentations and nonlinear feedback auxiliary signals was presented. Nonlinear feedback auxiliary signals have several important advantages over sensitivity enhancement via traditional linear feedback. These advantages include the complete control over the augmented degrees of freedom with no actuator (physical) effort. Also, augmented variables provide additional sensor knowledge for the augmented degrees of freedom. Additionally, the augmented (fictitious) system does not need to be stable, rather only the physical linearized system needs to be stable.

A major drawback to both traditional feedback and nonlinear feedback auxiliary signals is the need for complex active control to be built into the system. Hence, the ability to provide sensitivity enhancement with a reduced number of actuators and sensors is very important. This work demonstrates this ability, and shows the promise of the proposed nonlinear method for use in smart structures. In particular, two system were explored. The first system contains just one actuator and five sensors and demonstrated the effectiveness of the approach over linear feedback and an uncontrolled system. The additional sensor and control from the augmentation was shown to increase the number of parameters that can be detected. In the second system, a single actuator and just two sensors were used for sensitivity enhancement. In this case, traditional linear feedback methods are not useful in identifying multiple simultaneous parameter variations. However, nonlinear feedback auxiliary signals were shown to detect several simultaneous parameter variations.

In this work, there were several extensions to the method beyond using nonlinear feedback auxiliary signals with a reduced number of actuators and sensors. First, the work detailed a methodology for augmented frequency extraction using noisy and limited measurement data. Also, the work explores the detection of changes in local and global parameters. The local parameters in this case were added masses at the tip and midspan, which corresponded to sensing scenarios. However, if damage detection was the application, the local changes could just as well be stiffness changes. The global changes corresponded to uniform changes in mass and stiffness. These global changes can correspond to certain environmental (temperature or humidity fluctuations) or operational conditions that the user wants to detect. Additionally, an approach to desensitize the resonant frequencies to certain parameters (in this case the global parameters) and increase the sensitivity to other parameters (the local parameters) was introduced. This might prove especially useful in a sensing scenario where the goal is just to detect the mass(es) on a beam, while the environmental or operational conditions are not of interest.

The method was shown able to detect masses that were 0.1% of the mass of the physical beam simultaneously with uniform changes in mass and stiffness with limited physical sensing and actuation. Also, it was shown to be able to detect masses of the same size, while being insensitive to uniform mass and stiffness changes. Numerical simulations were conducted with limited measurements and noisy data.

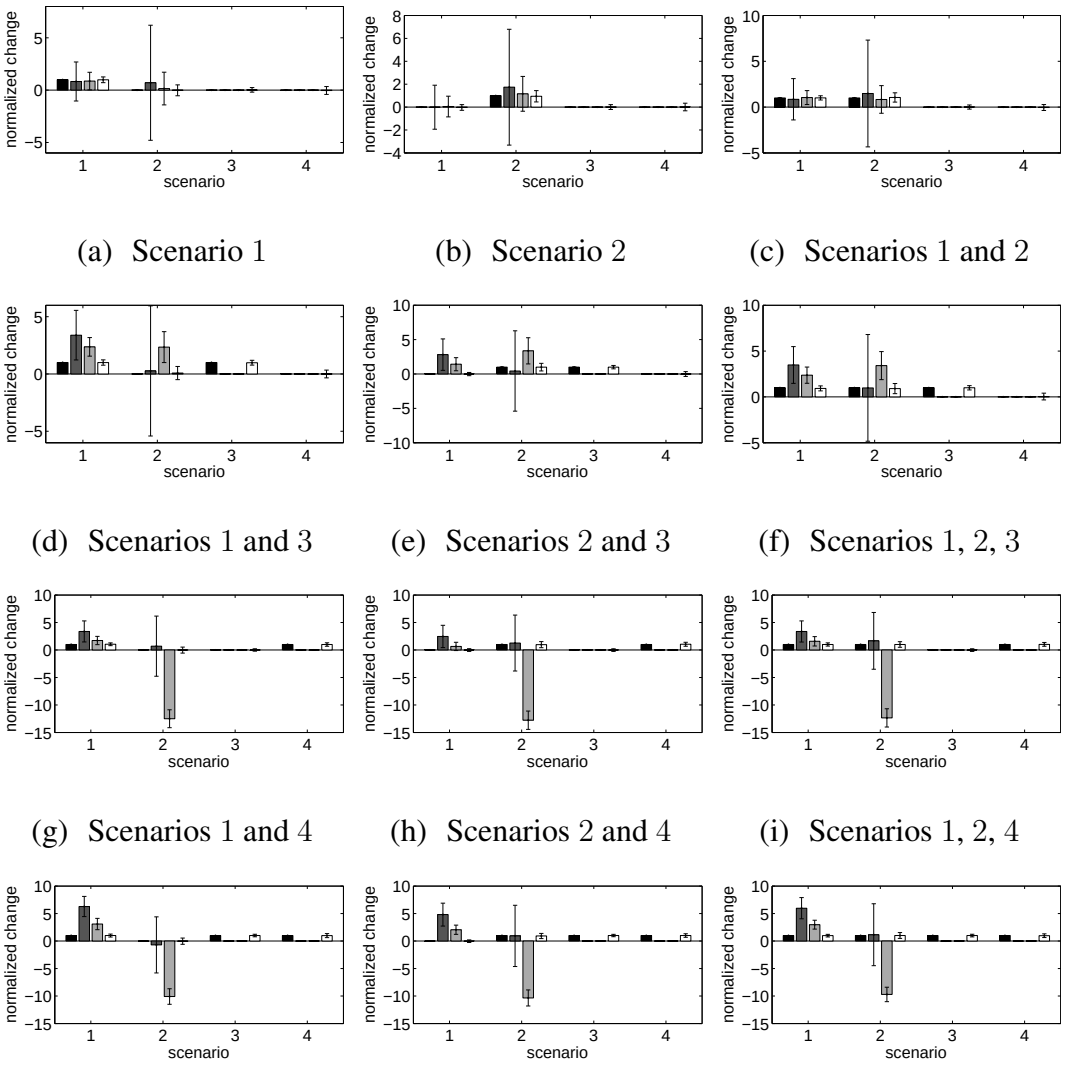

(a) Scenario 1 (b) Scenario 2 (c) Scenarios 1 and 2

(d) Scenarios 1 and 3 (e) Scenarios 2 and 3 (f) Scenarios 1, 2, 3

(g) Scenarios 1 and 4 (h) Scenarios 2 and 4 (i) Scenarios 1, 2, 4

(j) Scenarios 1, 3, 4 (k) Scenarios 2, 3, 4 (l) Scenarios $1-4$

Figure 7.4: Sensed mass: (i) by the open loop system (dark grey), (ii) by a system with linear feedback unable to detect uniform mass and stiffness changes (light grey), (iii) by a system with nonlinear feedback auxiliary signals which is able to detect uniform mass and stiffness changes (white), and (iv) the exact changes (black). Scenario 1 represents changes in mass at the tip. Scenario 2 represents changes in mass at the midspan. Scenario 3 represents a uniform change in mass. Scenario 4 represents a uniform change in stiffness.

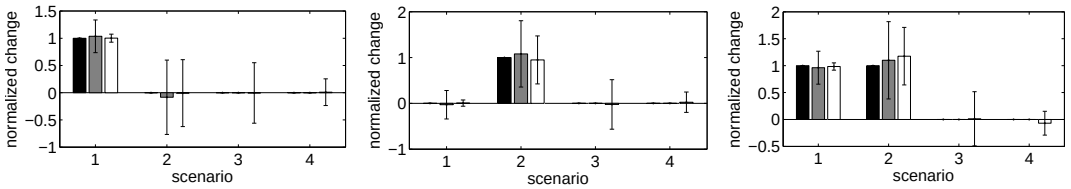

(a) Scenario 1 (b) Scenario 2 (c) Scenarios 1 and 2

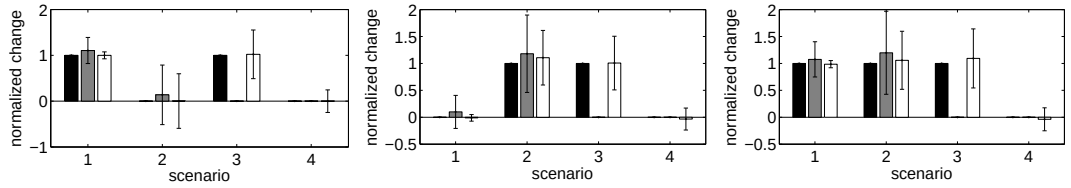

(d) Scenarios 1 and 3 (e) Scenarios 2 and 3 (f) Scenarios 1, 2, 3

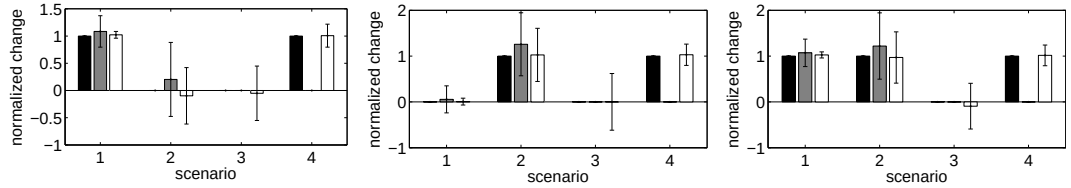

(g) Scenarios 1 and 4 (h) Scenarios 2 and 4 (i) Scenarios 1, 2, 4

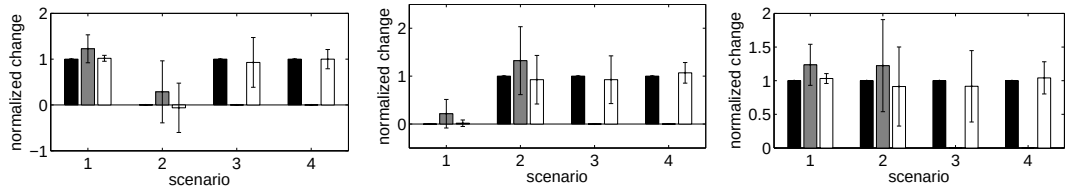

(j) Scenarios 1, 3, 4 (k) Scenarios 2, 3, 4 (l) Scenarios $1-4$

Figure 7.5: Sensed mass and/or stiffness: (i) by the open loop system (grey), (ii) by a closed loop system designed to detect uniform mass and stiffness changes using nonlinear feedback auxiliary signals (white), and (iii) the exact changes (black). Scenario 1 represents changes in mass at the tip. Scenario 2 represents changes in mass at the midspan. Scenario 3 represents a uniform change in mass. Scenario 4 represents a uniform change in stiffness.

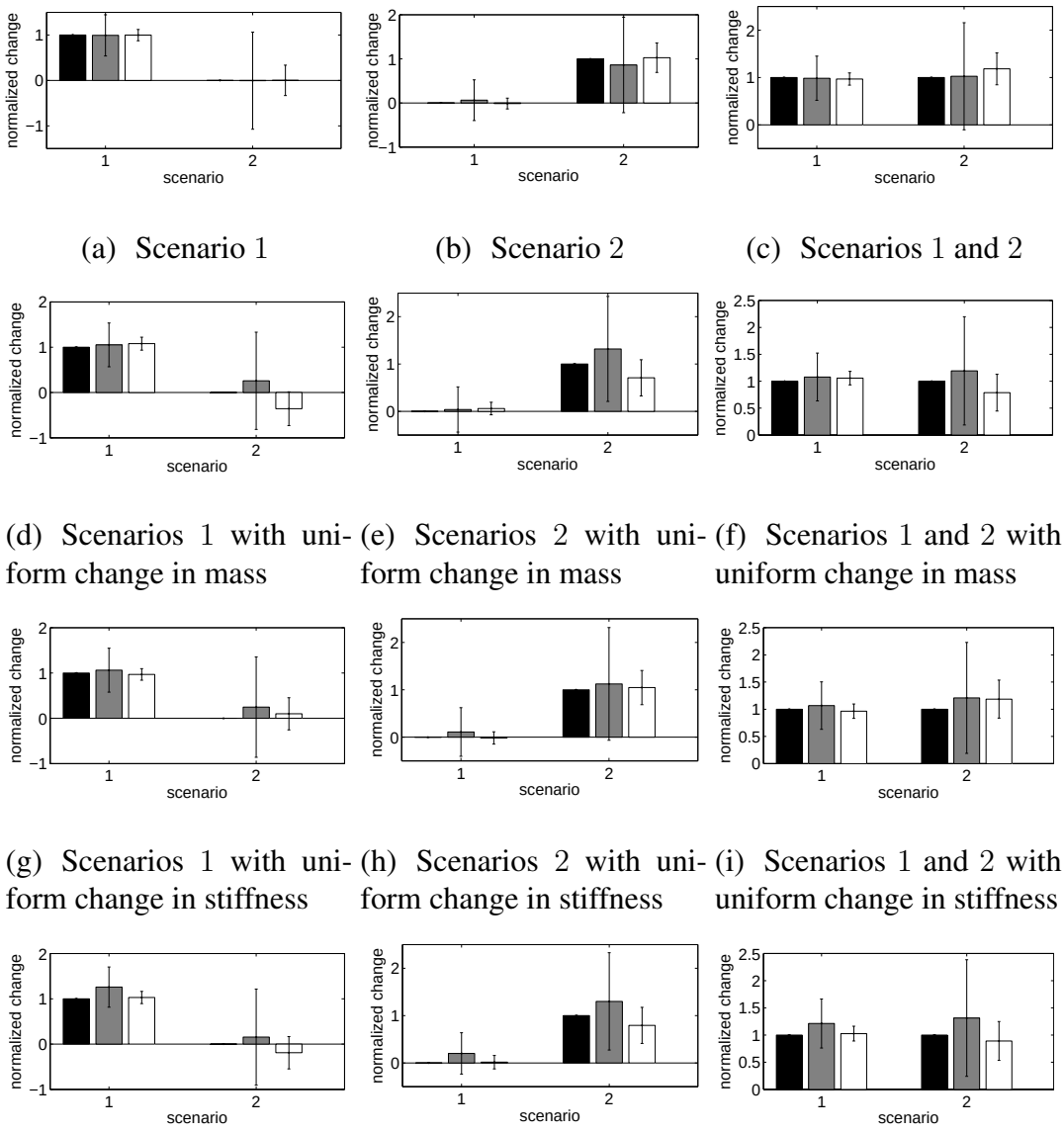

(a) Scenario 1 (b) Scenario 2 (c) Scenarios 1 and 2

(d) Scenarios 1 with uniform change in mass (e) Scenarios 2 with uniform change in mass (f) Scenarios 1 and 2 with uniform change in mass

(g) Scenarios 1 with uniform change in stiffness (h) Scenarios 2 with uniform change in stiffness (i) Scenarios 1 and 2 with uniform change in stiffness

(j) Scenarios 1 with uniform change in mass and stiffness (k) Scenarios 2 with uniform change in mass and stiffness (l) Scenarios 1 and 2 with uniform change in mass and stiffness

Figure 7.6: Sensed mass: (i) by the open loop system (grey), (ii) by a closed loop system designed to be **insensitive** to uniform mass and stiffness changes using *one set* of nonlinear feedback auxiliary signals (white), and (iii) the exact changes (black). Scenario 1 represents changes in mass at the tip. Scenario 2 represents changes in mass at the midspan.

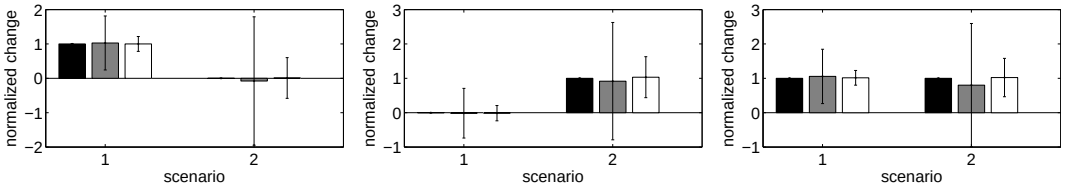

(a) Scenario 1 (b) Scenario 2 (c) Scenarios 1 and 2

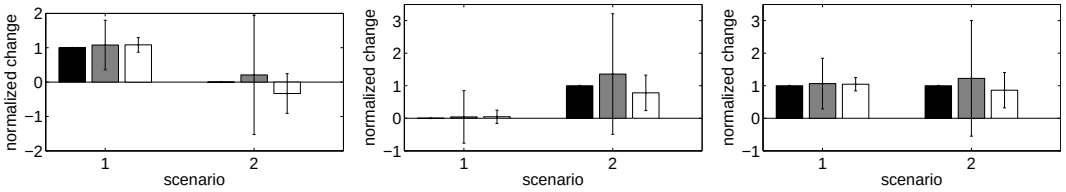

(d) Scenarios 1 with uniform change in mass (e) Scenarios 2 with uniform change in mass (f) Scenarios 1 and 2 with uniform change in mass

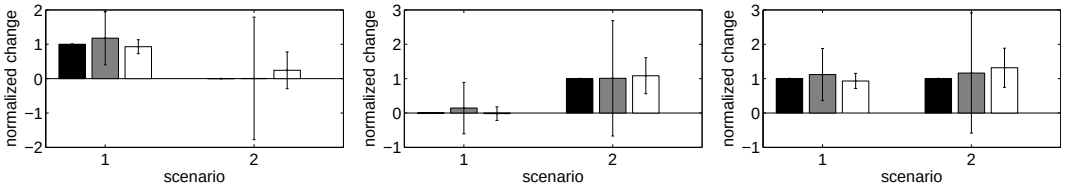

(g) Scenarios 1 with uniform change in stiffness (h) Scenarios 2 with uniform change in stiffness (i) Scenarios 1 and 2 with uniform change in stiffness

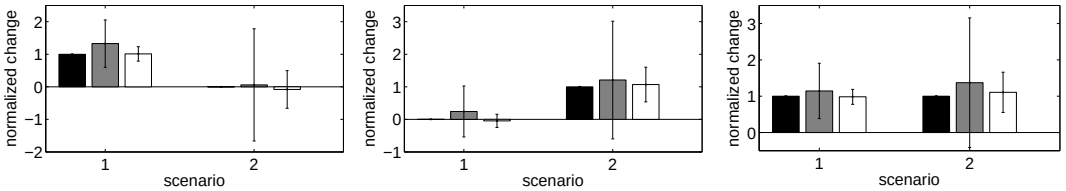

(j) Scenarios 1 with uniform change in mass and stiffness (k) Scenarios 2 with uniform change in mass and stiffness (l) Scenarios 1 and 2 with uniform change in mass and stiffness

Figure 7.7: Sensed mass: (i) by the open loop system (grey), (ii) by a closed loop system designed to be **insensitive** to uniform mass and stiffness changes using *two sets* of nonlinear feedback auxiliary signals (white), and (iii) the exact changes (black). Scenario 1 represents changes in mass at the tip. Scenario 2 represents changes in mass at the midspan.

CHAPTER VIII

Conclusions and Future Work

8.1 Contributions

The work presented in this dissertation presents several new tools for the analysis and interrogation of nonlinear systems. The original contributions of this dissertation can be summarized as follows:

- In Chapter II the concept of system augmentations for nonlinear systems was introduced. These system augmentations are higher dimensional than the corresponding linear system and are designed to follow a single trajectory of the nonlinear system. It was shown that the modes and frequencies of these augmented systems could be extracted using multi-input multi-output time-based modal analysis techniques such as DSPI [7]. These augmented modal properties could then be used for a variety of applications or methods. This chapter focused on using the augmented modal properties for damage detection. In particular, a generalized minimum rank perturbation theory (GMRPT) was developed from traditional minimum rank perturbation theory [1] (MRPT) to handle augmented systems. GMRPT was designed to handle the asymmetries that occur in the system matrices when damage occurs in the nonlinear parameters (but not in the undamageable augmented parameters). The nonlinearities considered in this chapter consist of cubic springs.

- In Chapter III the idea of system augmentations is explored further, and additional damage detection techniques were developed. Two other damage detection methodologies are introduced for augmented systems. The first, referred to as the iterative GMRPT approach, was designed to handle simultaneous changes in multiple system matrices (i.e. mass, damping and stiffness). The approach requires an iterative update of the mass and stiffness matrices using the GMRPT approach. The second, referred to as multiple augmentation GMRPT, exploits the fact that multiple augmentations exist for the same nonlinear system. This approach enables the solving of the asymmetries (nonlinear changes) in the system matrices first, allowng the use of only the right eigenvectors of the system. Two filtering algorithms were also discussed to improve the algorithms robustness to noise. The first was developed in this work, and exploits the fact that no damage can occur in the augmented equations. It can be employed before the damage location algorithm is used. The second was designed to filter the eigenvectors based on where damage is deemed to be. This filtering algorithm must be used after the results of the damage location algorithm are obtained. The nonlinearities considered in this chapter are both cubic springs and Colomb friction.

- In Chapter IV an integrated sensor placement and damage detection methodology was introduced. A key contribution of the method is the reduced order health assessment approach that uses the modes that contain the changes in the dynamics as opposed to conventional reduced order modeling which retains the modes that contain the dominant dynamics of the system. The method uses a filtering algorithm to remove frequency content of the modes outside the selected modes, and uses the knowledge about the damageable regions of the structure to expand the eigenvectors from the reduced (measured) space to the full (modal) space. The sensors are to be

placed at the hot spots of the system. When this is infeasible, a generalized effective independence distribution vector is used to place the remaining sensors. Also, a novel damage detection method called damage identification by hot spot projection (DIHSP) was introduced in this chapter. DIHSP is designed to project the full order model into the damaged subspace of the system, and filters out noise and damages outside of the hot spots of interest. This method can be used for linear and nonlinear (augmented) systems.

- In Chapter V nonlinear feedback auxiliary signals (NFAS) with system augmentation was introduced for sensitivity enhancing feedback control in *nonlinear* systems. Although the system is nonlinear (and also has a nonlinear controller), the system augmentation approach enables the use of linear methods such as modal analysis. Also, for the first time, the idea of an optimal augmentation is introduced (in this case for sensitivity enhancement). Several additional features of NFAS with system augmentation were discovered that make the use of this approach with linear systems desirable. These features include the ability to apply control in all the augmented equations of motion (without any physical control effort). Furthermore, a related benefit is the additional controller configurations that the added control of the augmented degrees of freedom enables. Finally, it was shown that the stability of the physical linearized system is what must be maintained, the (fictitious) augmented system can be unstable, which can result in significant sensitivity enhancement.

- In Chapter VI NFAS was used with system augmentation for increased sensitivity enhancement in *linear* systems. The focus of this chapter is exploring the benefits of NFAS over traditional sensitivity enhancing feedback. These benefits include the ability to have physically stable systems characterized by unstable augmented

systems for increased sensitivity enhancement. Also, the ability to control all augmented degrees of freedom with no actuator effort (only signal processing). Additionally, the added sensor-type knowledge of the augmented variables, and actuator-type control of the augmented degrees of freedom allow for a reduced number of physical sensors and actuators. Additionally, the NFASs are adaptively designed to the level of parameter variation expected in the system to ensure the linearity between the change in parameters and resonant frequencies. This chapter also used eigenstructure assignment for linear systems using NFAS and only partial measurement information. The benefits of modeling generalized damping were also shown.

- In Chapter VII the effectiveness of NFAS and system augmentation on linear systems with little physical actuation and control was shown. The key enabling features of NFAS that were exploited are the increased sensor knowledge, increased control authority, and additional controller configurations, which allow for sensitivity enhancement of multiple simultaneous parameter variations when traditional linear feedback is not feasible. In this chapter there are also several extensions to NFAS outside of its use with a reduced number of physical sensors and actuators. First, a method was detailed for augmented frequency extraction using noisy and limited measurement data. Also, the parameter variations whose sensitivity was enhanced and detected are both local (added mass at the tip and midspan) and global (uniform changes in mass and stiffness). Finally, a sensitivity reduction (for parameters that are not of interest) approach in conjunction with sensitivity enhancement (of parameters of interest) was introduced.

8.2 Future Research

The following are some suggested topics of future research to build upon the work presented in this dissertation.

- **Experimental work demonstrating system augmentation and nonlinear feedback auxiliary signals**

  A considerable amount of numerical studies have been conducted using system augmentation on a variety of nonlinear systems. A key next step is demonstrating the effectiveness of system augmentation and nonlinear feedback auxiliary signals experimentally. A linear cantilevered beam similar to the one discussed in Chapter VII would be ideal for experimentation on both system augmentation and nonlinear feedback auxiliary signals.

- **Integrated health monitoring of complex nonlinear systems using system augmentations and GMRPT**

  Failures in complex systems often result from problems from a few or a single component. If a healthy model of the system is known a priori then GMRPT is particularly well suited for identifying the damaged component(s) early. The integrated system can consist of structural (load bearing) components and non-structural components (controllers, pumps, etc.) as long as a healthy model is known and sufficient data is being extracted. A key unresolved challenge is to extract left eigenvectors from these systems (because these systems will be inherently asymmetric, the multiple augmentations GMRPT approach will not be sufficient). Modifying existing modal analysis approaches such as DSPI [7] or smooth orthogonal decomposition [108] to provide left eigenvectors are promising solutions to this challenge.

- **MEMS sensing devices using nonlinear feedback auxiliary signals**

  Exploiting the vibration of linear micro-structures such as micro-beams [40] and micro-cantilevers [37–39] has been carried out to sense small mass or stiffness variations using shifts in the resonant frequency. The resolution and robustness of these devices can be improved with the introduction of nonlinearity and feedback auxiliary signals. Numerical and experimental work in this area could have a significant impact on sensing in MEMS applications.

BIBLIOGRAPHY

BIBLIOGRAPHY

[1] D. C. Zimmerman and M. Kaouk. Structural damage detection using minimum rank update theory. *ASME Journal of Vibration and Acoustics*, 116(2):222–231, 1994.

[2] Q. J. Yang, P. Q. Zhang abd C. Q. Li, and X. P. Wu. A system theory approach to multi-input multi-output modal parameters identification methods. *Mechanical Systems and Signal Processing*, 8(2):159–174, 1994.

[3] H. Vold and G. T. Rocklin. The numerical implementation of a multi-input modal estimation for mini-computers. In *Proceedings of the 1st International Modal Analysis Conference*, pages 542–548, Orlando, Florida, 1982.

[4] J. N. Juang and R. S. Pappa. An eigensystem realisation algorithm for modal parameter identification and model reduction. *Journal of Guidance, Control, and Dynamics*, 8(5):620–627, 1985.

[5] W. Shong and P. Q. Zhang. MIMO ITD identifying technique for mini-computer. *Journal of University of Science and Technology of China*, 18(2):195–202, 1988.

[6] P. Q. Zhang, C. Q. Li, and Q. J. Yang. Identification of structural modal parameters by ARMAV model method. *Journal of Experimental Mechanics*, 4(1):137–145, 1989.

[7] J. Leuridan. *Some Direct Parameter Model Identification Methods Applicable For Multiple Modal Analysis,* PhD thesis. Department of Mechanical and Industrial Engineering, University of Cincinnati, 1984.

[8] K. Worden and G. R. Tomlinson. Nonlinearity in experimental modal analysis. *Philosophical Transactions of the Royal Society of London: A - Mathematical, Physical, and Engineering Sciences*, 359(1778):113–130, 2001.

[9] D. J. Ewins. *Modal Testing: Theory and Practice*. Research Studies Press, Taunton, 1984.

[10] S. J. Gifford. *Volterra Series Analysis of Nonlinear Structures,* PhD thesis. Department of Mechanical Engineering, Heriot-Watt University, 1989.

[11] D. Mirri, G. Iuculano, F. Filicori, G. Pasini G, G. Vannini, and G. P. Gualtieri. A modified Volterra series approach for nonlinear dynamic systems modeling. *IEEE Transactions on Circuits and Systems I - Fundamental Theory and Applications*, 49(8):1118–1128, 2002.

[12] S. J. Levinson. A padé approach for eigenvalue identification in underwater acoustic normal mode computations. *Journal of the Acoustical Society of America*, 99(2):831–835, 1996.

[13] X. Ma, M. F. A. Azeez, and A. F. Vakakis. Non-linear normal modes and non-parametric system identification of non-linear oscillators. *Mechanical Systems and Signal Processing*, 14(1):37–48, 2000.

[14] E. Pesheck, C. Pierre, and S. W. Shaw. Accurate reduced-order models for a simple rotor blade model using nonlinear normal modes. *Mathematical and Computer Modelling*, 33(10-11):1085–1097, 2001.

[15] S. W. Shaw and C. Pierre. Normal modes for non-linear vibratory systems. *Journal of Sound and Vibration*, 164(1):85–124, 1993.

[16] F. X. Wang, A. K. Bajaj, and K. Kamiya. Nonlinear normal modes and their bifurcations for an inertially coupled nonlinear conservative system. *Nonlinear Dynamics*, 42(3):233–265, 2005.

[17] W. Steiner, A Steindl, and H. Troger. Center manifold approach to the control of a tethered satellite system. *Applied Mathematics and Computation*, 70(2-3):315–327, 1995.

[18] M. Q. Xiao and T. Basar. Center manifold of the viscous Moore-Greitzer PDE model. *SIAM Journal on Applied Mathematics*, 61(3):855–869, 2000.

[19] S. R. Ibrahim and A. A. Saafan. Correlation of analysis in modeling and structures, assesment and review. In *Proceedings of the 5th IMAC*, volume 2, pages 1651–1660, London, England, 1987.

[20] W. Heylen and P. Sas. Review of model optimization techniques. In *Proceedings of the 5th IMAC*, volume 2, pages 1172–1182, London, England, 1987.

[21] A. Y. T. Leung, L. F. Chen, and W. L. Wang. A linearized procedure for solving inverse sensitivity equations of non-defective systems. *Journal of Sound and Vibration*, 259(3):513–524, 2003.

[22] A. N. Andry, E. Y. Shapiro, and J. C. Chung. Eigenstructure assignment for linear-systems. *IEEE Transactions on Aerospace and Electronic Systems*, 19(5):711–729, 1983.

[23] T. W. Lim. Structural damage detection using constrained eigenstructure assigment. *Journal of Guidance, Control, and Dynamics*, 18(3):411–418, 1995.

[24] L. J. Jiang, J. Tang, and K. W. Wang. An optimal sensitivity-enhancing feedback control approach via eigenstructure assignment for structural damage identification. *ASME Journal of Vibration and Acoustics*, 129(6):771–783, 2007.

[25] P. L. Liu. Identification and damage detection of trusses using modal data. *Journal of Structural Engineering*, 121(4):599–608, 1995.

[26] H. S. Kim and Y. S. Chun. Structural damage assessment of building structures using dynamic experimental data. *Structural Design of Tall and Special Buildings*, 13(1):1–8, 2004.

[27] D. C. Zimmerman. Looking into the crystal ball: The continued need for multiple viewpoints in damage detection. *Key Engineering Materials: Damage Assessment of Structures*, 167-168(1):76–90, 1999.

[28] D. C. Zimmerman. Model validation and verification of large and complex space structures. *Inverse Problems in Engineering*, 8(2):93–118, 2000.

[29] D. C. Zimmerman and T. Simmermacher. Model correlation using multiple static load and vibration tests. *AIAA Journal*, 33(11):2182–2188, 1995.

[30] M. Kaouk, D. C. Zimmerman, and T. W. Simmermacher. Assessment of damage affecting all structural properties using experimental modal parameters. *ASME Journal of Vibration and Acoustics*, 122(4):456–463, 2000.

[31] A. Cherng. Optimal sensor placement for modal parameter identification using signal subspace correlation techniques. *Mechanical Systems and Signal Processing*, 17(2):361–378, 2003.

[32] K. Yuen, L. S. Katafygiotis, C. Papadimitriou, and N. C. Mickleborough. Optimal sensor placement methodology for identification with unmeasured excitation. *Journal of Dynamic Systems, Measurement, and Control*, 123(4):677–686, 2001.

[33] J. E. T. Penny, M. I. Friswell, and S. D. Garvey. Automatic choice of measurement locations for dynamic testing. *AIAA Journal*, 32(2):407–414, 1994.

[34] R. G. Cobb and B. S. Liebst. Sensor placement and structural damage identification from minimal sensor information. *AIAA Journal*, 35(2):369–374, 1997.

[35] Z. Y. Shi, S. S. Law, and L. M. Zhang. Optimum sensor placement for structural damage detection. *Journal of Engineering Mechanics*, 126(11):1173–1179, 2000.

[36] H. Y. Guo, L. Zhang, L. L. Zhang, and J. X. Zhou. Optimal placement of sensors for structural health monitoring using improved genetic algorithms. *Smart Materials and Structures*, 13(3):528–534, 2004.

[37] B. Ilic, D. Czaplewski, M. Zalalutdinov, H. G. Craighead, P. Neuzil, C. Campagnolo, and C. Batt. Single cell detection with micromechanical oscillators. *Journal of Vacuum Science and Technology*, 19(6):2825–2828, 2001.

[38] T. Thundat, E. A. Wachter, S. L. Sharp, and R. L. Warmack. Detection of mercury-vapor using resonating microcantilevers. *Applied Physics Letters*, 66(13), 1995.

[39] G. Y. Chen, T. Thundat, E. A. Wachter, and R. J. Warmack. Adsorption-induced surface stress and its effects on resonance frequency of microcantilevers. *Journal of Applied Physics*, 77(8), 1995.

[40] D. DeVoe. Piezoelectric thin film micromechanical beam resonators. *Sensors and Actuators A*, 88(2):263–272, 2001.

[41] K. Wolf and O. Gottlieb. Nonlinear dynamics of a noncontacting atomic force microscope cantilever actuated by a piezoelectric layer. *Journal of Applied Physics*, 91(7):4701–4709, 2002.

[42] S. W. Doebling, C. R. Farrar, M. B. Prime, and D. W. Shevitz. *Damage identification and health monitoring of structural and mechanical systems from changes in their vibration characteristics: a literature review*. Los Alamos National Laboratory Report LA-13070-MS, Los Alamos, NM, 1996.

[43] S. W. Doebling, C. R. Farrar, and M. B. Prime. A summary review of vibration-based damage identification methods. *Shock and Vibration Digest*, 30(2):91–105, 1998.

[44] P. Cornwell, M. Kan, B. Carlson, L. B. Hoerst, S. W. Doebling, and C. R. Farrar. Comparative study of vibration-based damage identfication algorithms. In *Proceedings of the 16th International Modal Analysis Conference, Part 2*, pages 1710–1716, Santa Barbara, CA, 1998.

[45] M. I. Friswell and J.E.T. Penny. The practical limits of damage detection and location using vibration data. In *Proceedings of the 11th VPI & SU Symposium on Structural Dynamics and Control*, pages 31–40, Blacksburg, VA, 1997.

[46] A. S. J. Swamidas and Y. Chen. Monitoring crack growth through change of modal parameters. *Journal of Sound and Vibration*, 186(2):325–343, 1995.

[47] R. D. Adams, P. Cawley, C. J. Pye, and B. J. Stone. A vibrational technique for non-destructively assessing the integrity of structures. *Journal of Mechanical Engineering Science*, 20(2):93–100, 1978.

[48] L. R. Ray and L. Tian. Damage detection in smart structures using sensitivity enhancing feedback control. *Journal of Sound and Vibration*, 227(5):987–1002, 1999.

[49] L. R. Ray, B. H. Koh, and L. Tian. Damage detection and vibration control in smart plates: Towards multifunctional smart structures. *Journal of Intelligent Material Systems and Structures*, 11(9):725–739, 2000.

[50] J. N. Juang, K. B. Lim, and J. L. Junkins. Robust eigensystem assignment for flexible structures. *Journal of Guidance, Control, and Dynamics*, 12(3):381–387, 1989.

[51] N. G. Nalitolela, J. E. T. Penny, and M. I. Friswell. Mass or stiffness addition technique for structural parameter updating. *Modal Analysis: The International Journal of Analytical and Experimental Modal Analysis*, 7(3):157–168, 1992.

[52] J. S. Lew and J. N. Juang. Structural damage detection using virtual passive controllers. *Journal of Guidance, Control, and Dynamics*, 25(3):419–424, 2002.

[53] B. H. Koh and L. R. Ray. Feedback controller design for sensitivity-based damage localization. *Journal of Sound and Vibration*, 273(1-2):317–335, 2004.

[54] C. R. Farrar, S. W. Doebling, and D. A. Nix. Vibration-based structural damage identification. *Philosophical Transactions of the Royal Society of London: A - Mathematical, Physical and Engineering Sciences*, 359(1778):131–149, 2001.

[55] A. K. Pandey and M. Biswas. Damage detection in structures using changes in flexibility. *Journal of Sound and Vibration*, 169(1):3–17, 1994.

[56] M. S. Agbabian, S. F. Masri, R. F. Miller, and T. K. Caughey. System identification approach to detection of structural changes. *ASCE Journal of Engineering Mechanics*, 117(2):370–390, 1990.

[57] B. F. Feeny, C. M. Yuan, and J. P. Cusumano. Parametric identification of an experimental of an experimental magneto-elastic oscillator. *Journal of Sound and Vibration*, 247(5):785–806, 2001.

[58] L. Ljung. *System Identification - Theory for the User*. Prentice Hall, New York, 1999.

[59] S. F. Masri, R. K. Miller, A. F. Saud, and T. K. Caughey. Identification of nonlinear vibrating structures: Part I: Formulation. *Journal of Applied Mechanics*, 109(54):918–922, 1987.

[60] A. W. Smyth, S. F. Masri, A. G. Chassiakos, and T. K. Caughey. On-line parametric identification of MDOF nonlinear hysteretic systems. *ASCE Journal of Engineering Mechanics*, 125(2):133–142, 1999.

[61] M. J. Atalla and D. J. Inman. On model updating using neural networks. *Mechanical Systems and Signal Processing*, 12(1):135–161, 1998.

[62] T. Marwala and H. E. M. Hunt. Fault identification using finite element models and neural networks. *Mechanical Systems and Signal Processing*, 13(3):475–490, 1999.

[63] C. Zang and M. Imregun. Structural damage detection using artificial neural networks and measured FRF data reduced via principal component projection. *Journal of Sound and Vibration*, 242(5):813–827, 2001.

[64] A. Bazoune, Y. A. Khulief, N. G. Stephen, and M. A. Mohiuddin. Dynamic response of spinning tapered Timoshenko beams using modal reduction. *Finite Element Analysis and Design*, 37(3):199–219, 2001.

[65] R. Bladh, M. P. Castanier, and C. Pierre. Reduced order modeling and vibration analysis of mistuned bladed disk assemblies with shrouds. *Journal of Engineering for Gas Turbines and Power*, 121(3):515–522, 1999.

[66] R. Bladh, M. P. Castanier, and C. Pierre. Component-mode-based reduced order modeling techniques for mistuned bladed disks - Part II: Application. *Journal of Engineering for Gas Turbines and Power*, 123(1):100–108, 2001.

[67] M. P. Castanier, Y. C. Tan, and C. Pierre. Characteristic constraint modes for component mode synthesis. *AIAA Journal*, 39(6):1183–1187, 2001.

[68] B. I. Epureanu, K. C. Hall, and E. H. Dowell. Reduced order models of unsteady transonic viscous flows in turbomachinery. *Journal of Fluids and Structures*, 14(8):1215–1235, 2000.

[69] B. I. Epureanu, K. C. Hall, and E. H. Dowell. Reduced order models of unsteady viscous flows in turbomachinery using viscous-inviscid coupling. *Journal of Fluids and Structures*, 15(2):255–276, 2001.

[70] B. F. Farrell and P. J. Ioannou. Accurate low-dimensional approximation of the linear dynamics of fluid flow. *Journal of Atmosferic Sciences*, 58(18):2771–2789, 2001.

[71] P. Feldmann and R. W. Freund. Efficient linear circuit analysis by Padé approximation via the lanczos process. *IEEE Transactions on Computer Aided Design of Integrated Circuits and Systems*, 14(5):639–649, 1995.

[72] M. Kamon, F. Wang, and J. White. Generating nearly optimally compact models from Krylov-subspace based reduced-order models. *IEEE Transactions of Circuits and Systems II - Analog and Digital Signal Processing*, 47(4):239–248, 2000.

[73] K. D'Souza and B. I. Epureanu. Damage detection in nonlinear systems using system augmentation and generalized minimum rank perturbation theory. *Smart Materials and Structures*, 14(5):989–1000, 2005.

[74] K. D'Souza and B. I. Epureanu. System augmentation and matrix updating for damage detection in nonlinear systems. In *Proceedings of the 46-th AIAA/ASME/ASCE/AHS/ASC Structures, Structural Dynamics and Materials Conference*, volume AIAA-2005-1831, pages 1–9, Austin, Texas, 2005.

[75] J. S. Bay. *Fundamentals of Linear State Space Theory*. McGraw-Hill, Madison, 1999.

[76] P. E. Moraal and J. W. Grizzle. Observer design for nonlinear systems with dicrete-time measurements. *IEEE Transactions on Automatic Control*, 40(3):395–404, 1995.

[77] J. Tsinias. Observer design for nonlinear systems. *System and Control Letters*, 13(2):135–142, 1989.

[78] K. D'Souza and B. I. Epureanu. Minimum rank generalized subspace updating approach for nonlinear systems. In *Proceedings of the 2005 International Mechanical Engineering Conference and Exposition*, volume IMECE-2005-80135, pages 1–10, Orlando, Florida, 2005.

[79] Z. Y. Shi, S. S. Law, and L. M. Zhang. Damage detection by directly using incomplete mode shapes. *Journal of Engineering Mechanics*, 126(6):656–660, 1999.

[80] K. D'Souza and B. I. Epureanu. Multiple augmentations of nonlinear systems and generalized minimum rank perturbations for damage detection. *Journal of Sound and Vibration*, 316(1-5):101–121, 2008.

[81] C. Hung, W. Ko, and Y. Peng. Identification of modal parameters from measured input and output data using a vector backward auto-regressive with exogeneous model. *Journal of Sound and Vibration*, 276(3-5):1043–1063, 2004.

[82] E. Dascotte. Practical application of finite element tuning using experimental data. In *Proceeding of the 8th International Modal Analysis Conference*, pages 1032–1037, Orlando, FL, 1990.

[83] N. Stubbs and R. Osegueda. Global damage detection in solids-experimental verification. *Modal Analysis: The International Journal of Analytical and Experimental Modal Analysis*, 5(2):81–97, 1990.

[84] N. Stubbs and R. Osegueda. Global non-destructive damage evaluation in solids. *Modal Analysis: The International Journal of Analytical and Experimental Modal Analysis*, 5(2):67–79, 1990.

[85] P. Trivailo, L. A. Plotnikova, and L.A. Wood. Enhanced parameter identification for damage detection and structural integrity assessment using twin structures. In *The 5th International Congress on Sound and Vibration*, pages 1733–1741, Adelaide, Australia, 1997.

[86] L. R. Ray and S. Marini. Optimization of control laws for damage detection in smart structures. In *SPIE Symposium on Mathematics and Control in Smart Structures*, volume 3984, pages 395–402, Newport Beach, CA, March 2000. SPIE, SPIE.

[87] K. D'Souza and B. I. Epureanu. Sensor placement for damage detection in nonlinear systems using system augmentations. *AIAA Journal*, 46(10):2434–2442, 2008.

[88] T. B. Cunningham. Eigenspace selection procedures for closed-loop response shaping with modal control. In *Proceedings of the IEEE Conference on Decision and Control*, pages 178–186, 1980.

[89] F. J. Shelley and W. W. Clark. Active mode localization in distributed parameter systems with consideration of limited actuator placement, Part 1: Theory. *ASME Journal of Vibration and Acoustics*, 122(2):160–164, 2000.

[90] F. J. Shelley and W. W. Clark. Active mode localization in distributed parameter systems with consideration of limited actuator placement, Part 2: Simulations and experiments. *ASME Journal of Vibration and Acoustics*, 122(2):165–168, 2000.

[91] J. Tang and K. W. Wang. Vibration confinement via optimal eigenvector assignment and piezoelectric networks. *Journal of Vibration and Control*, 126(1):27–36, 2004.

[92] T. Y. Wang and K. W. Wang. Periodic isolator design enhancement via vibration confinement through eigenvector assignment and piezoelectric circuitry. *Journal of Vibration and Control*, 13(7):989–1006, 2007.

[93] T. Coleman, M. A. Branch, and A. Grace. *Opimization Toolbox User's Guide*. The MathWorks, Inc., 3rd edition, 1999.

[94] K. D'Souza and B. I. Epureanu. Damage detection in nonlinear systems using optimal feedback auxiliary signals. *ASME Journal of Vibration and Acoustics*, (accepted), 2009.

[95] S. L. Campbell and R. Nikoukhah. *Auxiliary Signal Design for Failure Detection*. Princeton University Press, 2004.

[96] T. P. Burg, M. Godin, S.M. Knudsen, W. Shen, G. Carlson, J. S. Foster, K. Babcock, and S. R. Manalis. Weighing of biomolecules, single cells and single nanoparticles in fluid. *Nature*, 446(7139):1066–1069, 2007.

[97] M. Godin, A. K. Bryan, and T. P. Burg. Measuring the mass, density, and size of particles and cells using a suspended microchannel resonator. *Applied Physics Letters*, 91(12):123121:1–123121:3, 2007.

[98] T. Braun, V. Barwich, M. K. Ghatkesar, A. H. Bredekamp, C. Gerber, M. Hegner, and H. P. Lang. Micromechanical mass sensors for biomolecular detection in a physiological environment. *Physical Review*, 72(3):031907:1–031907:9, 2005.

[99] A. Gupta, D. Akin, and R. Bashir. Single virus particle mass detection using microresonators with nanoscale thickness. *Applied Physics Letters*, 84(11):1976–1978, 2004.

[100] O. S. Salawu. Detection of structural damage through changes in frequency : a review. *Engineering Structures*, 19(9):718–723, 1997.

[101] J. M. W. Brownjohn. Structural health monitoring of civil infrastructure. *Philosophical Transactions of the Royal Society of London: A - Mathematical, Physical and Engineering Sciences*, 365:589–622, 2007.

[102] M. I. Friswell, J. E. Mottershead, and H. Ahmadian. Finite-element model updating using experimental test data: parameterization and regularization. *Philosophical Transactions of the Royal Society of London: A - Mathematical, Physical and Engineering Sciences*, 359:169–186, 2001.

[103] S. Yin and B. I. Epureanu. Structural health monitoring based on sensitivity vector fields and attractor morphing. *Philosophical Transactions of the Royal Society of London: A - Mathematical, Physical and Engineering Sciences*, 364:2515–2538, 2006.

[104] M. I. Friswell. Damage identification using inverse methods. *Philosophical Transactions of the Royal Society of London: A - Mathematical, Physical and Engineering Sciences*, 365:393–410, 2007.

[105] P. D. Cha and W. Gu. Model updating using an incomplete set of experimental modes. *Journal of Sound and Vibration*, 233(4):587–600, 2000.

[106] L. J. Jiang, J. Tang, and K. W. Wang. On the tuning of variable piezoelectric transducer circuitry network for structural damage identification. *Journal of Sound and Vibration*, 309(3-5):695–717, January 2008.

[107] K. D'Souza and B. I. Epureanu. Nonlinear feedback auxiliary signals for system interrogation and damage detection. *Philosophical Transactions of the Royal Society of London: A - Mathematical, Physical and Engineering Sciences*, 464(2100):3129–3148, 2008.

[108] U. Farooq and B. F. Feeny. Smooth orthogonal decomposition for modal analysis of randomly excited systems. *Journal of Sound and Vibration*, 316:137–146, 2008.